Strength of anchors in masonry

Arifovic, Fedja; Nielsen, Mogens Peter

Publication date:
2006

Document Version
Publisher's PDF, also known as Version of record

Fedja Arifovic
Mogens Peter Nielsen

Strength of anchors in masonry

DANMARKS
TEKNISKE
UNIVERSITET

Rapport
BYG · DTU
R-134
2006
ISSN 1601-2917
ISBN 87-7877-205-2

Strength of anchors in masonry

Fedja Arifović
M.P. Nielsen

Department of Civil Engineering
Technical University of Denmark
October, 2004

Abstract

Strength of anchors in masonry is treated by means of the upper bound theorem of the theory of plasticity. Thus, the theory of plasticity for bonded anchors is described.
The case of a single anchor in masonry far from edges and corners is treated by utilizing global and local failure mechanisms. Local failure mechanisms are characterized as those where the failure only occurs in the brick or the joint in which an anchor is installed. Those are: combined brick-cone failure, splitting failure and sliding failure. Global failure mechanisms are defined as those where most or the whole of masonry wall is involved in the failure. Those are: wall strip bending failure, punching shear failure and sliding failure at an edge. Cases of anchors close to a corner and an edge parallel to the bed joint are only treated experimentally.
The proposed upper bound expressions are determined in conjunction with the empirical data based on tests conducted for the purpose of this report and some other ones conducted recently.

Contents

1 Introduction **2**
1.1 Behavior of bonded anchors in masonry - tension loading 3

2 Theory of plasticity for bonded anchors **4**
2.1 Constitutive equations 4
2.2 Yield conditions 5
2.3 Extremum principles 7
2.3.1 The upper bound theorem 7
2.3.2 The lower bound theorem 7
2.3.3 The uniqueness theorem 7
2.4 Dissipation formulas 7
2.5 Strength of masonry wall 8
2.5.1 Compressive strength 8
2.5.2 Tensile strength 9
2.6 Local failure mechanisms 11
2.6.1 Sliding failure along a deformed bar 11
2.6.2 Combined brick-cone failure 13
2.6.3 The splitting failure 18
2.7 Global failure mechanisms 20
2.7.1 Wall strip bending failure 20
2.7.2 Punching shear failure 27
2.7.3 Sliding failure at an edge 28
2.8 Final remarks 29

3 Test results **31**
3.1 Far from edges and corners 33
3.1.1 Header arrangements 33
3.1.2 Stretcher arrangements 36
3.1.3 Joint arrangements 38
3.2 Close to edges and corners 40
3.2.1 Edge arrangements - normal to the bed joint 40
3.2.2 Edge arrangements - parallel to the bed joint 41
3.3 Corner arrangements 42

4 Theory and empirical data **43**
4.1 Combined brick-cone failure 43
4.2 Sliding failure of anchors in joints 45
4.3 Sliding failure of anchors in bricks 47
4.4 Punching shear 49
4.5 Edge arrangements 50

5 Conclusion **51**

Bibliography **53**

List of symbols **54**

Appendix **2**

A Test results - anchors in masonry **2**
A.1 Test setup 2
A.2 Far from edge and corners 4
A.2.1 Stretcher arrangement - 1, d = 12 mm 4
A.2.2 Stretcher arrangement - 2, d = 12 mm 6
A.2.3 Stretcher arrangement - 3, d = 12 mm 8
A.2.4 Stretcher arrangement - 1, d = 16 mm 10
A.2.5 Stretcher arrangement - 2, d = 16 mm 12
A.2.6 Stretcher arrangement - 3, d = 16 mm 14
A.2.7 Stretcher arrangement, d = 10 mm, h = 100 mm 16
A.2.8 Stretcher arrangement, d = 10 mm, h = 120 mm 18
A.2.9 Stretcher arrangement, d = 10 mm, h = 140 mm 20
A.2.10 Stretcher arrangement, d = 10 mm, h = 160 mm 22
A.2.11 Stretcher arrangement, d = 12 mm, h = 100 mm 24
A.2.12 Stretcher arrangement, d = 12 mm, h = 120 mm 26
A.2.13 Stretcher arrangement, d = 12 mm, h = 140 mm 28
A.2.14 Stretcher arrangement, d = 12 mm, h = 160 mm 30
A.2.15 Stretcher arrangement, d = 16 mm, h = 100 mm 32
A.2.16 Stretcher arrangement, d = 16 mm, h = 120 mm 34
A.2.17 Stretcher arrangement, d = 16 mm, h = 140 mm 36
A.2.18 Stretcher arrangement, d = 16 mm, h = 140 mm 38
A.2.19 Header arrangement - 1, d = 12 mm 40
A.2.20 Header arrangement - 2, d = 12 mm 42
A.2.21 Header arrangement - 3, d = 12 mm 44
A.2.22 Header arrangement - 1, d = 16 mm 46
A.2.23 Header arrangement - 2, d = 16 mm 48
A.2.24 Header arrangement - 3, d = 16 mm 50
A.2.25 Header arrangement, d = 10 mm, h = 90 mm 52
A.2.26 Header arrangement, d = 10 mm, h = 100 mm 54

A.2.27 Header arrangement, d = 10 mm, h = 110 mm 56
A.2.28 Header arrangement, d = 10 mm, h = 120 mm 58
A.2.29 Header arrangement, d = 10 mm, h = 130 mm 60
A.2.30 Header arrangement, d = 10 mm, h = 140 mm 62
A.2.31 Header arrangement, d = 10 mm, h = 150 mm 64
A.2.32 Header arrangement, d = 10 mm, h = 160 mm 66
A.2.33 Header arrangement, d = 10 mm, h = 170 mm 68
A.2.34 Header arrangement, d = 12 mm, h = 100 mm 70
A.2.35 Header arrangement, d = 12 mm, h = 120 mm 72
A.2.36 Header arrangement, d = 12 mm, h = 140 mm 74
A.2.37 Header arrangement, d = 12 mm, h = 160 mm 76
A.2.38 Header arrangement, d = 16 mm, h = 100 mm 78
A.2.39 Header arrangement, d = 16 mm, h = 120 mm 80
A.2.40 Header arrangement, d = 16 mm, h = 140 mm 82
A.2.41 Header arrangement, d = 16 mm, h = 160 mm 84
A.2.42 Joint arrangements, d = 10 mm, h = 100 mm 86
A.2.43 Joint arrangements, d = 10 mm, h = 120 mm 88
A.2.44 Joint arrangements, d = 10 mm, h = 140 mm 90
A.2.45 Joint arrangements, d = 10 mm, h = 160 mm 92
A.2.46 Joint arrangements, d = 12 mm, h = 100 mm 94
A.2.47 Joint arrangements, d = 12 mm, h = 120 mm 96
A.2.48 Joint arrangements, d = 12 mm, h = 140 mm 98
A.2.49 Joint arrangements, d = 12 mm, h = 160 mm 100
A.2.50 Joint arrangements, d = 16 mm, h = 100 mm 102
A.2.51 Joint arrangements, d = 16 mm, h = 120 mm 104
A.2.52 Joint arrangements, d = 16 mm, h = 140 mm 106
A.2.53 Joint arrangements, d = 16 mm, h = 160 mm 108
A.3 Close to a corner 110
A.3.1 Corner distance c = 100 mm, d = 12 mm 110
A.3.2 Corner distance c = 160 mm, d = 12 mm 112
A.3.3 Corner distance c = 230 mm, d = 12 mm 114
A.3.4 Corner distance c = 230 mm - 2, d = 12 mm 116
A.3.5 Corner distance c = 100 mm, d = 16 mm 118
A.3.6 Corner distance c = 160 mm, d = 16 mm 120
A.3.7 Corner distance c = 160 mm - 2, d = 16 mm 122
A.3.8 Corner distance c = 230 mm, d = 16 mm 124
A.3.9 Corner distance c = 230 mm - 2, d = 16 mm 126
A.4 Close to an edge - normal to the bed joint 128
A.4.1 Edge distance e = 90 mm, d = 12 mm 128
A.4.2 Edge distance e = 160 mm, d = 12 mm 130
A.4.3 Edge distance e = 230 mm, d = 12 mm 132
A.4.4 Edge distance e = 100 mm, d = 16 mm 134
A.4.5 Edge distance e = 160 mm, d = 16 mm 136
A.4.6 Edge distance e = 230 mm, d = 16 mm 138

A.5 Close to an edge - parallel to the bed joint 140
A.5.1 Edge distance e = 90 mm, d = 12 mm 140
A.5.2 Edge distance e = 160 mm, d = 12 mm 142
A.5.3 Edge distance e = 230 mm, d = 12 mm 144
A.5.4 Edge distance e = 100 mm, d = 16 mm 146
A.5.5 Edge distance e = 160 mm, d = 16 mm 148
A.5.6 Edge distance e = 230 mm, d = 16 mm 150

Foreword

The present report on anchors in masonry is based on tests conducted at the Department of Civil Engineering at the Technical University of Denmark.

The introduction of concentrated loads is unavoidable in building structures and this involves the use of fastening systems, mainly anchors. Since no empirical approaches are developed regarding the design of anchors in masonry the theoretical investigation becomes an obvious goal. The theory of plasticity has reached the level where it is natural to use it in practical design of anchors and some investigations have been conducted in recent years at the Department of Civil Engineering.

It is important to emphasize that we are under great obligation to the consulting company *AI-gruppen A/S* that made it possible for us to conduct this investigation and the present report.
For support regarding the experimental part of this investigation we are grateful to the staff at the laboratory of Department of Civil Engineering. Also, great thanks to Hilti Danmark A/S that kindly donated the anchors and some of the equipment used in the experiments. We also express gratitude to Karsten Findsen and Lars Z. Hansen for their valuable suggestions and advices.

Finally, we would like to thank MURO[1], particularly managing director, Architect MAA Søren Bøgh, who has initiated masonry research at the department and supported the production of the test specimens.

Fedja Arifović
M. P. Nielsen

[1]Danish abbreviation : Murerfagets oplysningsråd

1 Introduction

In this report strength of anchors in masonry is considered. The load carrying capacity of anchors in masonry is determined by means of the theory of plasticity. So far, the theory of plasticity has been successfully applied to anchors in concrete, firstly, by Olsen and Nielsen, [3], for a single anchor far from edges and corners and later by Arifović, [6], extending the treatment to anchors close to an edge and a corner as well as a group of anchors far from and close to an edge and a corner. In [6], single anchors in masonry far from edges and corners are treated and the pull-out tests are described (for the test results see Appendix A). This work is extended in this report.

As far as anchors in masonry are concerned the knowledge on their behavior is very limited. Thus, there exist no empirical formulas that can be used to verify the theoretical approach of the theory of plasticity developed in this report. For this reason pull-out tests of single anchors in masonry are necessary in order to observe the failure modes that govern the failures and in order to obtain the ultimate loads. In this report the test results obtained in [6] are used as well as the pull-outs carried out for the purpose of this report involving anchors near edges and corners - all shown in Appendix A.

The theory of plasticity for anchors in masonry is developed by analogy of the approach of the concrete-cone failure in punching shear of concrete slabs, [4] and by analogy of the anchorage theory, [4]. The latter is due to the anchors used in masonry being bonded anchors. Also, the approach of selecting the most dangerous mechanism in upper bound solutions is applied.

The description of the work starts off with a chapter on the theory of plasticity for bonded anchors. In this chapter the theory of plasticity is shortly introduced and the development of the necessary upper bound expressions is described. The upper bound expressions are described for two different kinds of failures : local and global failures. Local failures are those observed in tests and are of a local character, i.e. involving only the brick or the joint in which an anchor is installed. The global failures involve most of or the whole wall and are described by some simple failure mechanisms in cases where there is no edge and corner influence and by the splitting failure mechanism in the case of edge influence.

The test results obtained and the results from Appendix D in [6] (reproduced in Appendix A) are described in chapter 3. Finally, in chapter 4 the theoretical solutions are compared to the test results on which basis effectiveness factors are proposed for future design.

1.1 Behavior of bonded anchors in masonry - tension loading

When subjected to tension loading bonded anchors in masonry are seen to exhibit essentially the same failure modes as bonded anchors in concrete, Appendix A:

- steel failure
- combined brick-cone failure
- pull-out/sliding failure
- brick-splitting failure for anchors arranged close to an edge normal to the bed joint

Steel failure of anchors in masonry is rarely observed and takes place only in cases when the embedment depth and the strength of the masonry are very high.
Combined brick-cone failure is a cone-like failure that occurs in solid brick by analogy of the cone failure in concrete. This kind of failure is treated as a combined failure due to another failure that occurs simultaneously with the brick-cone failure. This is the sliding failure along the anchor or along the interface. The failure is demonstrated by the tests shown in Appendix A and Appendix D in [6].
Pure sliding failure occurs either by failure at the interface between resin mortar and the base material or by failure within the resin mortar.
Brick-splitting failure occurs in solid brick where the brick splits in two parts. This failure is believed to occur only when the anchor is arranged close to an edge normal to the bed joint Otherwise, this kind of failure is not possible due to to the necessary dilatation of the brick being prevented.

As mentioned, no predictive methods for determining the load-carrying capacity of anchors in masonry exist so far. Normally, failure loads are checked under actual conditions. It is known that a lot of factors influence the failure loads but in order to avoid comprehensive testings only the influence of the arrangement and the dimension of the anchor is investigated.

It should also be noticed that other failure mechanisms may occur. In this report those are treated as global failure mechanisms - as proposed in [1] or as corner and splitting failures observed in tests.
Also, punching shear failure is believed to govern the failure in some cases. The tests did not show any evidence of this kind of failure but anchor arrangements involving anchor plates might very easily impose this kind of failure, [1].

2 Theory of plasticity for bonded anchors

In this chapter a short introduction to the theory of plasticity for bonded anchors is given. The theory of plasticity is here applied to bodies made of rigid-plastic materials. Rigid-plastic material does not exist in reality since it is assumed that no deformation occurs up to a certain limit. This limit is called the yield point. At this point arbitrarily large plastic deformation may occur without any change in stresses. Stresses at this limit are recognized as yield stresses.

The strength of anchors is calculated by means of the work equation where the dissipation formulas defined in section 2.4 are used. The dissipation formulas describe the rate of work in the body, i.e. the resistance against the deformation. The strain rates are defined by the yield condition, the strain rate vector being perpendicular to the yield surface (associated plasticity).
The plasticity of masonry is primarily due to the mortar connecting the bricks and the interface between mortar and brick that is the weak part of masonry, [5].
Finally, the failure loads in upper bound solutions are determined by equalizing the external work and the dissipation. In order to find upper bound solutions a prediction of a failure mechanisms is necessary. This is done in sections 2.6 and 2.7.
Lower bound solutions are also of great interest but they are not considered because the statically admissible stress distributions are too complicated.

A more detailed description of the theory of plasticity and its application on concrete is given by Nielsen in [4].

2.1 Constitutive equations

In this section the constitutive equations for a rigid-plastic material are established. In this case elastic strains are disregarded, thus Hooke's law or any other relation between stress and strain is not applied. This is a valid assumption when plastic strains are much greater than elastic strains. The relation between stress and strain for a rigid-plastic material in uniaxial state is illustrated in figure 2.1. From this figure it is obvious that stresses are undetermined up to the yield stress f_y and that the strains corresponding to f_y can be arbitrarily large.

The constitutive equations for a rigid-plastic material may be based on an energy consideration. It is the work necessary to be performed to deform a rigid-plastic body that is sought. This work is found using *von Mises hypothesis on maximum work*. This means that of all the stress combinations that satisfy the yield condition the one is sought that gives the greatest possible work, i.e. the greatest possible resistance in the body.

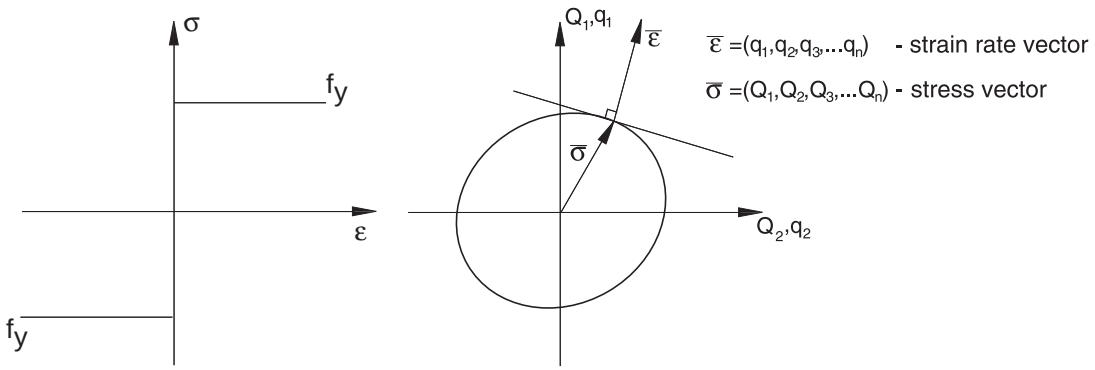

Figure 2.1: *Stress-strain relation for rigid-plastic material and the normality condition for two-dimensional case (n = 2)*

Assuming that the yield surface is smooth without plane surfaces or apexes and that it is convex and closed (as illustrated in figure 2.1 for a two-dimensional case) it can be shown that under given assumptions the strain rate vector $\bar{\epsilon}$ uniquely determines a stress vector $\bar{\sigma}$ on the yield surface, where $\bar{\epsilon}$ is normal to the surface. This is the associated flow rule called *the normality condition.*

2.2 Yield conditions

The failure of the bricks, mortar and interface between brick and mortar and between anchors and bricks is described by the modified Coulomb failure condition, [4]. Two kinds of failures are considered, sliding failure and separation failure. The shear stress τ determining the sliding resistance is composed of cohesion c and internal friction that equals a certain fraction μ of the normal stress σ in the section. Thus, this part of the failure conditions is given by $\mid \tau \mid = c - \mu\sigma$, σ being positive as tension. The separation failure is determined by the separation resistance which is normally equal to the tensile strength f_t. As shown in [4] these assumptions are equivalent to using a circular transition curve as shown in figure 2.2

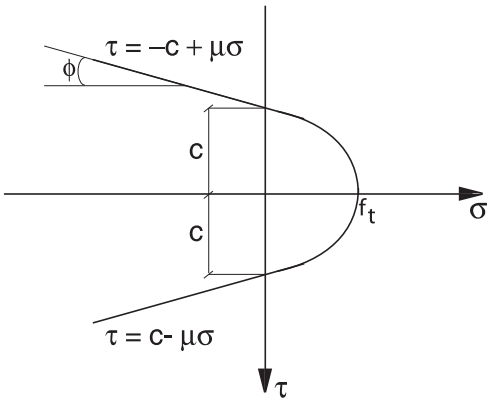

Figure 2.2: *Yield conditions for masonry - Modified Coulomb material*

If the tensile strength is set to zero, which is reasonable to assume, the modified Coulomb failure condition for masonry may be illustrated as shown in figure 2.3 (σ is here positive as compression).
Mohr's circle for uniaxial compression is shown in the figure and defines the compressive strength f_c. Even for a joint it might be convenient to define a formal compressive strength f_{ci}. The relation between c and f_c is in general

$$c = \frac{f_c}{2}\frac{1-\sin\phi}{\cos\phi} \tag{2.1}$$

where ϕ is the angle of friction defined by $\mu = \tan\phi$.

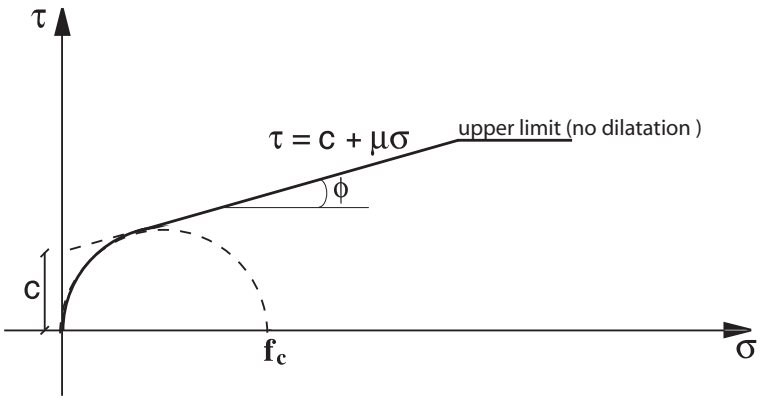

Figure 2.3: *Modified Coulomb friction law for masonry, [4]*

The angle of friction is still not known particularly well. Values between 30^o and 37^o are normally used.
There is some evidence that in Coulomb materials an upper limit of the shear strength may exist. This has been seen in the anchor tests (concrete, [3] and in the tests reported here). An upper limit is illustrated in figure 2.3. When the associated flow rule is valid there is no dilatation in this region.
Since the cohesion c is an important factor in determining the failure condition for masonry it is important to add that the cohesion may be found by means of an empirical equation, [2]. This equation reads

$$c = \Big(-0.11\frac{v}{k} + 0.03\Big)\mathrm{IRA} - 0.5\frac{v}{c} + 3.6 \tag{2.2}$$

where

- IRA is the initial rate of absorption in kg/m^2/min valid in the interval 1.7-3.9
- v/k is water-lime ratio
- v/c is water-cement ratio

2.3 Extremum principles

A body reaching the yield point is said to be subject to *collapse by yielding*. The corresponding load is called the *failure load* or the *load-carrying capacity*. In order to determine the load-carrying capacity the following extremum principles are developed.

2.3.1 The upper bound theorem

The upper bound theorem states that if various geometrically possible displacement fields are considered, the work equation can be used to find values of the load-carrying capacity that are greater than or equal to the true one. Thus the name *upper bound theorem*.

2.3.2 The lower bound theorem

The lower bound theorem states that if the load has such a magnitude that it is possible to find a safe and statically admissible stress distribution (stresses corresponding to stresses within the yield surface and satisfying the equilibrium conditions and statical boundary conditions for the actual load) this load will not be able to cause collapse of the body. Thus the load is then smaller than the collapse load - hence the name *lower bound theorem*.

2.3.3 The uniqueness theorem

From the upper bound and lower bound theorem it is seen that only one load exists that satisfies all of the conditions for a failure load. This is seen from the fact that the lower bound theorem determines a load smaller than or equal to the collapse load and the upper bound theorem describes a load greater than or equal to the collapse load. Thus, the failure load is uniquely determined. It should be noticed that only the load-carrying capacity is uniquely determined. The stresses, strains and displacements at the yield point are not uniquely determined.

For the proof of the upper bound and lower bound theorem see chapter 1 in [4].

2.4 Dissipation formulas

In the work equation the external work is set equal to the dissipation.
The dissipation per unit length for a modified Coulomb material for yield lines in case of plane strain reads, [4]

$$W_l = \frac{1}{2} f_c u b (l - m \sin \alpha), \quad \pi \leq \alpha \leq \pi - \phi \tag{2.3}$$

where f_c is the compressive strength, u the relative displacement of the bodies separated by the yield lines, α the angle between the displacement vector and the yield line and b is the thickness.
l and m are defined by

$$\begin{aligned} l &= 1 - 2\frac{f_t}{f_c}\frac{\sin\phi}{1-\sin(\phi)} \\ m &= 1 - 2\frac{f_t}{f_c}\frac{1}{1-\sin(\phi)} \end{aligned} \tag{2.4}$$

Here ϕ is, as before, the angle of friction defined by $\mu = \tan\phi$. It is seen that for $f_t = 0$ we have

$$W_l = \frac{1}{2} f_c u b (1 - \sin\alpha) \tag{2.5}$$

2.5 Strength of masonry wall

2.5.1 Compressive strength

In [5], the compressive strength of a masonry wall is found by an upper bound solution. The expression is complicated and must be optimized with respect to several geometrical parameters. However, the compressive strength can be found approximately by the following expression, also given in [5]

$$f_c = \left[1.81\left(\frac{\nu_j f_{cj}}{\nu_b f_{cb}}\right)^{0.66} - 0.81\left(\frac{\nu_j f_{cj}}{\nu_b f_{cb}}\right)^{1.38}\right]\nu_b f_{cb}, \quad (f_{cb} \text{ and} f_{cj} \text{ in MPa}) \tag{2.6}$$

where

- f_{cb} is the compressive strength of a brick
- f_{cj} is the compressive strength of the mortar
- ν_b is the effectiveness factor applied on the compressive strength of a brick f_{cb}
- ν_j is the effectiveness factor applied on the compressive strength of the mortar f_{cj}

Expressions for ν_b and ν_j are given in [5]

$$\left.\begin{aligned} \nu_b &= 0.34 {f_{cb}}^{0.34} \\ \nu_j &= \frac{1.18}{{f_{cj}}^{0.45}} \end{aligned}\right\} \leq 1, \quad (f_{cb} \text{ and} f_{cj} \text{ in MPa}) \tag{2.7}$$

2.5.2 Tensile strength

The tensile strength of masonry disks depends on the direction in which the tension is applied. The tensile strength normal to the bed joint is normally set to zero whereas the tensile strength parallel to the bed joint is found by considering the failure modes shown in figure 2.4, [1].

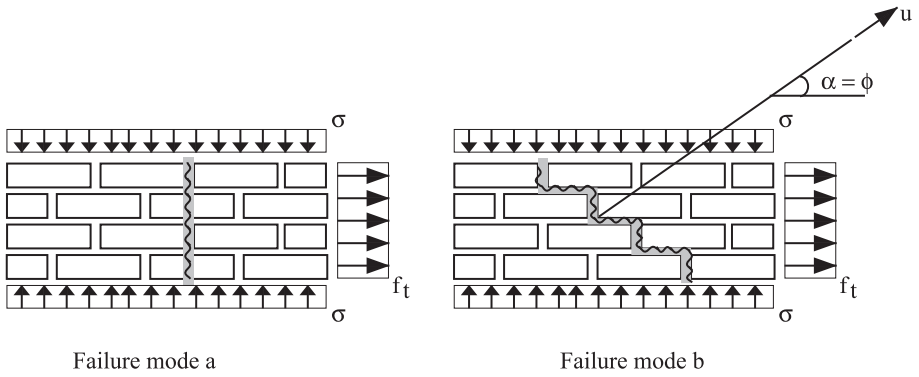

Figure 2.4: *Failure modes determining the tensile strength of a masonry wall parallel to the bed joint, [1]*

The failure mode a encloses the following tensile strength neglecting the strength of the cross joint

$$f_t = \frac{h_b}{2(h_b + h_j)} f_{tb} \tag{2.8}$$

where

- f_{tb} is the tensile strength of a brick, normally set to $\frac{1}{20} f_{cb}$
- h_b is the height of a brick
- h_j is the height of a joint

For zero cohesion failure mode b leads to zero dissipation. This is recommended in old masonry. In such case the work equation leads to the external work

$$W_{\text{ext}} = -\frac{1}{2}(l_b + h_j)\sigma u \sin\phi + (h_b + h_j) f_t u \cos\phi = 0 \Rightarrow f_t = \frac{l_b + h_j}{2(h_b + h_j)} \sigma \tan\phi \tag{2.9}$$

where l_b is the brick length.
Thus, the tensile strength is found by

$$f_t = \min \begin{cases} \dfrac{h_b}{2(h_b + h_j)} f_{tb} \\ \dfrac{l_b + h_j}{2(h_b + h_j)} \sigma \tan \phi \end{cases} \tag{2.10}$$

In order to find the strength of a masonry wall in one-way bending (strip action) it is necessary to define the effective width of the wall. The effective width may be determined by figure 2.5 assuming that the tensile strength parallel to the bed joint is reached in a vertical section through point A. Moment equilibrium about A gives

$$\frac{1}{8}\sigma b^2 = \frac{1}{2} y^2 f_t \Rightarrow b = 2y\sqrt{\frac{f_t}{\sigma}} \quad (b \leq y) \tag{2.11}$$

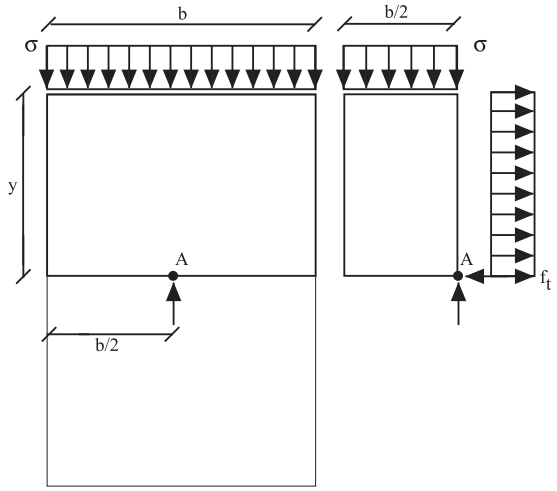

Figure 2.5: *Defining the effective width b of a masonry wall, [1]*

2.6 Local failure mechanisms

The local failure mechanisms are described in this section. In those mechanisms only the brick or the joint in which the anchor is installed is involved in the failure.
In order to predict the failure loads of anchors installed in masonry three different failure mechanisms are considered: the combined brick-cone failure, splitting failure and sliding failure.

The splitting failure governs the failure only in cases where the anchor is arranged near an edge normal to the bed joint. The cases of anchors close to edges parallel to the bed joint and close to corners are only treated experimentally. This limitation is not important since anchors should never be installed near a free edge parallel to the bed joint and thus also not near a corner. For the test results on those arrangements, see chapter 3.

The sliding failure always governs the failure in cases where the anchor is arranged in the joint and also in some cases where the anchor is arranged in the brick.

Firstly, the upper bound expression for the sliding failure is described since this failure is always present in combination with other failure modes.

2.6.1 Sliding failure along a deformed bar

The failure of an anchor in masonry always involves a kind of a local failure, i.e. bond failure. This kind of failure is characterized as a sliding failure along an anchor bar and is fundamental in all local failure mechanisms described. This failure mechanism is described in chapter 9 in [4].

A bar is shown in figure 2.6 where it is assumed to move a distance u_s in the direction of the bar axis and the surrounding material is assumed to move axisymmetrically perpendicular to the bar axis.

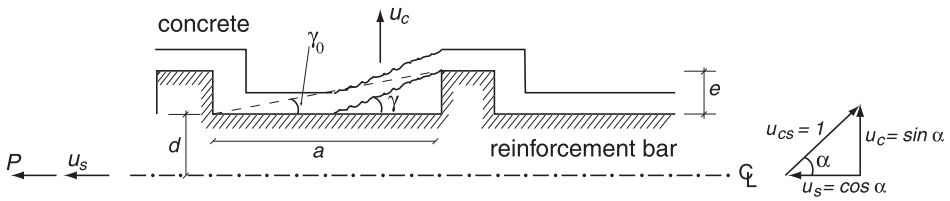

Figure 2.6: *Local failure mechanism, [4]*

The dissipation L along a length l is found by

$$L = \begin{cases} \dfrac{\pi}{2} f_c (d+e) \dfrac{el}{a} \dfrac{1-\sin\phi}{\sin(\alpha-\phi)}, & \gamma = \alpha - \phi \geq \gamma_0 \\ \dfrac{\pi}{2} f_c \Big[d + 2e - \alpha \tan(\alpha-\phi) \Big] l \dfrac{1-\sin\phi}{\cos(\alpha-\phi)}, & 0 \leq \alpha - \phi \leq \gamma_0 \end{cases} \tag{2.12}$$

For d and e, see figure 2.6.
When the upper bound expression for the load-carrying capacity of an anchor in masonry is to be described by means of an arbitrary failure mechanism the dissipation S in the surrounding material must be added to the local dissipation L as well as possible contribution from the transverse reinforcement B. Then the work equation is found assuming that n bars are involved in the failure

$$nP\cos\alpha = nL + S + B \tag{2.13}$$

Normalizing the equation with respect to $n\pi dlf_c$, the bond strength τ per bar is found to be

$$\frac{\tau}{f_c} = \frac{P}{\pi dlf_c} = \frac{L}{\pi dlf_c\cos\alpha} + \frac{S}{n\pi dlf_c\cos\alpha} + \frac{B}{n\pi dlf_c\cos\alpha} \tag{2.14}$$

$\gamma = 0$ gives an upper limit of the dissipation in the local failure mechanism.
As mentioned before experience seems to show, [3], that an upper limit of the bond strength must be introduced. When this limit is reached the dilatation is zero, see figure 2.3. Formally the limit may by found from (2.14) by setting $\gamma = \alpha = \phi = 0$. Without contribution from the surrounding material and from the transverse reinforcement the bond strength of a single anchor becomes

$$\frac{\tau}{f_c} = \frac{P}{\pi dlf_c} = \frac{L}{\pi dlf_c} = \frac{\frac{\pi}{2}f_c[d+2e]l}{\pi dlf_c} = \frac{1}{2} + \frac{e}{d} \Rightarrow P = \frac{1}{2}\nu f_c\pi dl, \quad (d >> e) \tag{2.15}$$

when the effectiveness factor ν is applied to f_c. Normally, ν is defined by the usual form ($\nu = K_n/\sqrt{f_c}$) and in this report an additional definition is also used: $\nu = (K_n/\sqrt{f_c})\sqrt{d/h}$. f_c is the formal compressive strength corresponding to the upper limit of the bond strength of the base material, the interface or the resin. K_n is found by comparison to the tests.

2.6.2 Combined brick-cone failure

The combined brick-cone failure is observed in the tests conducted and some typical brick-cones are shown in figure 2.8. The failure mechanism may be considered as composed of three contributions: the brick-cone failure and sliding failures along the anchor and along the interface between the mortar and the brick, see figure 2.7.

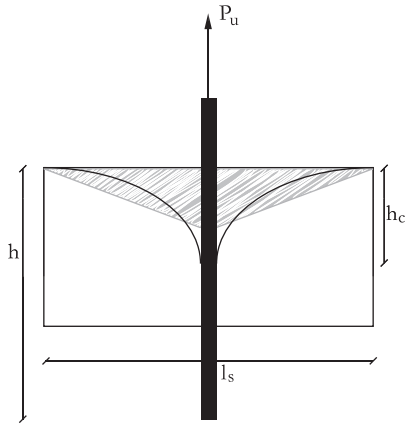

Figure 2.7: *The principle of the combined brick-cone failure*

In order to simplify the upper bound expression the combined brick-cone failure is preliminarily considered as a combination of the brick-cone failure and sliding failure along the anchor, i.e. by analogy of the case of a single bonded anchor in concrete. Finally, the failure is considered as a combination of the combined brick-cone failure and sliding failure along the interface between brick and mortar. The sliding failure at the interface takes place along an area on both bed sides of the brick. The area equals approximately the sliding area defined by the brick-cone generatrix, the length of the brick and the anchor diameter - see hatched area in figure 2.7.

Figure 2.8: *Brick-cone failures typically observed in masonry*

From the typical brick-cone failures shown in figure 2.8 it is easily seen that the failure involves only the brick in which the anchor is installed. The failure in the interface between the brick and the mortar is also obvious from the figure.

Firstly, the combined brick-cone and sliding failure along the anchor is treated. This is done by treating the brick-cone contribution by the theory of punching shear of concrete slabs, [4], and by treating the combined brick-cone and sliding failure along the anchor with the brick-cone height optimization, [3].

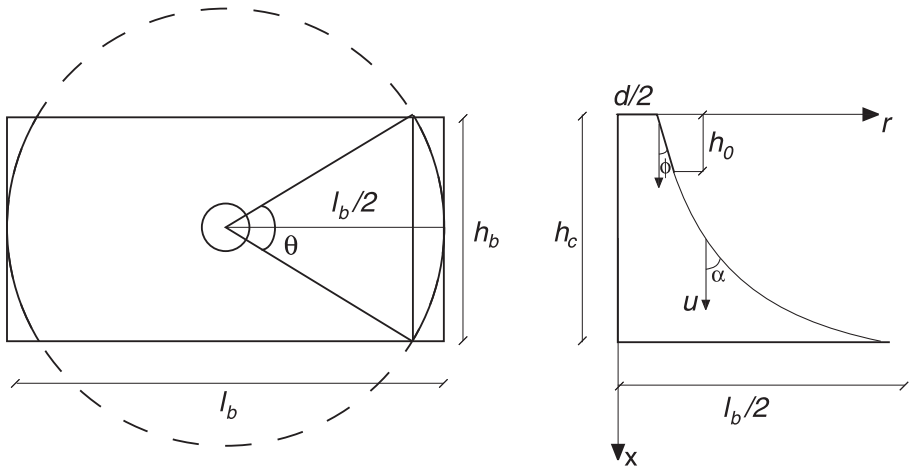

Figure 2.9: *Brick-cone failure modelling*

From the appearance of the shape of the failure surface it is obvious that the shape is close to the cone-like shape but slightly different from the one normally observed in concrete. Even though the shape is different (see Appendix C in [6]) it is treated similarly. Thus, the upper bound value of the failure load is governed by the dissipation in the failure surface, that is the two cone-like failure surfaces on each side of the anchor along the bed joint.

The approach is illustrated in figure 2.9 where the failure surface is described by a generatrix $r(x)$ that is a function composed of a linear[1] and a catenary part

$$r(x) = \begin{cases} \dfrac{d}{2} + x \tan\phi & \text{for } 0 \le x \le h_0 \\ a \cosh \dfrac{x - h_0}{c} + b \sinh \dfrac{x - h_0}{c} & \text{for } h_0 \le x \le h_c \end{cases} \tag{2.16}$$

[1]The linear part is due to the geometrical conditions that can not always be satisfied by the catenary part

and satisfies the geometrical conditions

$$c = \sqrt{a^2 - b^2} \tag{2.17a}$$

$$a = \frac{d}{2} + h_0 \tan\phi \tag{2.17b}$$

$$\tan\phi = \frac{b}{c} \tag{2.17c}$$

$$\frac{l_b}{2} = a\cosh\frac{h_c - h_0}{c} + b\sinh\frac{h_c - h_0}{c} \tag{2.17d}$$

The angular strains are equal to zero, thus the generatrix $r(x)$ may be considered as a yield line in plane strain.

The dissipation is calculated by involving only the arc of length $d/2\theta$, i.e. the arc limited by the radii of length $l_b/2$ making an angle θ with each other. The failure surface extends along the height h_c and the solid part of the circle with diameter l_b drawn left in figure 2.9 that is the limit of the failure surface seen from above.

The dissipation is written by means of eq. (2.3) as

$$dA = r\theta\frac{dx}{\cos\alpha} \Rightarrow D = 2\int_0^{h_c}\frac{1}{2}f_{cb}u(l - m\sin\alpha)r\theta\frac{dx}{\cos\alpha} \tag{2.18}$$

where factor 2 is due to one failure surface on each side of the anchor. Angle θ is

$$\theta = 2\sin^{-1}\left(\frac{h_b}{l_b}\right) \tag{2.19}$$

and f_c is the compressive strength of the brick in which the anchor is installed.

The upper bound expression is written as

$$P_u = \theta f_{cb}\int_0^{h_c}(l - m\sin\alpha)r\frac{dx}{\cos\alpha} \tag{2.20}$$

The linear part P_1 is found by inserting the linear part of $r(x)$ in (2.20) and integrating from 0 to h_0. P_1 is thus found to be (cf. [4])

$$P_1 = \theta f_{cb}\frac{h_0}{2}\frac{(l - m\sin\phi)(h_0\sin\phi + d\cos\phi)}{\cos^2\phi} \tag{2.21}$$

P_2 is the catenary part of the failure mechanism found by inserting the catenary part of $r(x)$ in (2.20) and integrating from h_0 to h_c. P_2 is thus found to be

$$\begin{aligned} P_2 &= \theta f_{cb}\Bigg[\frac{lc}{2}(h_c-h_0)+\frac{l_b}{4}\Bigg[l\Big(b\cosh\frac{h_c-h_0}{c}+a\sinh\frac{h_c-h_0}{c}\Big) \\ &\quad -m\Big(a\cosh\frac{h_c-h_0}{c}+b\sinh\frac{h_c-h_0}{c}\Big)-\frac{a}{2}(lb-ma)\Bigg]\Bigg] \end{aligned} \tag{2.22}$$

The ultimate failure load is the sum of the two parts and is determined by

$$P_{cu} = P_1 + P_2 \tag{2.23}$$

In order to obtain an easy design method the non-dimensional parameter τ/f_{cb} is introduced where $\tau = P/\pi(d+h_c)h_c$ is the nominal shear stress on a cylindrical surface with diameter $d+h_c$ (the control surface as seen in the punching shear capacity of concrete slabs). In figure 2.10 τ/f_{cb} is plotted for several d/h_c and l_b/h_c values. Here, the generatrix $r(x)$ is optimized in accordance to the geometrical conditions (2.17) (standard Danish brick sizes are assumed). Figure 2.10 can also be found by multiplying figure 7.2.4 in [4] by θ/π. This is seen from the comparison of equations (2.21) and (2.22) with the corresponding expressions in [4].
Furthermore it is evident that there is practically no variation of τ/f_{cb} when l_b/h_c becomes large. However, here we are mainly interested in τ/f_{cb} for rather small values of l_b/h_c and d/h_c. Using the $d/h_c = 0.1$ and the smallest value of l_b/h_c that satisfies the geometrical conditions it is seen that $\tau/f_{cb} = 0.02$ may be used as a design value. Thus the upper bound value for the brick-cone failure is approximately equal to

$$P_{cu} = 0.02\nu f_{cb}\pi(d+h_c)h_c \tag{2.24}$$

The combined brick-cone and sliding failure is found by calculating the sliding failure using equation (2.15). The load carried by the sliding failure is then

$$\frac{P}{\pi dl f_{cb}} = \frac{\frac{\pi}{2}f_{cb}[d+2e]l}{\pi dl f_{cb}} = \frac{1}{2}+\frac{e}{d} \Rightarrow P_{su} = \frac{\pi}{2}(h-h_c)d\nu f_{cb}, \quad (d >> e) \tag{2.25}$$

Formula (2.25) implies that we have related the upper limit of the bond strength to the compressive strength of the brick f_{cb} by introducing the effectiveness factor ν.
The sliding occurs along the length $l = h - h_c$ of the anchor and the load carrying capacity for the failure combined by the brick-cone failure and sliding failure along the anchor is found to be

$$P_{\mathrm{comb},u} = 0.02\nu f_{cb}\pi(d+h_c)h_c + \frac{\pi}{2}(h-h_c)d\nu f_{cb} \tag{2.26}$$

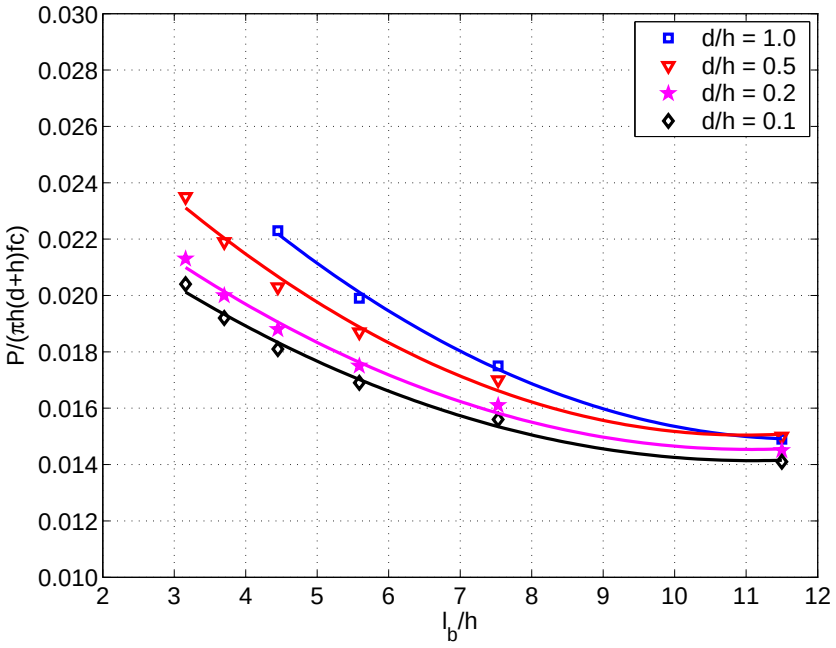

Figure 2.10: *The normalized load-carrying capacity τ/f_c for different d/h and l_b/h ratios. In the figure h_c is named h*

assuming the effectiveness factor on f_{cb} to be the same in the two terms.
The minimum value is found by optimizing (2.26) with respect to h_c

$$\frac{\partial P_{\text{comb},u}}{\partial h_c} = 0 \Rightarrow h_c = 12d \Rightarrow P_{\text{comb},u} = \frac{1}{2} d\nu f_{cb}\pi(h - 5.76d) \tag{2.27}$$

Finally, using the trapezoidal surface along which the sliding failure in the interface between brick and mortar occurs and the fact that the maximum bond strength is $\tau = \frac{1}{2} f_{ci}^{\max}$ where $f_{ci}^{\max}$ is the formal compressive strength corresponding to the upper limit of the bond strength in the interface the upper bound expression for the combined brick-cone failure is found to be

$$P_u = \frac{1}{2}\nu f_{cb} d\pi(h - 5.76d) + \nu_2 f_{ci}(l_b + d)12d \tag{2.28}$$

The maximum bond strength is introduced due to experience, [3], and in this stage no dilatation occurs - see figure 2.3.
Since the upper limit $f_{ci}^{\max}$ is not yet known the effective strength has been related to the formal interface compressive strength f_{ci} through the effectiveness factor ν_2.
Thus, ν_2 covers both the conversion from f_{ci} to $f_{ci}^{\max}$ and an effectiveness factor on $f_{ci}^{\max}$.
ν is the effectiveness factor applied to the brick strength f_{cb}. The factors are defined by

analogy of the effectiveness factors usually suggested in concrete (dependence on the square root of the compressive strength of concrete), [4], with the addition of the embedment depth dependence defined by $\sqrt{d/h}$ (introduced in the anchorage theory - the bond strength of reinforcement bars, [4]). Thus, the factors are defined

$$\nu = \frac{K_1}{\sqrt{f_{cb}}}\sqrt{\frac{d}{h}}, \qquad \nu_2 = \frac{K_2}{\sqrt{f_{ci}}}\sqrt{\frac{d}{h}} \tag{2.29}$$

For the determination of K_1 and K_2 on basis of the pull-out tests see chapter 4.
The formula (2.28) implies that the sliding along the interface is supposed not to change the parameters governing the failure geometry.

2.6.3 The splitting failure

The splitting failure mechanism is similar to the face splitting mechanism in the case of bonded anchors in concrete, [4]. This kind of failure occurs only when the anchor is close to an edge normal to the bed joint where dilatation may take place without much resistance. In the tests the failures are recognized as splitting of either the brick in which the anchor is installed or the splitting of the same brick together with one of the neighbouring bricks (including the joints, see figure 2.11). Since both of these failures eventually will result in the same upper bound value they are treated equally considering the first one only to be a special case of the last one. Thus, in order to simplify the calculations one upper bound expression is found.

Figure 2.11: *Typical splitting failures in masonry*

The upper bound expression for the splitting failure is written in analogy to the expression valid for the face splitting in concrete, thus the expression for a number of bars $n = 1$ becomes, [4]

$$\frac{\tau}{f_{cb}} = \frac{P_u}{f_{cb}\pi dh} = \min \begin{cases} 0.12\nu + 0.89\left(\frac{b}{d} - 1\right)\rho \\ \\ 0.28\nu + 0.48\left(\frac{b}{d} - 1\right)\rho \end{cases} \tag{2.30}$$

b being the width of the brick and d the anchor diameter. These expressions are only valid if the dissipation in the surroundings can be neglected, since in (2.30) the only contribution is from the brick (i.e. the sliding failure in the interface between the brick and mortar is neglected).
The effectiveness factors ν and ρ introduced in equation (2.30) are defined by analogy of the case of bonded anchors in concrete, [4]. By setting the tensile strength of the brick $f_{tb} = 1/20 f_{cb}$ as reported in [5], we get

$$\begin{aligned} \nu &= \frac{K_1}{\sqrt{f_{cb}}} \\ \rho &= \frac{\nu_t f_{tb}}{f_{cb}} = \frac{K_2}{20}\sqrt{\frac{d}{h}} \end{aligned} \tag{2.31}$$

For the determination of K_1 and K_2, see chapter 4.

2.7 Global failure mechanisms

The global failure mechanisms are applied to arrangements where most of or the whole of the wall is involved in the failure. The mechanisms are described in the following.

2.7.1 Wall strip bending failure

The global strength of masonry may be determined by the wall strip bending failure, shown in figure 2.12, [1].
The wall may be supported both at the top and bottom and along an additional vertical support. The latter case may be due to a cross wall. In the vertical support a vertical displacement may occur but it will sometimes be prevented for instance due to the wall being bricklayed with the neighbouring wall. Thus, this case is treated both with and without a free vertical displacement of the support. In both cases the bending tensile strength is set to zero.

The prediction of the load-carrying capacity is carried out by using an effective width of the wall t_{eff} that is found by subtracting the compression zone depth y_0 from the actual thickness t. Thus, t_{eff} is found to be

$$y_0 = \frac{\sigma}{f_c} t \Rightarrow t_{\text{eff}} = t\Big(1 - \frac{\sigma}{f_c}\Big) \tag{2.32}$$

Firstly, the wall strip supported only at the top and bottom is considered, as shown in figure 2.12. The load-carrying capacity P_u is found by the work equation in which the dissipation is zero due to the bending tensile strength being zero. The external work W_{ext} is found by the contributions from P, q and σbt as well as from G_1 and G_2 that are the weights of the wall strips.
The external work for $x \geq \eta$ is found to be

$$W_{\text{ext}} = P\frac{\eta}{x}\delta - \sigma btu - G_2\Big(u_1 + \frac{1}{2}u_2\Big) - \frac{1}{2}G_1 u_1 + \frac{1}{2}qbh\delta \tag{2.33}$$

where u,u_1 and u_2 are defined by the geometrical conditions obvious from figure 2.12. Thus

$$u_1 = \frac{t_{\text{eff}}}{x}\delta, \quad u_2 = \frac{t_{\text{eff}}}{h-x}\delta, \quad u = \frac{1}{2}u_2 + u_1 \tag{2.34}$$

Equalizing the external work form eq. (2.33) to zero dissipation and utilizing the definitions of the deflections u,u_1 and u_2 an upper bound expression for P is found

$$P_u = \frac{x}{\eta}\left[\sigma bt\Big(\frac{t_{\text{eff}}}{x} + \frac{1}{2}\frac{t_{\text{eff}}}{h-x}\Big) + G_2\Big(\frac{t_{\text{eff}}}{x} + \frac{1}{2}\frac{t_{\text{eff}}}{h-x}\Big) + \frac{1}{2}G_1\frac{t_{\text{eff}}}{x} - \frac{1}{2}qbh\right] \tag{2.35}$$

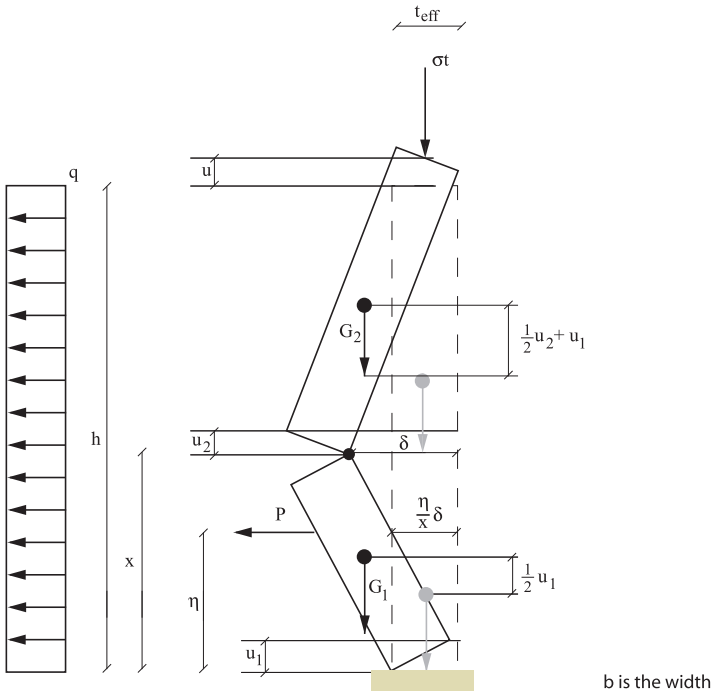

Figure 2.12: *The wall strip bending failure mechanism, [1]*

Notice that the work of the normal stress σ at the top of the wall has been calculated for a uniform stress distribution. If it can be assumed that the total force per unit length σt moves to the corner with the larger vertical displacement the work will be greater.
In the case of $x < \eta$ the definition of the displacements u,u_1 and u_2 remains the same. Only the work done by the pull-out force P changes, thus in this case the upper bound expression becomes

$$P_u = \frac{h-\eta}{h-x}\left[\sigma bt\left(\frac{t_{\text{eff}}}{x} + \frac{1}{2}\frac{t_{\text{eff}}}{h-x}\right) + G_2\left(\frac{t_{\text{eff}}}{x} + \frac{1}{2}\frac{t_{\text{eff}}}{h-x}\right) + \frac{1}{2}G_1\frac{t_{\text{eff}}}{x} - \frac{1}{2}qbh\right] \tag{2.36}$$

The addition of a vertical support produces additional skew yield lines. A possible failure mechanism is shown in figure 2.13.
The external forces are the same as in the previous failure mechanism shown in figure 2.12. The displacements are determined for the rotation axes of the different slab parts lying in a face of the slab. The dissipations in the skew yield lines as well as in the horizontal yield line are neglected here. While the dissipation in the horizontal yield line should always be neglected the contributions from the skew yield lines might be included.
The external work is the work done by external forces P, q and σbt and the weights of the different wall parts shown in figure 2.13.
By analogy of the previous approach the external work for $x \geq \eta$ is found to be

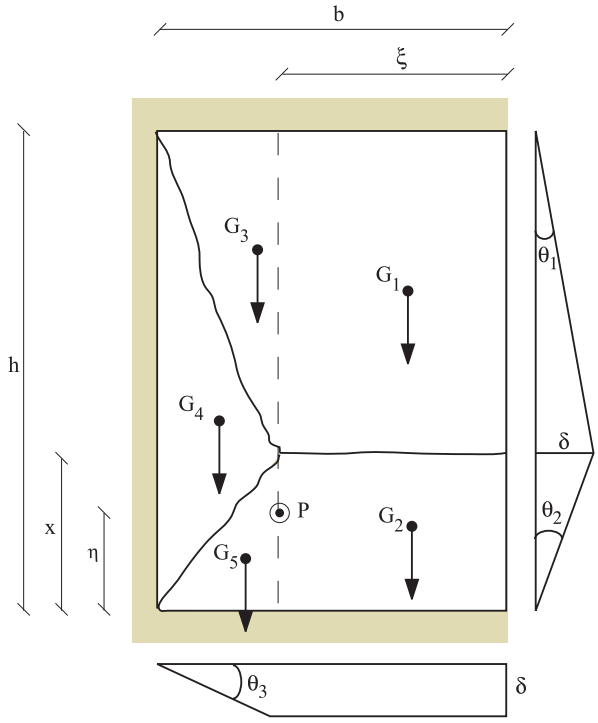

Figure 2.13: *The wall strip bending failure mechanism with an additional vertical support, [1]*

$$\begin{aligned} W_{\text{ext}} = \quad & q\delta\Big(\frac{1}{3}bh + \frac{1}{6}h\xi\Big) - \sigma t b t_{\text{eff}}\Big(\frac{1}{2}\theta_1 + \theta_2\Big) + P\frac{\eta}{x}\delta \\ & -\Big((G_1 + G_3)\Big(\frac{1}{2}\theta_1 + \theta_2\Big)t_{\text{eff}} + \frac{1}{2}(G_2 + G_5)\theta_2 t_{\text{eff}} + G_4\theta_2 t_{\text{eff}}\Big) \end{aligned} \tag{2.37}$$

The rotations θ_1 and θ_2 expressed by the displacement δ in figure 2.13 are

$$\theta_1 = \frac{\delta}{h-x}, \quad \theta_2 = \frac{\delta}{x} \tag{2.38}$$

Using the equations (2.37) and (2.38) an upper bound expression for P is found to be

$$\begin{aligned} P_u = \quad & \frac{x}{\eta}\Big[- q\Big(\frac{1}{3}bh + \frac{1}{6}h\xi\Big) + \sigma t b\Big(\frac{1}{2}\frac{t_{\text{eff}}}{h-x} + \frac{t_{\text{eff}}}{x}\Big) \\ & +(G_1 + G_3)\Big(\frac{1}{2}\frac{t_{\text{eff}}}{h-x} + \frac{t_{\text{eff}}}{x}\Big) + \frac{1}{2}(G_2 + G_5)\frac{t_{\text{eff}}}{x} + G_4\frac{t_{\text{eff}}}{x}\Big] \end{aligned} \tag{2.39}$$

In the case of $x < \eta$ only the work of pull-out force P changes and this gives by analogy of the previous approach the upper bound expression for this case

$$P_u = \frac{h-\eta}{h-x}\Big[-q\delta\Big(\frac{1}{3}bh+\frac{1}{6}h\xi\Big)+\sigma tb\Big(\frac{1}{2}\frac{t_{\text{eff}}}{h-x}+\frac{t_{\text{eff}}}{x}\Big) \\ +(G_1+G_3)\Big(\frac{1}{2}\frac{t_{\text{eff}}}{h-x}+\frac{t_{\text{eff}}}{x}\Big)+\frac{1}{2}(G_2+G_5)\frac{t_{\text{eff}}}{x}+G_4\frac{t_{\text{eff}}}{x}\Big] \tag{2.40}$$

In figure 2.14 the upper bound expressions defined in (2.35),(2.36), (2.39) and (2.40) are compared. It is evident that the gain in the load-carrying capacity introduced by an additional vertical support with free vertical displacement when the dissipation in the skew yield lines is neglected is small, $\Delta P_u = 1.01$ kN. The optimum value of the load-carrying capacity is achieved for $x \cong \eta$. Data from table 2.1 are used in the comparison presented in the figure - for the notation see the list of symbols at the end of the report.

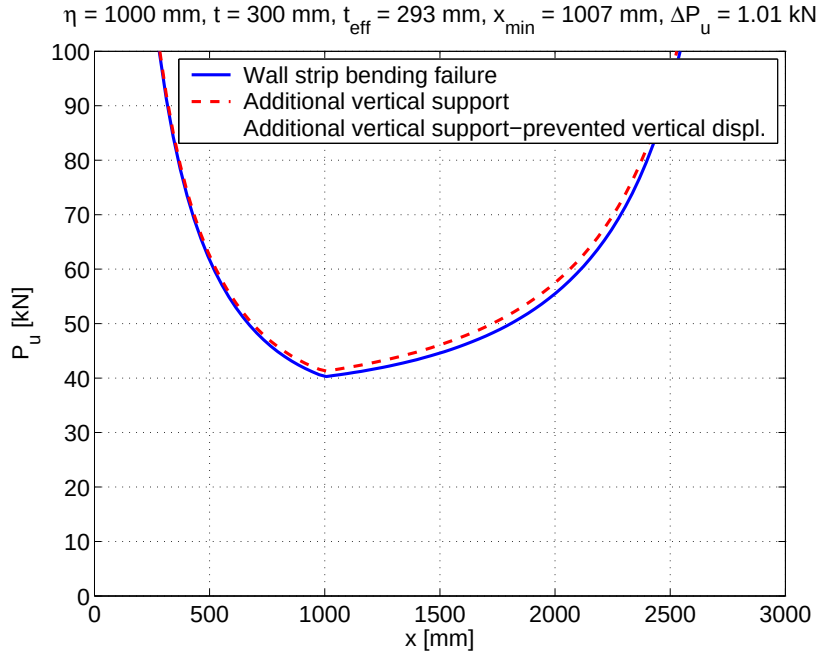

Figure 2.14: *The load-carrying capacity vs. the positions of the force P for two cases : simple wall strip bending failure and failure of wall with an additional vertical support, [1]*

σ	f_c	t	l_b	h_b	b_b	h_j	q	d
0.10	4.0	300	228	56	108	12	1.0	20
[MPa]	[MPa]	[mm]	[mm]	[mm]	[mm]	[mm]	[kN/m^2]	[mm]
ρ	h	b	η	ξ	t_{eff}	l		
15	3000	3000	1000	1500	292.50	150		
[kN/m^3]	[mm]	[mm]	[mm]	[mm]	[mm]	[mm]		

(l is the embedment depth)

Table 2.1: *Data used for the comparison in figure 2.14, [1]*

Finally, it remains to investigate the influence of the vertical support where the vertical displacement is prevented. If the failure mechanism, shown in figure 2.13, is activated and the vertical displacement of the support is prevented a shear failure through the bricks is required for the mechanism to occur.

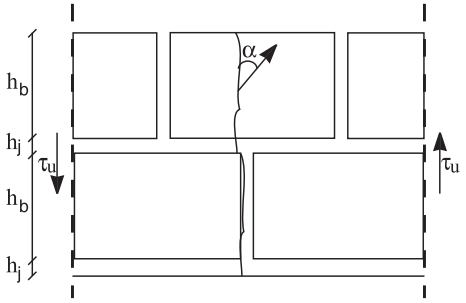

Figure 2.15: *The vertical failure of a single brick - the unit cell, [1]*

The treatment of the shear failure is simple, see figure 2.15 where the unit cell is shown. In the figure, a unit cell of a facing bond is shown with a vertical yield line.
The dissipation in the yield line is found by the dissipation formula for a modified Coulomb material, i.e. eq. (2.3), thus the case of plane strain is assumed. This implies that the angle between the displacement vector and the yield line is larger than the angle of friction for the interface between the brick and mortar and the brick, respectively. The angle of friction is here set to $\phi = 30^o$. Because the cross joints can not be assumed to be properly filled with mortar their contribution to the load-carrying capacity is neglected.

The dissipation per unit cell is formulated as

$$W_{\text{int}} = \frac{1}{2} f_{cb}(l - m\sin\alpha) h_b u b \tag{2.41}$$

where l and m are defined in eq. (2.4) and b is the width. The external work is (see figure 2.15)

$$W_{\text{ext}} = 2\tau_u \cos(\alpha)(h_b + h_j) u b \tag{2.42}$$

By means of the work equation τ_u is found to be

$$\tau_u = \frac{1}{4} \frac{h_b}{h_b + h_j} f_{cb} \frac{l - m\sin\alpha}{\cos\alpha} \tag{2.43}$$

The optimal value of α is found by the non-trivial solution to $\frac{\partial \tau_u}{\partial \alpha} = 0$. Thus,

t_{eff}	l_b	h_b	b_b	h_f	f_{cb}	ϕ	l	m	α
292.5	228	56	108	12	15	30	0.9	0.8	62.7
[mm]	[mm]	[mm]	[mm]	[mm]	[MPa]	[Deg.]	-	-	[Deg.]

Table 2.2: *Data used for the calculation of the additional part of the dissipation for the failure mechanism in figure 2.13, [1]*

$$\frac{\partial \tau_u}{\partial \alpha} = \frac{1}{4} f_{cb} \frac{h_b}{h_b + h_j} \frac{l \sin\alpha - m}{\cos^2 \alpha} = 0 \Rightarrow \alpha = \sin^{-1}\left(\frac{m}{l}\right), \quad (\alpha \geq \phi) \tag{2.44}$$

The shear failure through the bricks (when the vertical displacement of the additional support is prevented) governs the additional part of the dissipation. Thus, the additional dissipation is found by using

$$\Delta W_{\text{int}} = \tau_u A \frac{\delta}{x} t_{\text{eff}} \tag{2.45}$$

where A is the total sectional area of the yield line and $\frac{\delta}{x} t_{\text{eff}}$ is the vertical displacement defined by the failure mechanism from figure 2.13.

The additional part of the dissipation shown in (2.45) may be calculated by using the data from table 2.2 ($x = \eta$). The increase in the load-carrying capacity is found by first finding τ_u

$$\tau_u = \frac{1}{4} 15 \frac{56}{56 + 12} \frac{0.9 - 0.8 \sin(62.7^o)}{\cos(62.7^o)} = 1.27 \text{ MPa} \tag{2.46}$$

Subsequently, ΔW is found from eq. (2.45). Thus the increase in the load-carrying capacity when the shear failure in the bricks is introduced is found to be

$$\Delta W_{\text{int}} = 1.27 \cdot \frac{3000 \cdot 108 \cdot 292.5}{1000} = 120.7 \text{ kN} \tag{2.47}$$

Here, δ is neglected because in the work equations it vanishes.
The increase in the load-carrying capacity for other values of x is illustrated in figure 2.16. However, it should be kept in mind that the increase in the load-carrying capacity may in reality be smaller since an effectiveness factor needs to be applied on the compressive strength of the brick f_{cb} used in the upper bound expression for τ_u, eq. (2.43).
In such case it may be suggested to use the effectiveness factor ν_b used when calculating the compressive strength of a masonry wall from eq. (2.7). Then τ_u is found to be

$$\tau_u = \frac{1}{4} \frac{h_b}{h_b + h_j} \nu_b f_{cb} \frac{l - m \sin\alpha}{\cos\alpha} \tag{2.48}$$

where ν_b is found to be

$$\nu_b = 0.34 \cdot 15^{0.34} = 0.85 \tag{2.49}$$

thus, the increase is reduced by 15 %.

It is evident that the calculated increase in the load-carrying capacity is different from the one calculated in [1] (33.1 kN). This is due to a calculation error in [1].
It should be kept in mind that the upper bound expression found in (2.43) only applies to a masonry wall with the facing bond (figure 2.15) and the calculations are carried out for a half-brick wall. In the case of other types of bond a new upper bound expression should be established on basis of the unit cell of the actual bond.

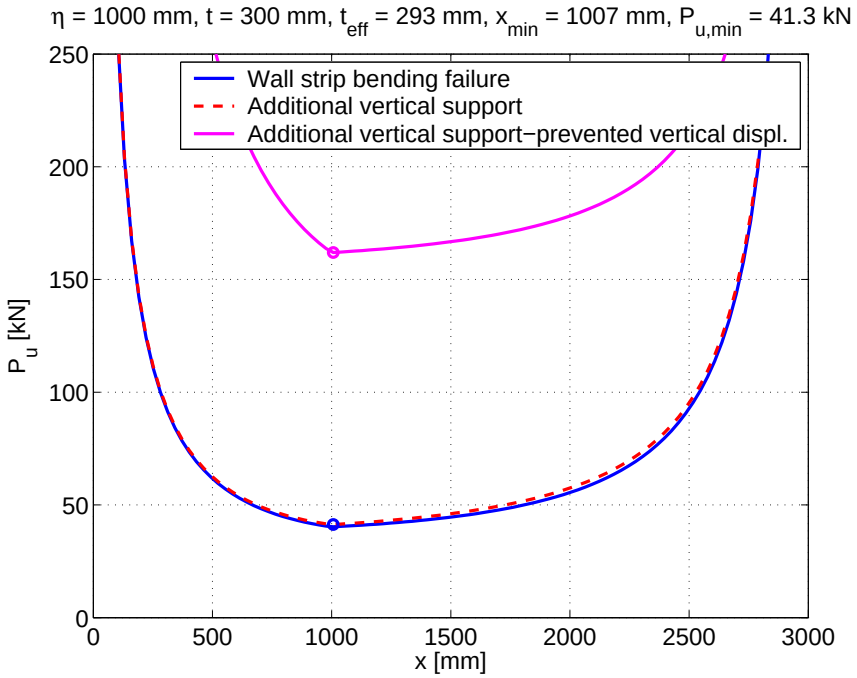

Figure 2.16: *The load-carrying capacity vs. the arrangements of force P for three cases : simple wall strip bending failure, wall with an additional vertical support with free and prevented vertical displacement*

2.7.2 Punching shear failure

The load-carrying capacity of a single anchor in concrete is successfully treated by the theory of punching shear of slabs in [3]. In [1], the punching shear mechanism is stated as the possible failure mechanism for a single anchor in masonry too.
In the tests reported in [6] and the recent ones, given in Appendix A, there was no evidence of punching shear failure. However, this failure mechanisms still needs to be considered when designing the anchors in masonry especially in cases of anchors installed by use of an anchor plate.

As explained in [1], the application of the punching shear analogy to anchors in masonry is the same as the one in concrete. Thus, the developed simple form of the upper bound expression for the concrete-cone failure is applied to masonry substituting the compressive strength of concrete with the compressive strength of masonry. The upper bound expression for the load-carrying capacity P_u is thus found by introducing the shear stress τ which is the nominal shear stress along a control surface defined by the circumference around the anchor in a radius of half the embedment depth, see figure 2.17.

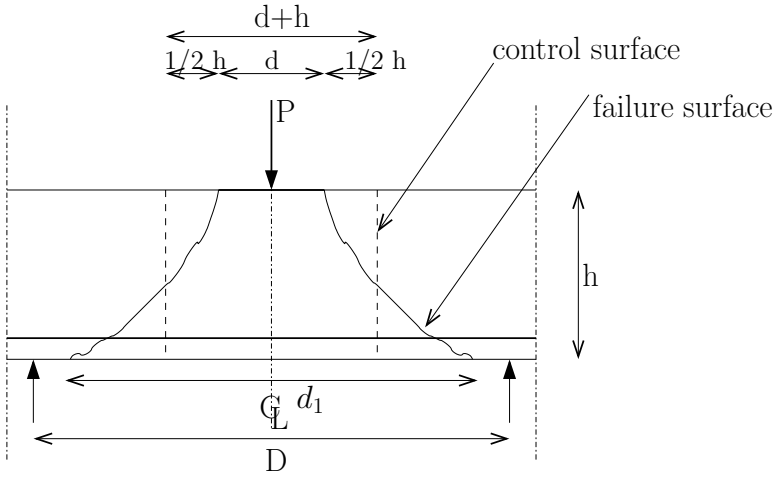

Figure 2.17: *Punching shear in a reinforced concrete slab, [4]. Applied to masonry in the present section*

P_u is found to be

$$P_u = \pi(d+h)h\tau, \quad \tau = 0.08\nu f_c, \quad (f_c \text{ in MPa}) \tag{2.50}$$

where

- d is the anchor diameter
- h is the embedment depth of the anchor

- f_c is the compressive strength of masonry

and ν is the effectiveness factor applied to the compressive strength of masonry assumed to be of the usual form used in concrete. Thus,

$$\nu = \frac{K_1}{\sqrt{fc}}, \quad (f_c \text{ in MPa}) \tag{2.51}$$

In [1], as a result of the comparison to the tests, K_1 is suggested a value of 3.82.

2.7.3 Sliding failure at an edge

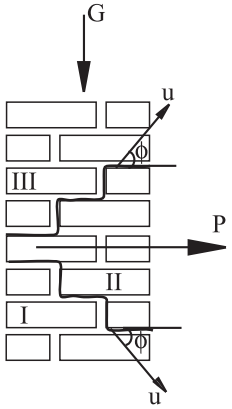

Figure 2.18: *Sliding failure at an edge, [1]*

Another global failure mechanism is sliding failure at an edge. The anchor arrangement is shown in figure 2.18 together with the failure mechanism.
The upper bound expression is determined by the external work since the dissipation is set to zero.
The part I has displacement zero while the part III is subjected to vertical displacements only. The mutual displacement between the parts u is assumed to make an angle equal to the angle of friction ϕ with the line of discontinuity.

The external work is formulated as usual

$$W_{\text{ext}} = u(P\cos\phi - 2G\sin\phi) \tag{2.52}$$

Setting the dissipation to zero P_u is found from (2.52) to

$$P_u = 2G\tan\phi \tag{2.53}$$

where G is the vertical load originating from the forces including the weight of the structure above.

2.8 Final remarks

It is seen that the theory of plasticity provides some important formulas for the prediction of the ultimate load for anchors in masonry.
In order to achieve an easy and simple design procedure the new expression for the combined brick-cone failure is formulated using a rather simple approach (by analogy of the punching shear problem in concrete). This involves the use of a cylindrical surface (control surface) with a radius of half the embedment depth around the anchor. In practice, this may for larger embedment depths extend beyond the brick surface involving the neighboring bricks and joints. Since the theoretical approach disregards this fact this should also be done in the design situation still of course using the strength of the single brick in which the anchor is installed.
Furthermore, a rather rough estimate of the upper limit of the bond strength of the interface between the brick and mortar is made. The strength is related to the formal compressive strength f_{ci} through an effectiveness factor ν_2.

When predicting the strength of an anchor in masonry by means of the upper bound theorem of the theory of plasticity the most dangerous mechanism needs to be found. This is illustrated by the comparisons made in figure 2.19 where the load-carrying capacity of an anchor in masonry is found by means of the investigated failure mechanisms. The data from tables 2.1 and 2.2 are used and the normal pressure on the top of the wall (σ) is varied.
It is evident that the combined brick-cone failure governs the failure for almost any σ applied. However, here f_{ci} is set to zero and thus in the case of large f_{ci} the sliding failure mechanism may govern the failure. For very small σ the sliding failure at an edge is the critical failure mode though with a reminder on the fact that this kind of failure is dependent on the arrangement (i.e. the failure occurs only for anchors installed near an edge).

Since the comparison shown in figure 2.19 is only valid for the data from tables 2.1 and 2.2 it is natural to show the effect of some other values. In figure 2.20 the data are slightly changed: the compressive strength of the brick f_{cb} is changed to 21.1 MPa and the compressive strength of masonry f_c is changed to 7.5 MPa. Finally the anchor embedment depth is changed to $h = 230$ mm - this corresponds to the masonry walls used in the tests.
It is then seen that the wall strip bending failure governs the failure, thus the local failure modes, the combined brick-cone failure and the sliding failure no longer predict the lowest failure loads. The sliding failure at an edge appears to govern the failure for almost no σ but again with the reminder on the fact that this failure is dependent on the arrangement.
It is obvious from the above that all the possible failure mechanisms need to be checked when designing anchors in masonry since in some cases global failure mechanisms are likely to govern the failure. This is also supported by the fact that the determination of the upper bound expressions is done in conjunction with pull-outs with no pre-compression of the walls (i.e. $\sigma = 0$). Thus, it is reasonable to expect the local failure loads to be higher in reality for which reason some global failure loads might govern the failure.

Finally, it should be noted that the sliding failure applied in the comparisons mentioned

above is the sliding failure along the anchor installed in a brick. If the anchor is installed in a joint the load carrying capacity is expected to be much lower due to a usually lower compressive strength of mortar. Since the failure loads are low it is not recommended to install anchors in joints.
In the comparison shown in figure 2.20 a formal compressive strength $f_{ci} = 2.71$ MPa is used. In the comparison in figure 2.19 the cohesion is set to zero and consequently the same is f_{ci}. The comparisons shown in figures 2.19 and 2.20 are based on the effectiveness factors defined in chapter 4.

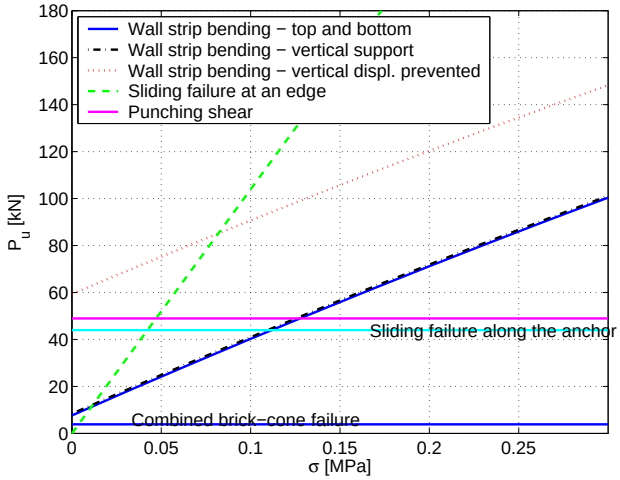

Figure 2.19: *Failure loads in relation to the normal pressure σ on top of the wall using the different failure mechanisms - data from tables 2.1 and 2.2*

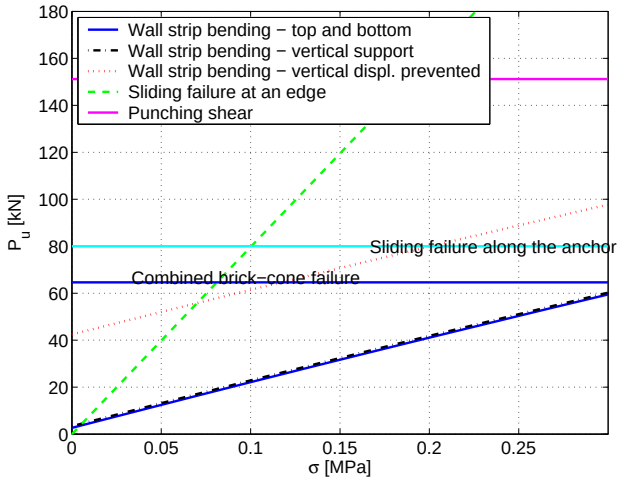

Figure 2.20: *Failure loads in relation to the normal pressure σ on top of the wall using the different failure mechanisms - data from tables 2.1 and 2.2 with different strengths of masonry and bricks, different wall thickness and anchor embedment depth*

3 Test results

In this chapter the test results are described.
The test results are due to pull-outs that involve cases of anchors arranged near edges and corners as well as those arranged far from edges and corners, see Appendix A.
Also, the test results of the pull-outs of anchors arranged far from edges and corners carried out in [6] are shortly described. For more information on those, see [6], Appendix D.

The test results contain cases of a single anchor far from edges and corners with the maximum embedment depth. Maximum embedment depth of anchors of size M16 is the wall thickness, $h = 230$ mm, and for anchors of size M12 it is $h = 185$ mm (maximum drill length). The test results achieved in [6] contain cases of anchors in stretcher and header side of a brick as well as those arranged in joints. The embedment depth is varied as well as the anchor diameter for all the arrangements tested.
The arrangements of the tests carried out are shown in figure 3.1. The figure shows the principle of the anchor edge arrangement (parallel and normal to the bed joint) and corner arrangement. The arrangement of anchors far from edges and corners is randomly chosen in the interior of the wall with no edge and corner influence, i.e. the edge and corner distance is chosen greater than 150 mm which is the minimum distance prescribed by Hilti, [7].

The test results are presented in tables 3.3, 3.4 and 3.5 where the failure loads and the failure modes are described. The graphs showing the relation between the failure loads and the embedment depth are supplemented with the so-called normal probability assessment plots, i.e. the plots where it is graphically assessed whether the data (test results) may come from a normal distribution.

The nomenclature used in the description of the failure loads observed is

- SF - sliding failure (e.g. see figures A.85, A.95 and A.105)
- SPF - splitting failure of the brick or of the wall (edge arrangement) (e.g. see figures A.133 and A.137)
- BPU - brick pull-out failure (e.g. see figures A.47, A.57 and A.143)
- BCF - combined brick-cone failure (e.g. see figures A.31 and A.35)
- CF - corner failure of the masonry wall (e.g. see figures A.109, A.111 and A.121)
- CBF - cover bending failure of the masonry wall (e.g. see figures A.139, A.141 and A.145)

The pull-out tests are carried out using masonry walls with mean compressive strength of 7.5 MPa layed with bricks with the mean compressive strength of 21.1 MPa. The strengths of the masonry walls and bricks are found by means of compressive strength testing. The test results are shown in tables 3.1 and 3.2, respectively.

no	1	2	3	4	5	6
f_c	8.1	6.6	7.6	7.7	8.1	6.9

$f_{c,m} = 7.5$ MPa

Table 3.1: *The compressive strength of masonry walls, [MPa]*

no :	1	2	3	4	5	6	7	8	8	9	10
f_{cb}	20.7	21.0	19.1	20.8	21.2	19.6	21.9	22.3	19.2	22.9	19.7

no :	12	13	14	15	16
f_{cb}	20.2	22.7	20.8	20.1	21.1

$f_{c,m} = 21.1$ MPa

Table 3.2: *The compressive strength of bricks, [MPa]*

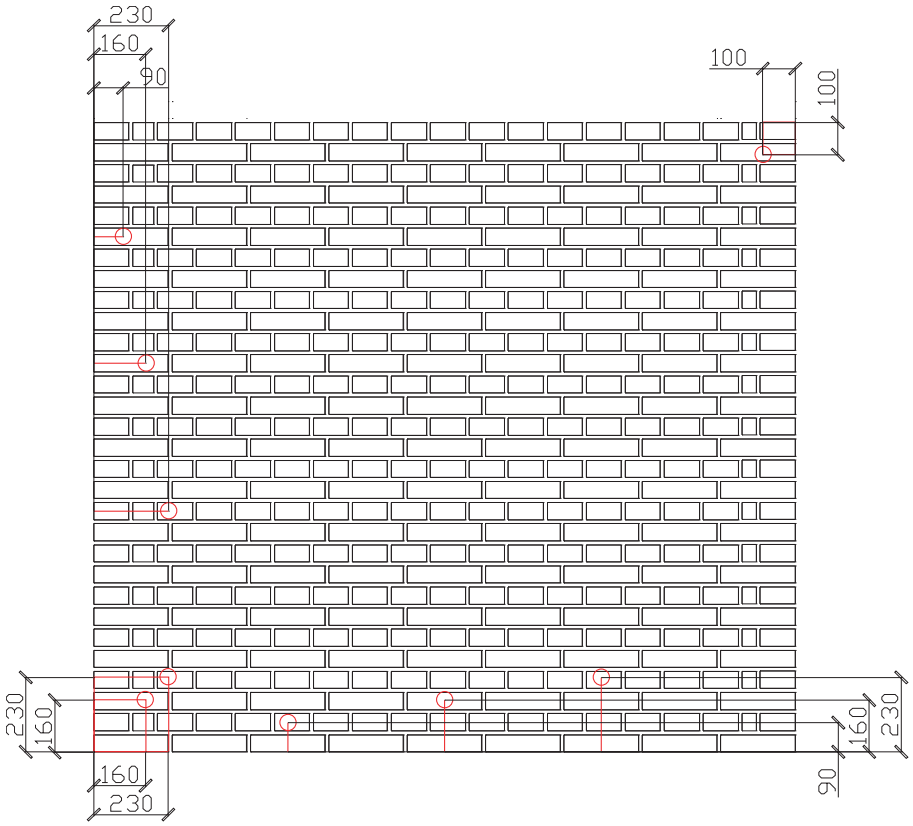

Figure 3.1: *The anchor arrangement. It should be noticed that in spite of what is shown in the figure the anchors are always arranged in the mid point of the brick*

3.1 Far from edges and corners

3.1.1 Header arrangements

The testing of the header arrangements, table 3.3, shows no clear dependency of the anchor size on the load-carrying capacity - see also figure 3.3 (failure loads at the maximum embedment depth are plotted as the mean values).
The tendency of increasing load-carrying capacity for increasing embedment depth is recognized for anchors of size $d = 12$ mm, though only for embedment depths up to 140 mm. The increasing load-carrying capacity for embedment depths higher than 140 mm should, however, not be excluded since the failure mode of this particular arrangement at the embedment dept of 160 mm is the brick pull-out that most likely originates from bad laying of the masonry. In a recently conducted pull-out at the embedment depth of 185 mm the mean failure load increases in relation to that of embedment depth of 160 mm, though it is still lower than that of 140 mm depth.
The tendency of increasing load-carrying capacity for increasing embedment depth is clearly recognized for anchors of size $d = 16$ and 10 mm though the failure load of the 160 mm embedment depth arrangement is not in favor of the claimed tendency for neither of the anchor sizes.
From table 3.3 it is evident that failures of anchors arranged in the header side of a brick is the brick pull-out failure that in most cases is combined with a sliding failure along the anchor. In the table, h is the embedment depth and h^* is the height of the brick pull-out, i.e. the sliding failure along the anchor occurs along the length $h - h^*$. This is illustrated in figure 3.2.

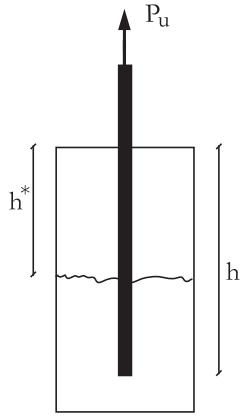

Figure 3.2: *The principle of the brick pull-out failure*

	d = 10 mm								
h [mm]	90	100	110	120	130	140	150	160	170
h^* [mm]	90	60	20	100	90	60	100	0	85
f.m.	SF	BPU+ SF	BPU+ SF	BPU+ SF	BPU+ SF	BPU+ SF	BPU+ SF	SF	BPU+ SF
P_u [kN]	11.8	26.7	28.6	26.6	23.9	39.1	32.1	42.7	45.7

	d = 12 mm				
h [mm]	100	120	140	160	185
h^* [mm]	80	55	55	160	1. 155 2. 0 3. 55
f.m.	BPU+ SF	BPU+ SF	BPU+ SF	BPU	BPU+ SF (2. only SF)
P_u [kN]	27.2	29.6	38.8	15.2	1. 28.3 2. 36.3 3. 35.9

	d = 16 mm				
h [mm]	100	120	140	160	230
h^* [mm]	100	120	-	160	1. 120 2. 80 3. 120
f.m.	BPU	BPU	SPF	BPU	BPU+SF
P_u [kN]	17.1	25.4	45.2	28.6	1. 40.5 2. 73.4 3. 55.7

Table 3.3: *Test results for the header arrangements (f.m. is the failure mode) [6]*

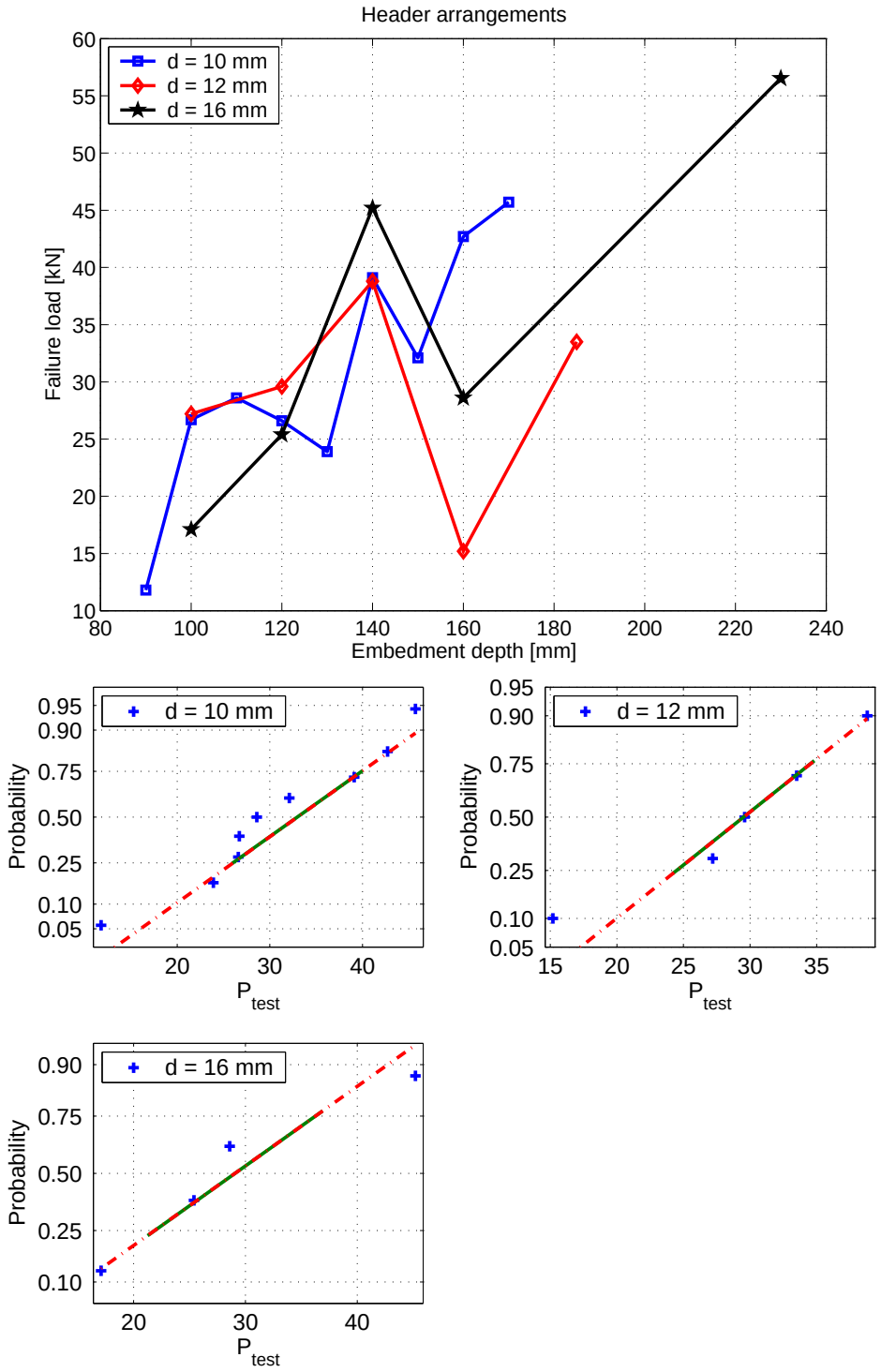

Figure 3.3: *Failure loads for anchors arranged in the header side of a brick against the embedment depth, ([6] - see table 3.3) and the normal probability assessment of the test results*

3.1.2 Stretcher arrangements

From table 3.4 it is evident that the failure of anchors of size $d = 16$ mm arranged in the stretcher side of a brick is governed by the combined brick-cone failure. This kind of failure is also seen for anchor of size $d = 12$ mm though the sliding failure and the brick pull-out failure normally seem to govern the failure of anchors of sizes $d = 10$ and 12 mm.
The failure loads listed in table 3.4 are shown in figure 3.4.
It is seen that tendency of increasing load-carrying capacity for increasing embedment depth is recognized for all anchor sizes though a drop in the capacity is observed at the embedment depth of 140 mm. The drop of the load carrying capacity of an anchor of size $d = 16$ mm at the maximum embedment depth is surprising but the explanation is most likely to be found in the different failure modes that govern the capacity at the maximum embedment depth (see last column in table 3.4 for $d = 16$ mm).
Also, it is evident that the anchors of size $d = 10$ mm exhibit higher failure loads than those of size $d = 12$ mm, which is in contrary to the expectations. This is most likely due to the high deviation of the test result and the fact that anchors of size $d = 10$ and 12 mm have rather close dimensions in comparison with anchors of size $d = 16$ mm.

	d = 10 mm				
h [mm]	100	120	140	160	
h^* [mm]				55	
P_u [kN]	21.8/SF	34.2/SF	22.3/SF	37.8/BPU+SF	
	d = 12 mm				
h [mm]	100	120	140	160	185
h^* [mm]	55				100 (3.)
P_u [kN]	18.2/BPU+SF	21.6/SF	11.6/SF	27.6/BCF	1. 35.8/BCF 2. 41.7/BCF 3. 34.0/BPU+SF
	d = 16 mm				
h [mm]	100	120	140	160	230
h^* [mm]					100 (2. and 3.)
P_u [kN]	42.3/BCF	58.3/BCF	52.9/BCF	63.9/SF	1. 63.1/SF 2. 36.8/BPU+SF 3. 33.7/BPU+SF

Table 3.4: *Test results for the stretcher arrangements*

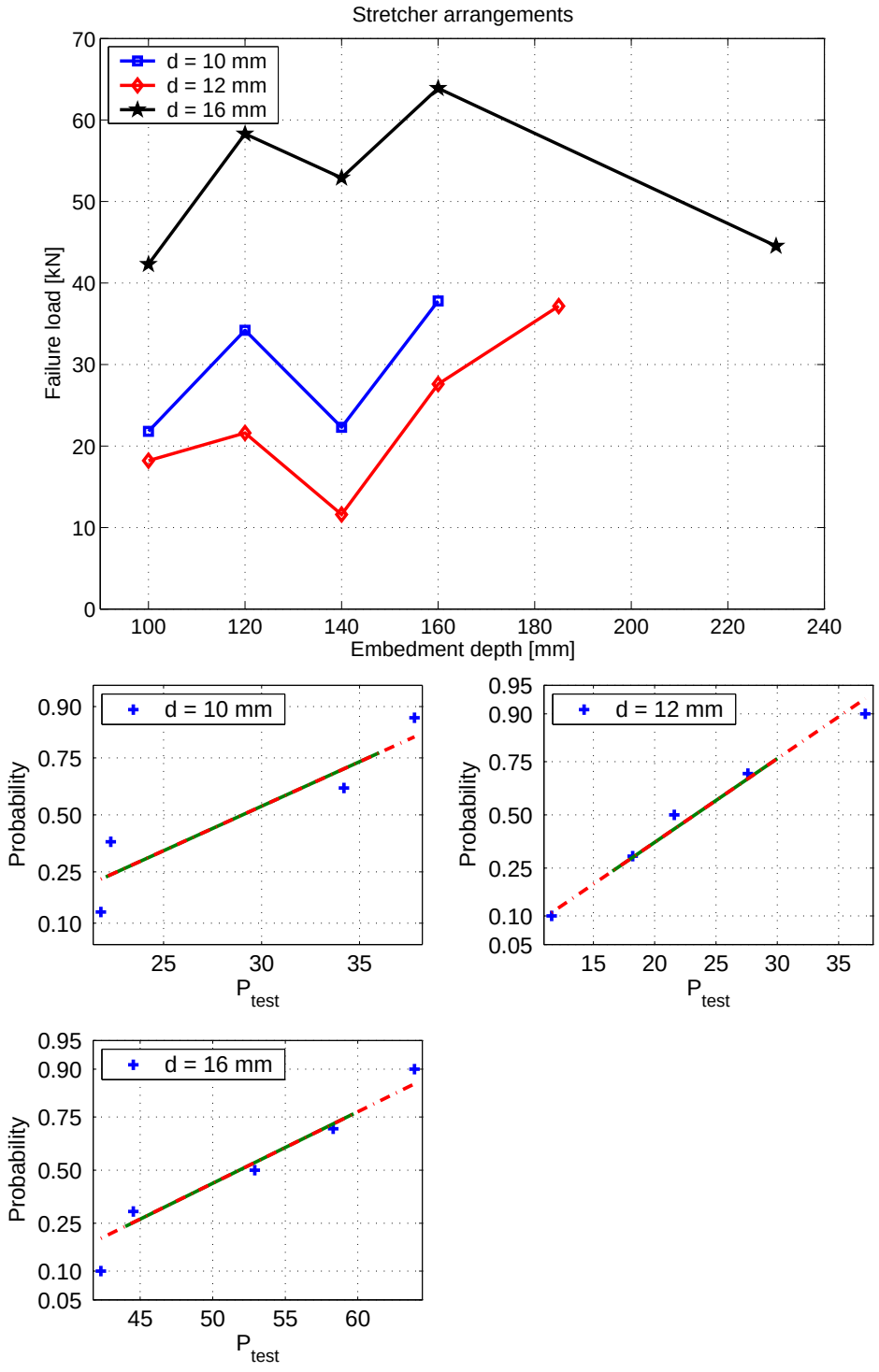

Figure 3.4: *Failure loads for anchors arranged in the stretcher side of a brick against the embedment depth,([6] - see table 3.4) and the normal probability assessment of the test results*

3.1.3 Joint arrangements

From table 3.5 it is evident that the failure of anchors arranged in the joints is governed by the sliding failure regardless of the anchor sizes and the embedment depth. It is observed that the failure occurs in the interface between the mortar resin and the anchor which is in accordance with the expectations.
The tendency of increasing load-carrying capacity, see figure 3.5, for increasing embedment depth is recognized for anchors of size $d = 16$ mm. This is also the case for anchors of sizes $d = 10$ and 12 mm though an unexpected drop in the capacities is observed at the embedment depth of 160 and 140 mm, respectively. As for anchors arranged in the stretcher side of a brick the anchors of size $d = 12$ mm exhibit failure loads lower than those of size $d = 10$ mm. The same explanation applies as in the case of the stretcher arrangements.

	d = 10 mm			
h [mm]	100	120	140	160
1.	17.7/SF	22.6/SF	30.9/SF	22.6/SF
	d = 12 mm			
h [mm]	100	120	140	160
	16.3/SF	17.6/SF	15.2/SF	21.2/SF
	d = 16 mm			
h [mm]	100	120	140	160
	21.7/SF	28.4/SF	35.7/SF	53.2/SF

Table 3.5: *Test results for the stretcher arrangements (P_u[kN]/failure mode), [6]*

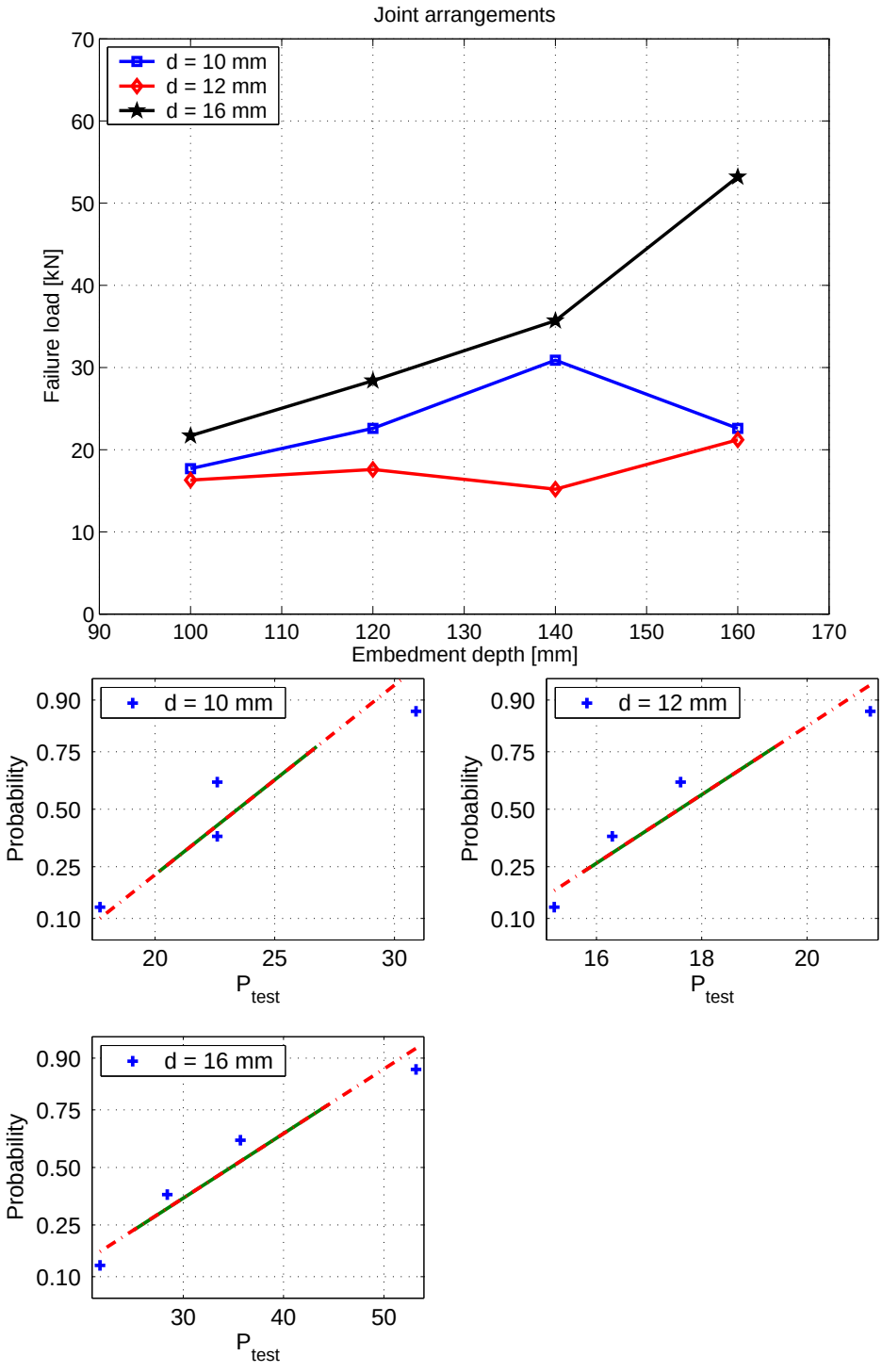

Figure 3.5: *Failure loads for anchors arranged in the joint against the embedment depth, ([6] - see table 3.5) and the normal probability assessment of the test results*

3.2 Close to edges and corners

3.2.1 Edge arrangements - normal to the bed joint

In table 3.6 failure loads for anchors arranged close to an edge normal to the bed joint are shown. Here e is the edge distance.
It is evident that the splitting failure governs the failure. Two different kinds of splitting failure are recognized : the one that only involves the brick in which the anchor is installed and the one that involves part of the masonry wall. It is evident that the latter kind occurs in larger edge distances (especially for anchors of size $d = 12$ mm). Also, for anchors of size $d = 12$ mm the tendency of increasing failure load for increasing edge distance is recognized (see figure 3.6) but for anchors of size $d = 16$ mm this is not the case. Anchors of size $d = 12$ mm demonstrate greater load-carrying capacity.

d [mm]	e [mm]	P_u [kN]	Failure mode
12	90	30.4	SPF
12	160	36.9	SPF
12	230	45.4	SPF
16	100	34.4	SPF
16	160	27.5	SPF
16	230	36.0	SPF

Table 3.6: *Test results for the edge arrangements - edge normal to the bed joint*

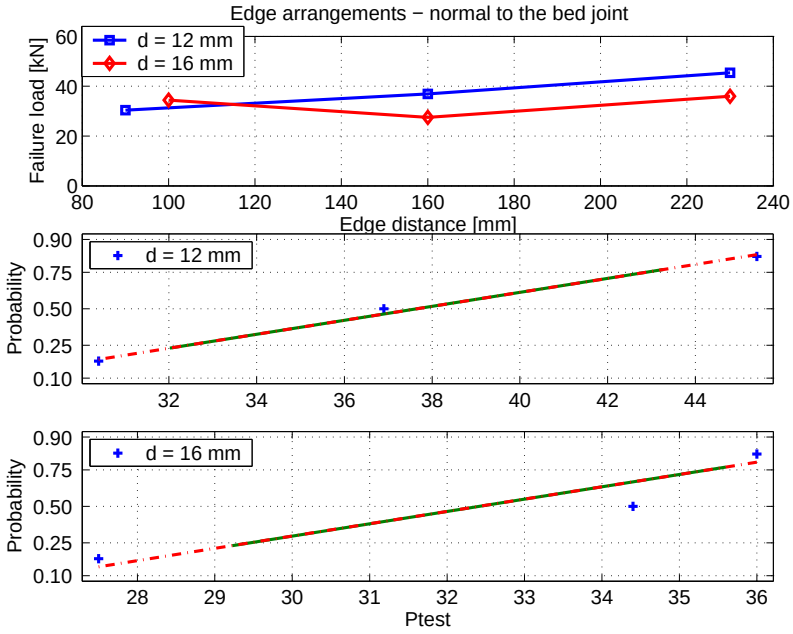

Figure 3.6: *Failure loads for anchors arranged close to an edge normal to the bed joint and the normal probability assessment of the test results*

3.2.2 Edge arrangements - parallel to the bed joint

The failure loads of anchors arranged close to an edge parallel to the bed joints appear to be lower than those obtained for anchors arranged close to an edge normal to the bed joint - compare tables 3.6 and 3.7.
The failure mode that governs the failure is the cover bending failure and the brick pull-out failure.
From figure 3.7 it is evident that for this kind of arrangement the load-carrying capacity is increasing with the edge distance e.

d [mm]	e [mm]	P_u [kN]	Failure mode
12	90	10.3	CBF
12	160	14.9	CBF
12	230	42.7	BPU
16	100	43.6	CBF
16	160	45.1	BPU
16	230	57.5	BPU

Table 3.7: *Test results for the edge arrangements - edge normal to the bed joint*

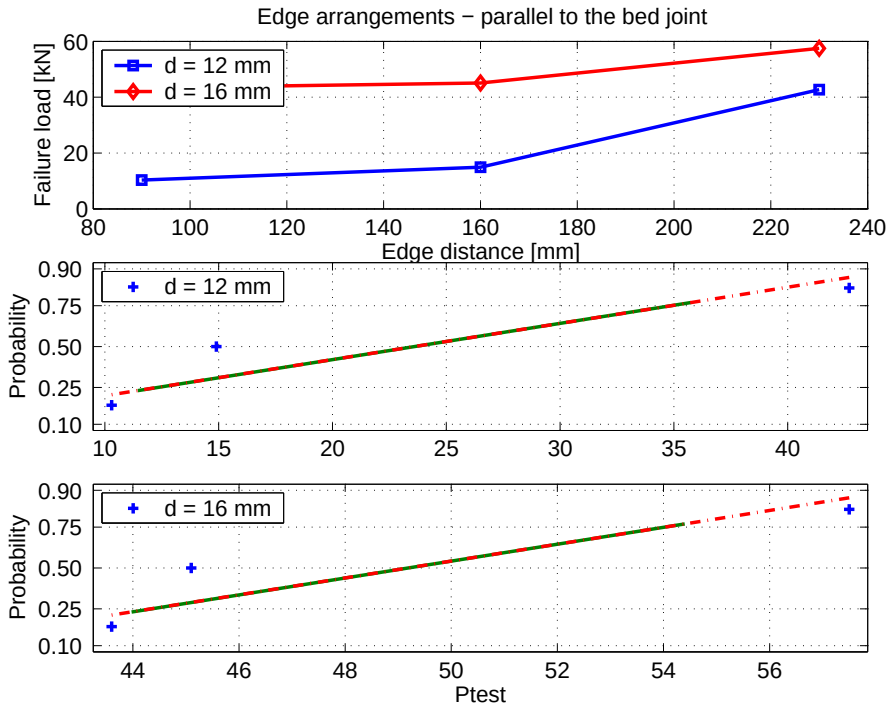

Figure 3.7: *Failure loads for anchors arranged close to an edge parallel to the bed joint and the normal probability assessment of the test results*

3.3 Corner arrangements

Testing of anchors arranged close to a corner reveals that the most common failure mode is the corner failure, see table 3.8.
From figure 3.8, where mean failure loads are plotted, it is evident that the load carrying capacity increases with increasing corner distance. This is valid for both anchor sizes tested. Surprisingly, it is anchors of size $d = 12$ mm that have the greatest load carrying capacity in most of the cases.

d [mm]	e [mm]	P_u [kN]	Failure mode
12	100	17.1	CF
12	160	21.3	CF
12	230	21.9	SF
12	230	35.5	CF
16	100	12.5	CF
16	160	9.53	CF
16	160	19.6	CF
16	230	32.5	SPF
16	230	25.5	BPU

Table 3.8: *Test results for the corner arrangements*

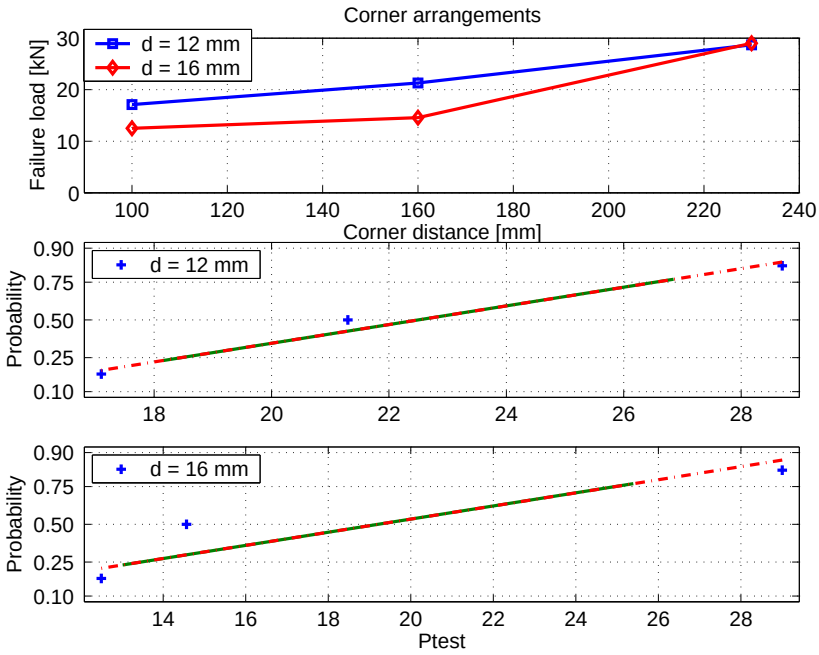

Figure 3.8: *Failure loads for anchors arranged close to a corner and the normal probability assessment of the test results*

4 Theory and empirical data

In this chapter failure loads predicted by the theory of plasticity are compared to those achieved by the pull-out tests. On this basis the effectiveness factors applied to the material constants (strength of bricks, mortar and masonry) are chosen so that the predicted failure loads fit well to the empirical ones. The effectiveness factors defined by the usual form are proposed ($\nu = K_n/\sqrt{f_c}$). In the case of the brick-cone failure and sliding failure of anchors in joints d and h dependence is introduced by applying factor $\sqrt{d/h}$ to ν-expression, see eq. (2.29). This is done in order to satisfy the correlation for different anchor sizes.
The test results are summarized in chapter 3 and a more detailed description is found in Appendix A.

4.1 Combined brick-cone failure

In figure 4.2 the failure loads predicted by assuming the combined brick-cone failure are compared to the corresponding pull-out tests (see table 4.1). The anchors in the pull-outs were arranged far from edges and corners.

	d = 12 mm				
h [mm]	100	120	140	160	185
P_u [kN]				27.6	35.8
					43.7
P_{um} [kN]				27.6	38.80
$P_{\text{brick-cone}}$ [kN]				33.66	32.68
$P_{\text{brick-cone}}/P_u$				1.22	0.84
P_{sliding}/P_u				1.21	1.00
P_{punch}/P_u				2.62	2.47
	d = 16 mm				
h [mm]	100	120	140	160	230
P_u [kN]	42.3	58.3	52.9		
$P_{\text{brick-cone}}$	56.88	54.04	51.98		
$P_{\text{brick-cone}}/P_u$	1.34	0.93	0.98		
P_{sliding}/P_u	0.66	0.57	0.74		
P_{punch}/P_u	0.72	0.74	1.09		

Table 4.1: *Failure loads achieved by the pull-outs exhibiting the combined brick-cone failure*

The effectiveness factors are proposed so that the predicted failure loads correlate well to the empirical ones. The upper bound expression for the combined brick-cone failure is composed of three contributions: the brick-cone failure and sliding failure along the anchor and the sliding failure in the interface between brick and mortar, see eq. (2.28). It is necessary to define two effectiveness factors: one on the compressive strength of the brick in which the anchor is installed (f_{cb}) and the other one on the formal compressive strength of the interface between a brick and the mortar (f_{ci}).
If cohesion c is known f_{ci} may be found by eq. (2.1). In order to obtain c the empirical

equation (2.2) is utilized.
Masonry used in the testing is bricklayed with bricks having mean IRA of 3,4 kg/m^2/min (Appendix B in [6]). Thus c may be found by the cohesion graphs shown in figure 4.1 which are the graphs for the commonly used mortars (for the mortar specifications see section 8.1 Supplement 1 in [2]). Thus, the cohesion for a mortar type with greater amount of lime (hydrophobic mortar necessary in conjunction with bricks having high IRA, [5]), i.e. the mortar 60/40/850, having IRA = 3,4 is 0.7 MPa. Using eq. (2.1) and inserting $\phi = 37^o$ and $f_c = f_{ci}$, f_{ci} is found to be

$$0.7 = \frac{f_{ci}}{2}\frac{1-\sin\phi}{\cos\phi} \Rightarrow f_{ci} = 2.71 \text{ MPa} \tag{4.1}$$

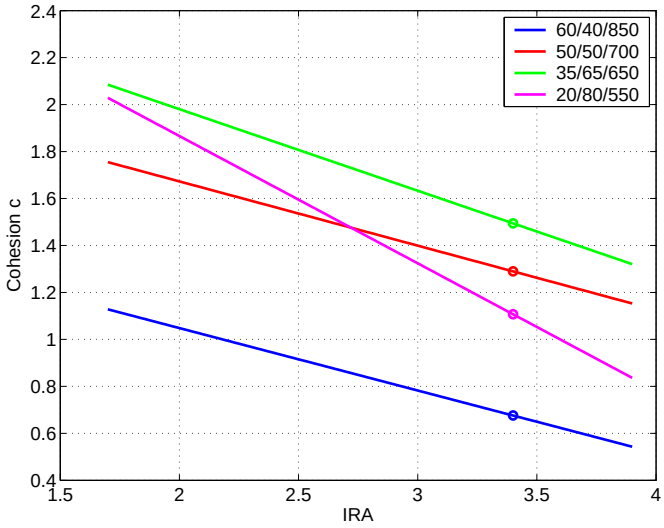

Figure 4.1: *Cohesion c vs. IRA using eq.* (2.2)*, [2], for some commonly used mortars*

Finally, applying the brick strength $f_{cb} = 21.1$ MPa and the interface strength $f_{ci} = 2.71$ MPa the effectiveness factors ν and ν_2 are defined by choosing $\underline{K_1 = 2.5}$ and $\underline{K_2 = 1.8}$. Thus, by means of eq. (2.29) the effectiveness factors are found to be

$$\nu = \frac{2.5}{\sqrt{21.1}}\sqrt{\frac{d}{h}} = 0.54\sqrt{\frac{d}{h}}, \quad \nu_2 = \frac{3.12}{\sqrt{2.71}}\sqrt{\frac{d}{h}} = 1.15\sqrt{\frac{d}{h}} \tag{4.2}$$

From figure 4.2 it is evident that the correlation is good.
From table 4.1 it should be noted that the sliding failure criterion for an anchor installed in a brick predicts lower failure loads than those predicted by the combined brick-cone failure. This is conflicting with the upper bound theorem since the failure mechanism governing the failure also has to be the most dangerous one (i.e. the lowest failure loads). This may be explained by the fact that the proposed value of the effectiveness factors are only based on

the correlation to the empirical values. In order to remain obligated to achieving the best possible correlation to the observed failure modes the choice of the effectiveness factors remains unchanged regardless of the fact that this might not always produce the lowest upper bound values.

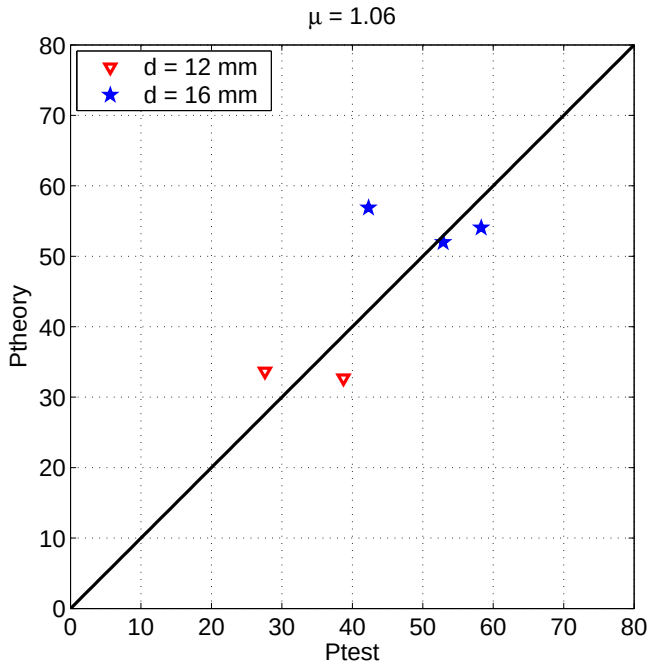

Figure 4.2: *Predicted failure loads vs. empirical data for the combined brick-cone failure*

4.2 Sliding failure of anchors in joints

The pull-out tests of anchors arranged in the joints show that the failure occurs by sliding failure. The sliding failure takes place along a deformed bar. Eq. (2.15) describes the simple upper bound expression when the failure is expected to occur in the mortar resin or the interface between the resin and the anchor. The effectiveness factor ν applied to the compressive strength of the mortar is defined by analogy of the effectiveness factor defined for the combined brick-cone failure, i.e. eq. (2.29). This means that both the dependence on the compressive strength of mortar and the anchor embedment depth is assumed.

A good correlation is found between the predicted and empirical failure loads when the effectiveness factor ν, defined by $K_1 = 14.25$, is applied to the compressive strength of the mortar. It should be noticed that ν is here defined by introducing the embedment depth and anchor size dependence (i.e. $\sqrt{d/h}$). The compressive strength of the mortar (f_{cj}) is found by the means of the approximative formula for the compressive strength of a masonry wall (i.e. eq. (2.6)) by utilizing the known mean compressive strength of the bricks and masonry. The effectiveness factor is thus defined as

$$\nu = \frac{14.25}{\sqrt{2.91}}\sqrt{\frac{d}{h}} = 8.35\sqrt{\frac{d}{h}} \tag{4.3}$$

The pull-out test results for different embedment depths are summarized in table 4.2 and in figure 4.3 the predicted failure loads are compared to the empirical ones.
It is evident that the correlation is good, i.e. the mean value of the ratio between the predicted failure loads and the empirical ones is 0.95. The ratio becomes 1.0 if the one test that does not comply well with the theory is neglected.

Finally, it should be noticed that the effectiveness factor defined by $K_1 = 14.25$ is greater than 1. This is due to the very low compressive strength of the mortar f_{cj} and due to the fact that f_{cj} is found by an approximative formula, eq. (2.6), and not by tests.

	d = 12 mm			
h [mm]	100	120	140	160
P_u [kN]	16.3	17.6	15.2	21.2
P_{sliding} [kN]	15.85	17.36	18.75	20.04
P_{sliding}/P_u	0.97	0.99	1.23	0.95

	d = 16 mm			
h [mm]	100	120	140	160
P_u[kN]	21.7	28.4	35.7	53.2
P_{sliding}[kN]	24.40	26.72	28.87	30.86
P_{sliding}/P_u	1.12	0.94	0.81	0.58

Table 4.2: *Failure loads achieved by the pull-outs exhibiting the joint failure (the interface failure) - [kN]*

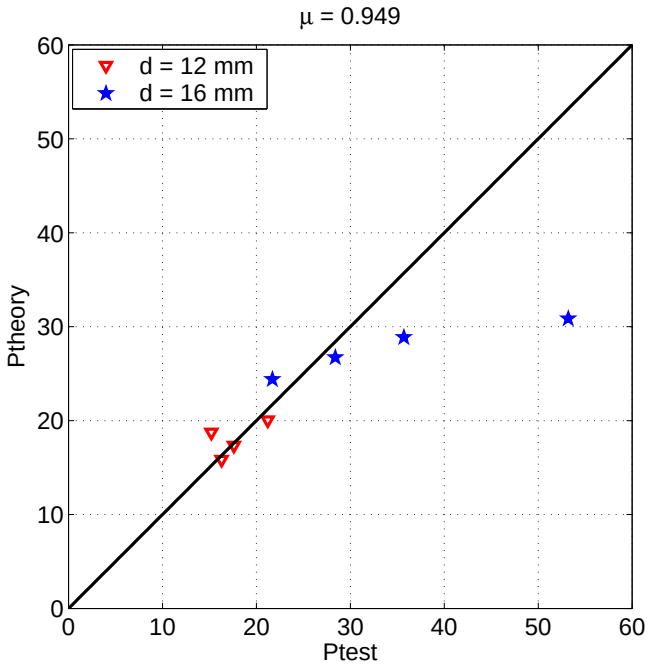

Figure 4.3: *Predicted failure loads vs. empirical data.* $f_{cj} = 2.9$ *MPa.*

4.3 Sliding failure of anchors in bricks

It is seen from the tests that the failure of anchors installed in bricks may also be governed by the sliding failure. In this case the strength of the brick in which the anchor is installed governs the failure. Thus, the upper bound expression for the sliding failure along a deformed bar, eq. (2.15), is used.

In table 4.3 the failure loads obtained are shown. Using the usual definition of ν, i.e. the dependence on the square root of the compressive strength of brick, and suggesting $K_1 = 2.41$ a good correlation between the predicted and the empirical failure loads is obtained. This is shown in figure 4.4 from which it is evident that the correlation is different for different anchor sizes.
$K_1 = 2.41$ yields a value of ν (here, ν is suggested in the usual form)

$$K_1 = 2.41 \Rightarrow \nu = \frac{K_1}{\sqrt{21.1}} = 0.52 \tag{4.4}$$

	d = 10 mm				
h [mm]	90	100	120	140	160
P_u [kN]	11.8	21.8	34.2	22.3	42.7
P_{sliding} [kN]	15.65	17.39	20.87	24.34	27.82
P_{sliding}/P_u [kN]	1.33	0.80	0.61	1.10	0.65
P_{brick}/P_u [kN]	2.20	1.19	0.76	1.16	0.61
P_{punch}/P_u [kN]	1.20	0.79	0.72	1.48	1.00
	d = 12 mm				
h [mm]	100	120	140	160	185
P_u [kN]		21.6	11.6		36.3
P_{sliding} [kN]		25.04	29.21		38.60
P_{sliding}/P_u [kN]		1.16	2.52		1.06
P_{brick}/P_u [kN]		1.51	2.82		0.90
P_{punch}/P_u [kN]		1.15	2.88		1.57
	d = 16 mm				
h [mm]	100	120	140	160	230
P_u [kN]				63.9	63.1
P_{sliding} [kN]				44.52	64.00
P_{sliding}/P_u [kN]				0.70	1.01
P_{brick}/P_u [kN]				0.74	0.75
P_{punch}/P_u [kN]				0.69	1.41

Table 4.3: *Failure loads of the anchors installed in a brick exhibiting the sliding failure*

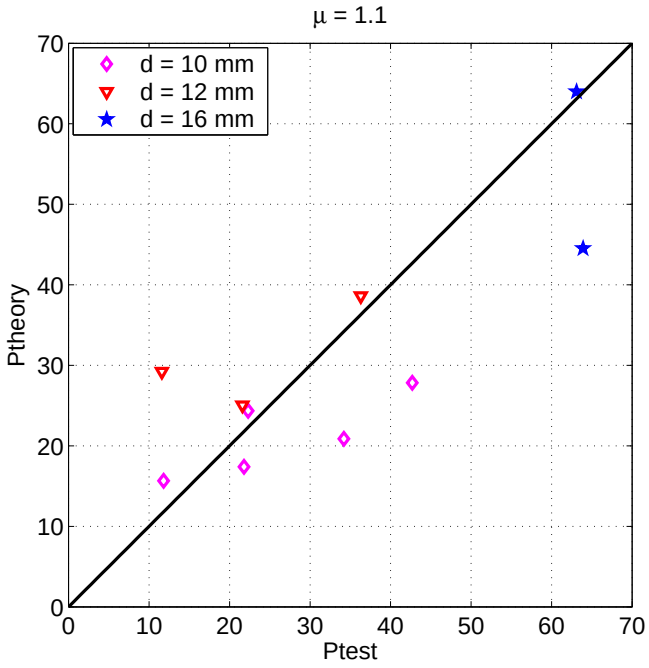

Figure 4.4: *Predicted failure loads vs. empirical data.* $f_{cb} = 21.1$ *MPa.*

Furthermore, it is evident from table 4.3 that none of the suggested failure mechanisms for anchors installed in a brick (combined brick-cone and punching shear failure) predict lower failure loads than those predicted by the sliding failure of an anchor in a brick.

4.4 Punching shear

The punching shear solution for concrete slabs is applied by introducing a new effectiveness factor ν (eq. (2.51)).
Since there has not been any evidence of this kind of failure in the pull-outs carried out in [6] and the recent ones (Appendix A) the empirical data used are the ones referred to in [1], see table 4.4. Here, in the light of the empirical data, K_1 is suggested to 3.82.
It is evident from figure 4.5 that the correlation is good, i.e. 0.98-1.0 with a coefficient of variation of 2.24 %.

d	[mm]	10	10
h	[mm]	90	90
f_c	[MPa]	3.66	6.87
f_{cb}	[MPa]	12.7	12.7
f_{cj}	[MPa]	1.00	5.93
P_u	[kN]	16.80	22.30
P_{punch}/P_u		0.98	1.02
P_{brick}/P_u		1.07	0.87
P_{sliding}/P_u		0.46	0.47

Table 4.4: *Empirical failure loads exhibiting the punching shear failure, [1]*

From table 4.4 it is evident that applying the punching shear failure does not produce the lowest failure loads. However, it should be kept in mind that the punching shear failure is dependent on the arrangement (the use of a back plate) for which reason it is still likely that this kind of failure might govern the failure.

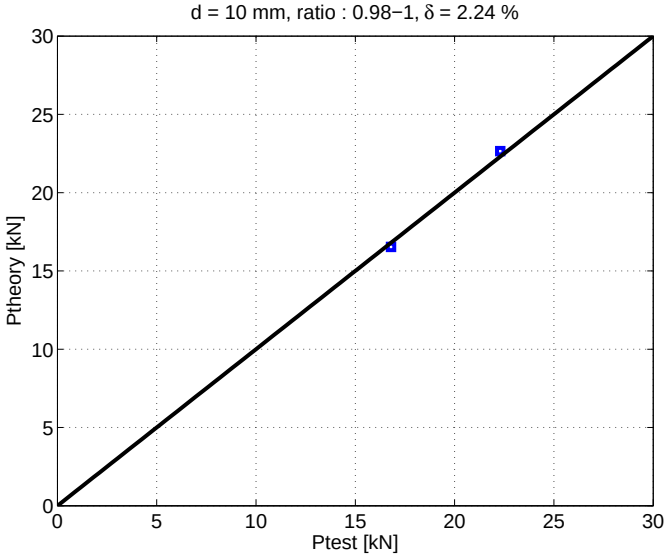

Figure 4.5: *Predicted failure loads vs. empirical data, [1]*

4.5 Edge arrangements

When anchors in masonry are arranged near an edge, so far it has only been possible to treat the case where the edge is normal to the bed joint. Thus, only for this case the predicted failure loads are compared to the empirical ones. The empirical data are reproduced in table 4.5. Since the splitting failure mechanism appears to govern the failure the failure loads are predicted using eq. (2.30).

d [mm]	e [mm]	P_u [kN]	P_{theory}	P_{theory}/P_u
12	90	30.4	30.39	0.99
12	160	36.9	30.39	0.82
12	230	45.4	30.39	0.67
16	100	34.4	41.75	1.21
16	160	27.5	41.75	1.52
16	230	36.0	41.75	1.16

Table 4.5: *Test results for the edge arrangements - edge normal to the bed joint*

The comparison between the predicted failure loads and the empirical ones is shown in figure 4.6. Here, a good correlation is achieved by suggesting the effectiveness factors defined by $K_1 = 3.35$ and $K_2 = 3.0$, thus the effectiveness factors defined by eq. (2.31) are found to be

$$\nu = \frac{K_1}{\sqrt{21.1}} = 0.73, \quad \rho = \frac{\nu_t f_{tb}}{f_{cb}} = \frac{K_2}{20}\sqrt{\frac{d}{h}} = 0.15 \tag{4.5}$$

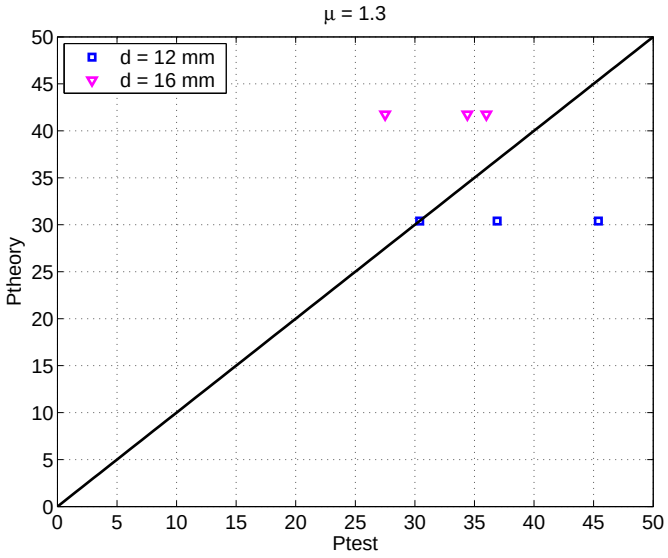

Figure 4.6: *Predicted failure loads vs. empirical data for anchors exhibiting the local splitting failure*

5 Conclusion

It has been shown that the upper bound expressions developed using the upper bound theorem of the theory of plasticity predict reasonable failure loads for anchors in masonry.
The introduction of the effectiveness factors is done in conjunction with the test results, i.e. the factors are introduced so that the predicted failure loads comply well with the empirical ones.

Combined brick-cone failure

The use of the combined brick-cone failure is proposed by using the effectiveness factors defined by $K_1 = 2.5$ and $K_2 = 3.12$. Thus, the upper bound expression becomes

$$P_u = \left(3.93\sqrt{f_{cb}}(h - 5.76d)d + 37.44\sqrt{f_{ci}}(l_b + d)d\right)\sqrt{\frac{d}{h}}, \quad (f_{cb} \text{ and } f_{ci} \text{ in MPa}) \quad (5.1)$$

Splitting failure

In similar manner it is found that the splitting failure as a local phenomenon is to be applied defining the effectiveness factors by $K_1 = 3.35$ and $K_2 = 3.0$. Thus, the upper bound expression becomes

$$\frac{P_u}{\pi dh} = \min \begin{cases} 0.40\sqrt{f_{cb}} + 0.13 f_{cb}\left(\dfrac{b}{d} - 1\right)\sqrt{\dfrac{d}{h}} \\ \\ 0.94\sqrt{f_{cb}} + 0.07 f_{cb}\left(\dfrac{b}{d} - 1\right)\sqrt{\dfrac{d}{h}} \end{cases} \quad (f_{cb} \text{ in MPa}) \quad (5.2)$$

Sliding failure of an anchor in the joint

The sliding failure that occurs in the joint is treated by introducing the effectiveness factor ν defined by $K_1 = 14.25$. This way the upper bound expression is found to be

$$P_u = 22.38\sqrt{f_{cj}h}d^{\frac{3}{2}}, \quad (f_{cj} \text{ in MPa}) \quad (5.3)$$

Sliding failure of an anchor in the brick

If the anchor is installed in the brick and the sliding failure mechanism governs the failure the upper bound expression is found by applying the suggested effectiveness factor defined by $K_1 = 2.41$. Thus, the upper bound expression is found to be

$$P_u = 3.79dh\sqrt{f_{cb}}, \quad (f_{cb} \text{ in MPa}) \quad (5.4)$$

Punching shear failure

The upper bound expression for the failure load by punching shear, after utilizing the effectiveness factor by $K_1 = 3.82$, is found to be

$$P_u = 0.96(d + h)h\sqrt{f_c}, \quad (f_c \text{ in MPa}) \quad (5.5)$$

Final remarks

Other global failure mechanisms (the wall strip bending failure and the sliding failure at the side) are not verified by the empirical data for which reason it still stays uncertain whether these mechanisms are reasonable to expect. This remains to be investigated and until that these mechanisms need to be checked in similarity to the verified failure mechanisms.

The prediction of the failure loads of anchors arranged close to corners and edges (parallel to the bed joint) remains to be investigated. As far as the edge arrangements are considered the tests show that anchors arranged close to edges normal to the bed joint exhibit higher failure loads than those arranged close to edges parallel to the bed joints.
This is not strange since the resistance against the dilatation of the surrounding material is smaller for anchors close to an edge parallel to the bed joint. It has also been pointed out that an anchor should never been installed near a free edge parallel to the bed joint nor a corner.

At last the following remark: It appears that in some cases the load carrying capacity of an anchor is far from average value indicating some error in the prediction of the masonry and/or in the installment of the anchor. Thus in important cases the anchor should be checked on the site after installment.

Bibliography

[1] L.Z. Hansen, Karsten Findsen and M.P. Nielsen, *Beregning af indlimede ankre i murede vægge (Strength of bonded anchors in masonry)*, Department of Civil Engineering, Technical University of Denmark, Lyngby 2004

[2] L.Z. Hansen and T. Gudmand-Høyer, *Strength effects from the initial rate of absorption on masonry*, Danish Society for Structural Science and Engineering Volume 68, No. 2-3, pp. 35-113, 1997

[3] M.K. Olsen and M.P. Nielsen, *The strength of anchors*, Bygningsstatiske Meddelelser, Vol. 68, No.1, pp. 1-34, 1997

[4] M.P. Nielsen, *Limit Analysis and Concrete Plasticity*, CRC Press LLC, 2nd ed., 1998

[5] M.P. Nielsen and L.G. Hagsten, *Murværk (Masonry)*, Forlaget Tegl, 1st edition, November 2002

[6] Fedja Arifović, *Anchors in concrete and masonry*, M.Sc. thesis, Department of Civil Engineering, Technical University of Denmark, October 2004

[7] Hilti, *Ankerhåndbogen (Anchor handbook)*, Hilti Danmark A/S, 2002

List of symbols

b_b	brick width
c	cohesion or the geometrical parameter in optimizing
	the shape generatrix of failure surface
d	anchor diameter
f_c	masonry compressive strength
f_{cb}	compressive strength of brick
f_{ci}	formal compressive strength of the interface between the mortar and the brick
f_{cj}	compressive strength of mortar
f_t	tensile strength of masonry wall
f_{tb}	tensile strength of brick
f_y	yield stress
G	weight of masonry wall
h	anchor embedment depth
h_b	brick height
h_c	brick-cone height
h_j	joint height
l	anchor length, or a constant in the dissipation formula
l_b	brick length
m	constant in the dissipation formula
P_u	ultimate failure load of an anchor (load-carrying capacity)
t	width of a masonry wall
t_{eff}	effective width of a masonry wall
u	virtual displacement
w	displacement
q	uniform load acting on a masonry wall in the transverse direction
x	distance from the bottom of the bending point in the case of the wall strip bending failure
α	angle between displacement and corresponding yield surface
δ	virtual displacement
η	distance from bottom to force P in wall strip bending failure
μ	coefficient of friction
ν_b	effectiveness factor of compressive strength of brick
ν_j	effectiveness factor of compressive strength of mortar
ξ	distance from vertical support to force P in
	wall strip bending failure

ρ	effectiveness factor of masonry tensile strength $\rho f_c = \nu_t f_t$, or the density of masonry wall
ν	effectiveness factor
σ	normal compressive stress or standard deviation
τ	shear stress
ϕ	angle of friction

Appendix A

test results

A Test results - anchors in masonry

The pull-outs are executed on masonry walls with the following strengths. The compressive strength of bricks is measured on 16 bricks as shown in table A.1. The mean strength is found to be $f_{c,m} = 21.1$ MPa.

no :	1	2	3	4	5	6	7	8	8	9	10
f_c	20.7	21.0	19.1	20.8	21.2	19.6	21.9	22.3	19.2	22.9	19.7

no :	12	13	14	15	16
f_c	20.2	22.7	20.8	20.1	21.1

$f_{c,m} = 21.1$ MPa

Table A.1: *The compressive strength of bricks*

The compressive strength of a masonry wall is found by subjecting six masonry piers to compressive testing, thus the mean compressive strength of a masonry wall is shown in table A.2.

no :	1	2	3	4	5	6
f_c	8.1	6.6	7.6	7.7	8.1	6.9

$f_{c,m} = 7.5$ MPa

Table A.2: *The compressive strength of masonry walls*

A.1 Test setup

The pull-out tests are carried out using a steel frame retainer to hold the upstroke press. The same setup is used in the anchor pull-out tests in the case of anchors in concrete, [6]. Here, the steel plate used to pull several anchors at once is replaced by a single bar pulling out the anchor installed in masonry (the plate shown in the detailed drawing in figure A.1).
The test set up is illustrated in figures A.2 and A.1.

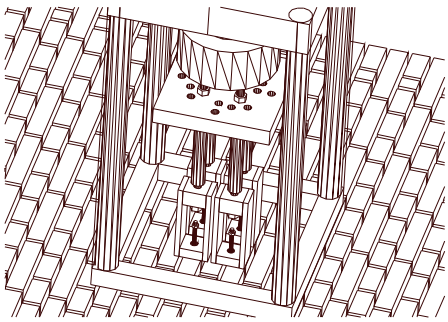

Figure A.1: *Principle of the test setup near the anchor (changed in the tests carried out for the purpose of this report)*

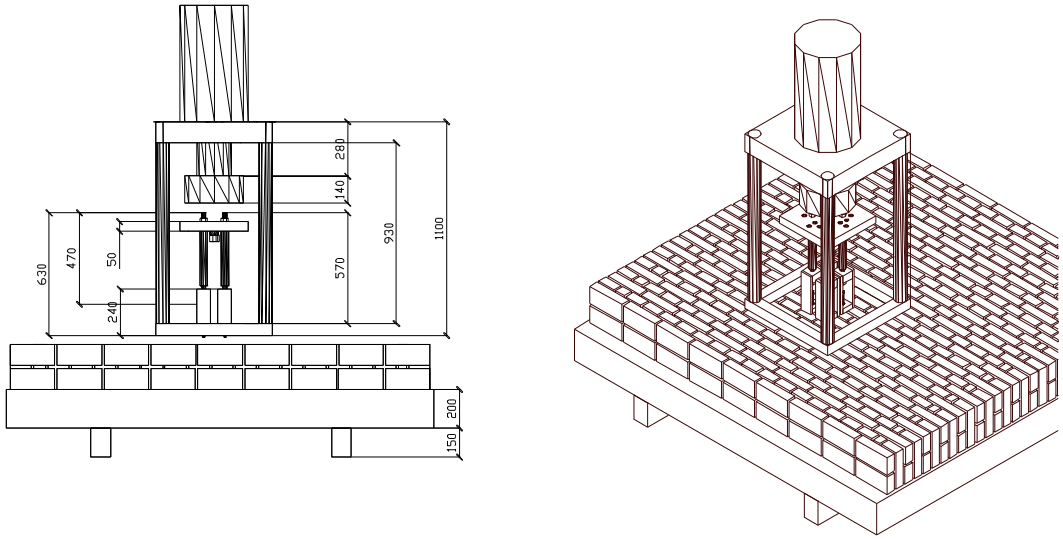

Figure A.2: *Principle of the test setup*

A.2 Far from edge and corners

A.2.1 Stretcher arrangement - 1, d = 12 mm

Figure A.3: *The failure mode observed*

Failure mode: Brick-cone failure

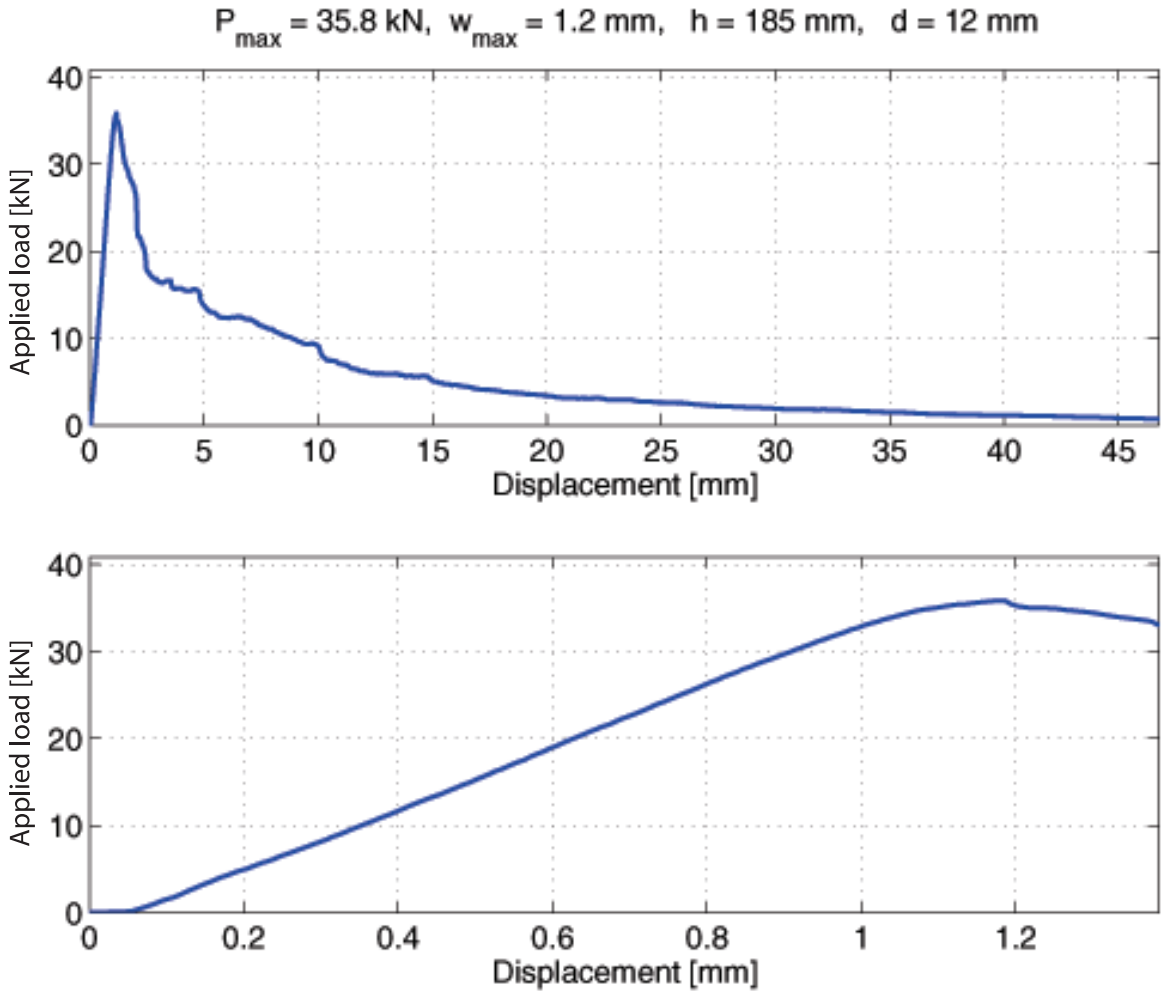

Figure A.4: *Load-deflection curve for the anchors pull-out*

A.2.2 Stretcher arrangement - 2, d = 12 mm

Figure A.5: *The failure mode observed*

Failure mode: Brick-cone failure

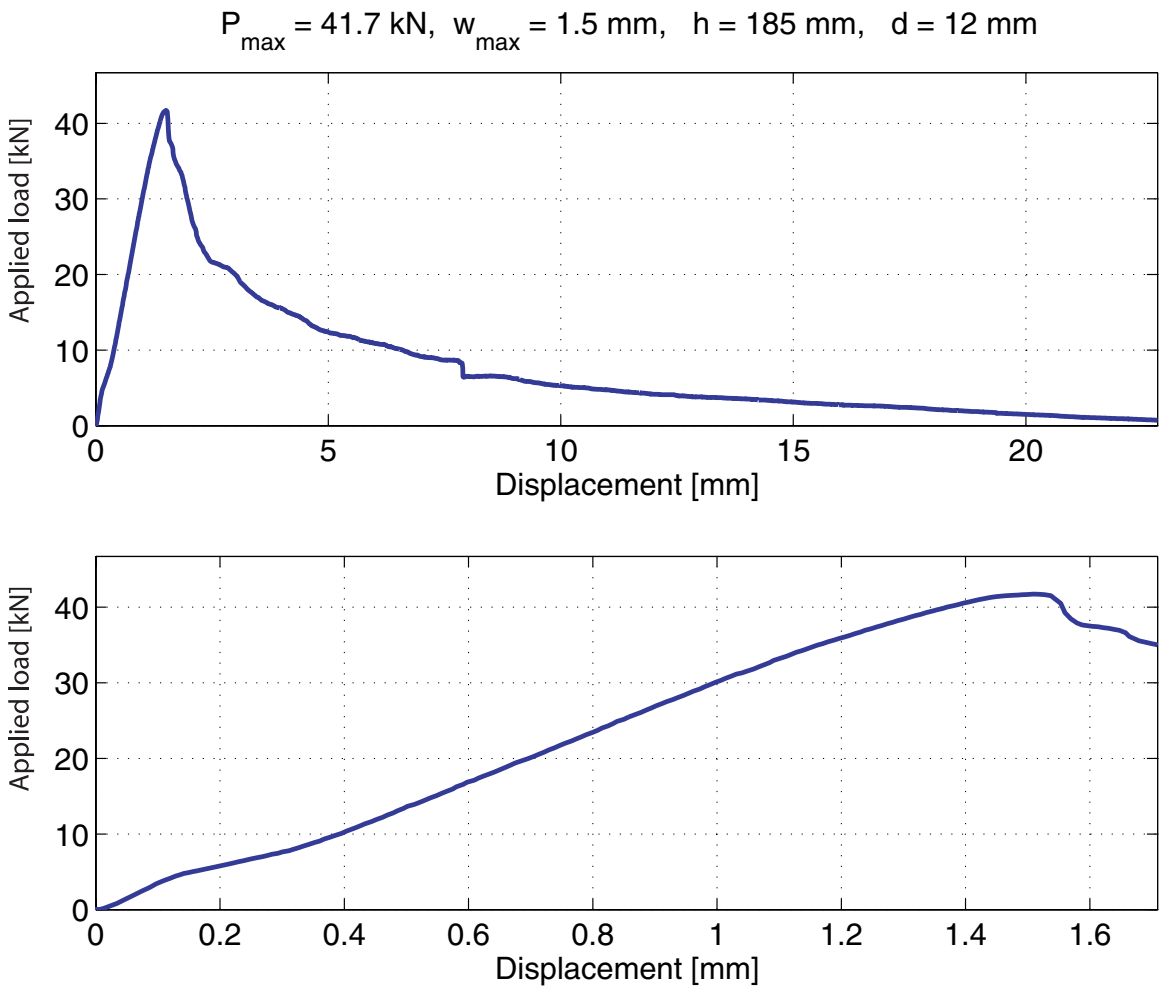

Figure A.6: *Load-deflection curve for the anchors pull-out*

A.2.3 Stretcher arrangement - 3, d = 12 mm

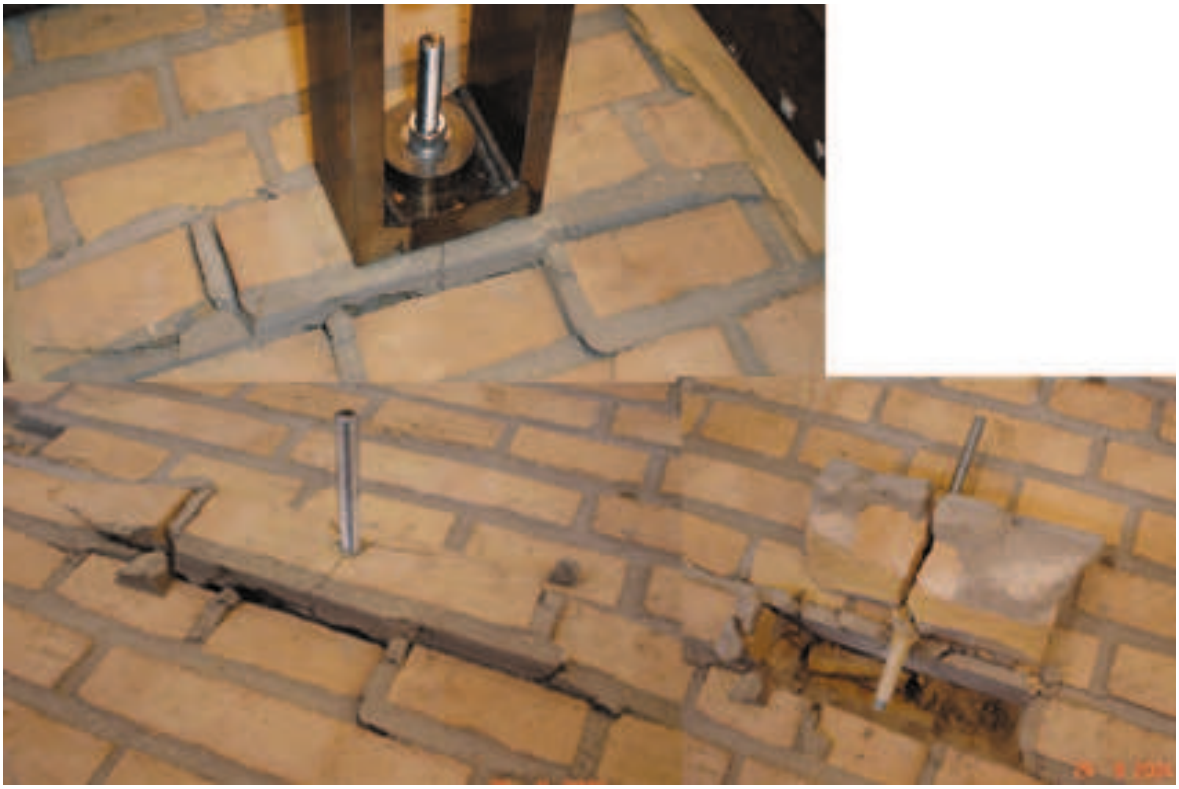

Figure A.7: *The failure mode observed*

Failure mode: Combined brick pull-out and sliding failure

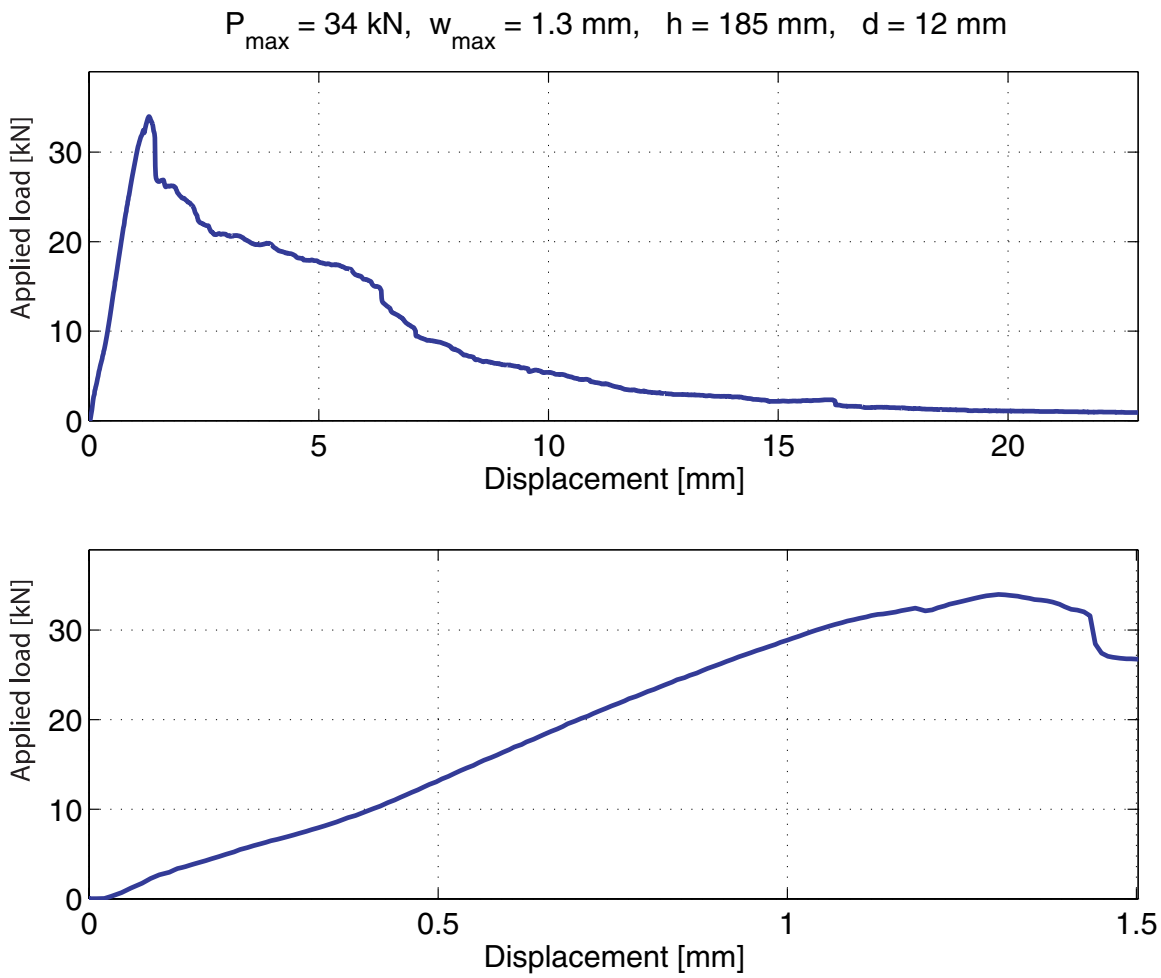

Figure A.8: *Load-deflection curve for the anchors pull-out*

A.2.4 Stretcher arrangement - 1, d = 16 mm

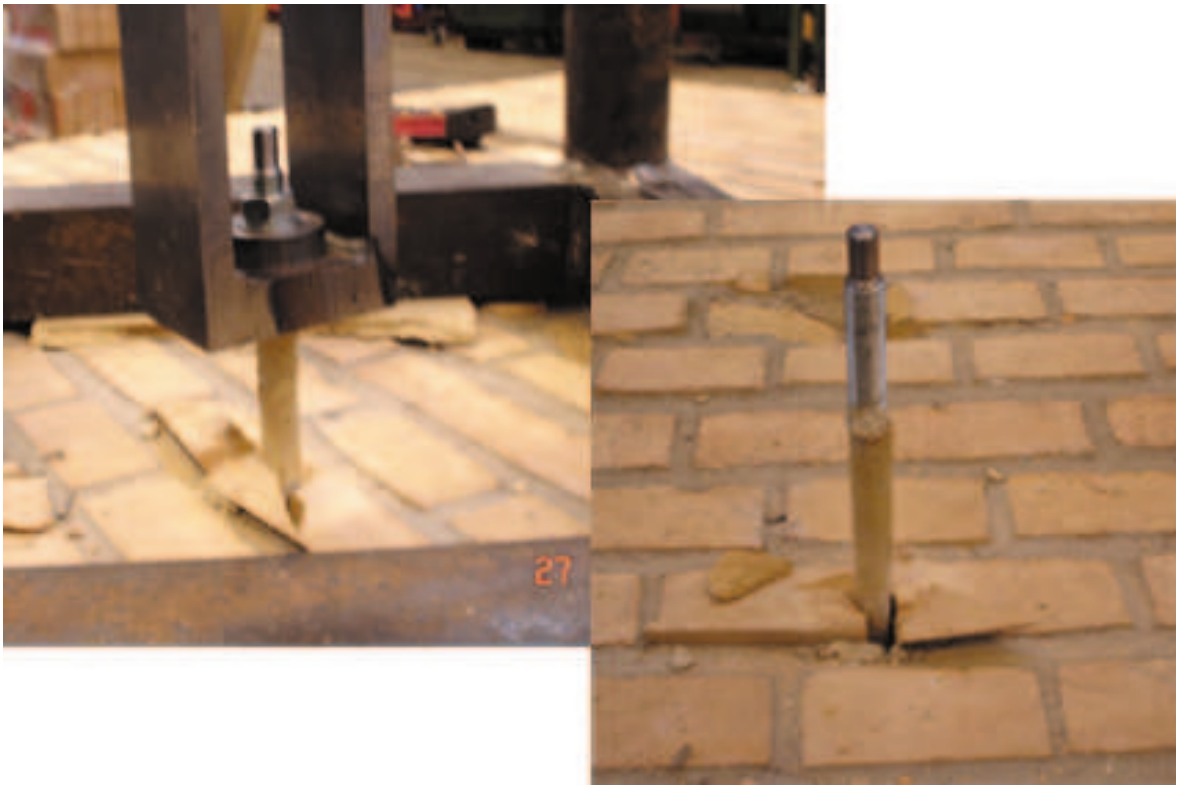

Figure A.9: *The failure mode observed*

Failure mode: Sliding failure

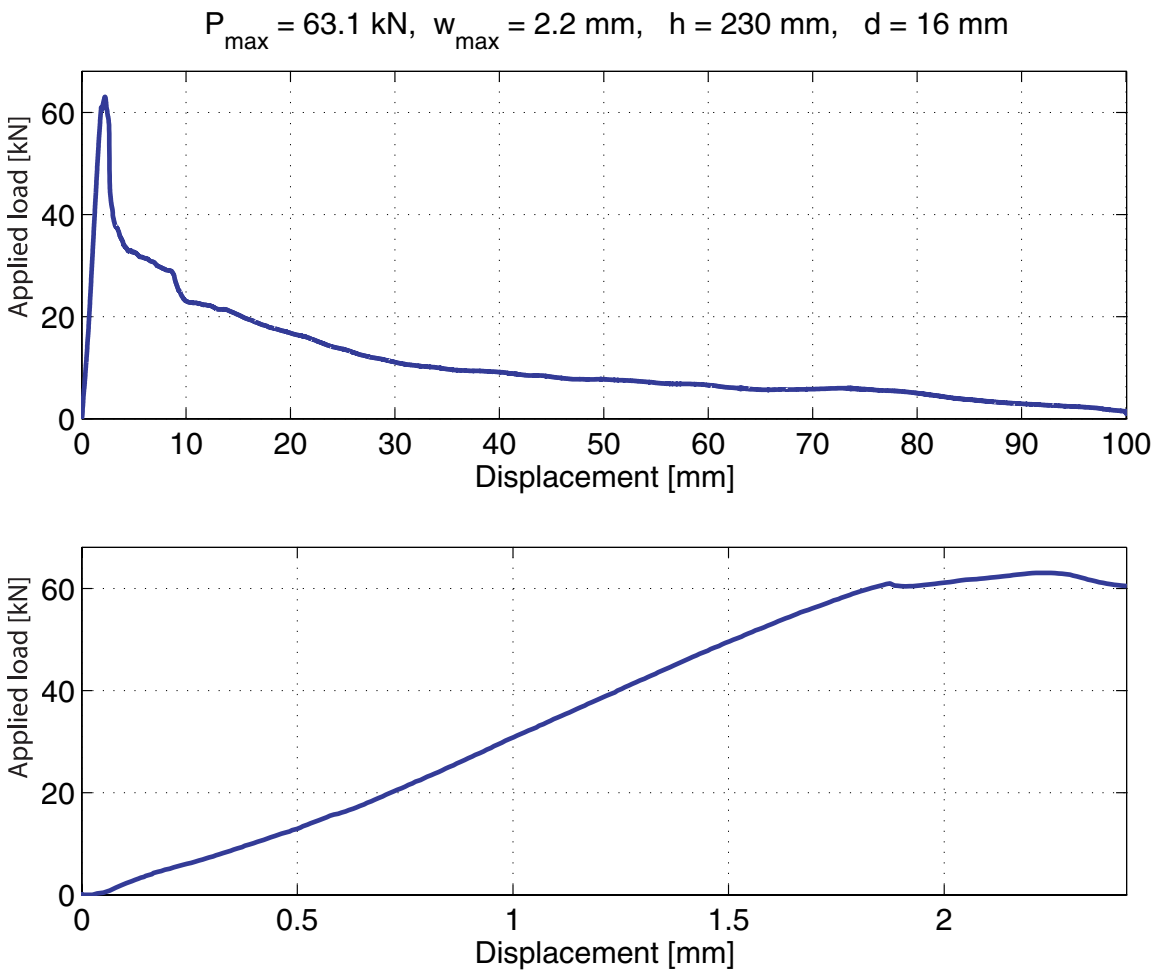

Figure A.10: *Load-deflection curve for the anchors pull-out*

A.2.5 Stretcher arrangement - 2, d = 16 mm

Figure A.11: *The failure mode observed*

Failure mode: Combined brick pull-out and sliding failure

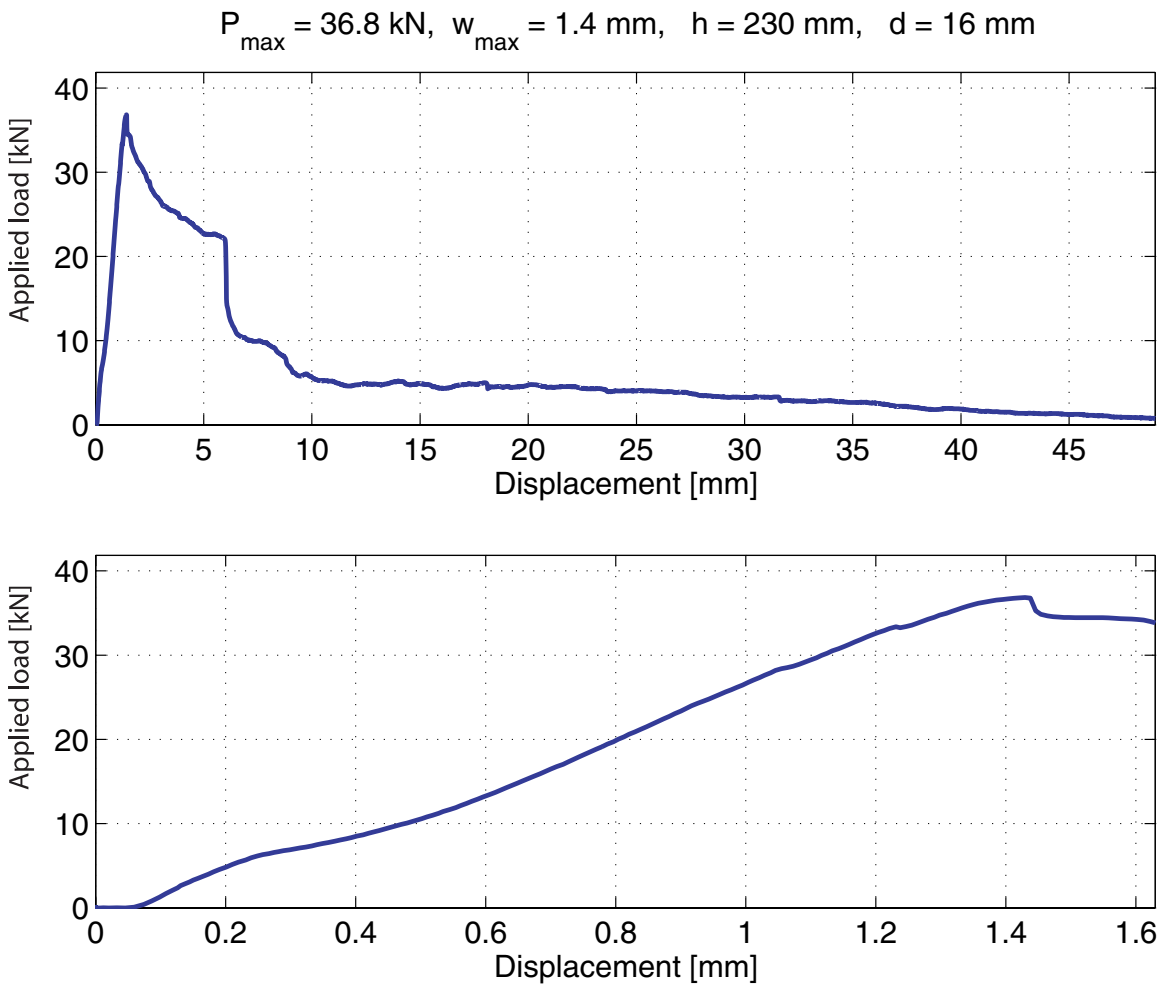

Figure A.12: *Load-deflection curve for the anchors pull-out*

A.2.6 Stretcher arrangement - 3, d = 16 mm

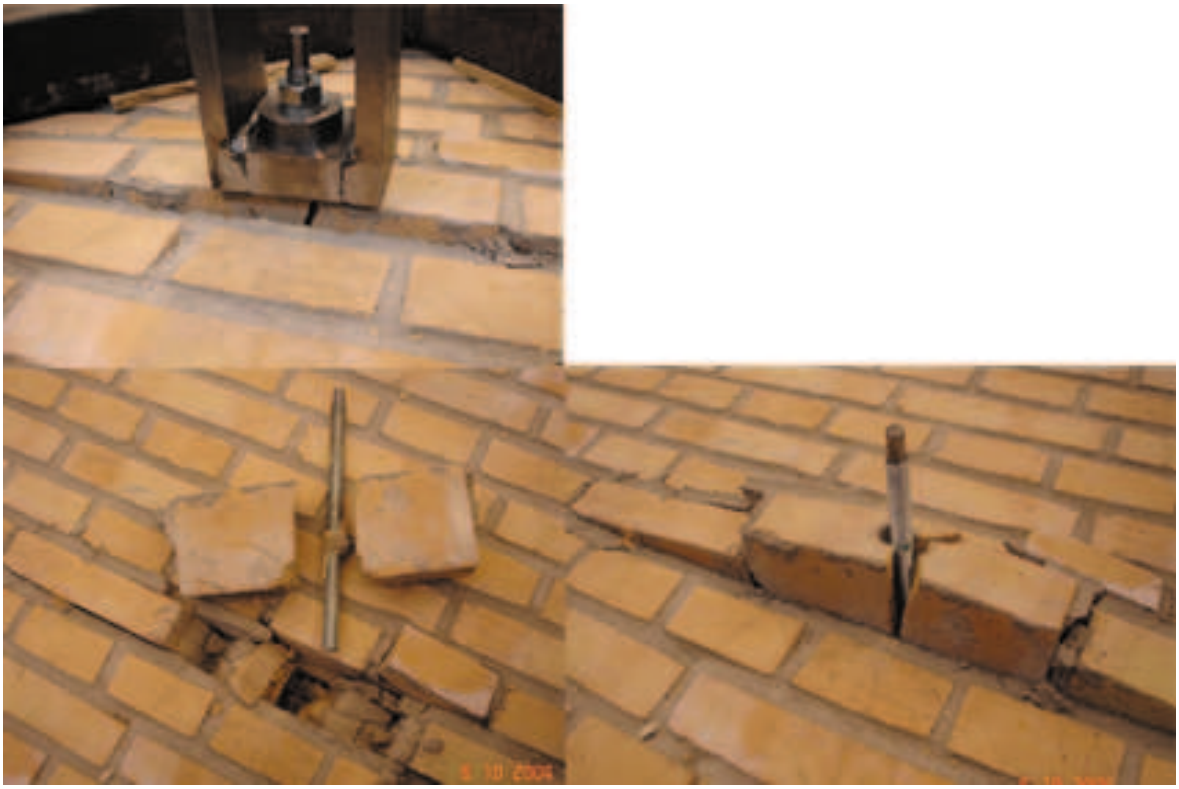

Figure A.13: *The failure mode observed*

Failure mode: Combined brick pull-out and sliding failure

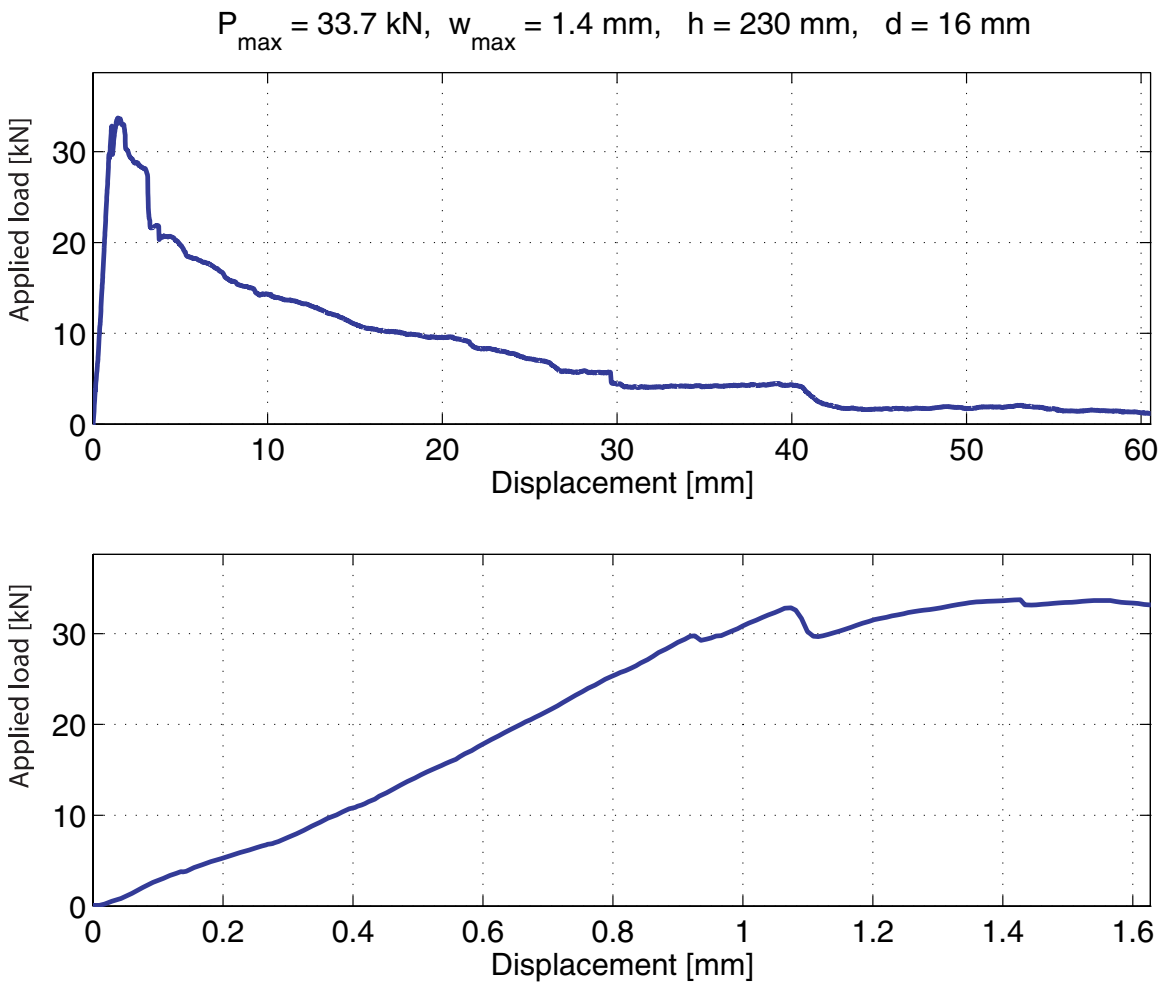

Figure A.14: *Load-deflection curve for the anchors pull-out*

A.2.7 Stretcher arrangement, d = 10 mm, h = 100 mm

Figure A.15: *The failure mode observed*

Failure mode: Sliding failure

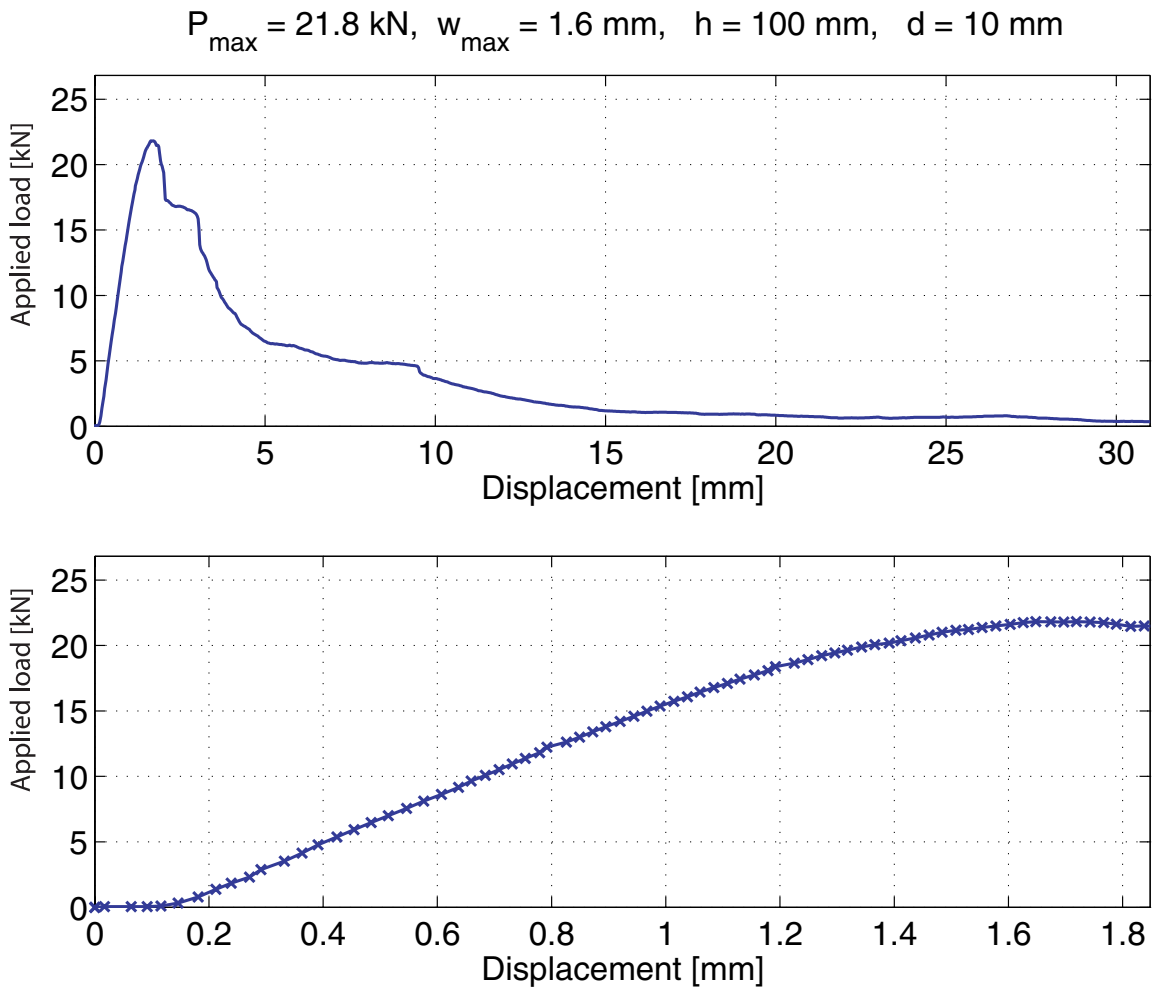

Figure A.16: *Load-deflection curve for the anchor pull-out*

A.2.8 Stretcher arrangement, d = 10 mm, h = 120 mm

Figure A.17: *The failure mode observed*

Failure mode: Sliding failure

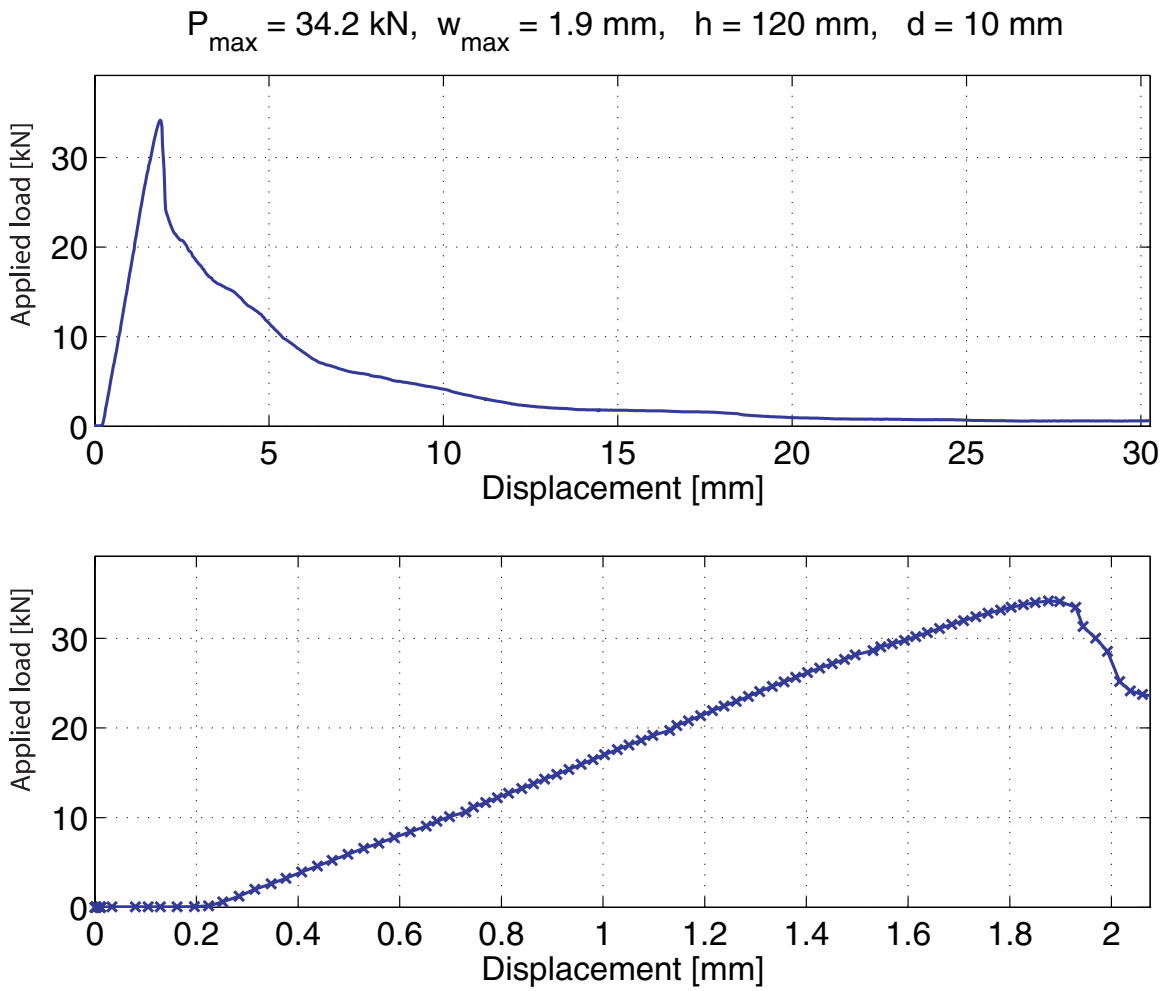

Figure A.18: *Load-deflection curve for the anchor pull-out*

A.2.9 Stretcher arrangement, d = 10 mm, h = 140 mm

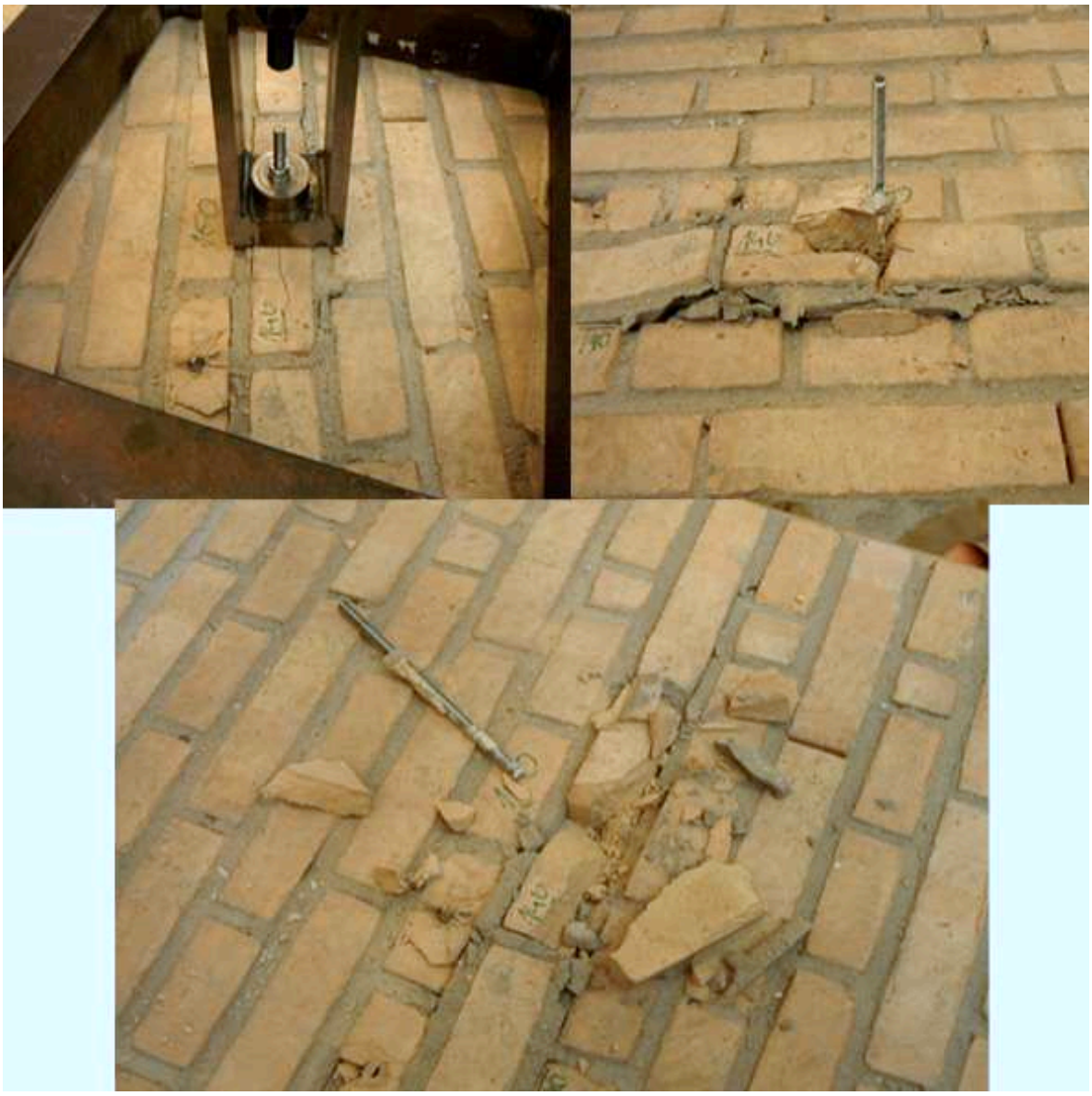

Figure A.19: *The failure mode observed*

Failure mode: Sliding failure

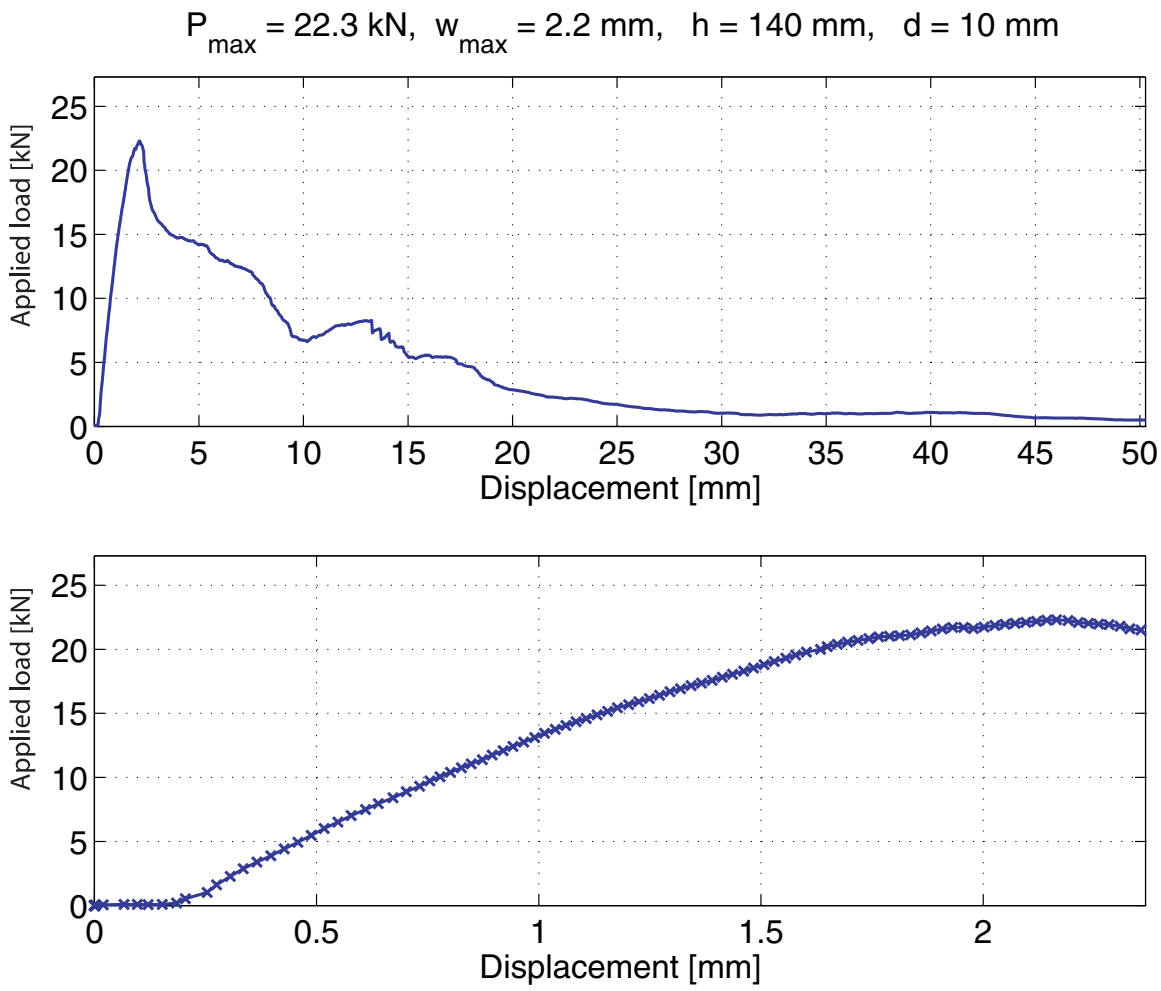

Figure A.20: *Load-deflection curve for the anchor pull-out*

A.2.10 Stretcher arrangement, d = 10 mm, h = 160 mm

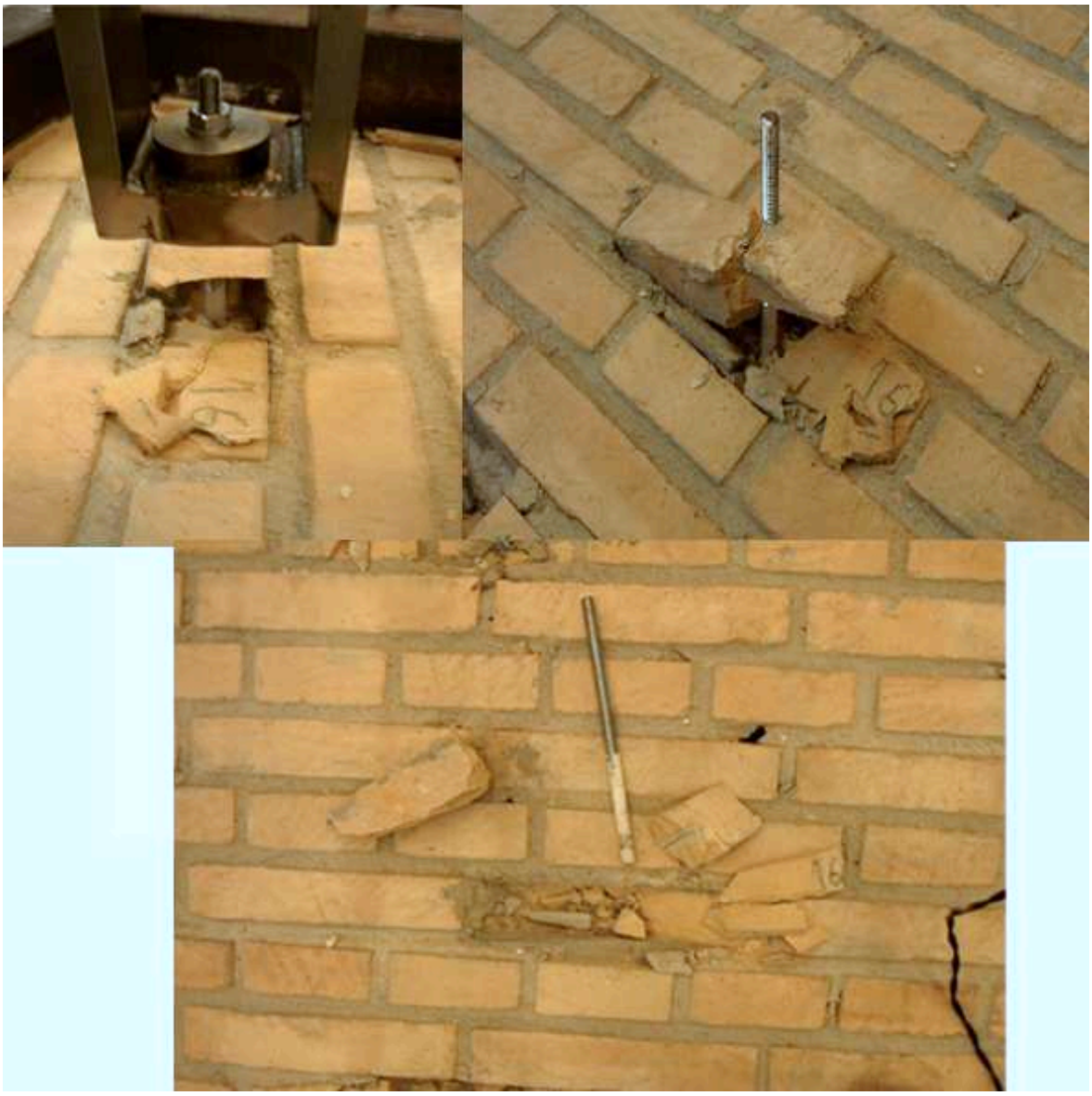

Figure A.21: *The failure mode observed*

Failure mode: Combined brick pull-out and sliding failure

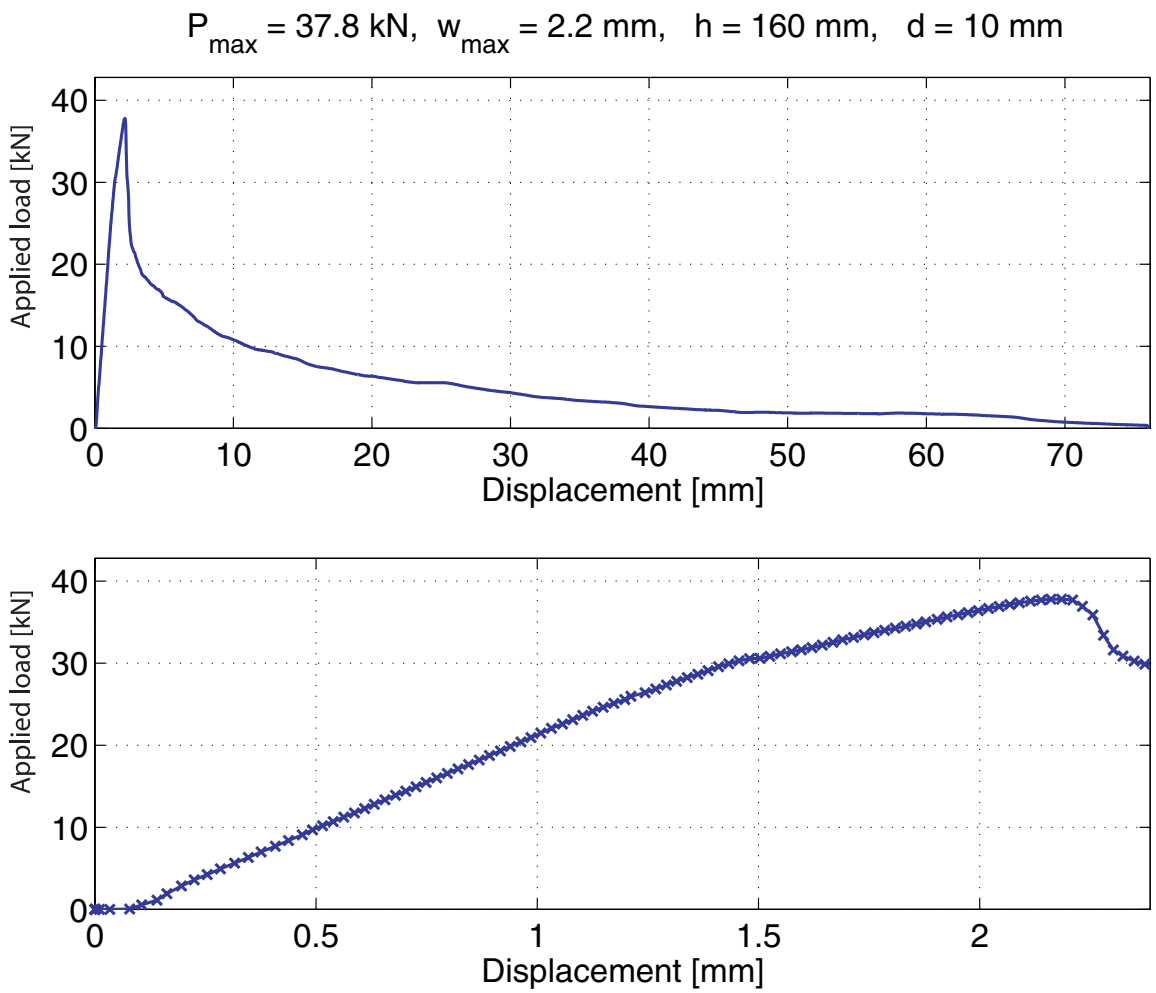

Figure A.22: *Load-deflection curve for the anchor pull-out*

A.2.11 Stretcher arrangement, d = 12 mm, h = 100 mm

Figure A.23: *The failure mode observed*

Failure mode: Combined brick pull-out and sliding failure

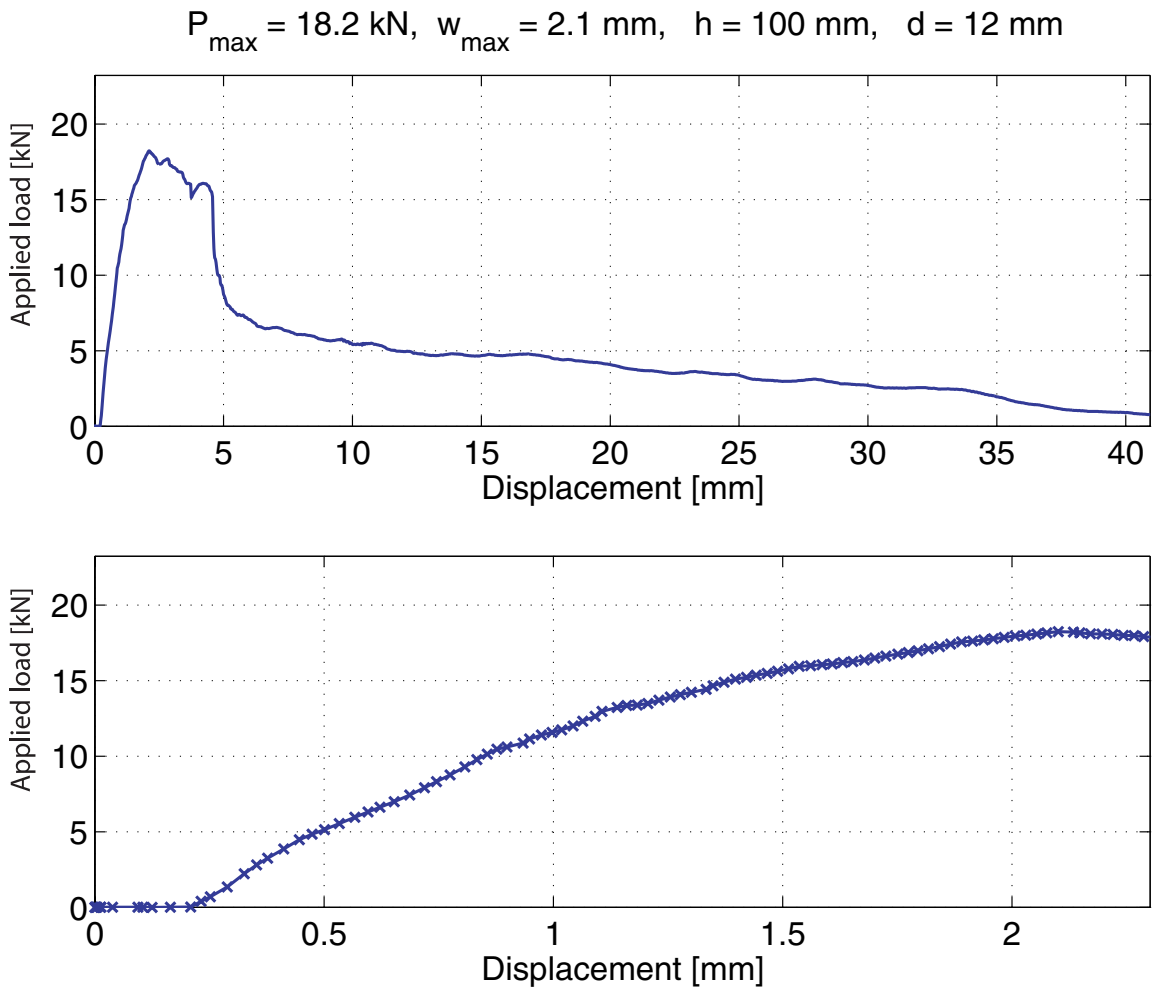

Figure A.24: *Load-deflection curve for the anchor pull-out*

A.2.12 Stretcher arrangement, d = 12 mm, h = 120 mm

Figure A.25: *The failure mode observed*

Failure mode: Sliding failure

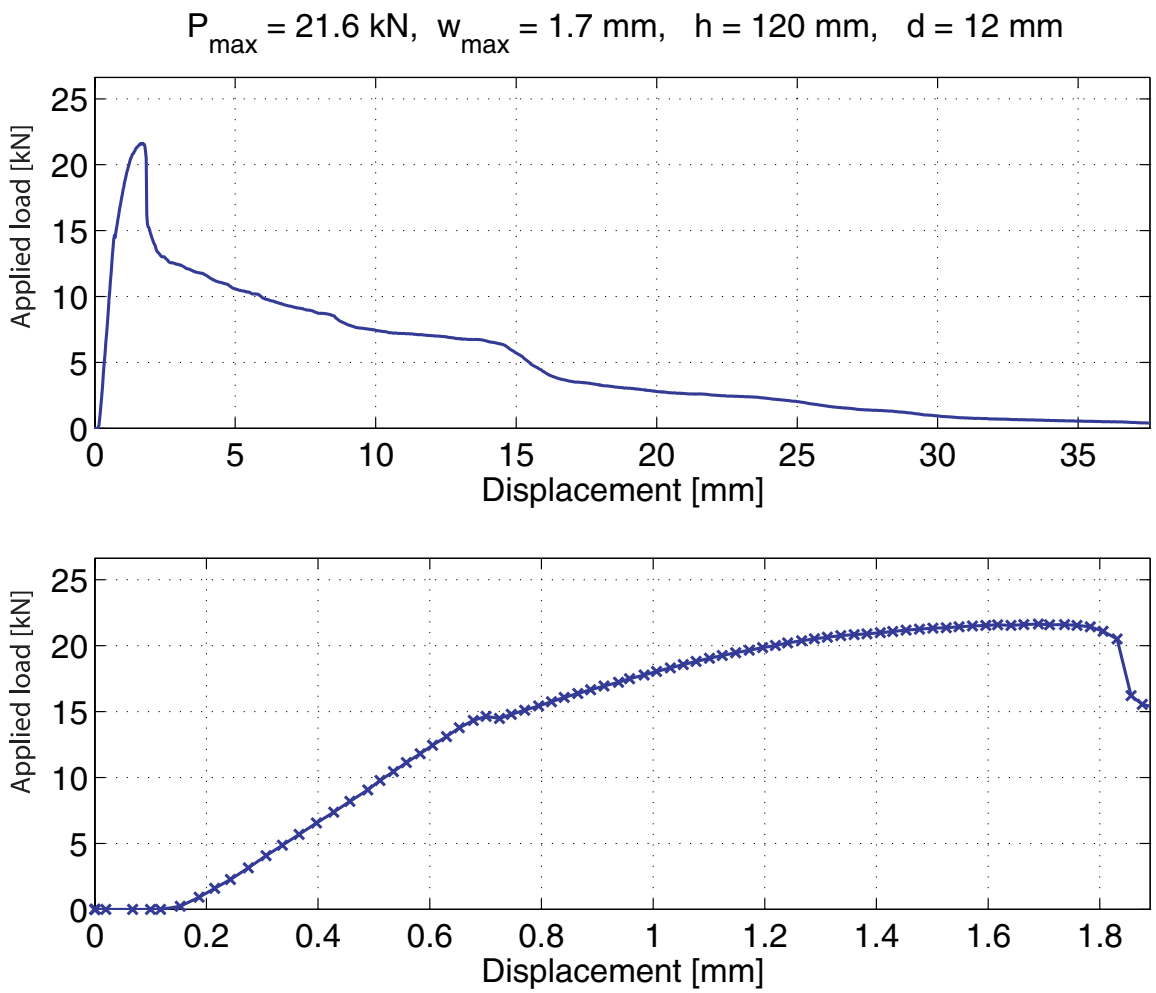

Figure A.26: *Load-deflection curve for the anchor pull-out*

A.2.13 Stretcher arrangement, d = 12 mm, h = 140 mm

Figure A.27: *The failure mode observed*

Failure mode: Sliding failure

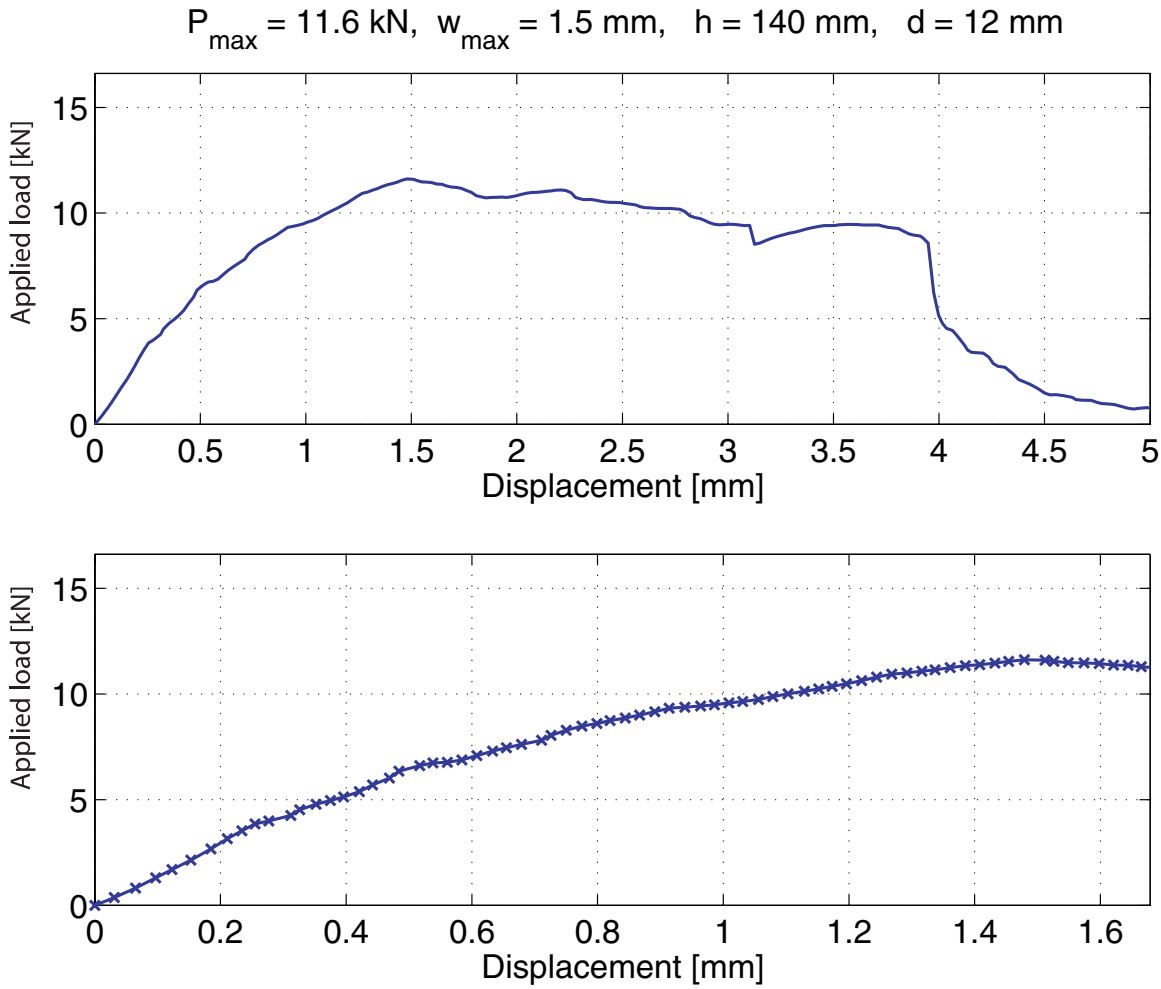

Figure A.28: *Load-deflection curve for the anchor pull-out*

A.2.14 Stretcher arrangement, d = 12 mm, h = 160 mm

Figure A.29: *The failure mode observed*

Failure mode: Brick-cone failure

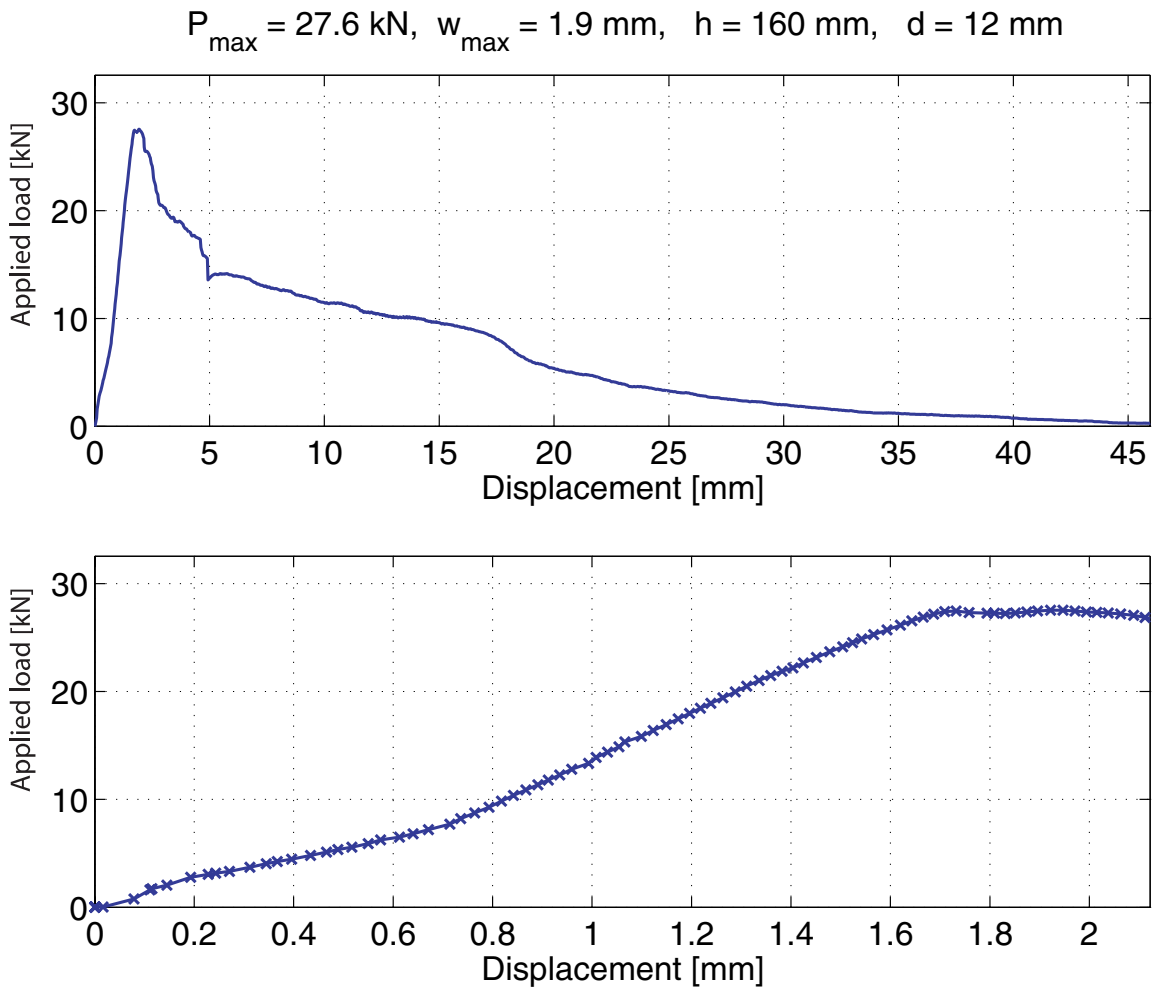

Figure A.30: *Load-deflection curve for the anchor pull-out*

A.2.15 Stretcher arrangement, d = 16 mm, h = 100 mm

Figure A.31: *The failure mode observed*

Failure mode: Brick-cone failure failure

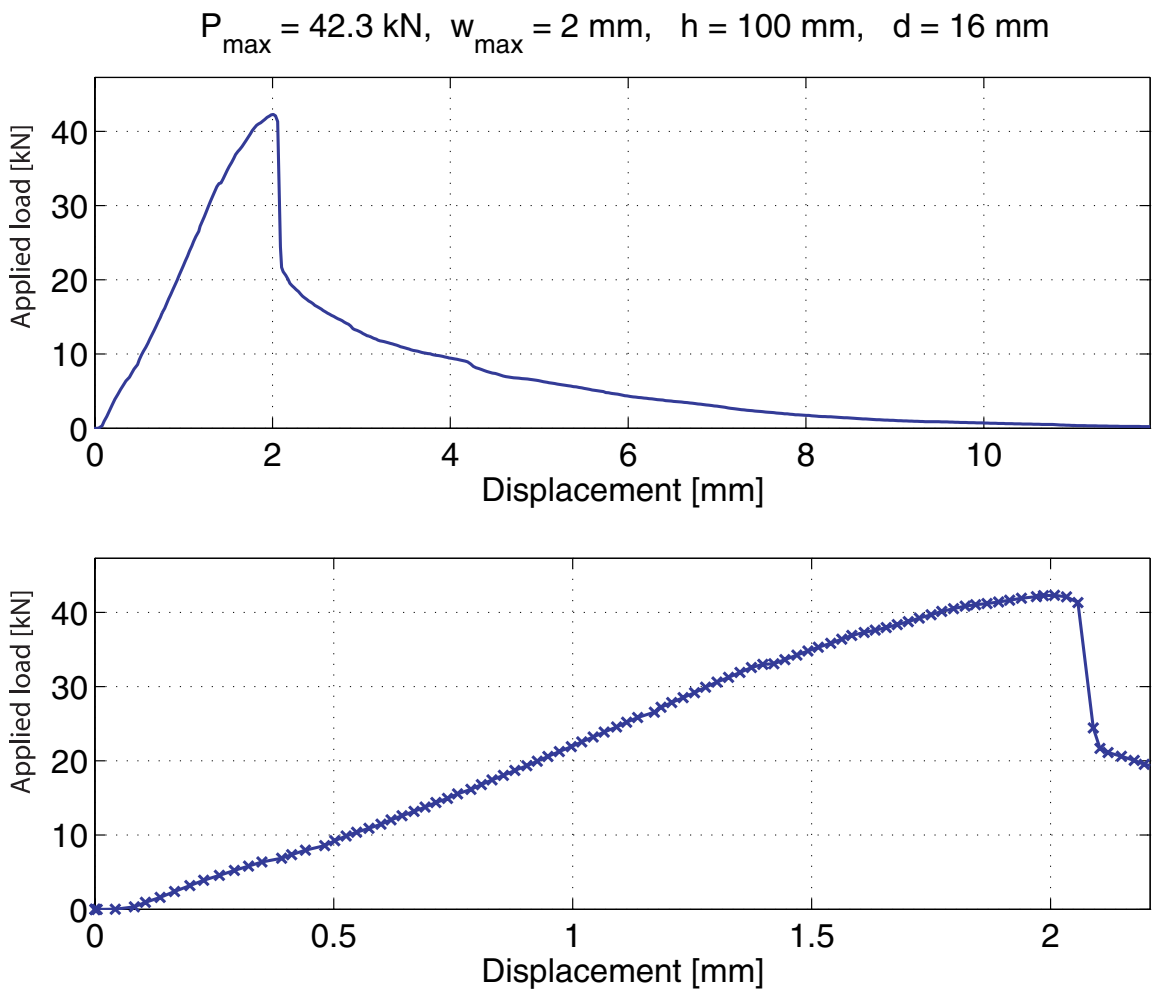

Figure A.32: *Load-deflection curve for the anchor pull-out*

A.2.16 Stretcher arrangement, d = 16 mm, h = 120 mm

Figure A.33: *The failure mode observed*

Failure mode: Brick-cone failure

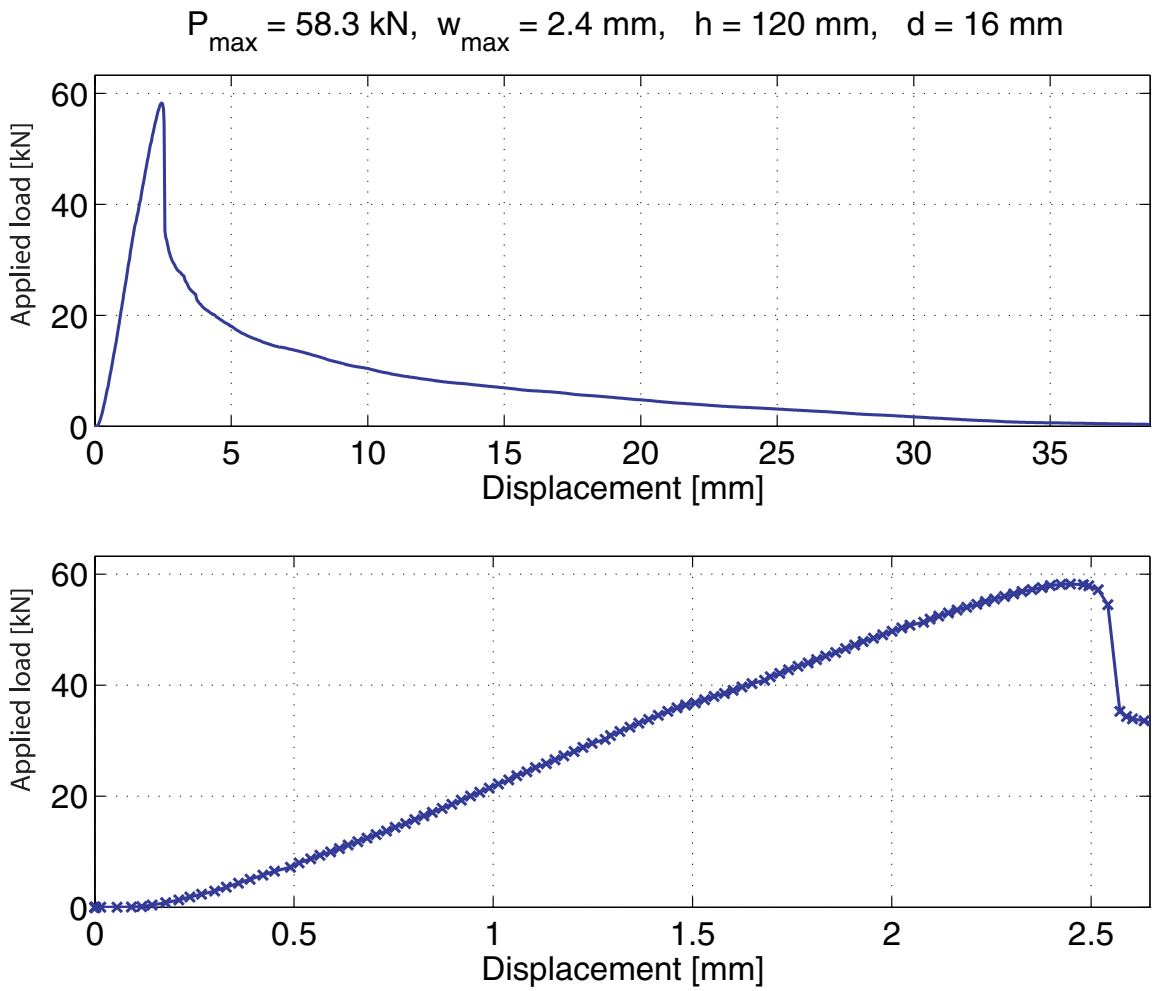

Figure A.34: *Load-deflection curve for the anchor pull-out*

A.2.17 Stretcher arrangement, d = 16 mm, h = 140 mm

Figure A.35: *The failure mode observed*

Failure mode: Brick-cone failure

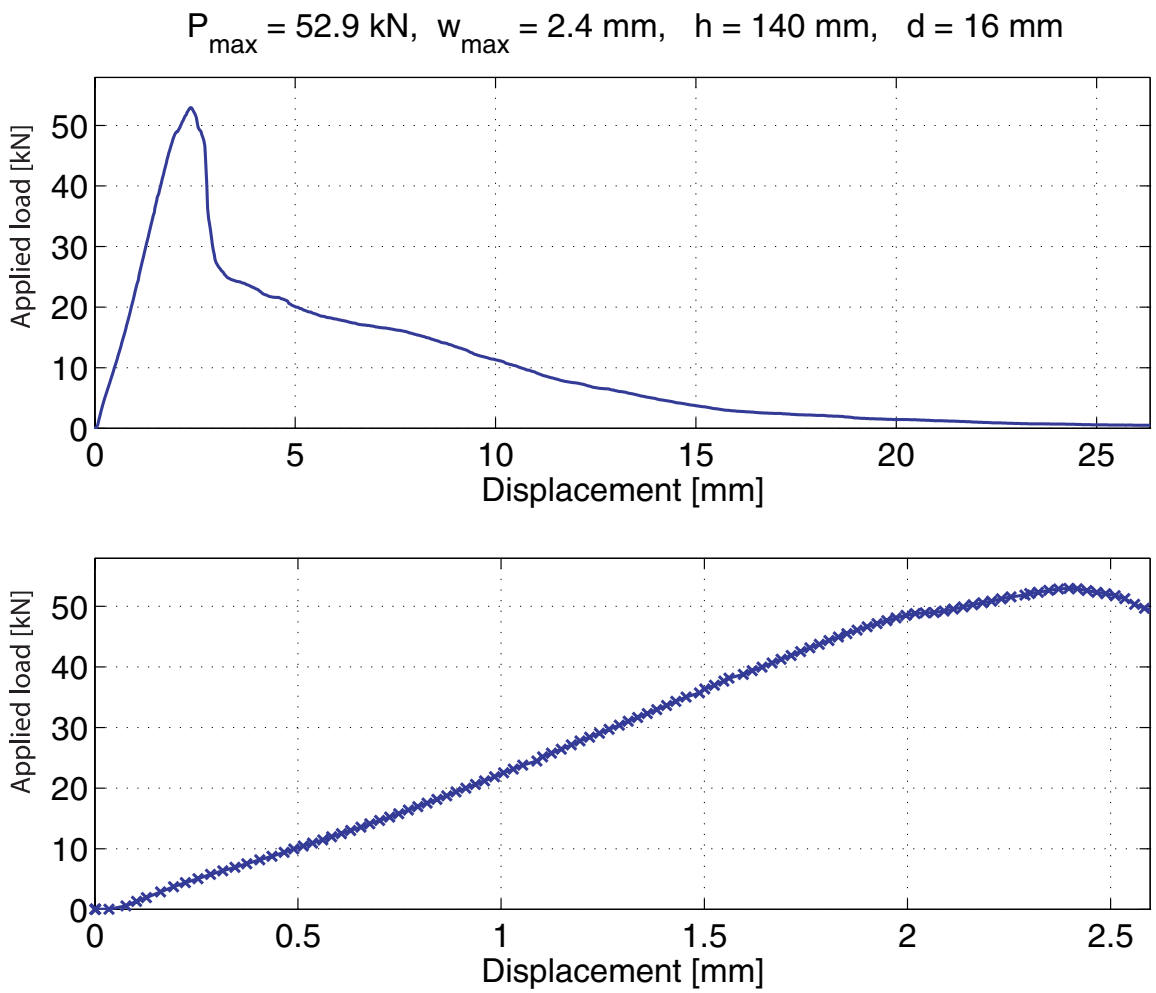

Figure A.36: *Load-deflection curve for the anchor pull-out*

A.2.18 Stretcher arrangement, d = 16 mm, h = 140 mm

Figure A.37: *The failure mode observed*

Failure mode: Sliding failure

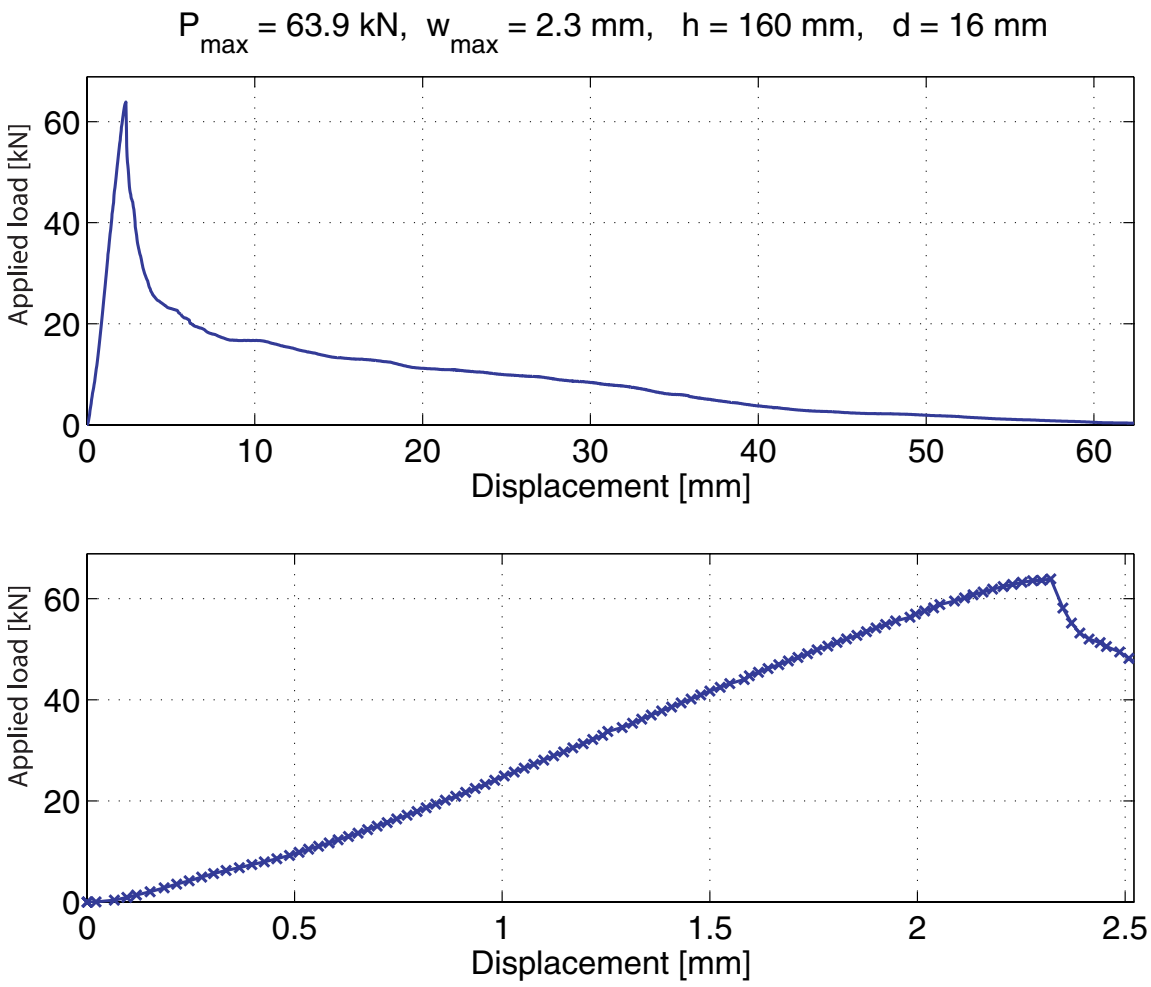

Figure A.38: *Load-deflection curve for the anchor pull-out*

A.2.19 Header arrangement - 1, d = 12 mm

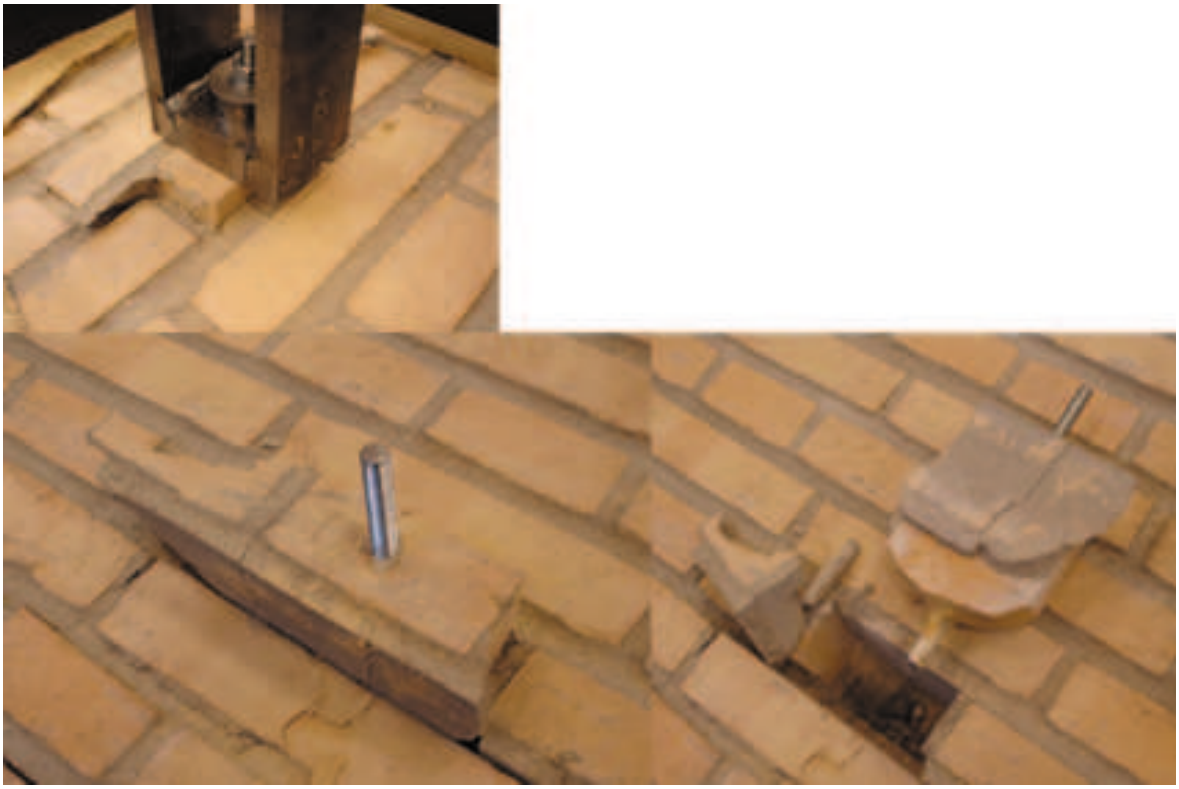

Figure A.39: *The failure mode observed*

Failure mode: Combined brick pull-out and sliding failure

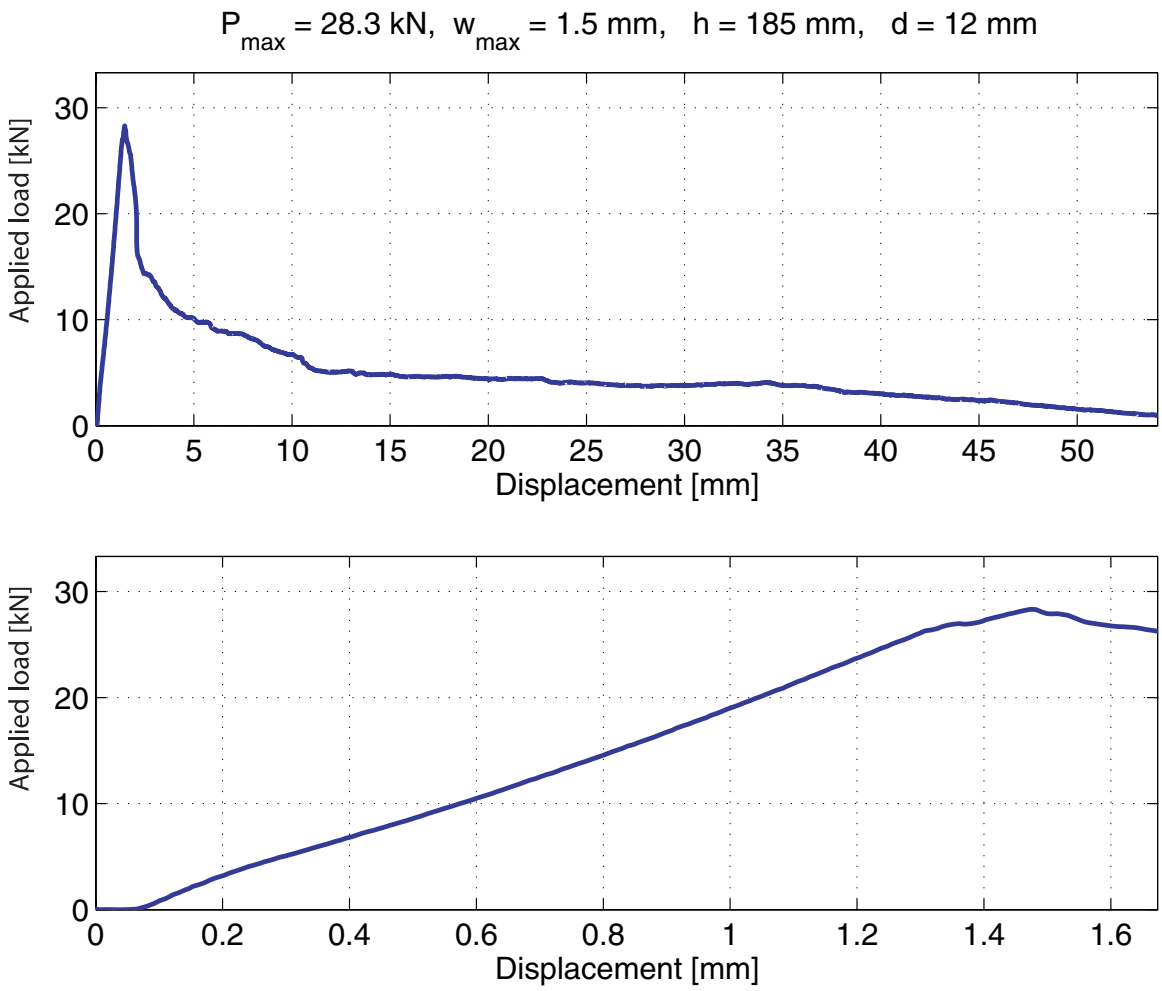

Figure A.40: *Load-deflection curve for the anchors pull-out*

A.2.20 Header arrangement - 2, d = 12 mm

Figure A.41: *The failure mode observed*

Failure mode: Sliding failure

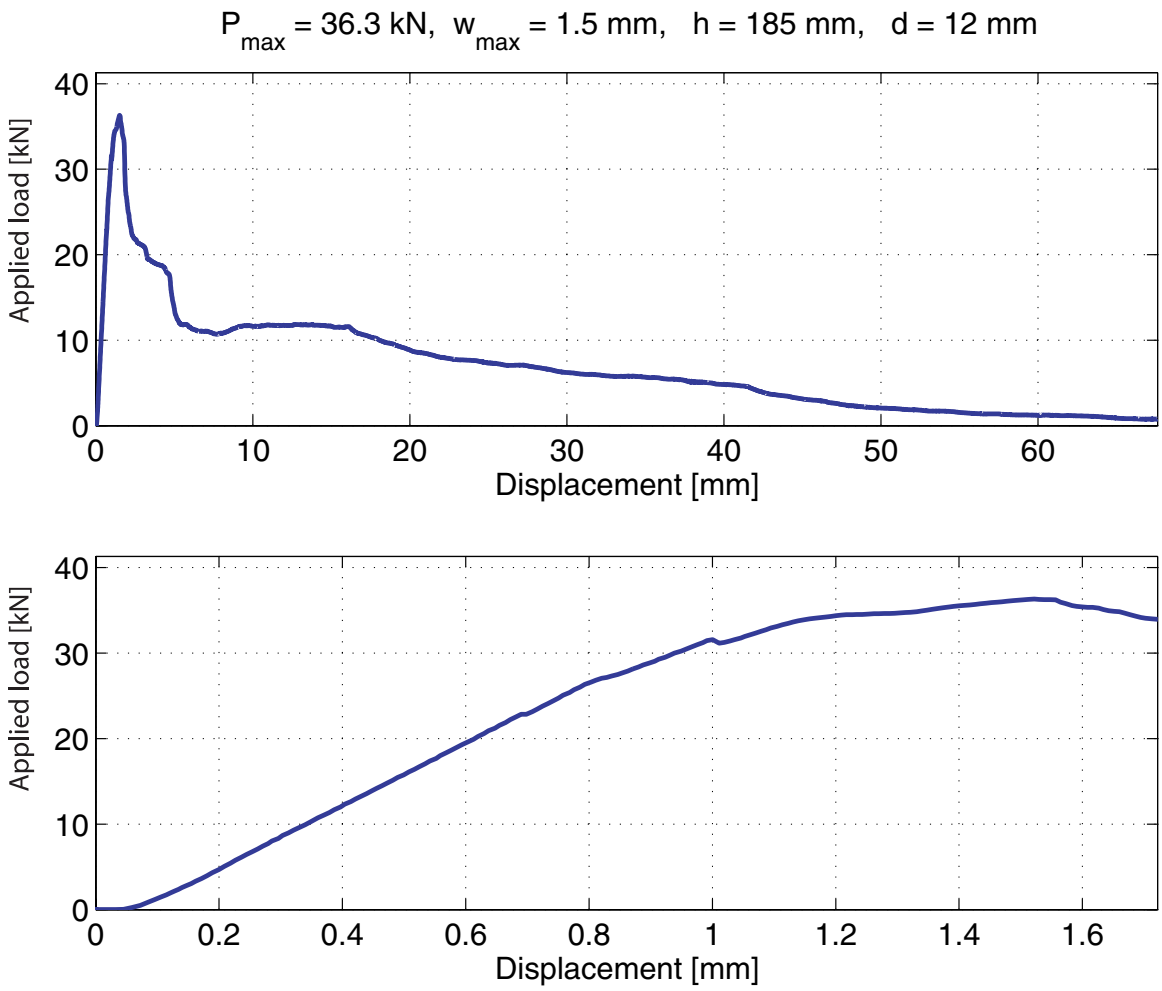

Figure A.42: *Load-deflection curve for the anchors pull-out*

A.2.21 Header arrangement - 3, d = 12 mm

Figure A.43: *The failure mode observed*

Failure mode: Combined brick pull-out and sliding failure

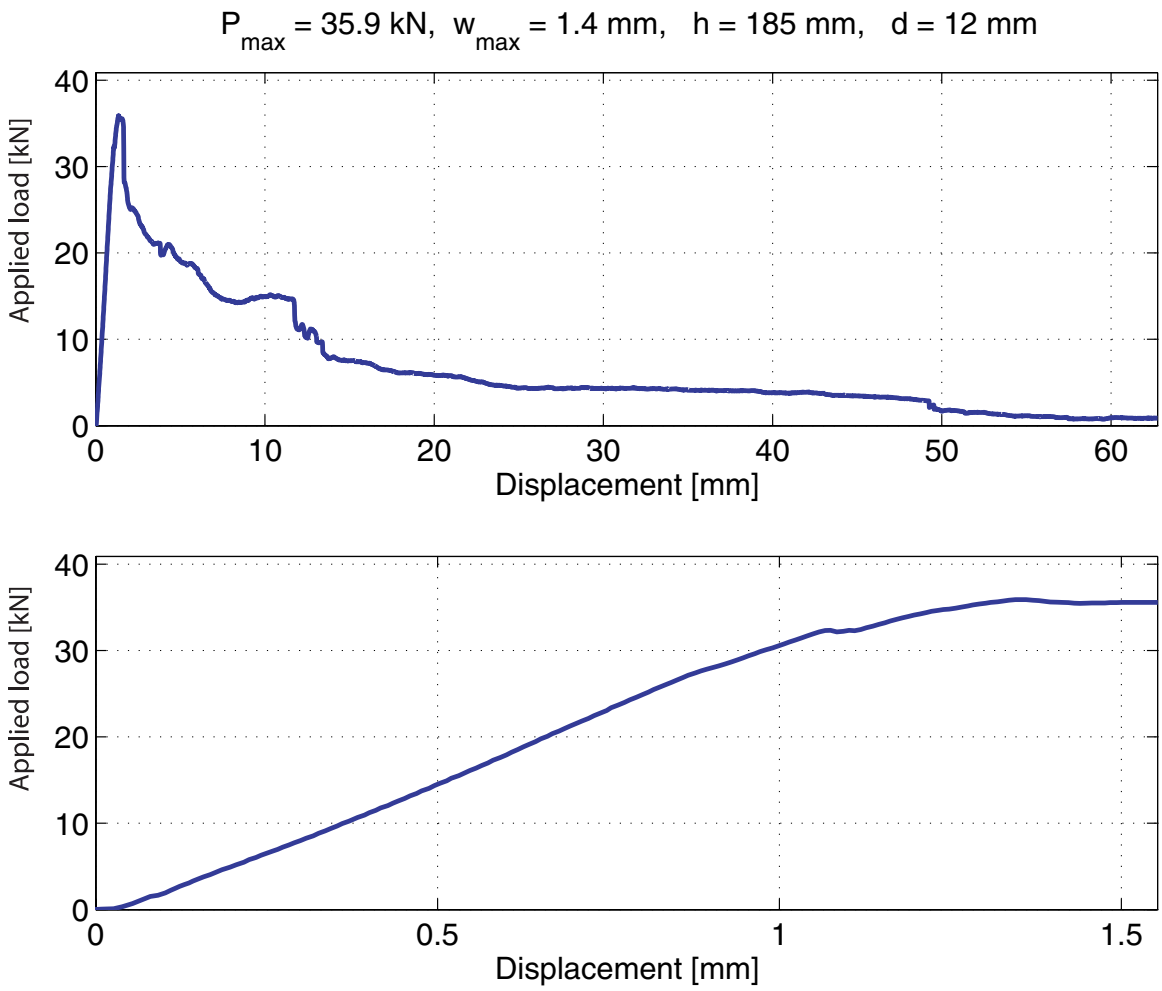

Figure A.44: *Load-deflection curve for the anchors pull-out*

A.2.22 Header arrangement - 1, d = 16 mm

Figure A.45: *The failure mode observed*

Failure mode: Combined brick pull-out and sliding failure

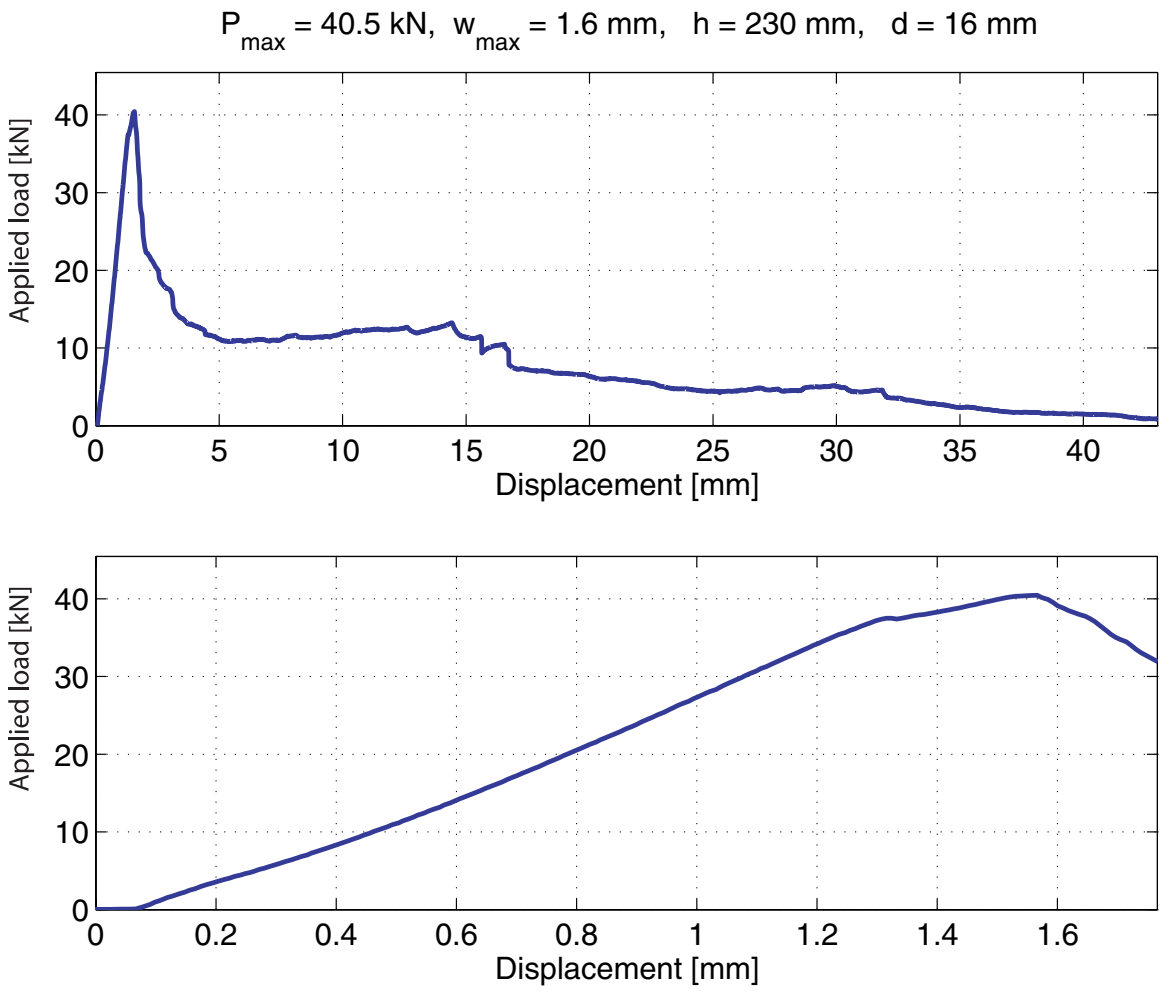

Figure A.46: *Load-deflection curve for the anchors pull-out*

A.2.23 Header arrangement - 2, d = 16 mm

Figure A.47: *The failure mode observed*

Failure mode: Combined brick pull-out and sliding failure

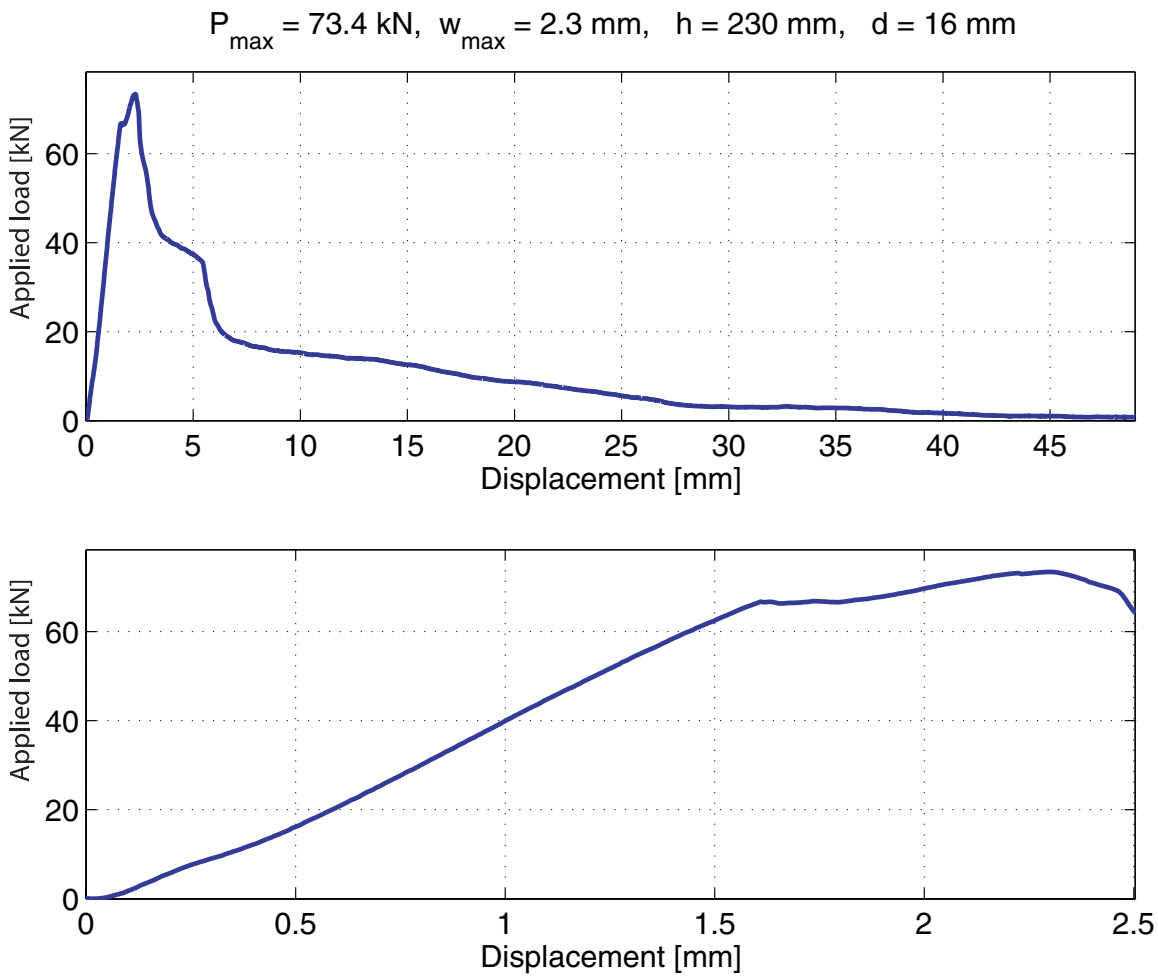

Figure A.48: *Load-deflection curve for the anchors pull-out*

A.2.24 Header arrangement - 3, d = 16 mm

Figure A.49: *The failure mode observed*

Failure mode: Combined brick pull-out and sliding failure

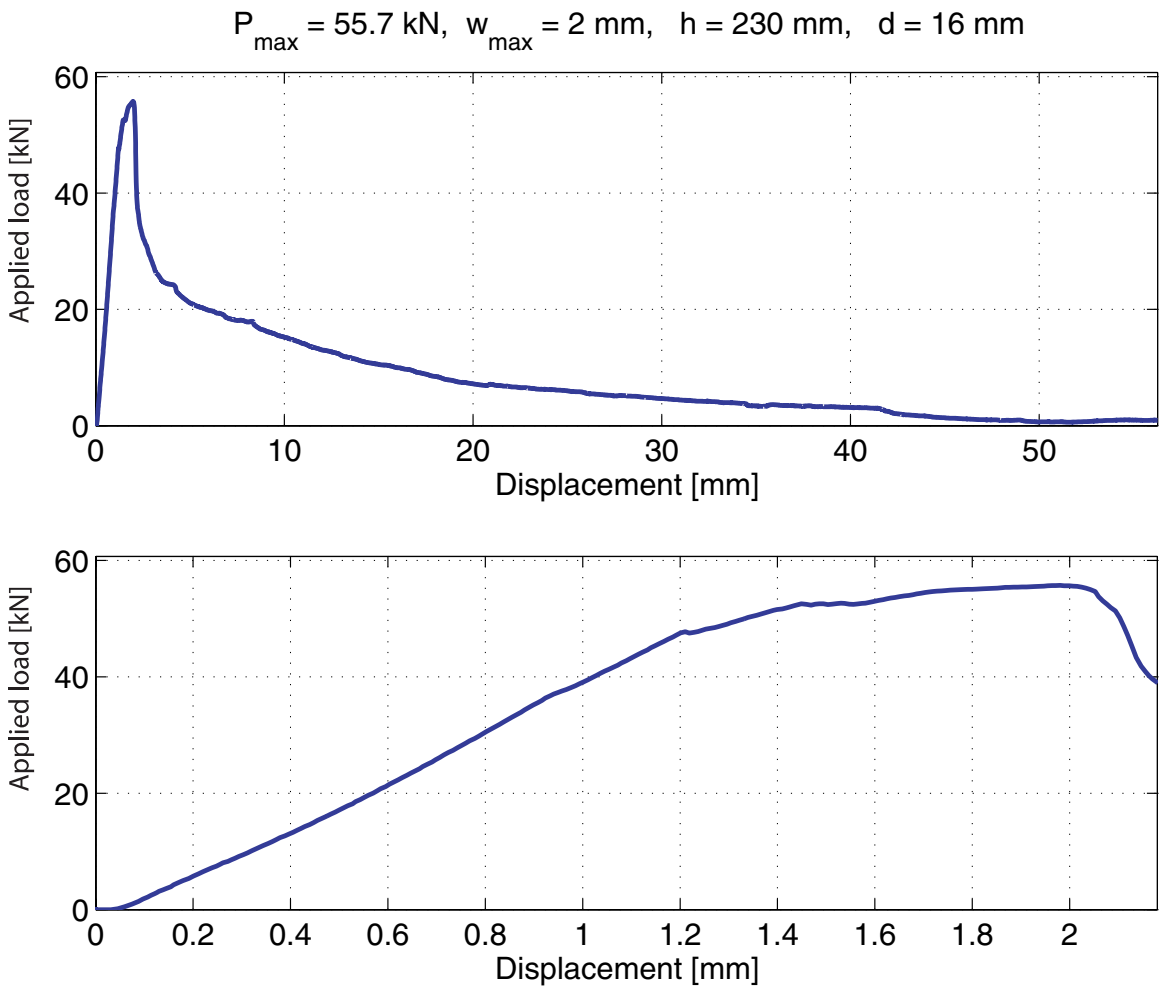

Figure A.50: *Load-deflection curve for the anchors pull-out*

A.2.25 Header arrangement, d = 10 mm, h = 90 mm

Figure A.51: *The failure mode observed*

Failure mode: Sliding failure

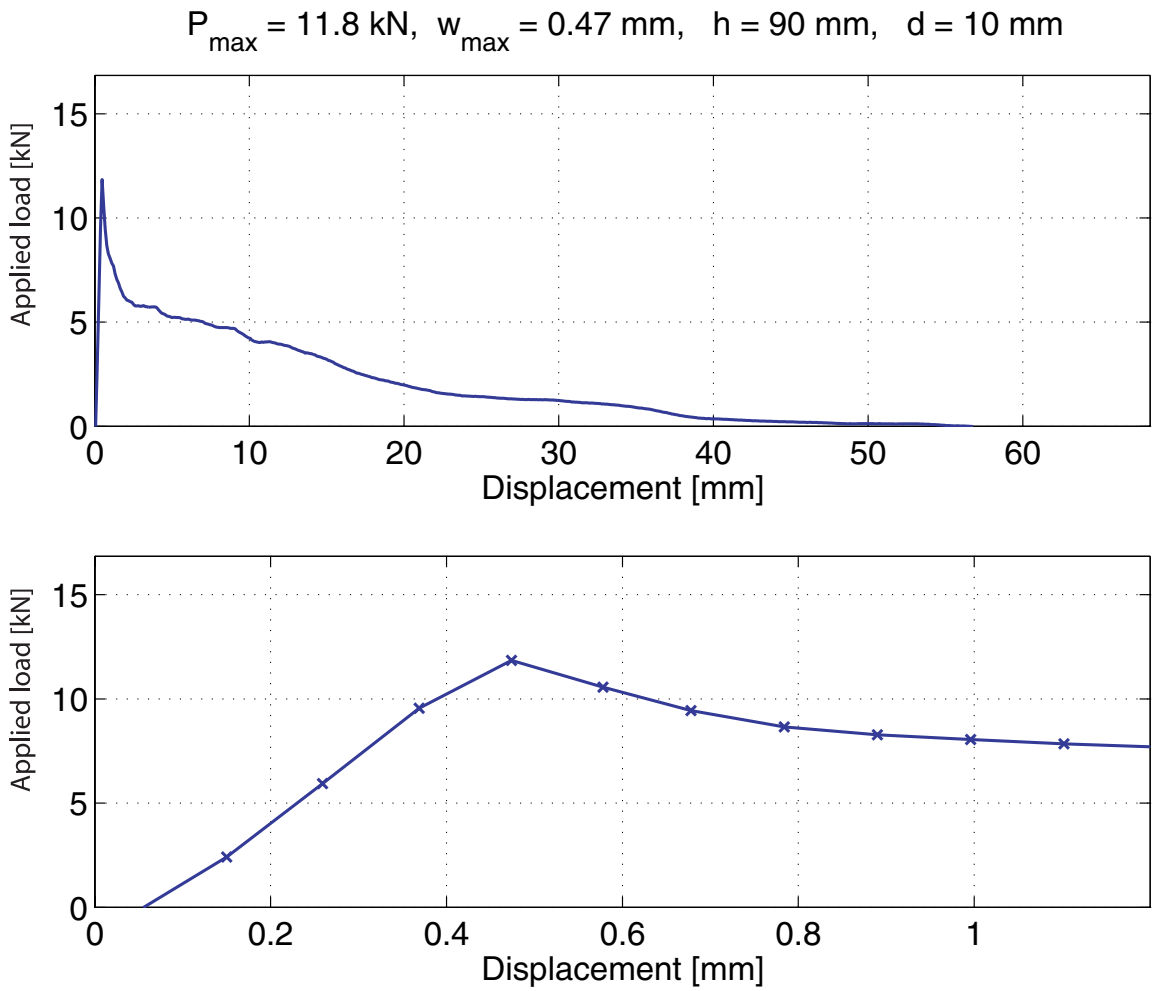

Figure A.52: *Load-deflection curve for the anchor pull-out*

A.2.26 Header arrangement, d = 10 mm, h = 100 mm

Figure A.53: *The failure mode observed*

Failure mode: Combined brick pull-out and sliding failure

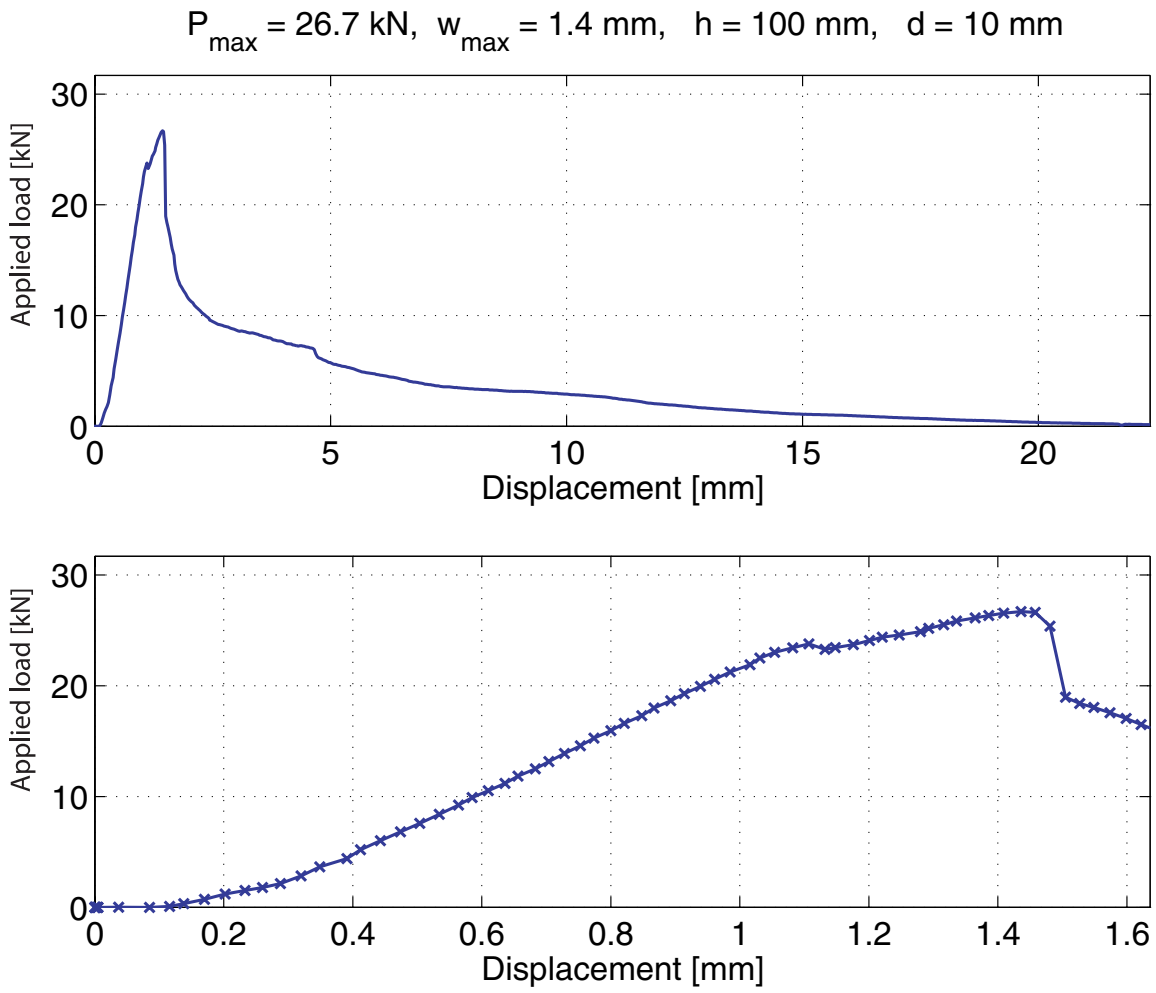

Figure A.54: *Load-deflection curve for the anchor pull-out*

A.2.27 Header arrangement, d = 10 mm, h = 110 mm

Figure A.55: *The failure mode observed*

Failure mode: Combined brick pull-out and sliding failure

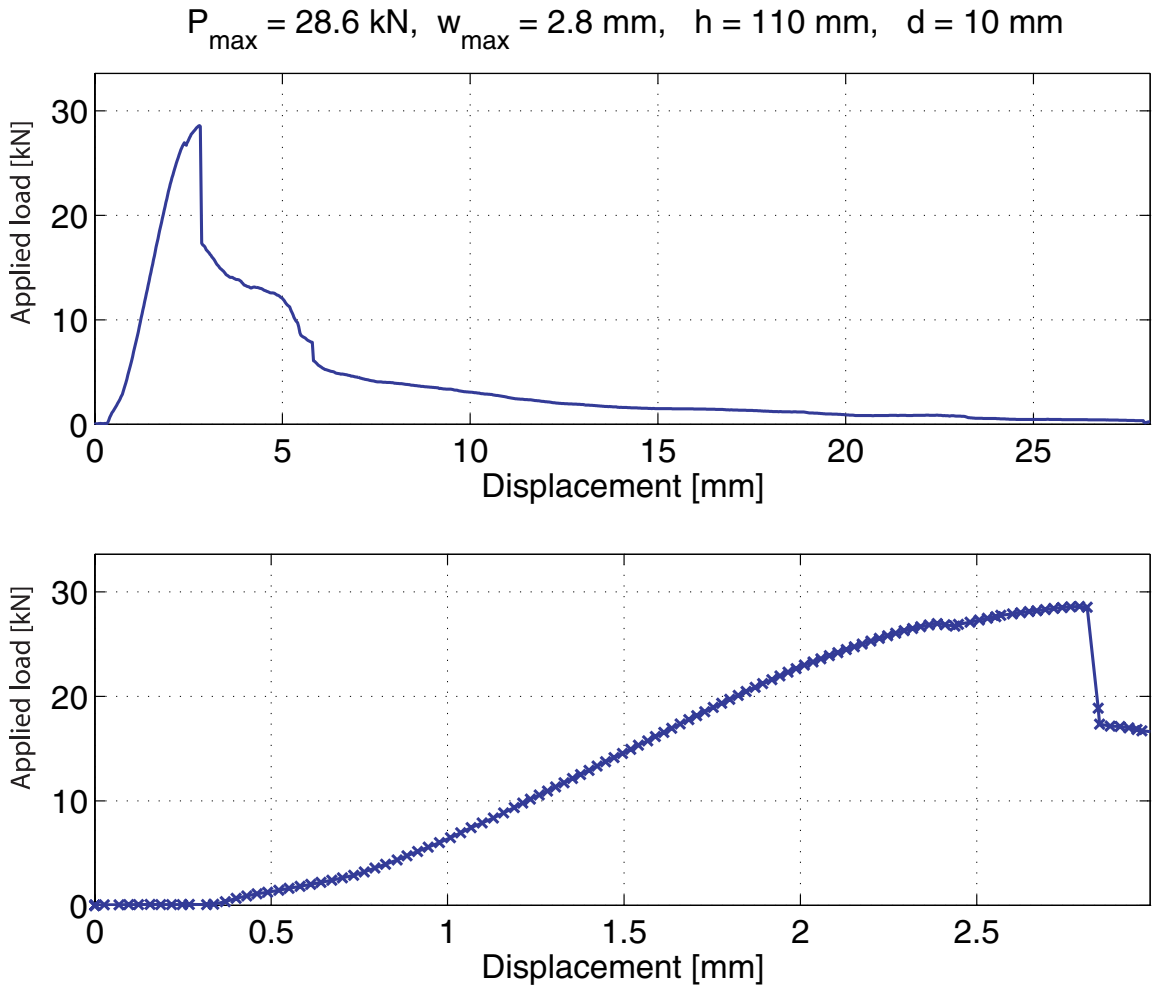

Figure A.56: *Load-deflection curve for the anchor pull-out*

A.2.28 Header arrangement, d = 10 mm, h = 120 mm

Figure A.57: *The failure mode observed*

Failure mode: Combined brick pull-out and sliding failure

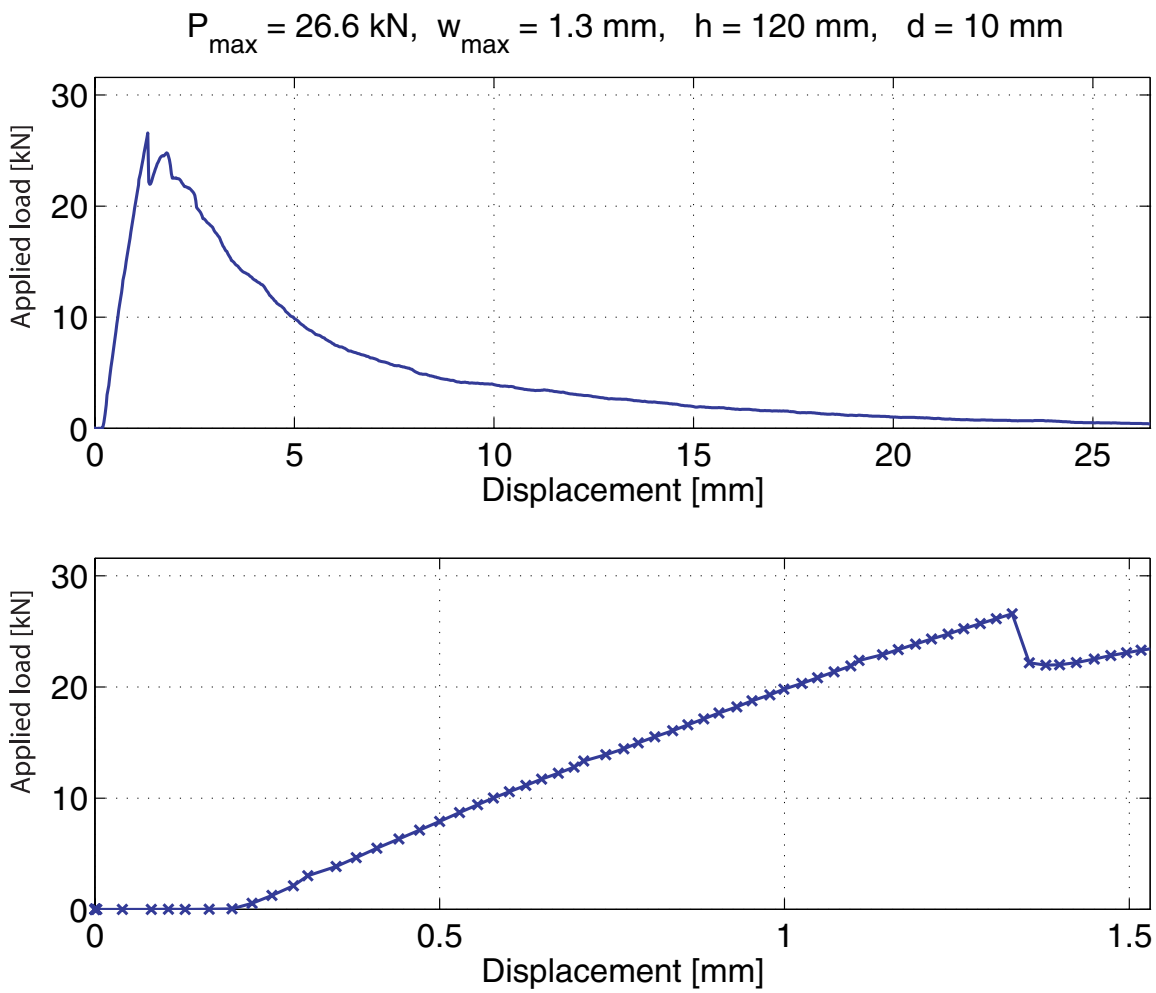

Figure A.58: *Load-deflection curve for the anchor pull-out*

A.2.29 Header arrangement, d = 10 mm, h = 130 mm

Figure A.59: *The failure mode observed*

Failure mode: Combined brick pull-out and sliding failure

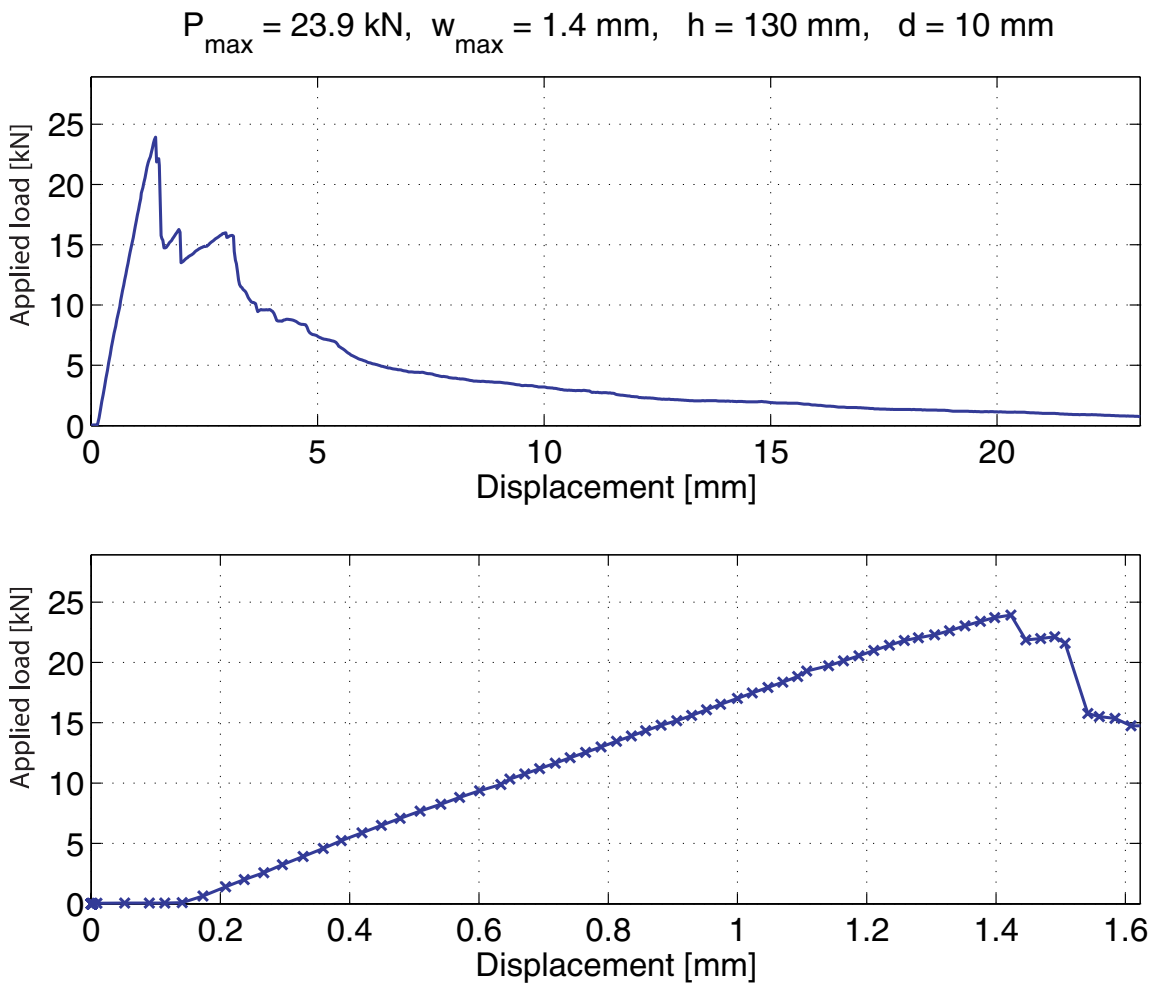

Figure A.60: *Load-deflection curve for the anchor pull-out*

A.2.30 Header arrangement, d = 10 mm, h = 140 mm

Figure A.61: *The failure mode observed*

Failure mode: Combined brick pull-out and sliding failure

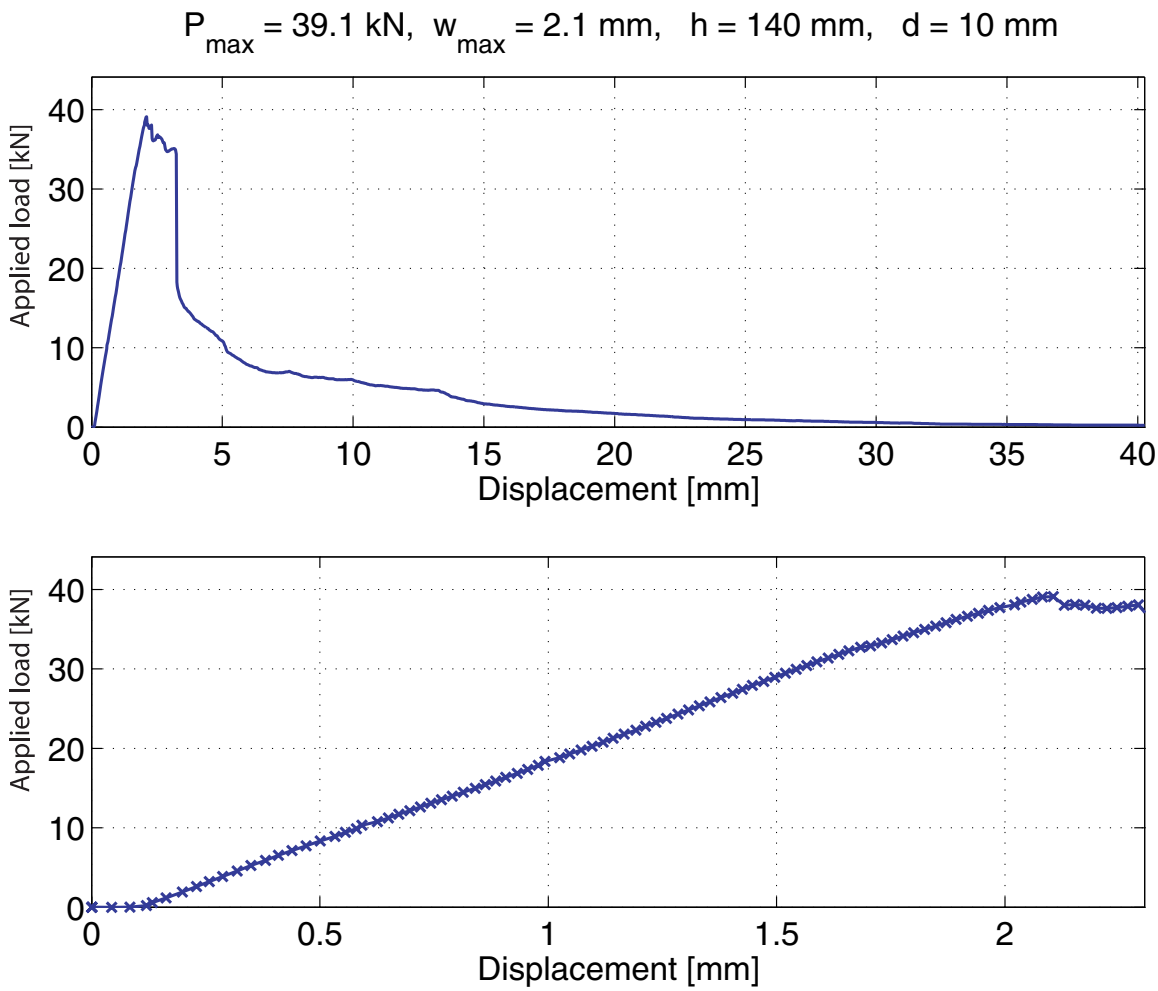

Figure A.62: *Load-deflection curve for the anchor pull-out*

A.2.31 Header arrangement, d = 10 mm, h = 150 mm

Figure A.63: *The failure mode observed*

Failure mode: Combined brick pull-out and sliding failure

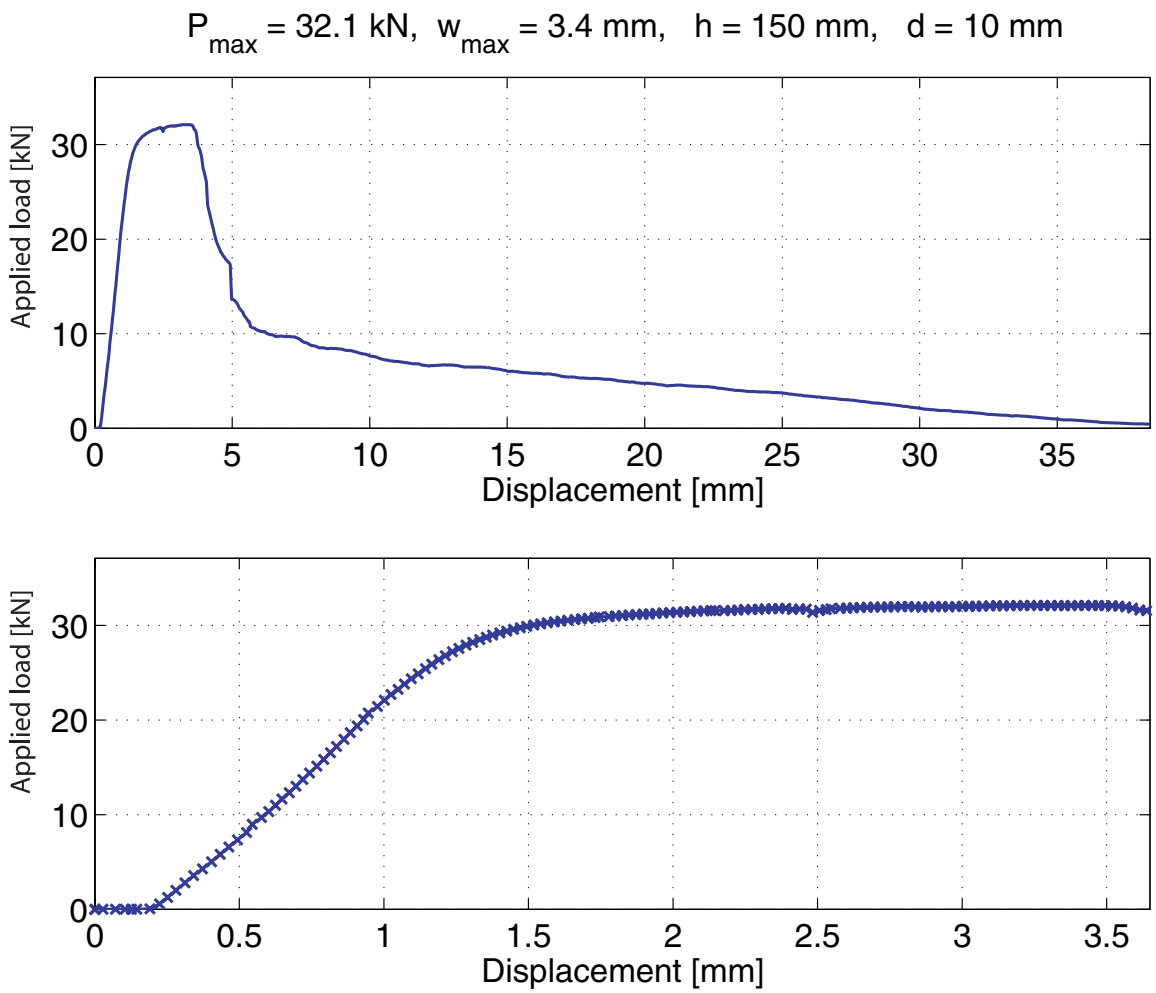

Figure A.64: *Load-deflection curve for the anchor pull-out*

A.2.32 Header arrangement, d = 10 mm, h = 160 mm

Figure A.65: *The failure mode observed*

Failure mode: Sliding failure

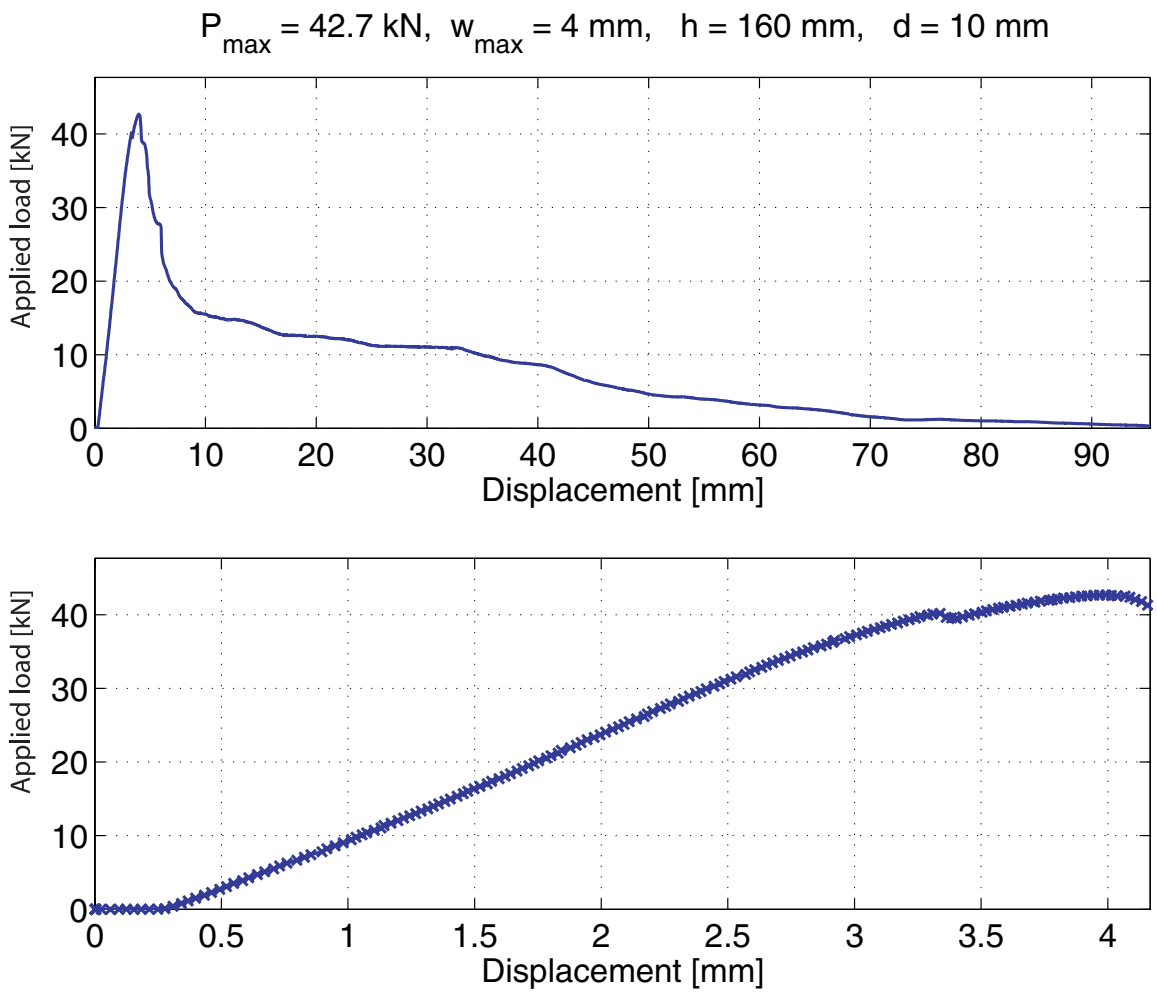

Figure A.66: *Load-deflection curve for the anchor pull-out*

A.2.33 Header arrangement, d = 10 mm, h = 170 mm

Figure A.67: *The failure mode observed*

Failure mode: Combined brick pull-out and sliding failure

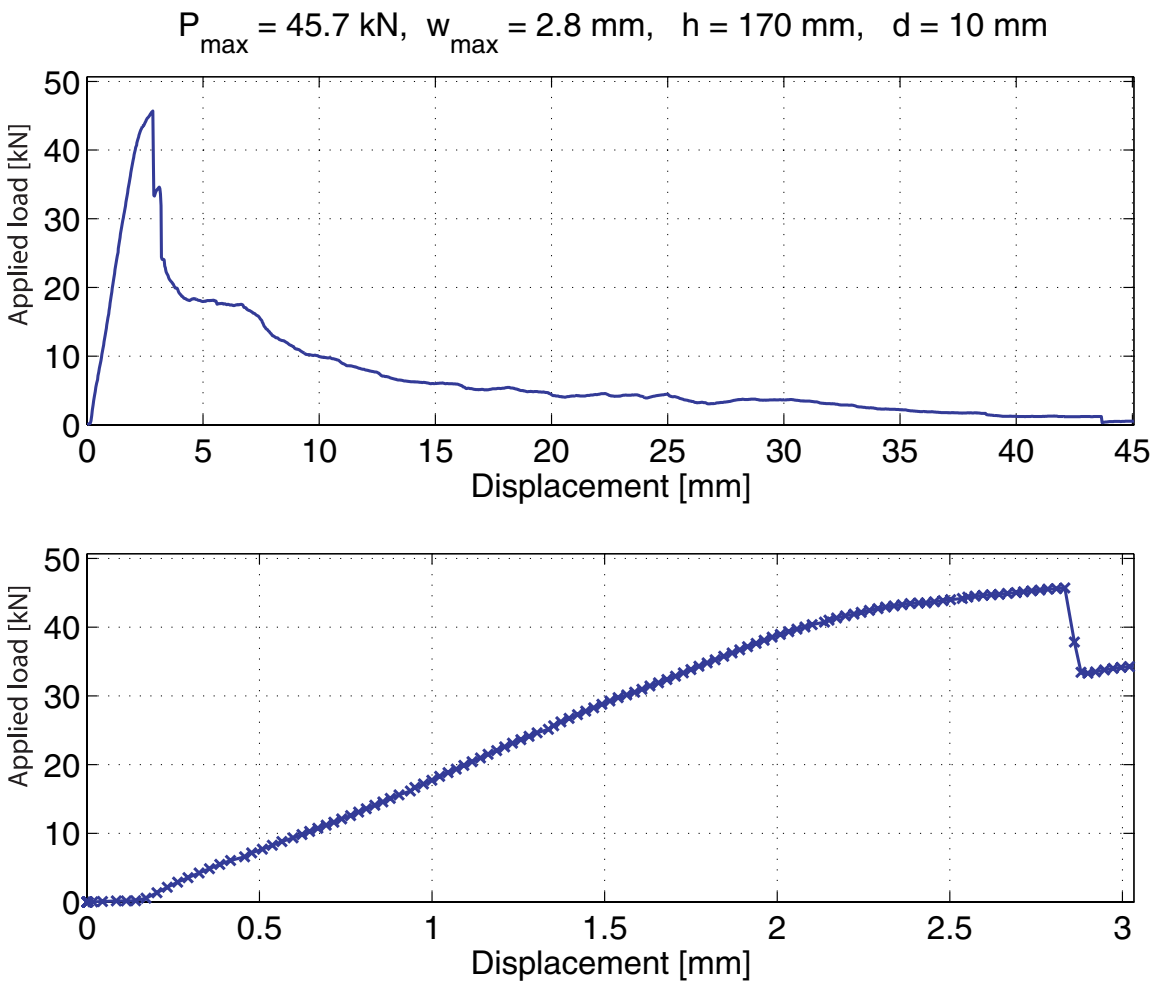

Figure A.68: *Load-deflection curve for the anchor pull-out*

A.2.34 Header arrangement, d = 12 mm, h = 100 mm

Figure A.69: *The failure mode observed*

Failure mode: Combined brick pull-out and sliding failure

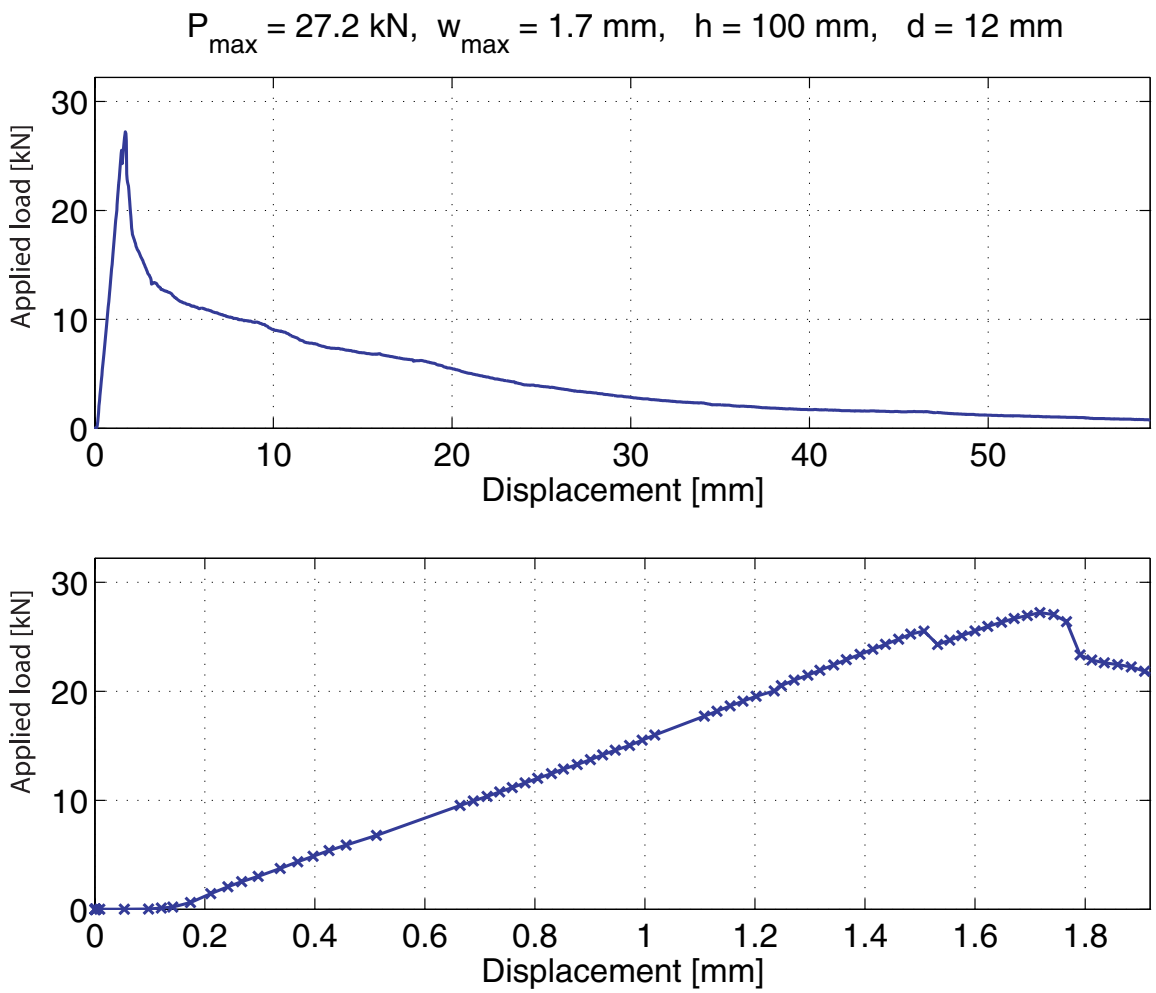

Figure A.70: *Load-deflection curve for the anchor pull-out*

A.2.35 Header arrangement, d = 12 mm, h = 120 mm

Figure A.71: *The failure mode observed*

Failure mode: Combined brick pull-out and sliding failure

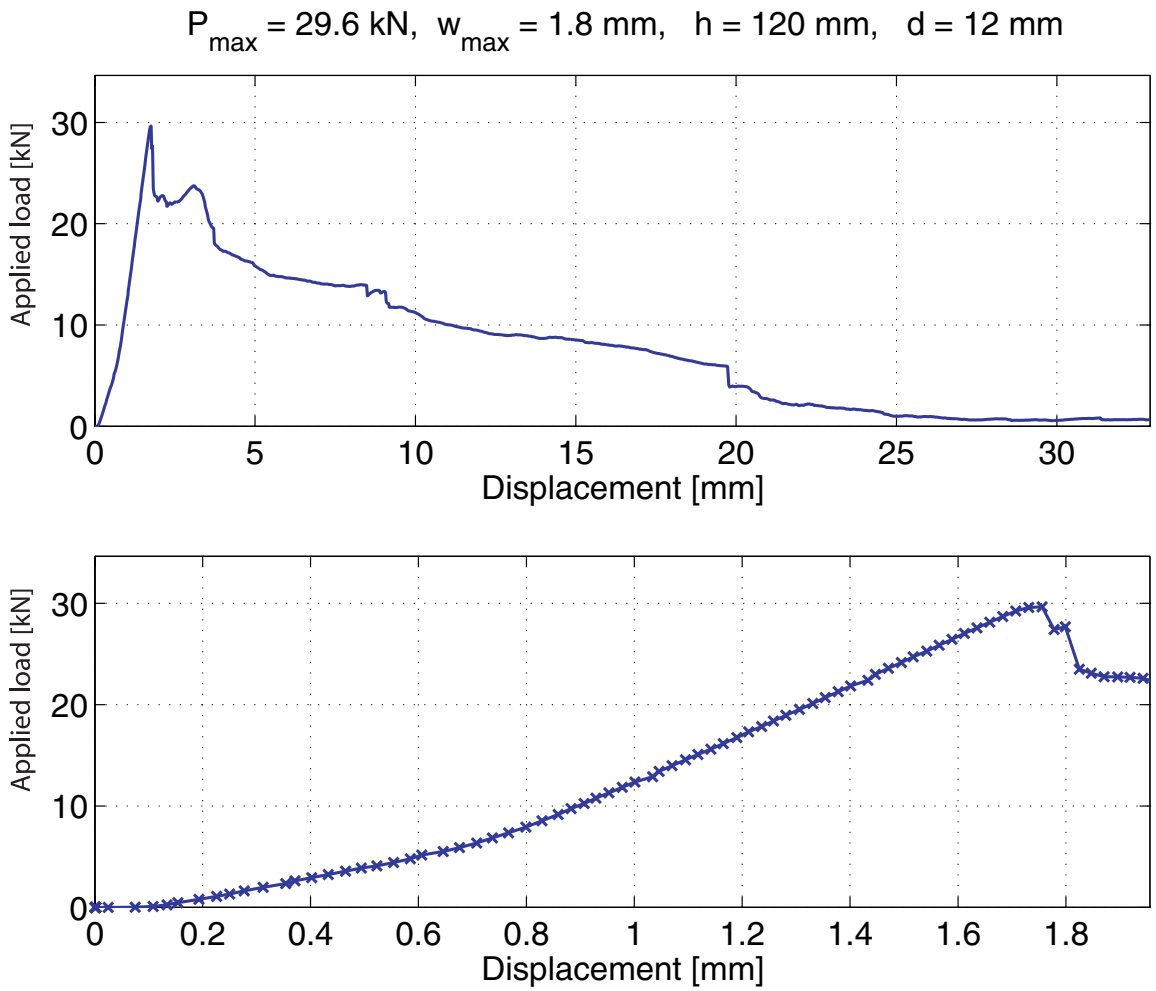

Figure A.72: *Load-deflection curve for the anchor pull-out*

A.2.36 Header arrangement, d = 12 mm, h = 140 mm

Figure A.73: *The failure mode observed*

Failure mode: Combined brick pull-out and sliding failure

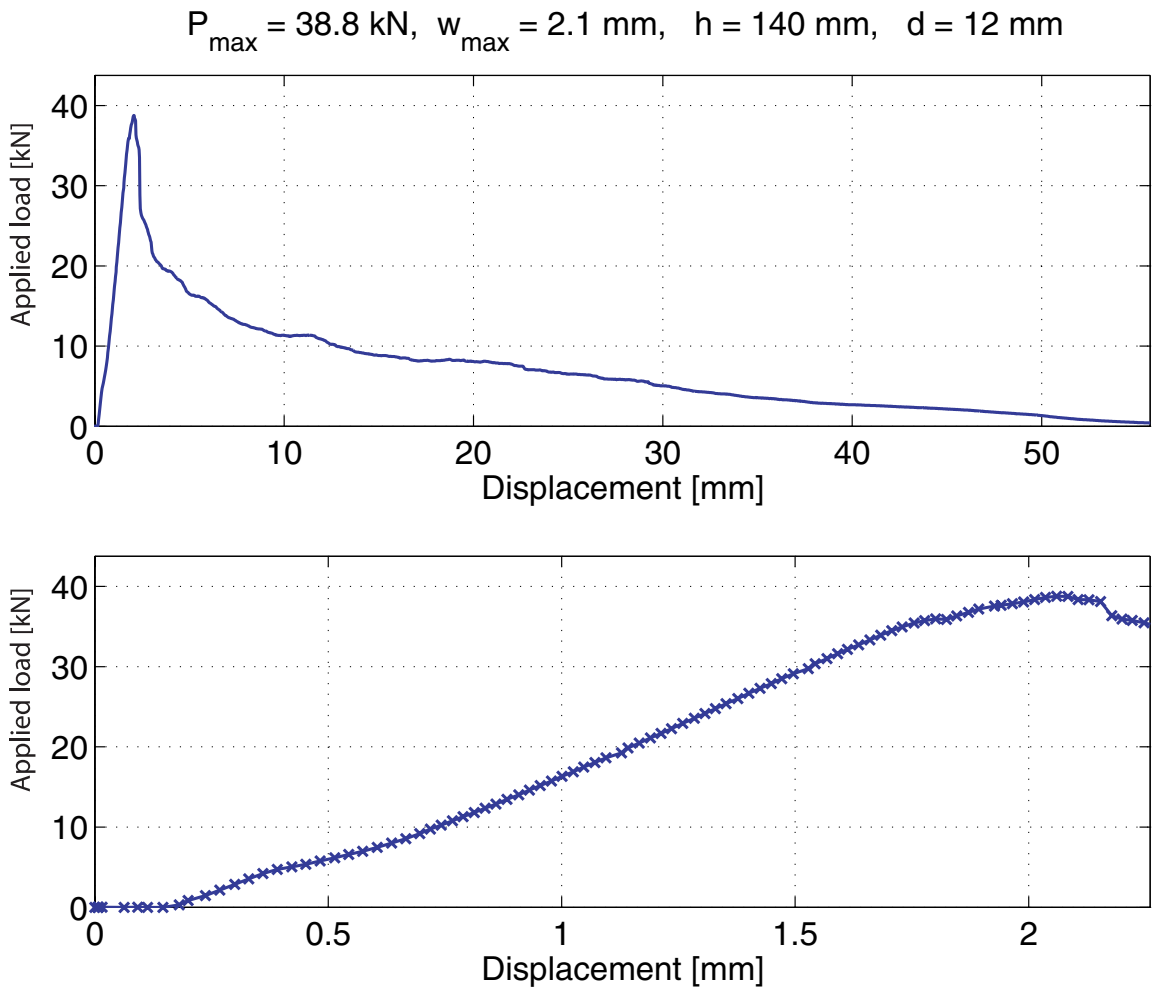

Figure A.74: *Load-deflection curve for the anchor pull-out*

A.2.37 Header arrangement, d = 12 mm, h = 160 mm

Figure A.75: *The failure mode observed*

Failure mode: Brick pull-out failure

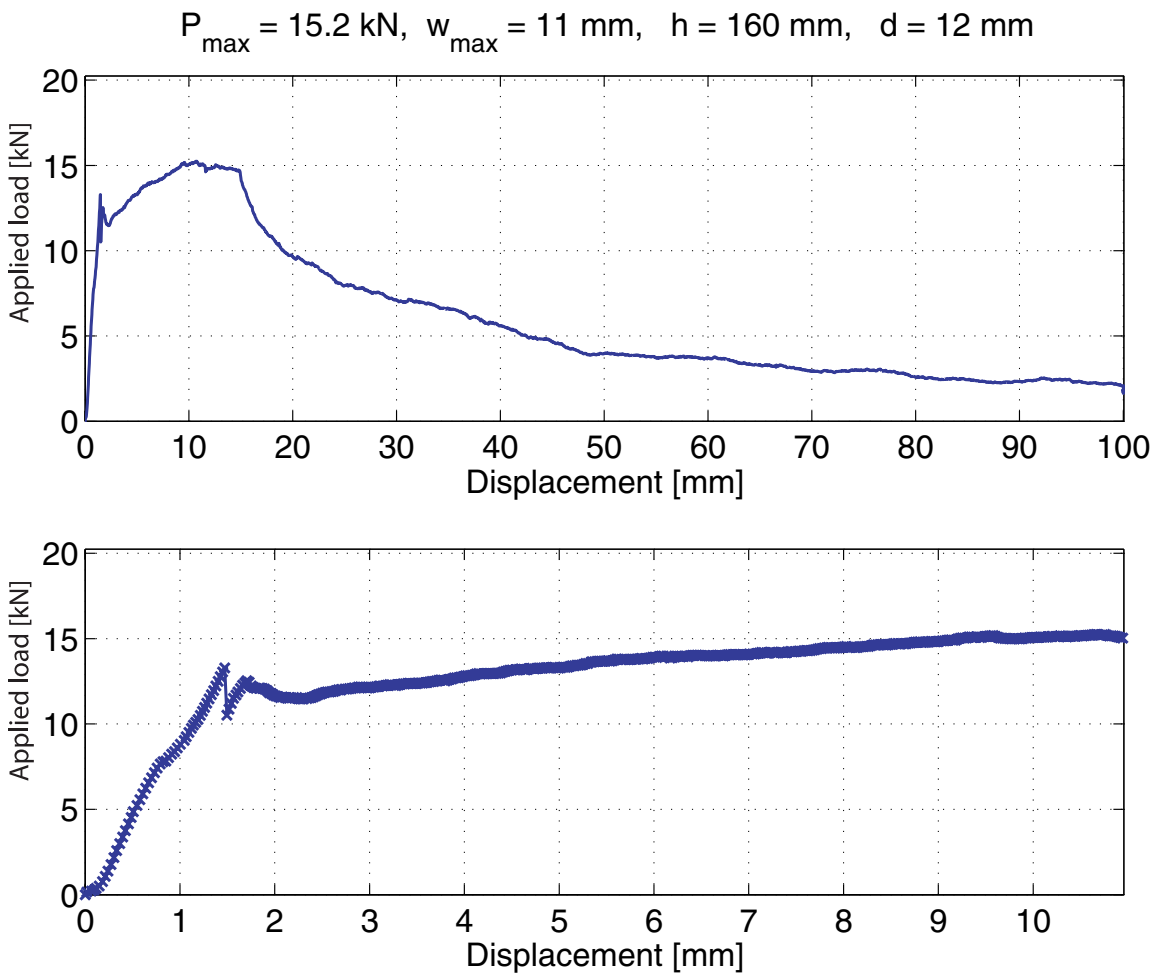

Figure A.76: *Load-deflection curve for the anchor pull-out*

A.2.38 Header arrangement, d = 16 mm, h = 100 mm

Figure A.77: *The failure mode observed*

Failure mode: Brick pull-out failure

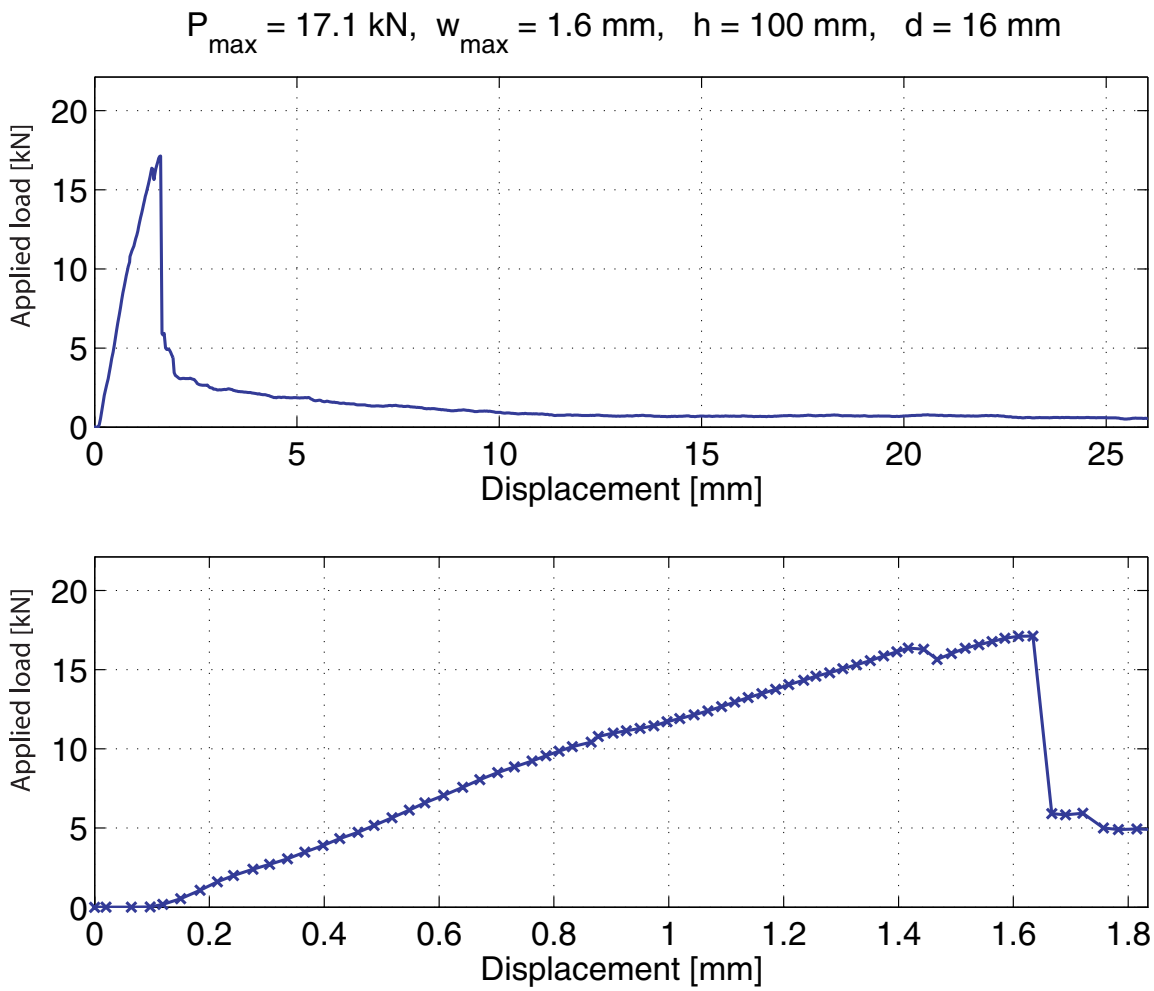

Figure A.78: *Load-deflection curve for the anchor pull-out*

A.2.39 Header arrangement, d = 16 mm, h = 120 mm

Figure A.79: *The failure mode observed*

Failure mode: Brick pull-out failure

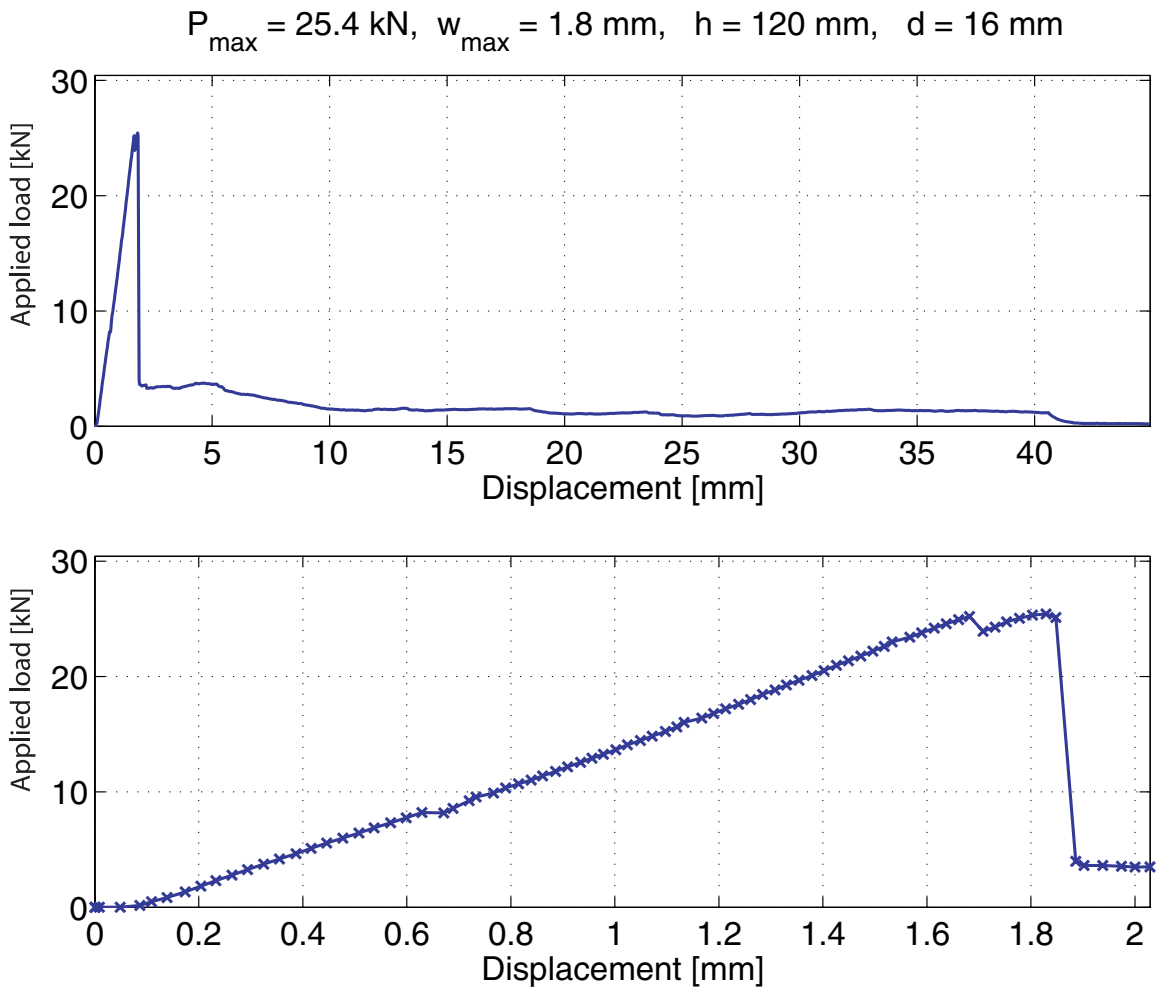

Figure A.80: *Load-deflection curve for the anchor pull-out*

A.2.40 Header arrangement, d = 16 mm, h = 140 mm

Figure A.81: *The failure mode observed*

Failure mode: Splitting failure in masonry

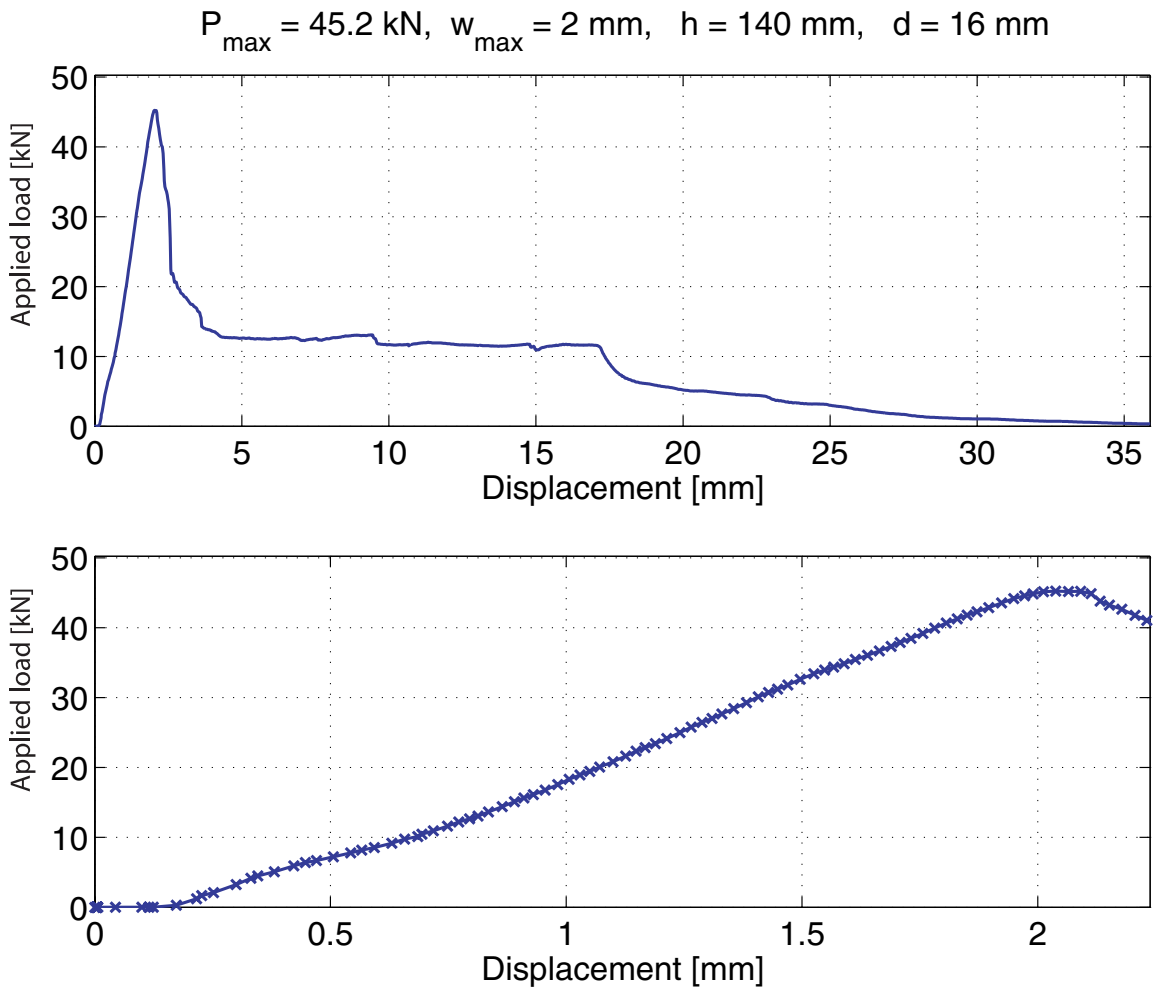

Figure A.82: *Load-deflection curve for the anchor pull-out*

A.2.41 Header arrangement, d = 16 mm, h = 160 mm

Figure A.83: *The failure mode observed*

Failure mode: Brick pull-out failure

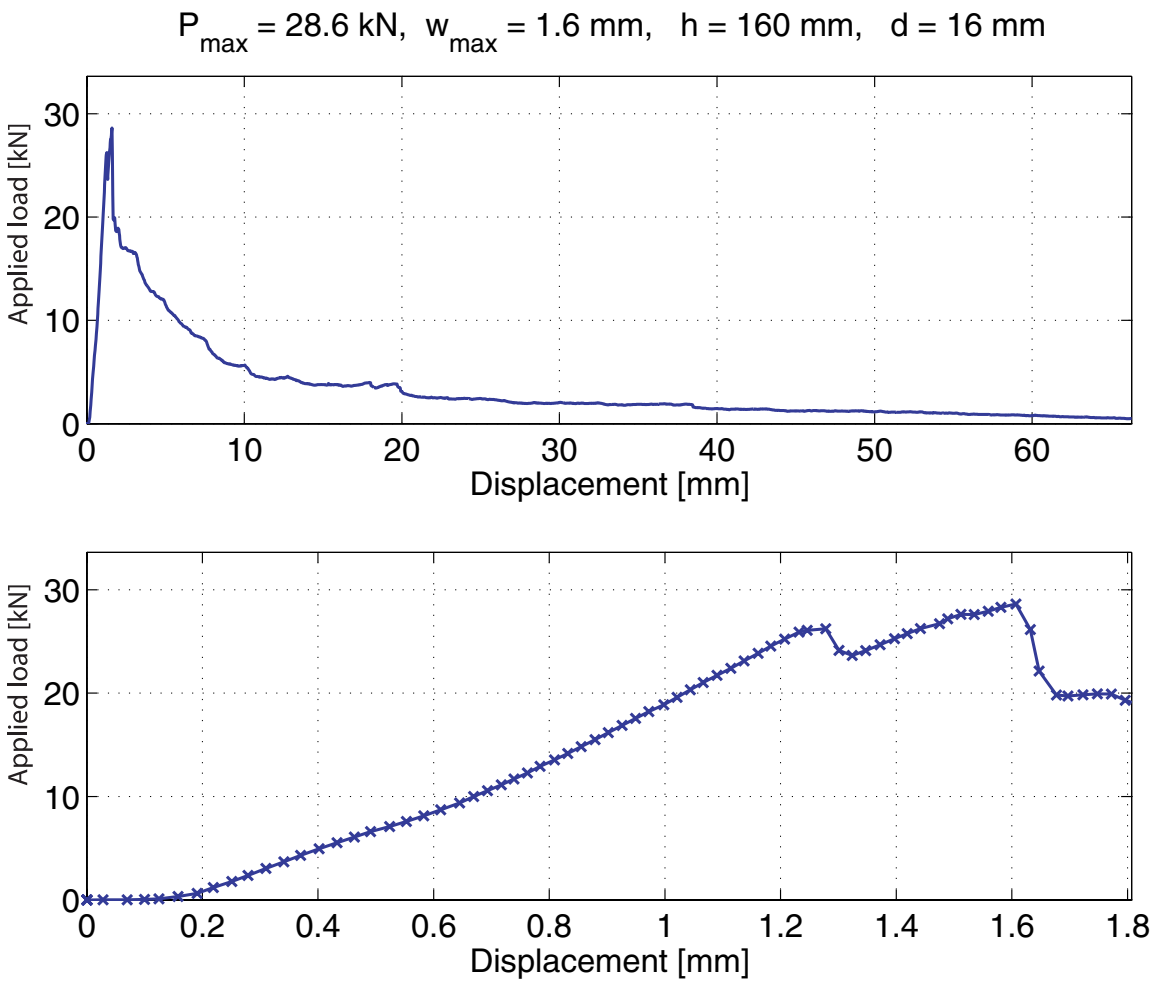

Figure A.84: *Load-deflection curve for the anchor pull-out*

A.2.42 Joint arrangements, d = 10 mm, h = 100 mm

Figure A.85: *The failure mode observed*

Failure mode: Sliding failure

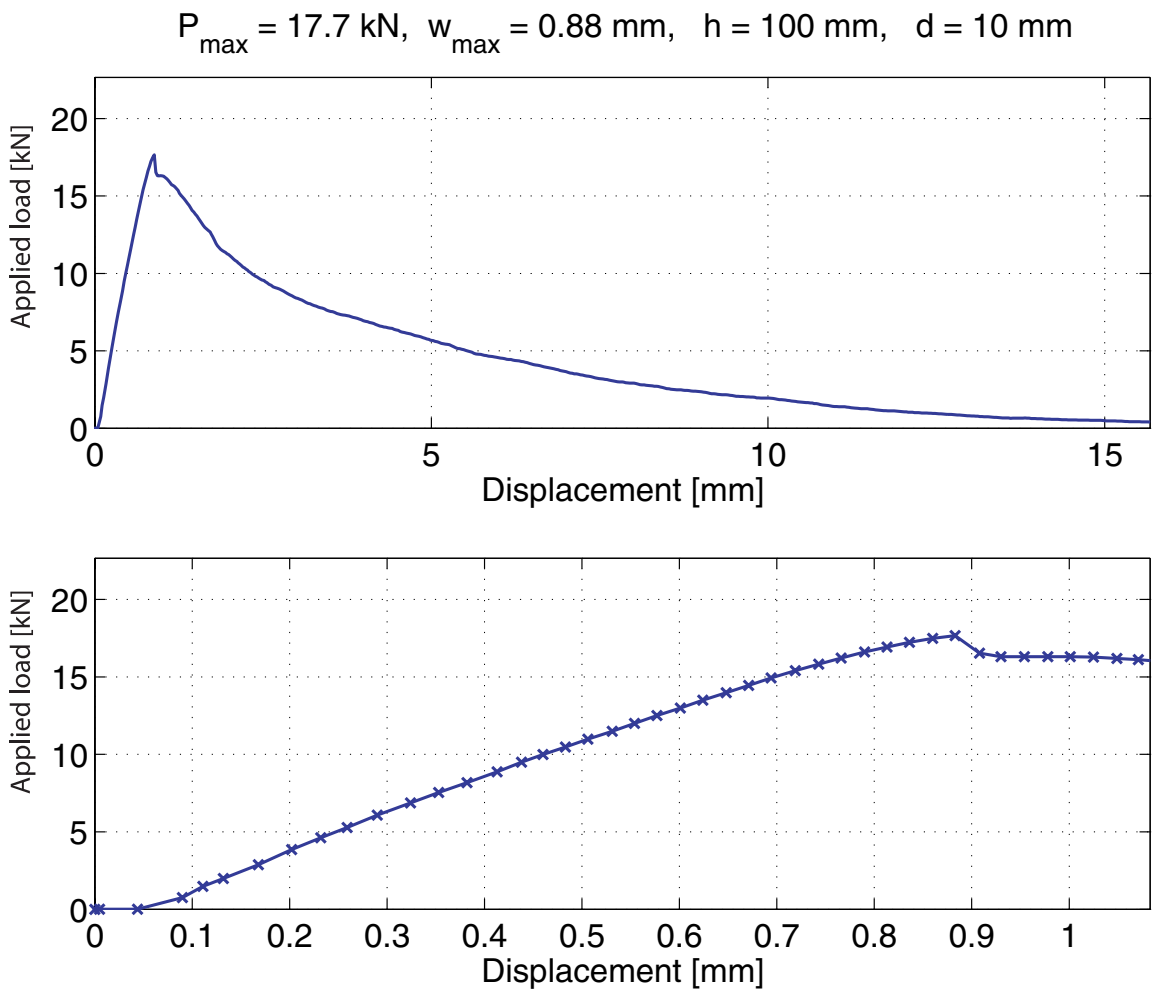

Figure A.86: *Load-deflection curve for the anchor pull-out*

A.2.43 Joint arrangements, d = 10 mm, h = 120 mm

Figure A.87: *The failure mode observed*

Failure mode: Sliding failure

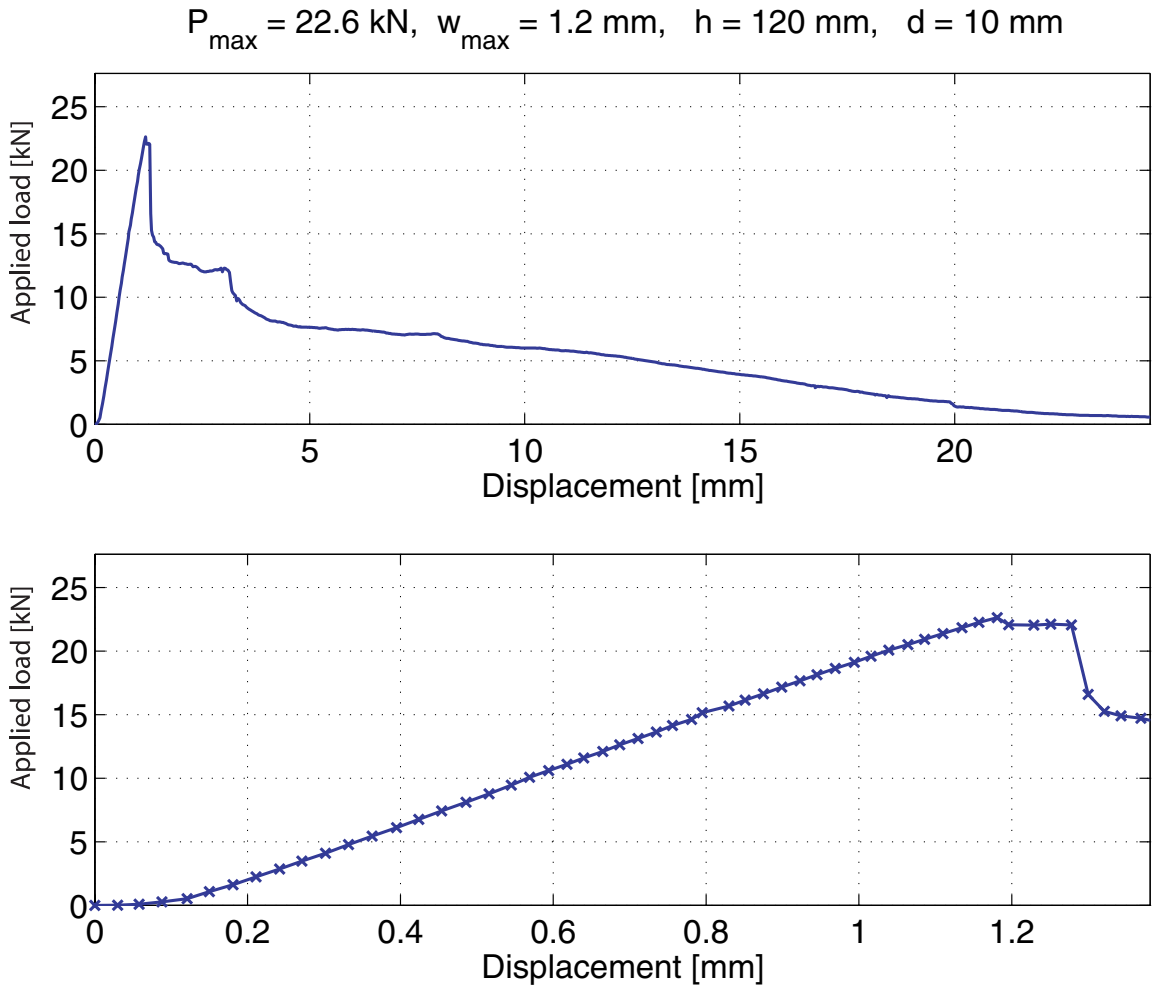

Figure A.88: *Load-deflection curve for the anchor pull-out*

A.2.44 Joint arrangements, d = 10 mm, h = 140 mm

Figure A.89: *The failure mode observed*

Failure mode: Sliding failure

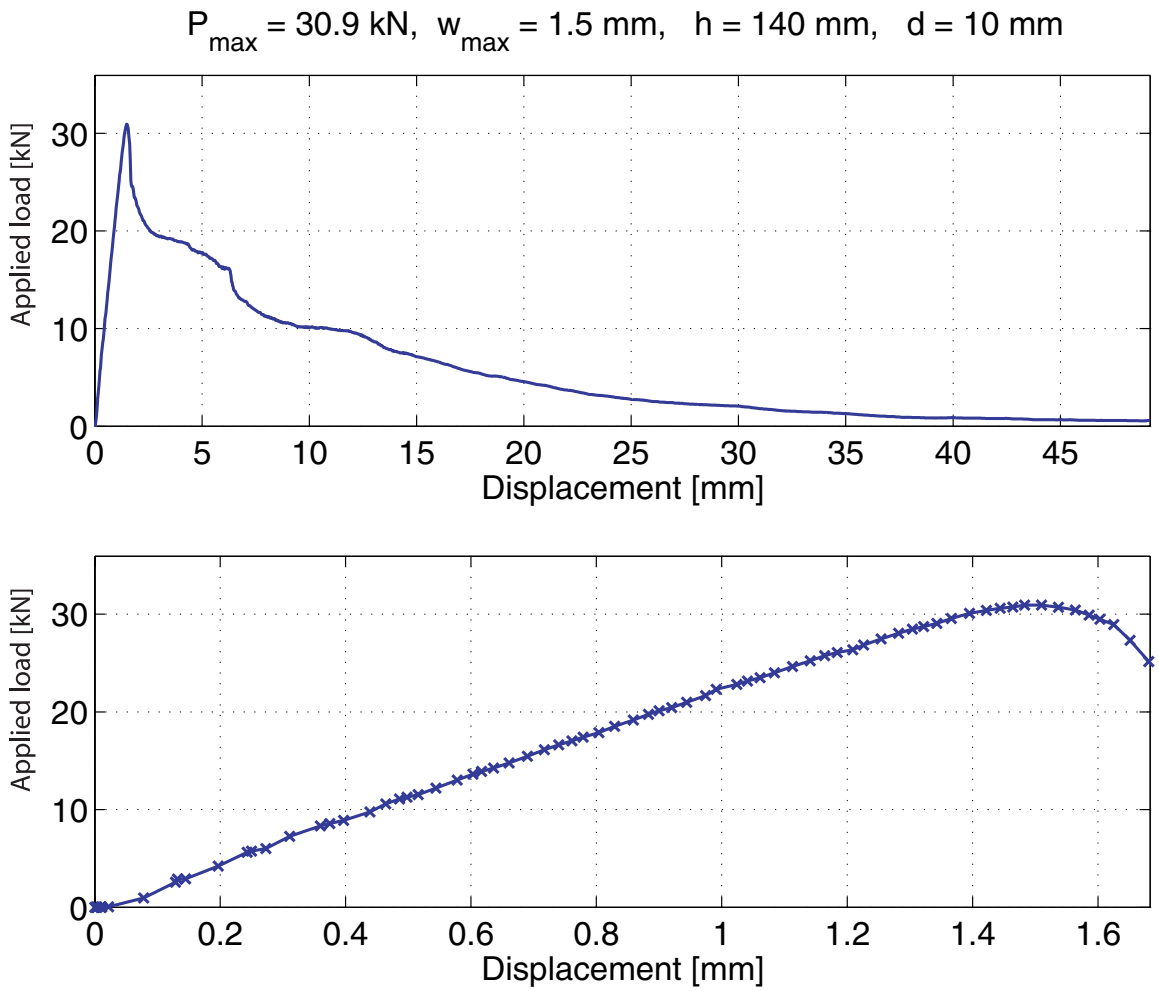

Figure A.90: *Load-deflection curve for the anchor pull-out*

A.2.45 Joint arrangements, d = 10 mm, h = 160 mm

Figure A.91: *The failure mode observed*

Failure mode: Sliding failure

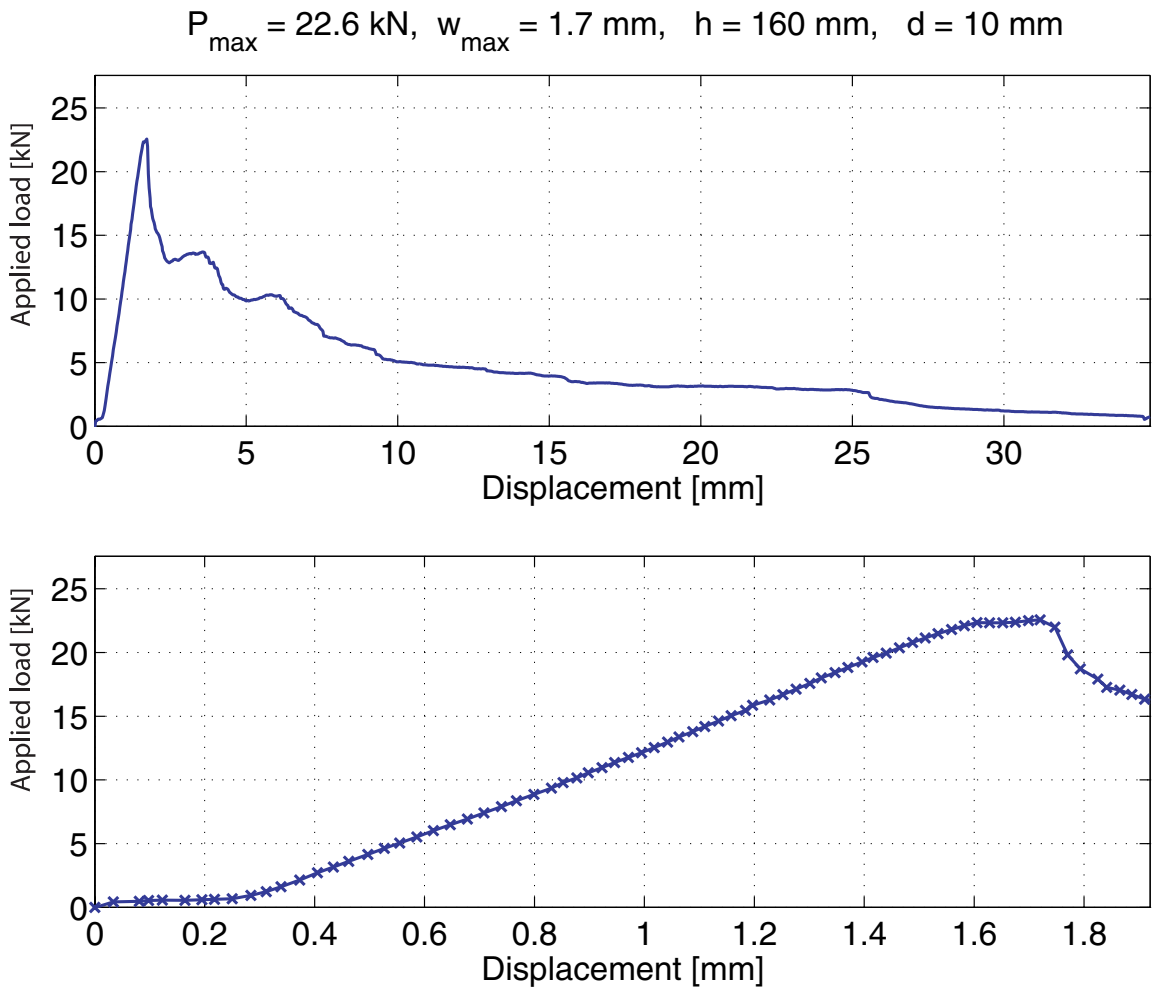

Figure A.92: *Load-deflection curve for the anchor pull-out*

A.2.46 Joint arrangements, d = 12 mm, h = 100 mm

Figure A.93: *The failure mode observed*

Failure mode: Sliding failure

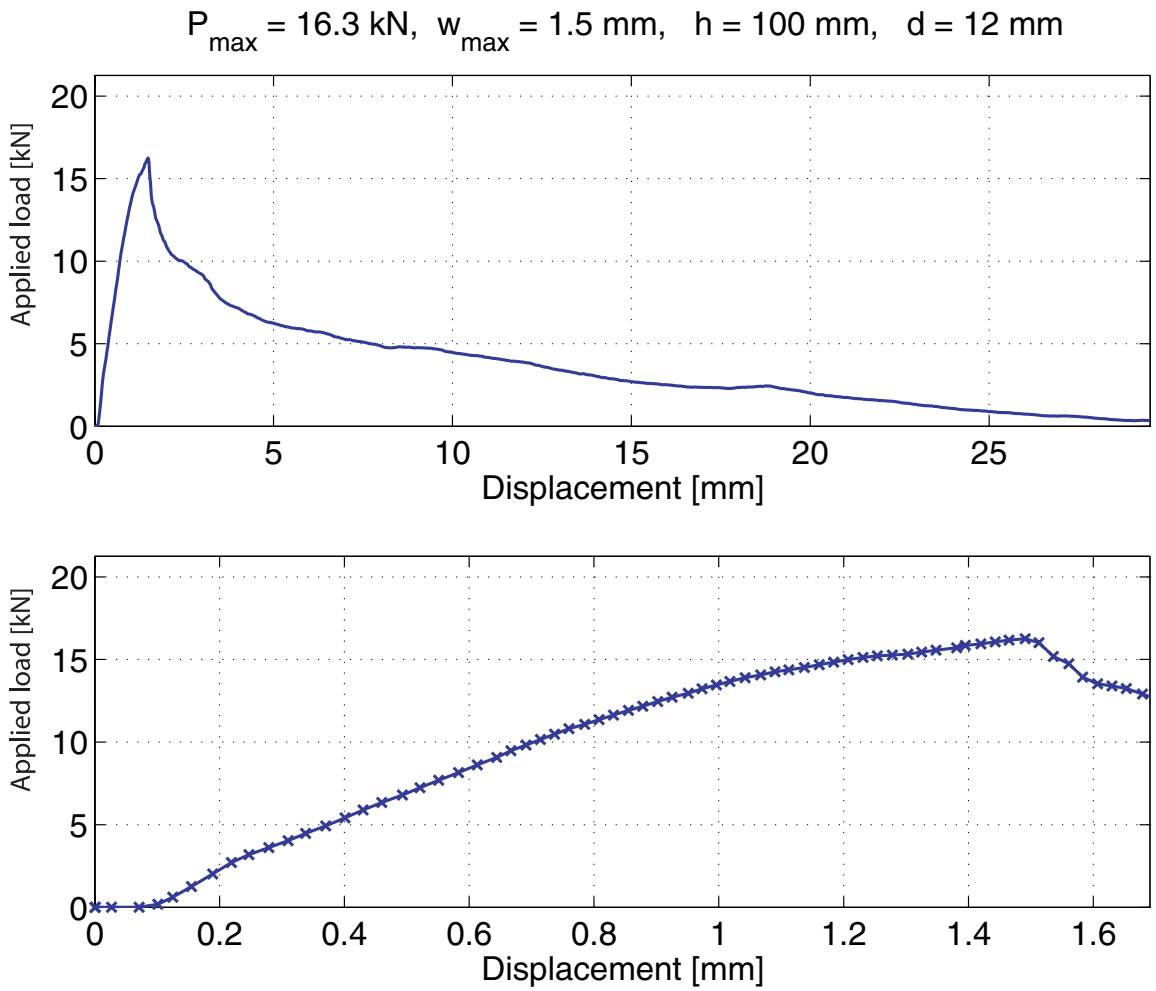

Figure A.94: *Load-deflection curve for the anchor pull-out*

A.2.47 Joint arrangements, d = 12 mm, h = 120 mm

Figure A.95: *The failure mode observed*

Failure mode: Sliding failure

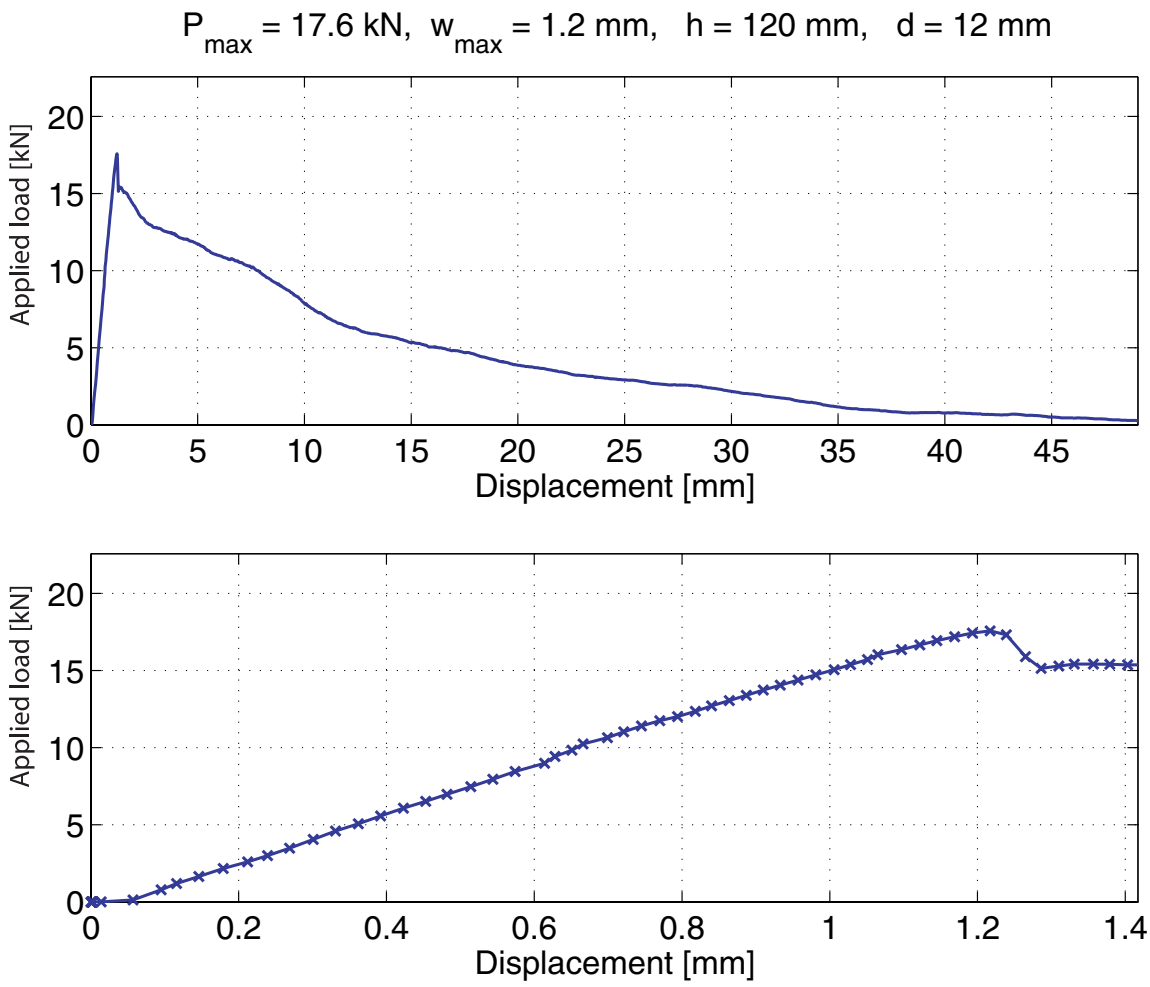

Figure A.96: *Load-deflection curve for the anchor pull-out*

A.2.48 Joint arrangements, d = 12 mm, h = 140 mm

Figure A.97: *The failure mode observed*

Failure mode: Sliding failure

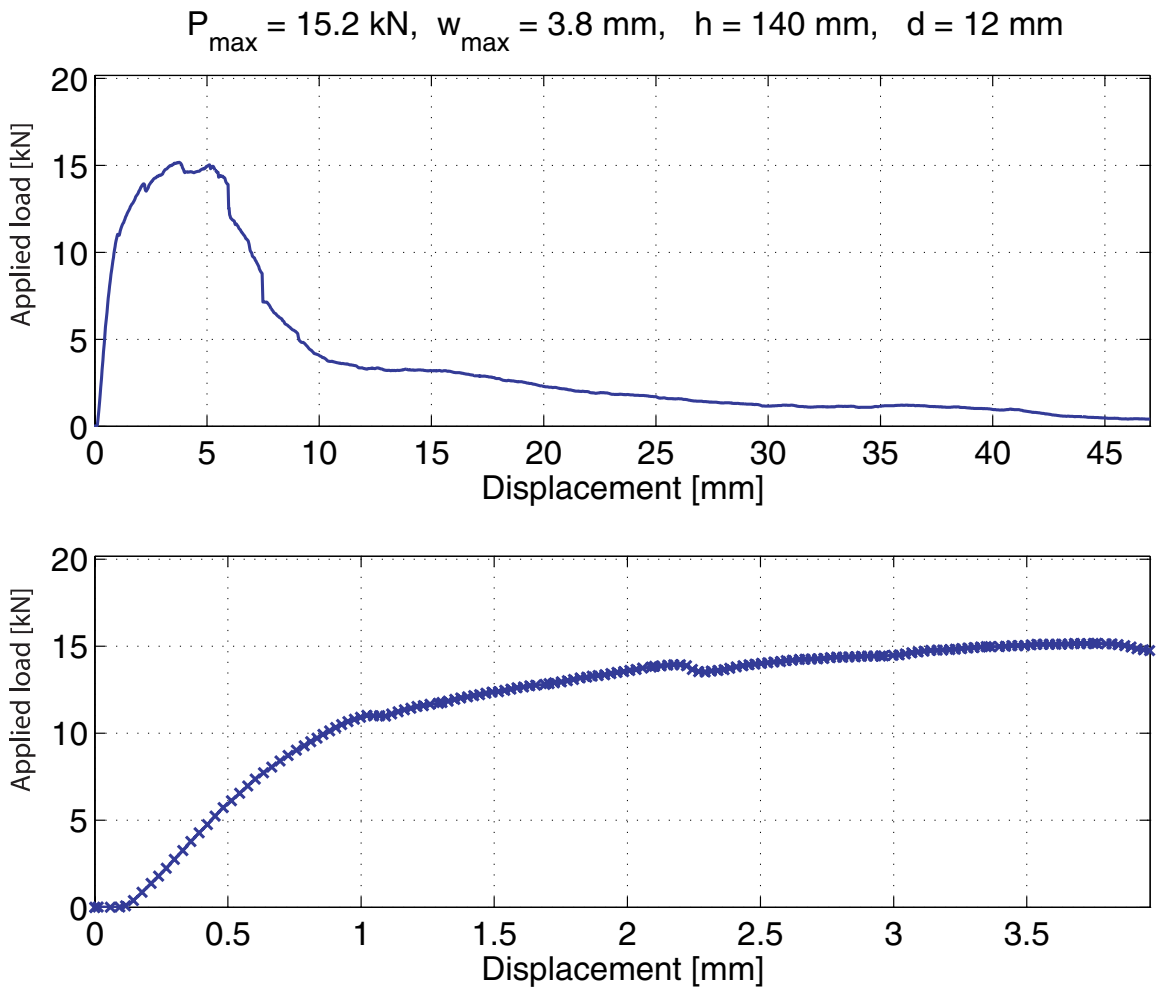

Figure A.98: *Load-deflection curve for the anchor pull-out*

A.2.49 Joint arrangements, d = 12 mm, h = 160 mm

Figure A.99: *The failure mode observed*

Failure mode: Sliding failure

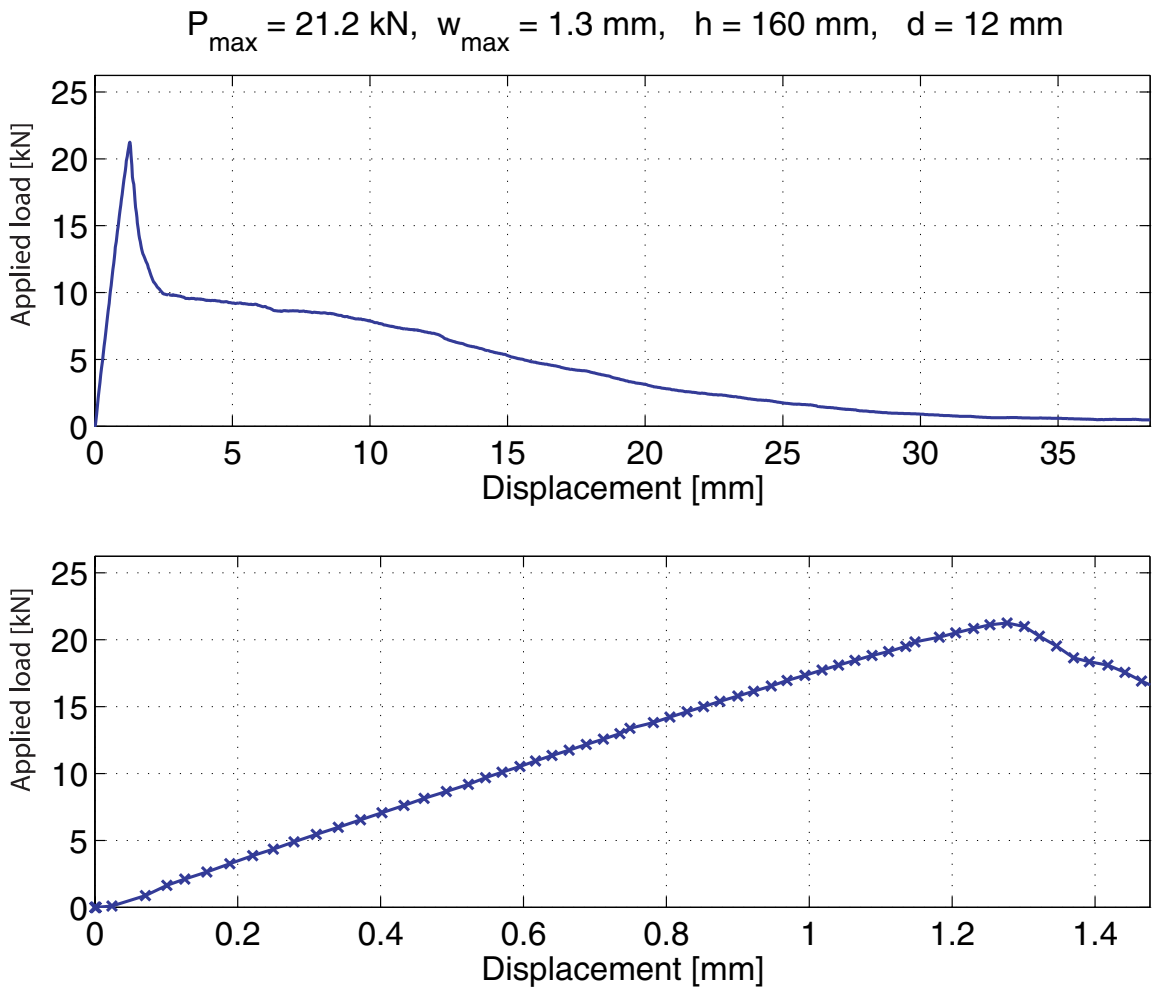

Figure A.100: *Load-deflection curve for the anchor pull-out*

A.2.50 Joint arrangements, d = 16 mm, h = 100 mm

Figure A.101: *The failure mode observed*

Failure mode: Sliding failure

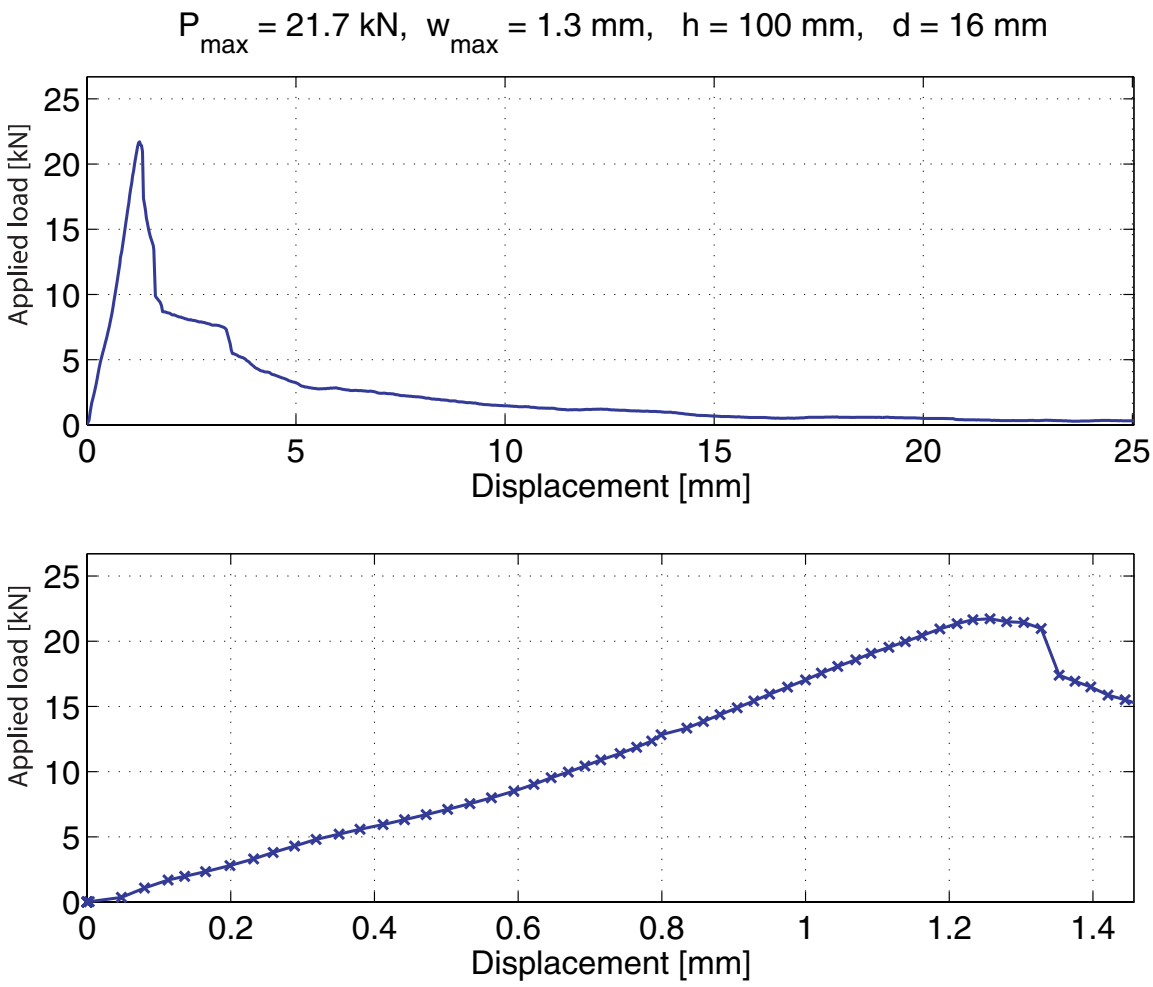

Figure A.102: *Load-deflection curve for the anchor pull-out*

A.2.51 Joint arrangements, d = 16 mm, h = 120 mm

Figure A.103: *The failure mode observed*

Failure mode: Sliding failure

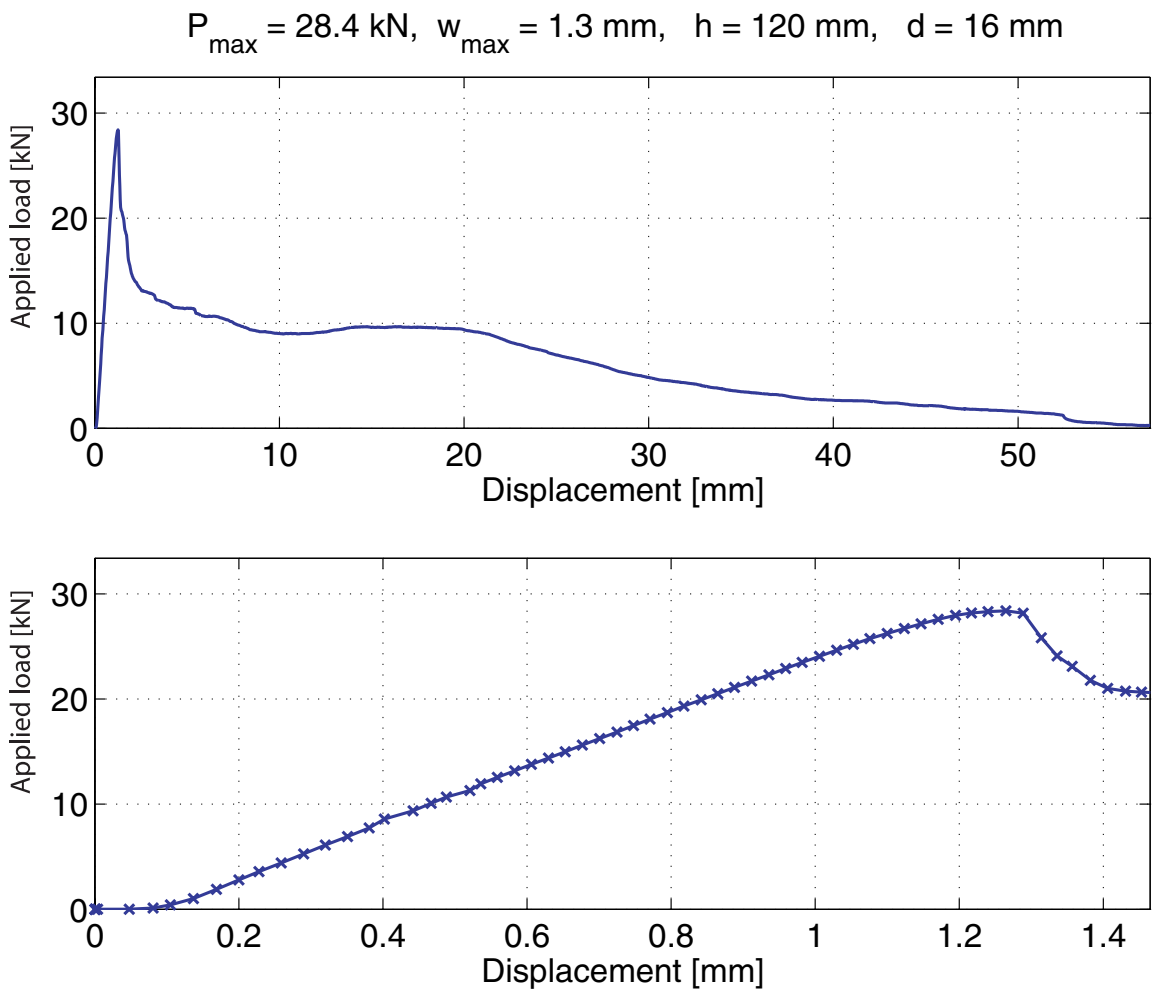

Figure A.104: *Load-deflection curve for the anchor pull-out*

A.2.52 Joint arrangements, d = 16 mm, h = 140 mm

Figure A.105: *The failure mode observed*

Failure mode: Sliding failure

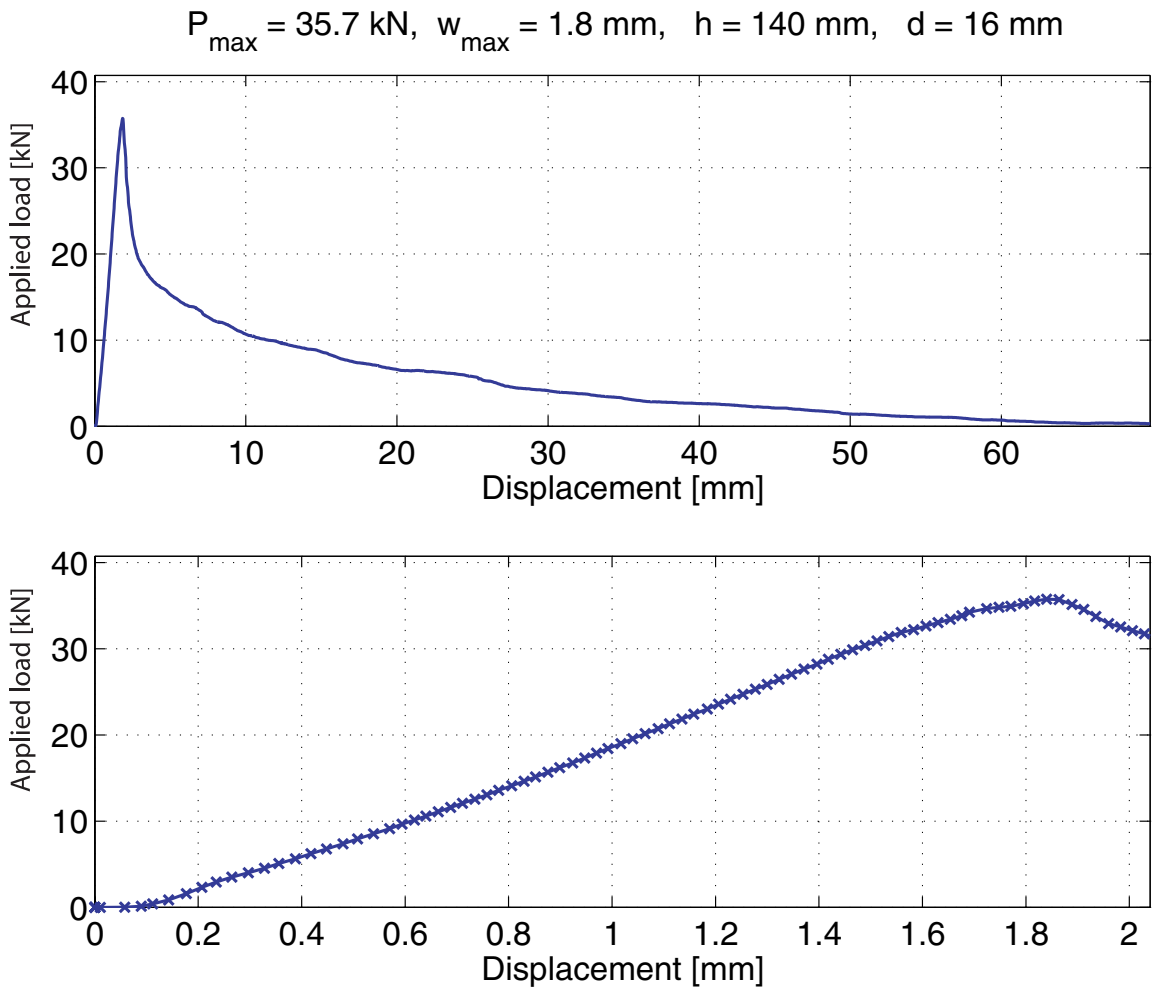

Figure A.106: *Load-deflection curve for the anchor pull-out*

A.2.53 Joint arrangements, d = 16 mm, h = 160 mm

Figure A.107: *The failure mode observed*

Failure mode: Sliding failure

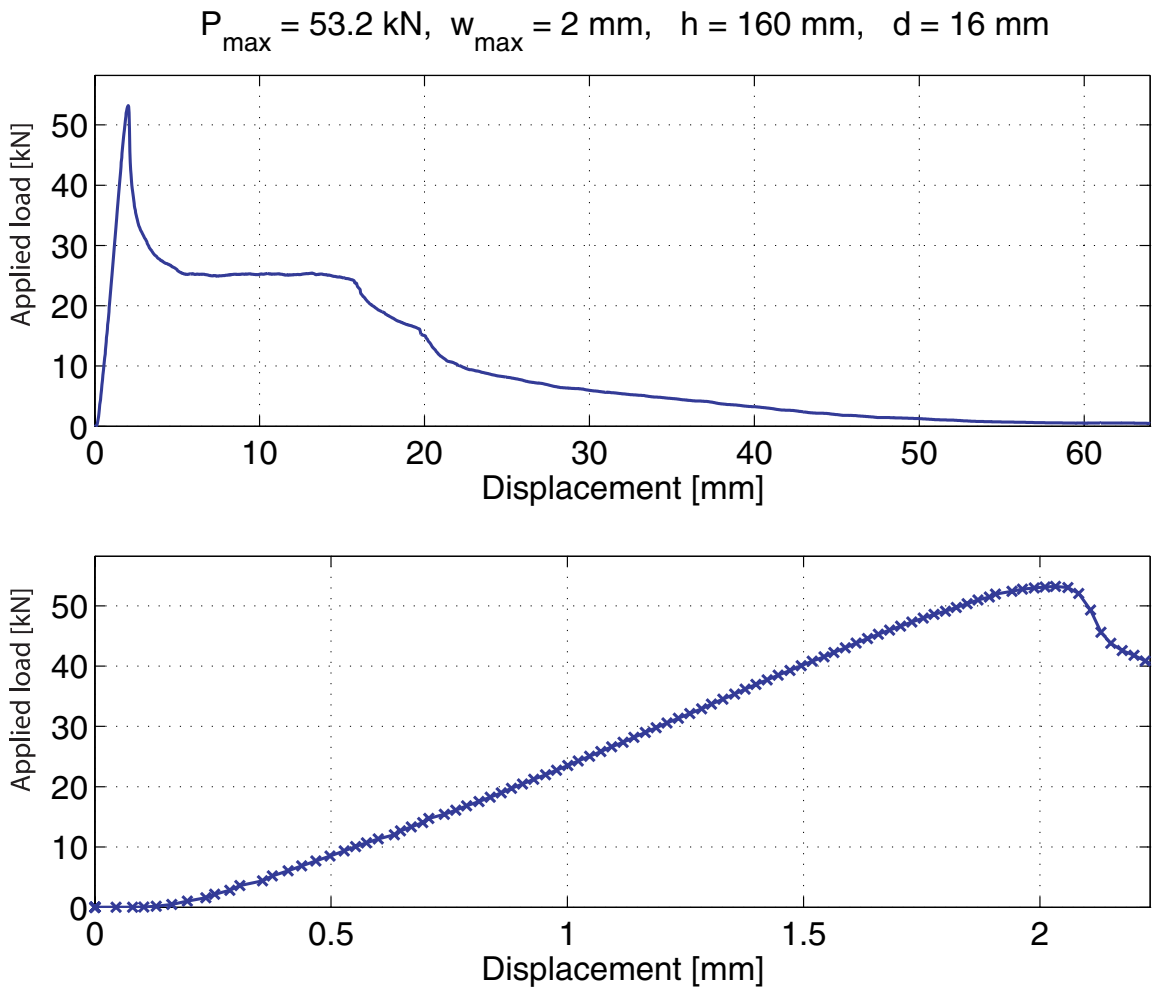

Figure A.108: *Load-deflection curve for the anchor pull-out*

A.3 Close to a corner

A.3.1 Corner distance c = 100 mm, d = 12 mm

Figure A.109: *The failure mode observed*

Failure mode: Corner failure

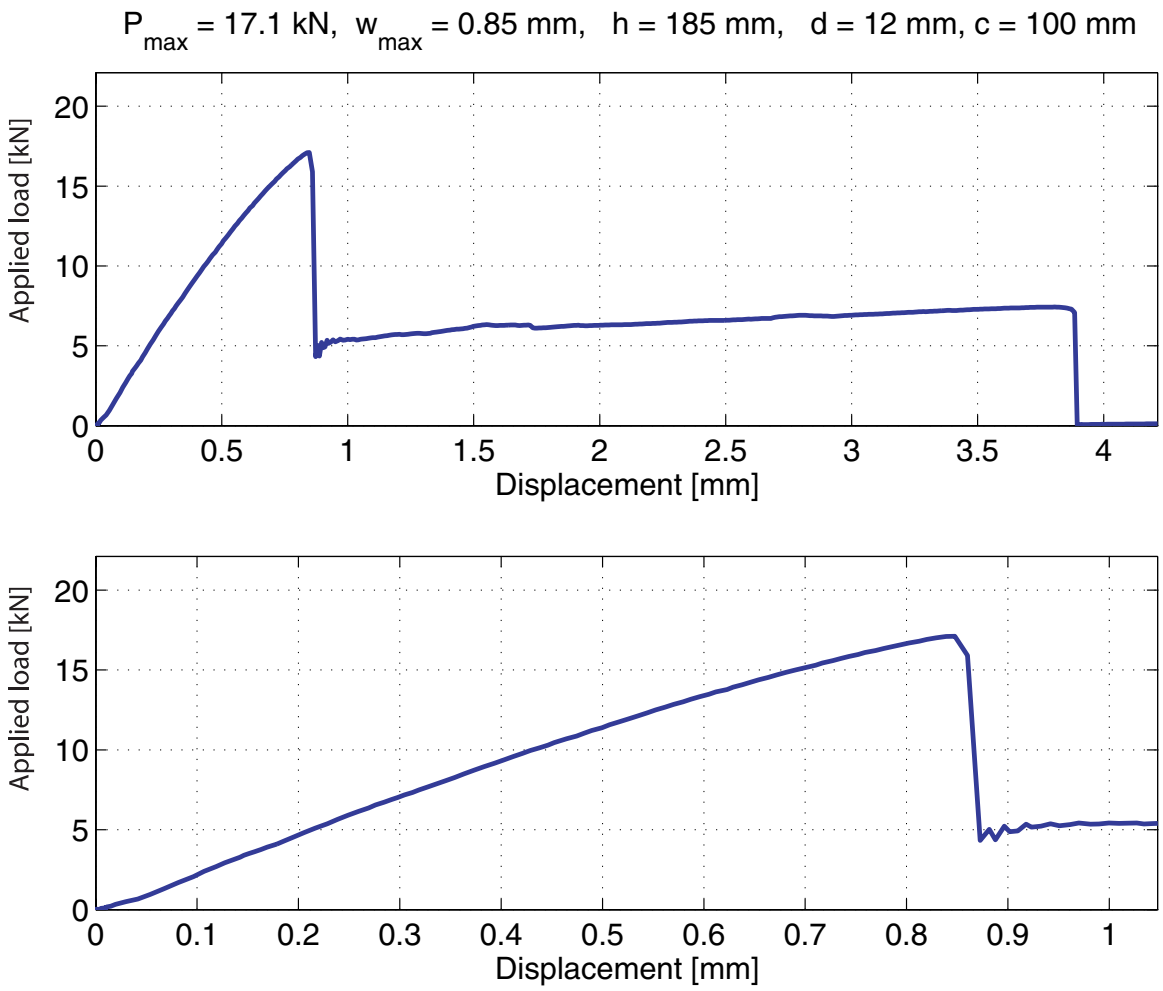

Figure A.110: *Load-deflection curve for the anchors pull-out*

A.3.2 Corner distance c = 160 mm, d = 12 mm

Figure A.111: *The failure mode observed*

Failure mode: Corner failure

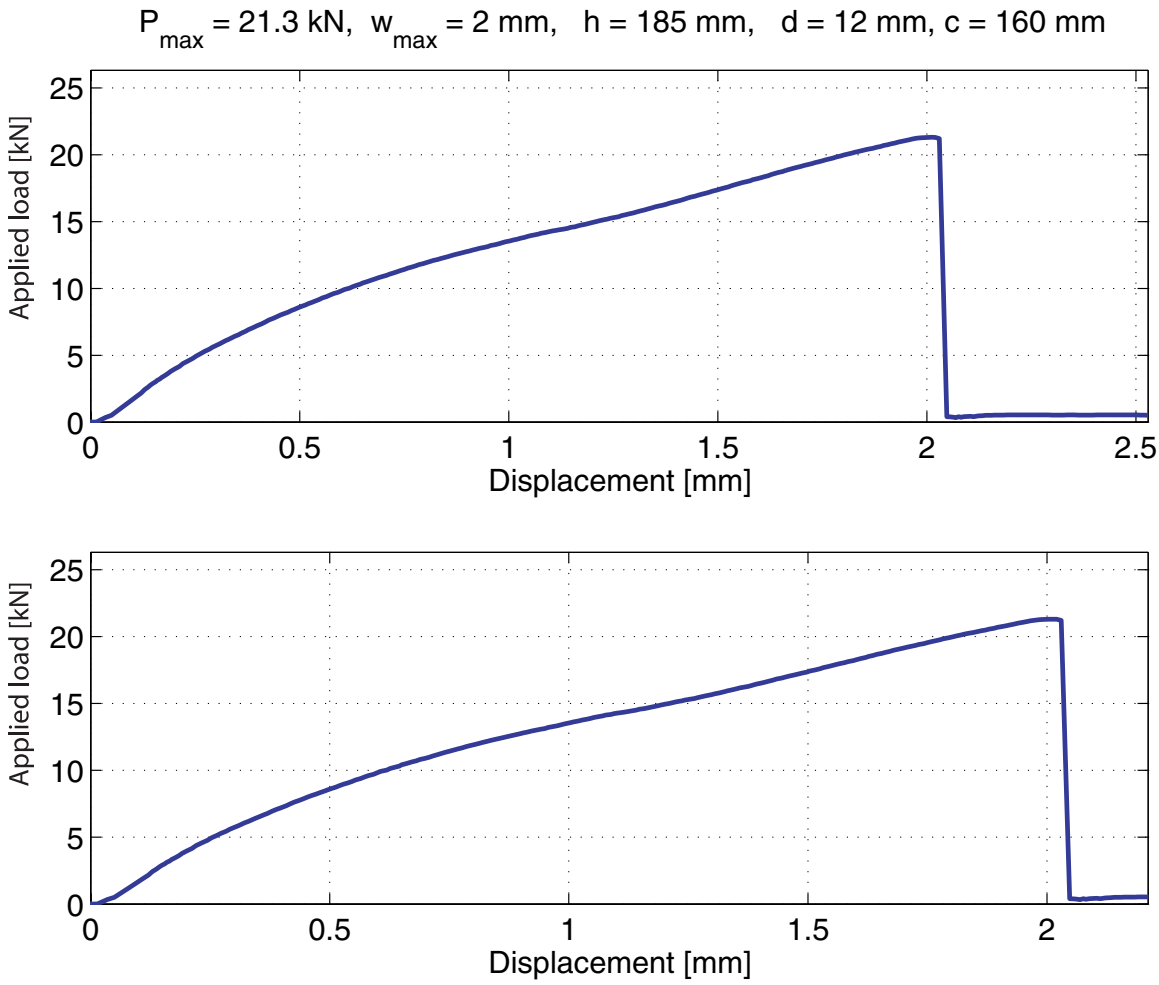

Figure A.112: *Load-deflection curve for the anchors pull-out*

A.3.3 Corner distance c = 230 mm, d = 12 mm

Figure A.113: *The failure mode observed*

Failure mode: Sliding failure

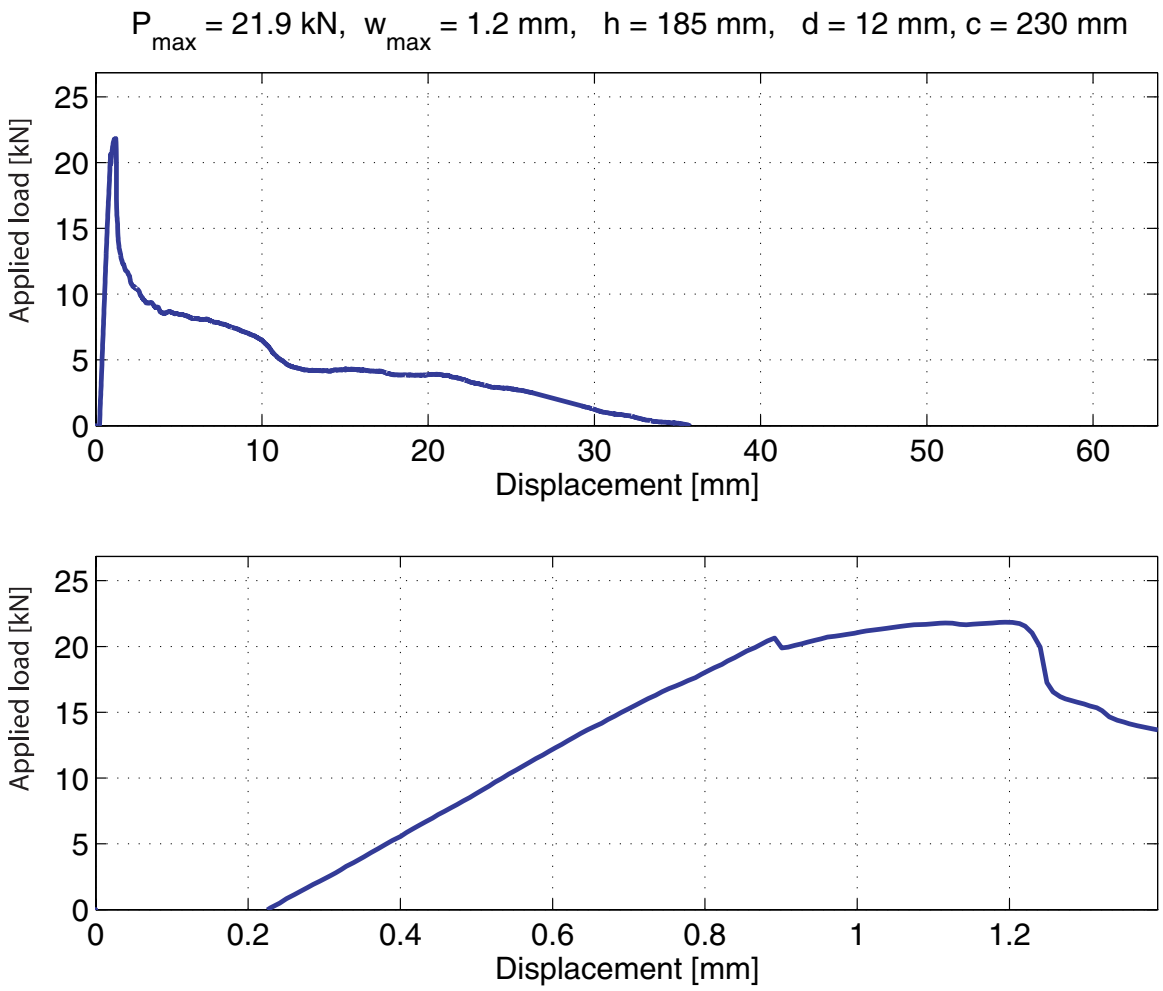

Figure A.114: *Load-deflection curve for the anchors pull-out*

A.3.4 Corner distance c = 230 mm - 2, d = 12 mm

Figure A.115: *The failure mode observed*

Failure mode: Corner failure

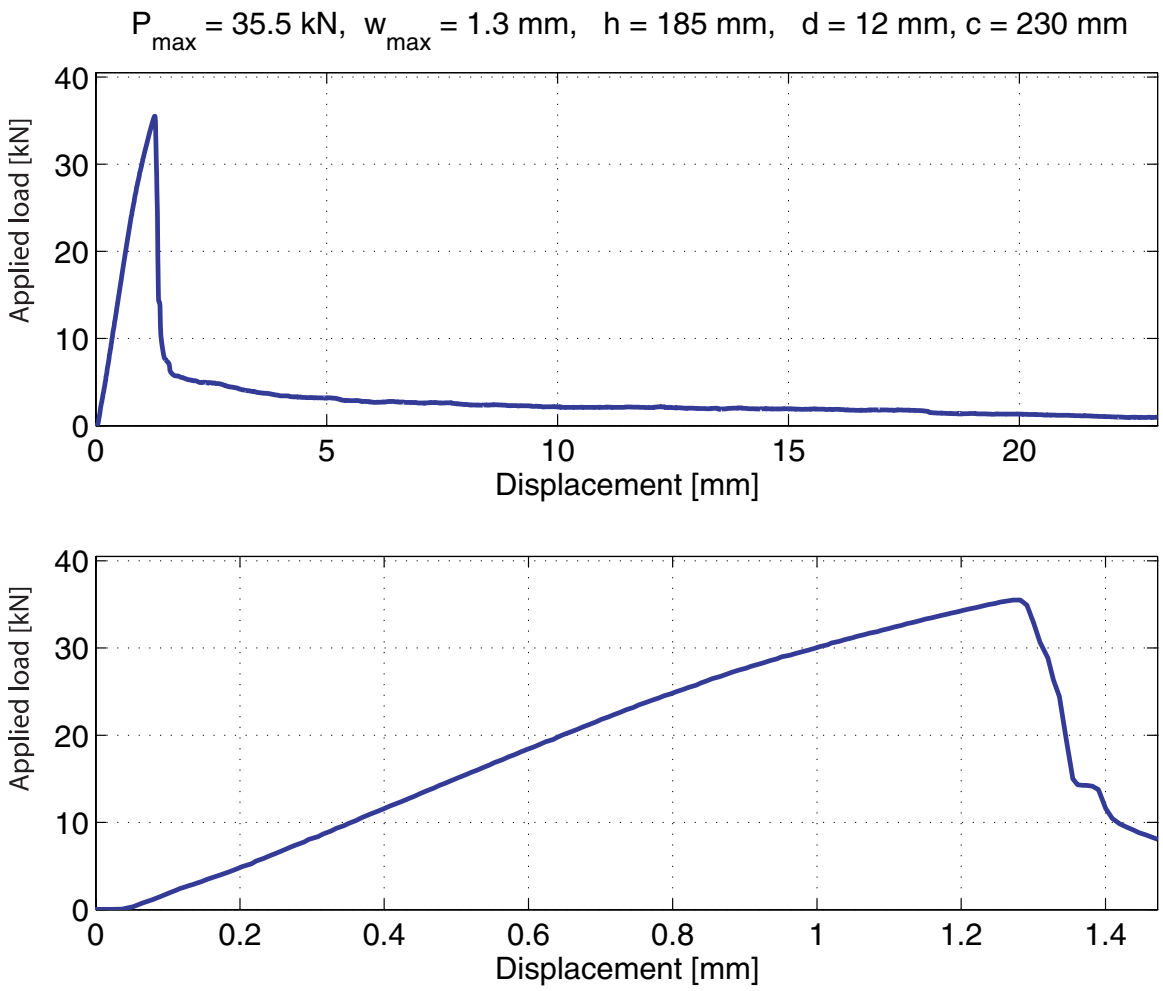

Figure A.116: *Load-deflection curve for the anchors pull-out*

A.3.5 Corner distance c = 100 mm, d = 16 mm

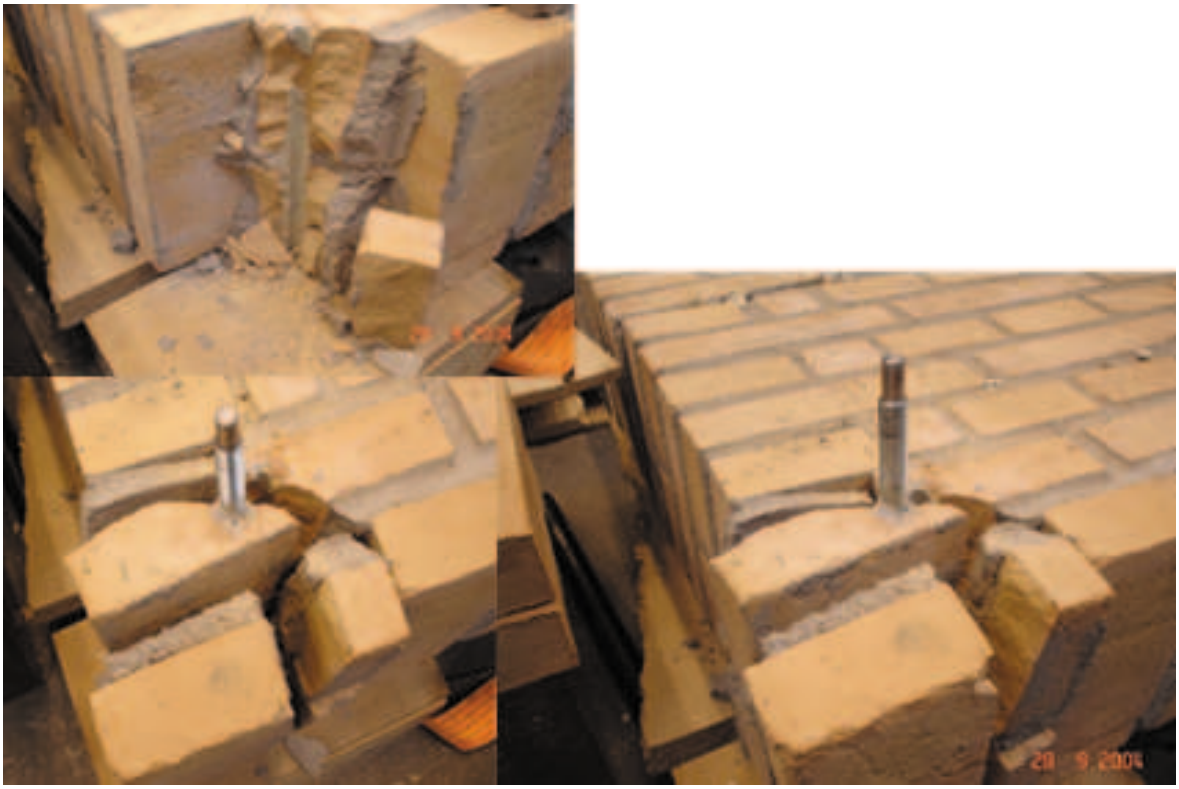

Figure A.117: *The failure mode observed*

Failure mode: Corner failure

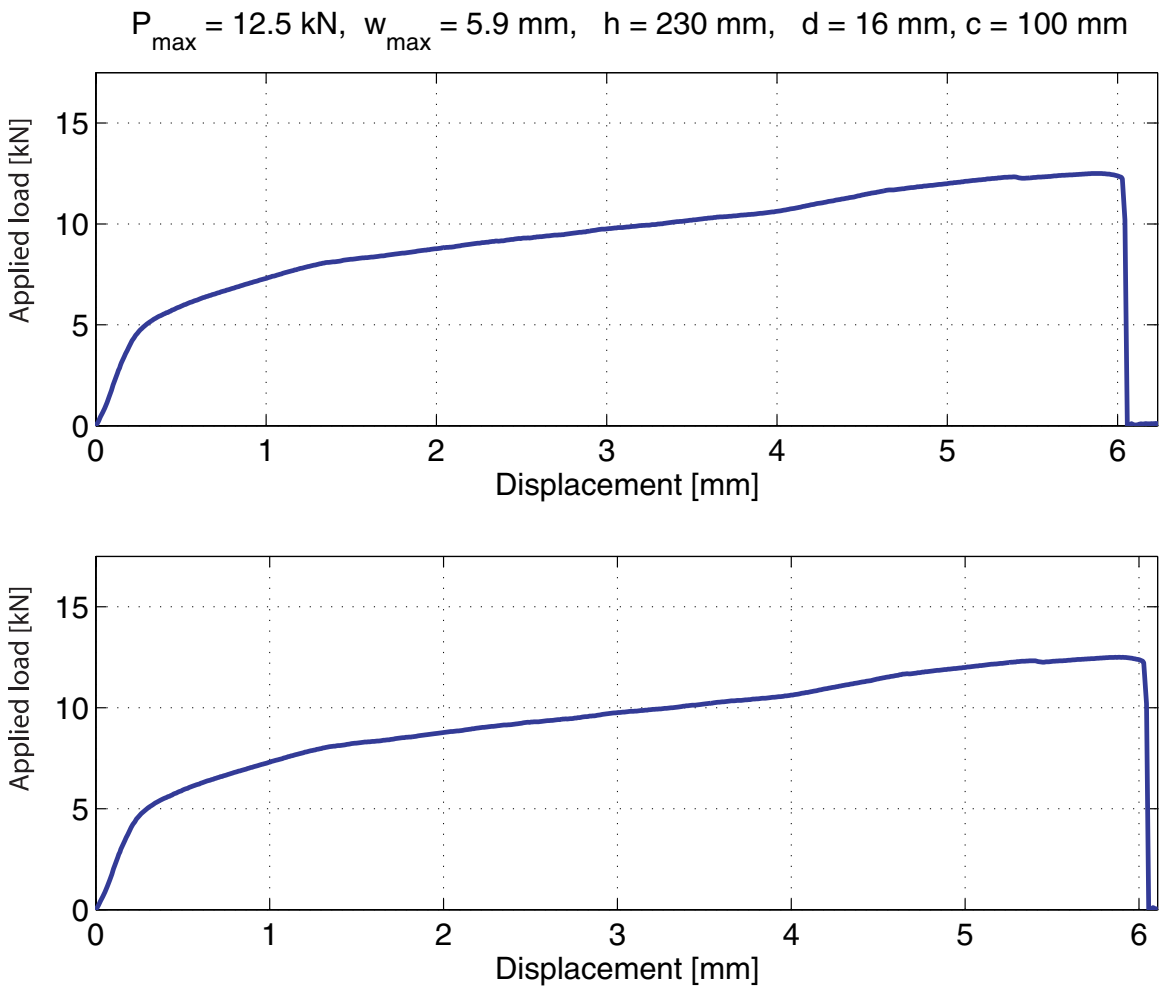

Figure A.118: *Load-deflection curve for the anchors pull-out*

A.3.6 Corner distance c = 160 mm, d = 16 mm

Figure A.119: *The failure mode observed*

Failure mode: Corner failure

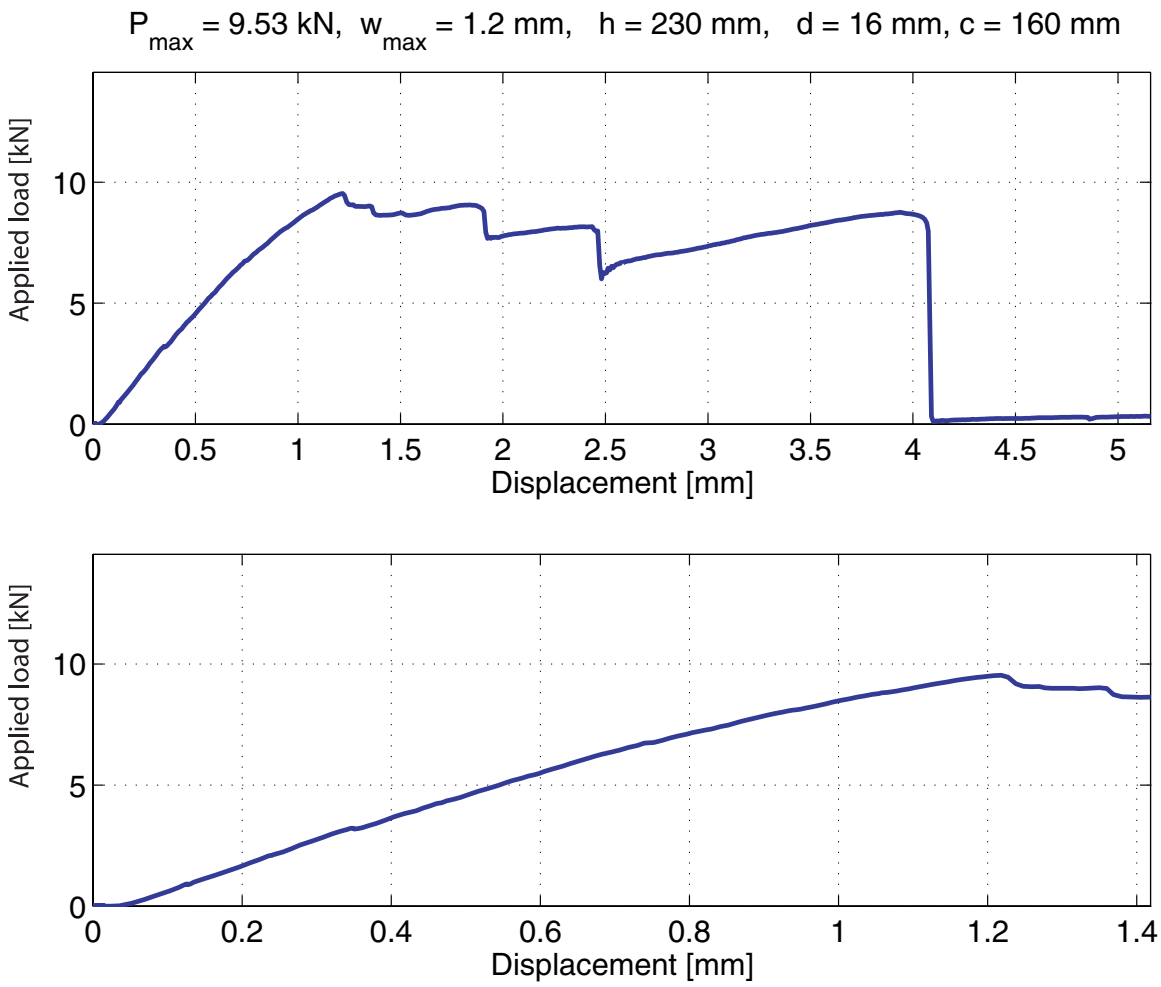

Figure A.120: *Load-deflection curve for the anchors pull-out*

A.3.7 Corner distance c = 160 mm - 2, d = 16 mm

Figure A.121: *The failure mode observed*

Failure mode: Corner failure

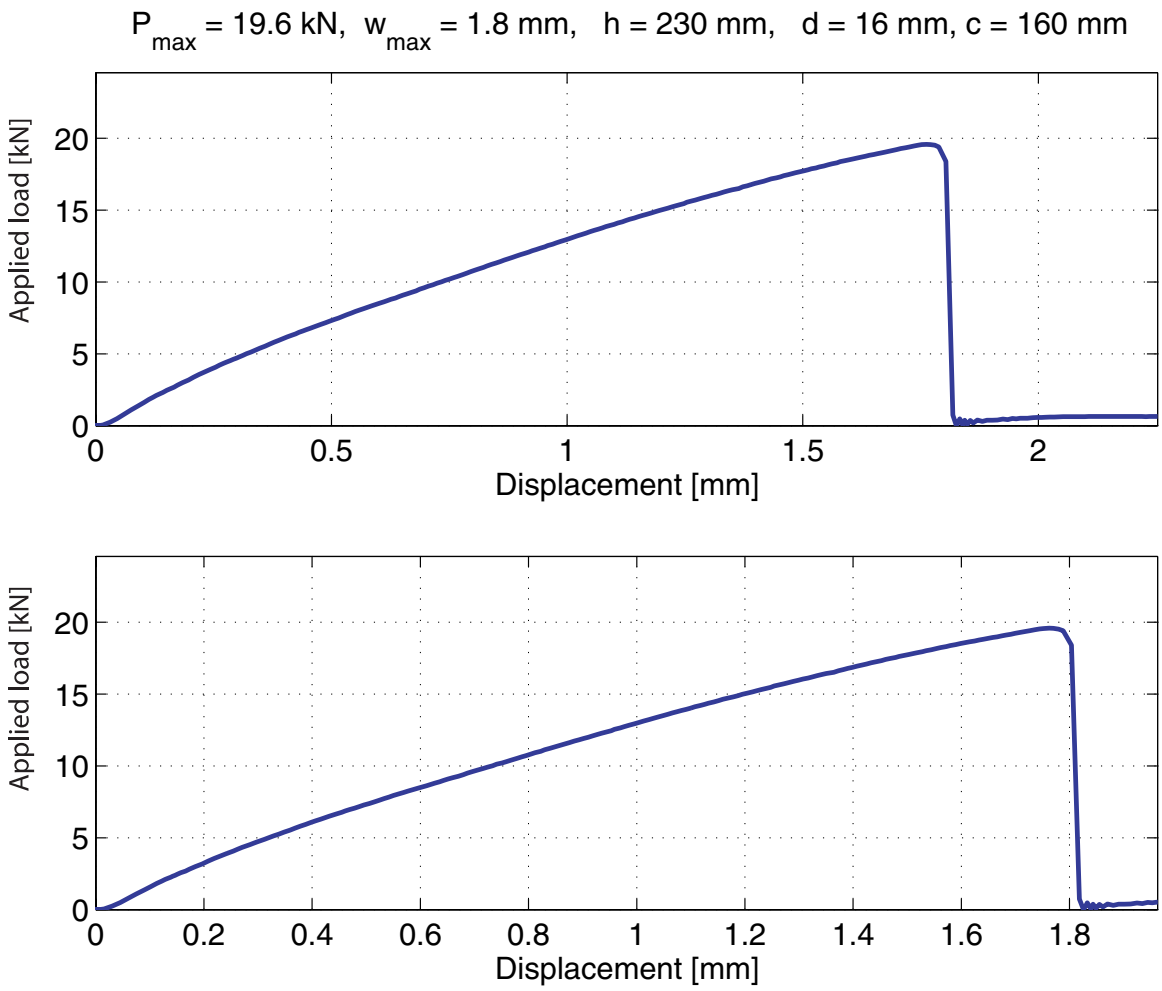

Figure A.122: *Load-deflection curve for the anchors pull-out*

A.3.8 Corner distance c = 230 mm, d = 16 mm

Figure A.123: *The failure mode observed*

Failure mode: Splitting failure in the brick

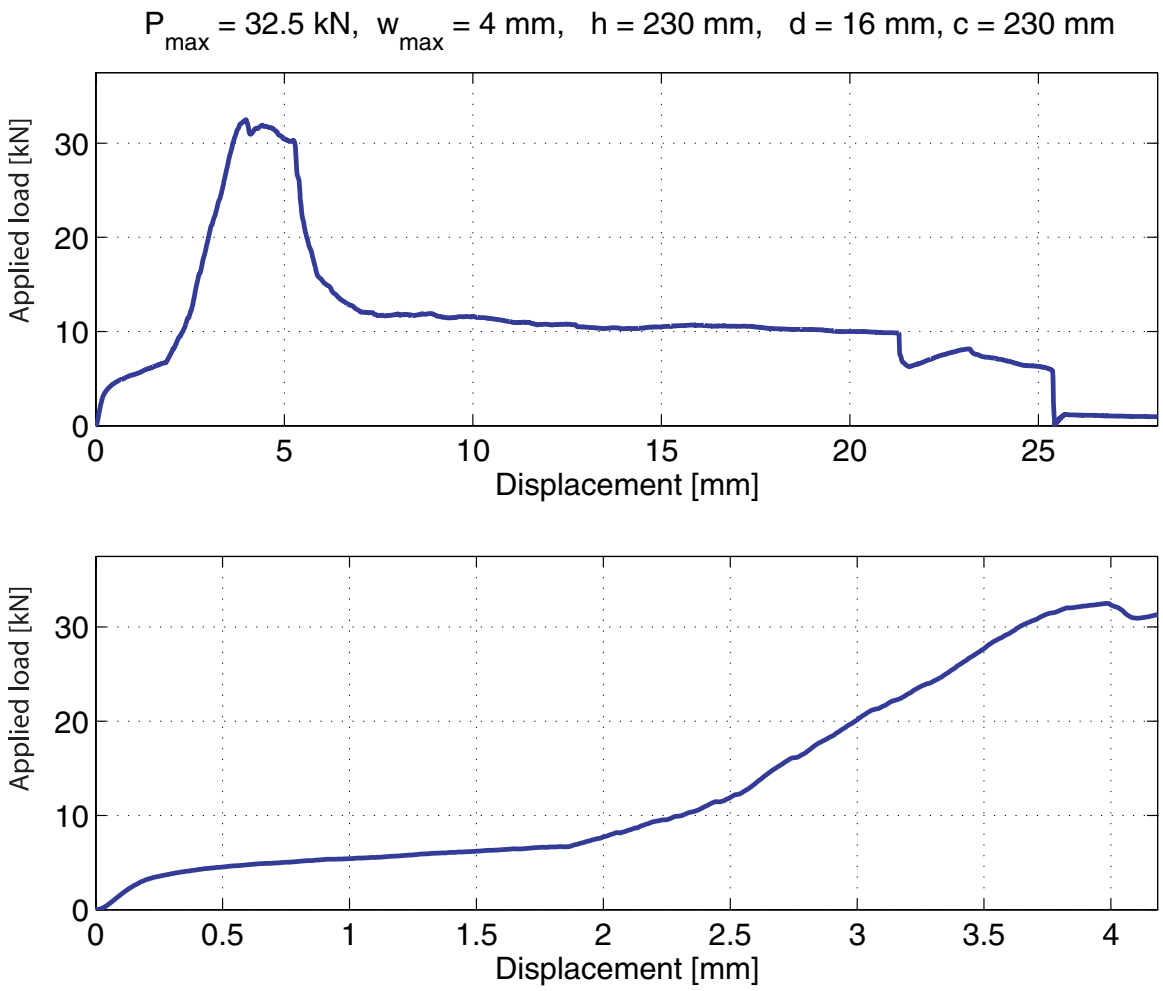

Figure A.124: *Load-deflection curve for the anchors pull-out*

A.3.9 Corner distance c = 230 mm - 2, d = 16 mm

Figure A.125: *The failure mode observed*

Failure mode: Brick pull-out failure failure

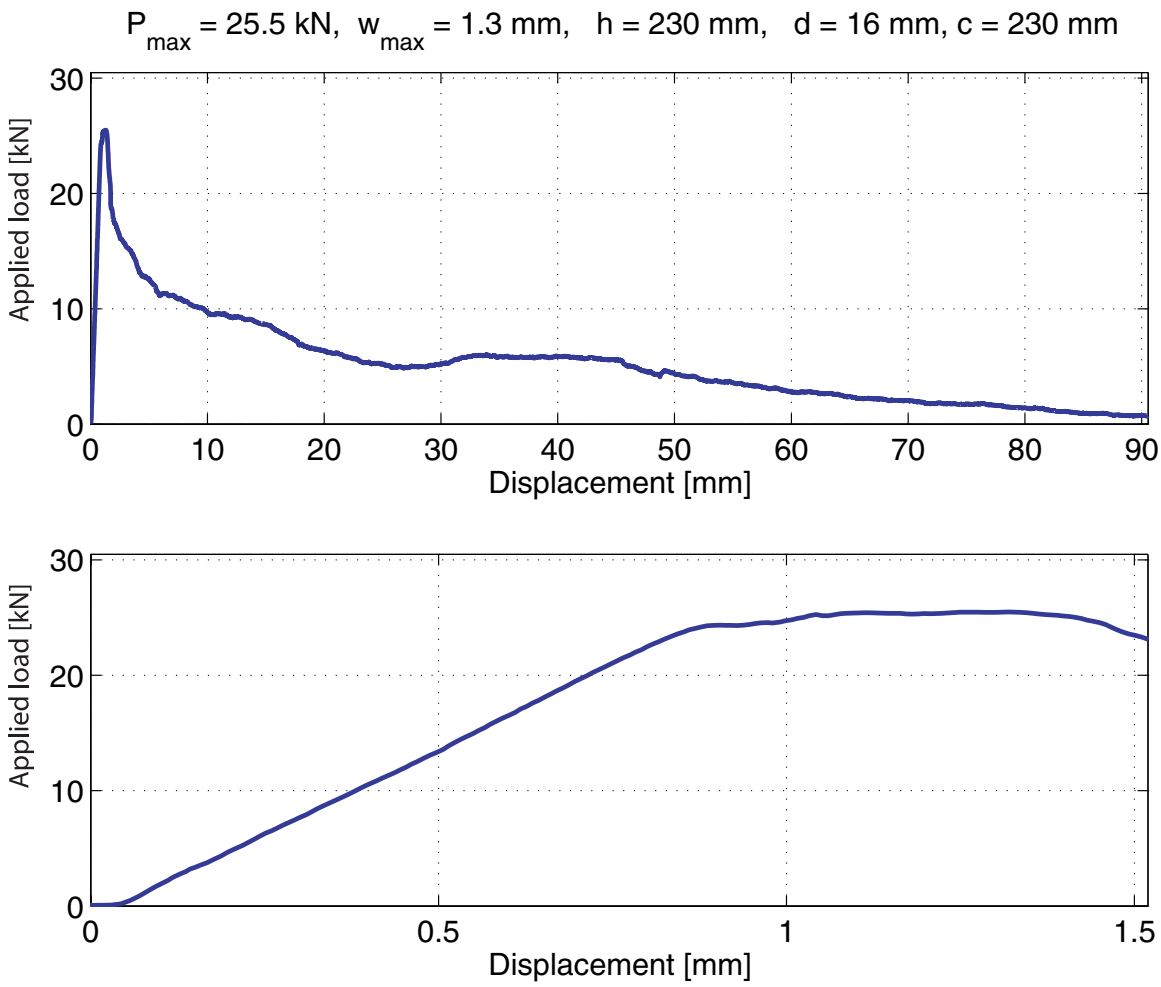

Figure A.126: *Load-deflection curve for the anchors pull-out*

A.4 Close to an edge - normal to the bed joint

A.4.1 Edge distance e = 90 mm, d = 12 mm

Figure A.127: *The failure mode observed*

Failure mode: Splitting failure in the brick

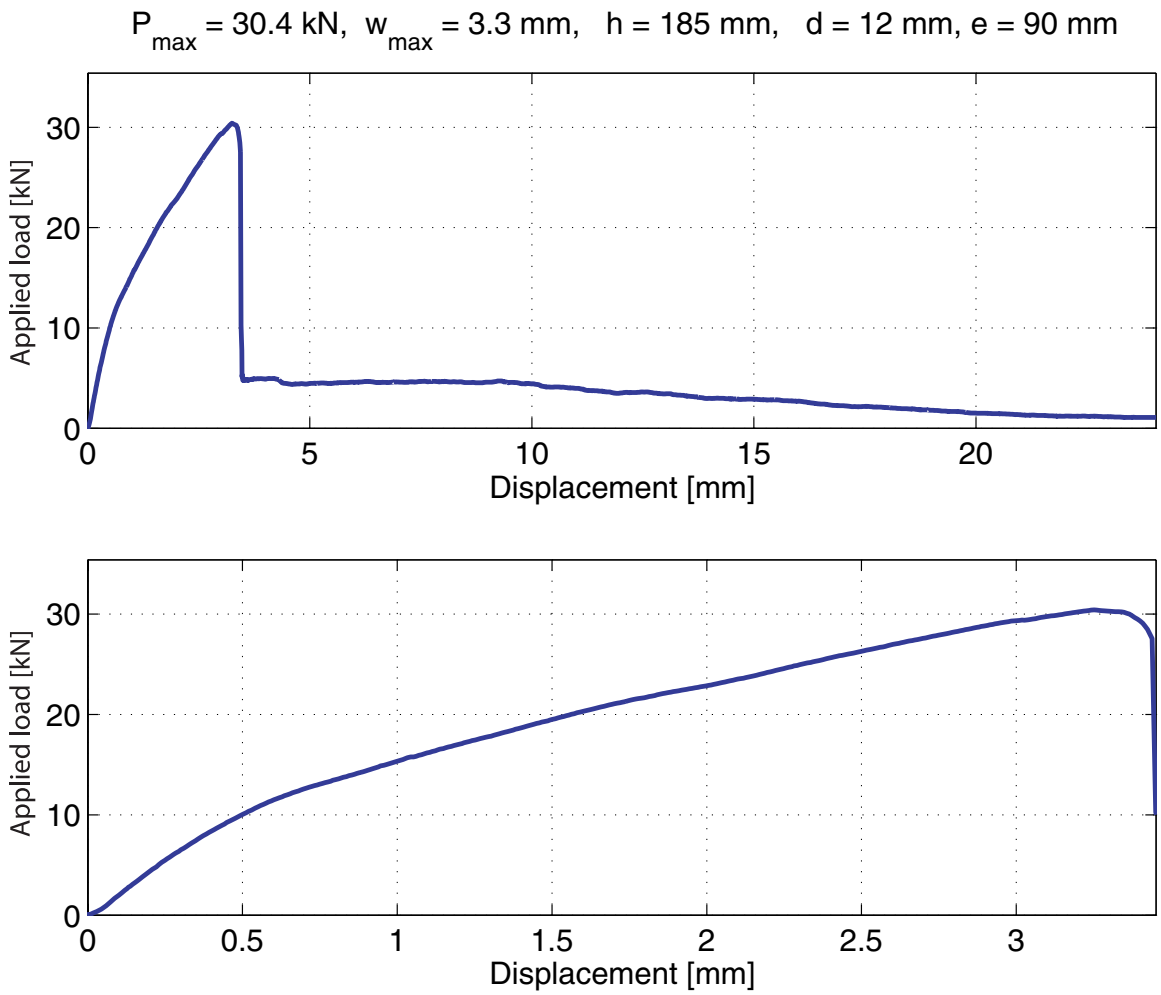

Figure A.128: *Load-deflection curve for the anchors pull-out*

A.4.2 Edge distance e = 160 mm, d = 12 mm

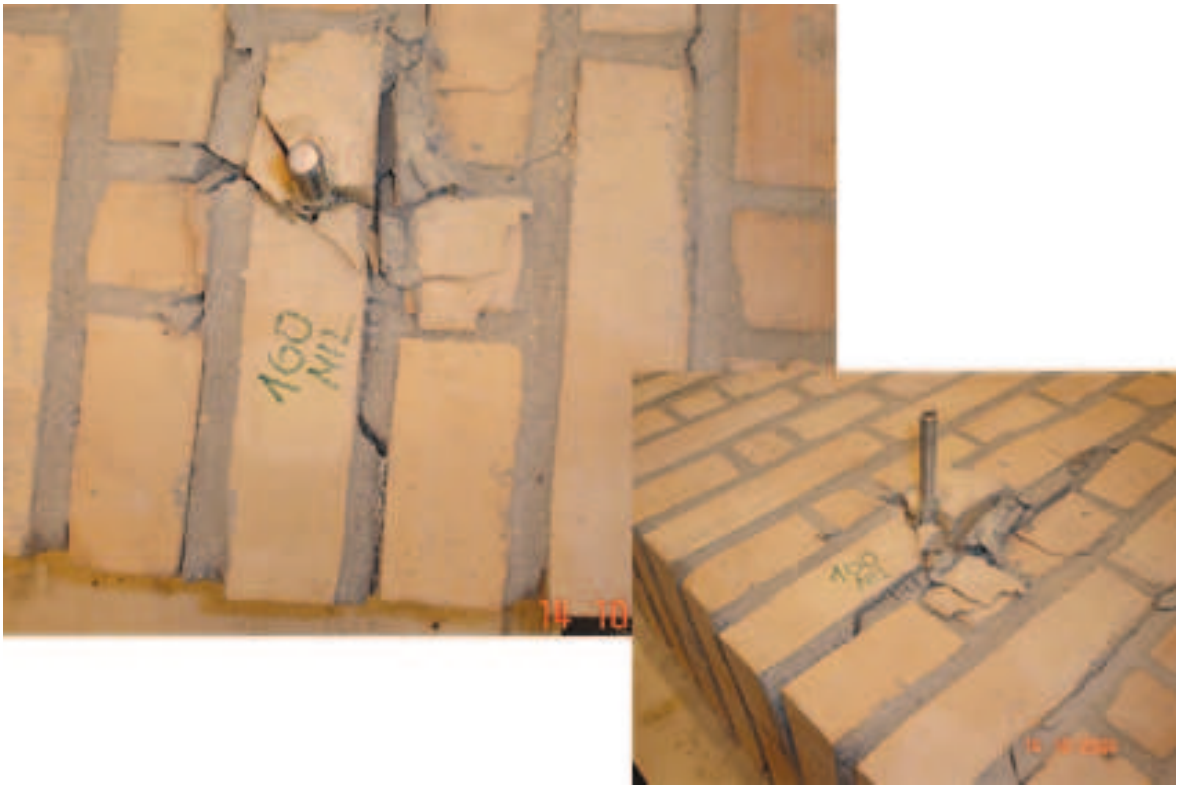

Figure A.129: *The failure mode observed*

Failure mode: Splitting failure in the brick

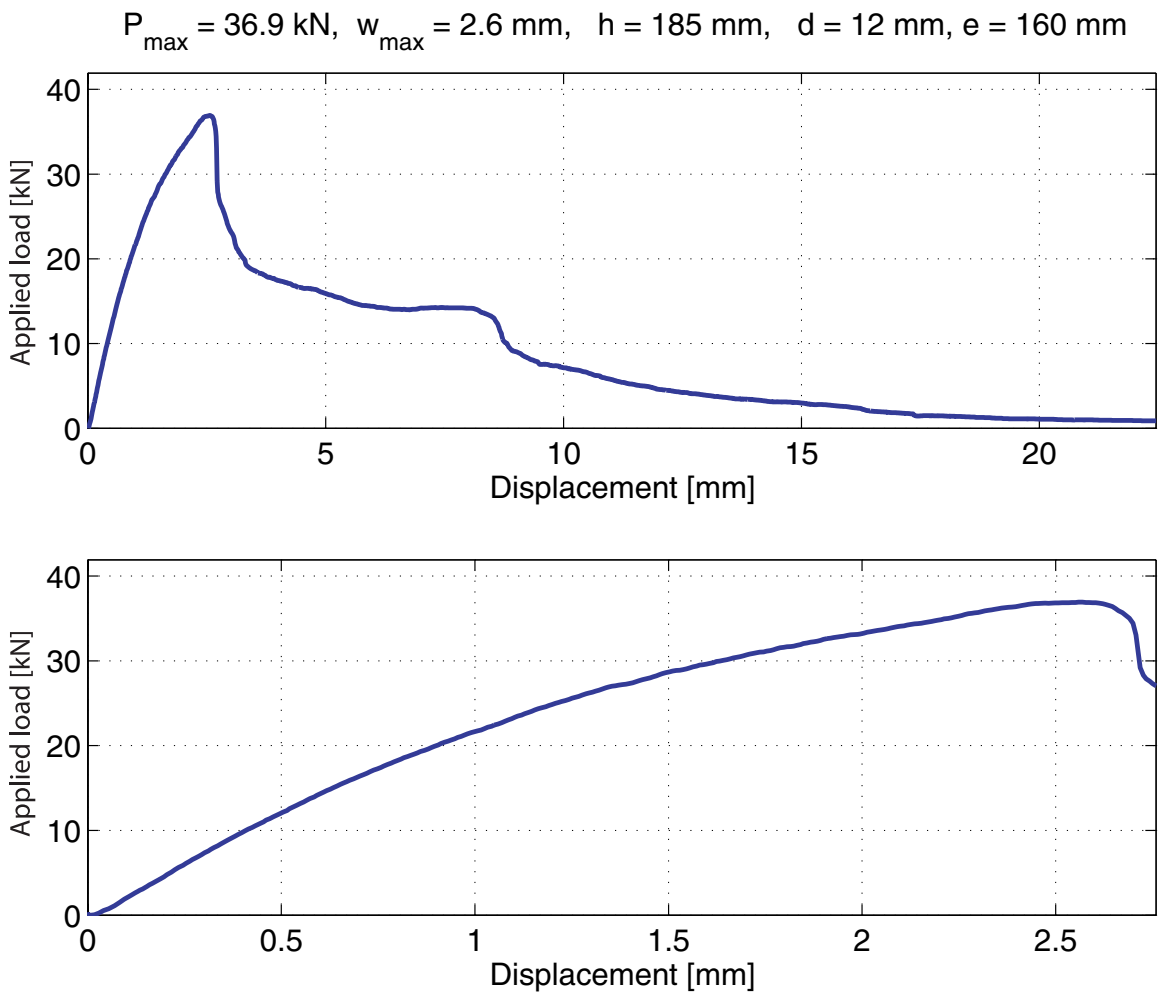

Figure A.130: *Load-deflection curve for the anchors pull-out*

A.4.3 Edge distance e = 230 mm, d = 12 mm

Figure A.131: *The failure mode observed*

Failure mode: Sliding failure in the wall

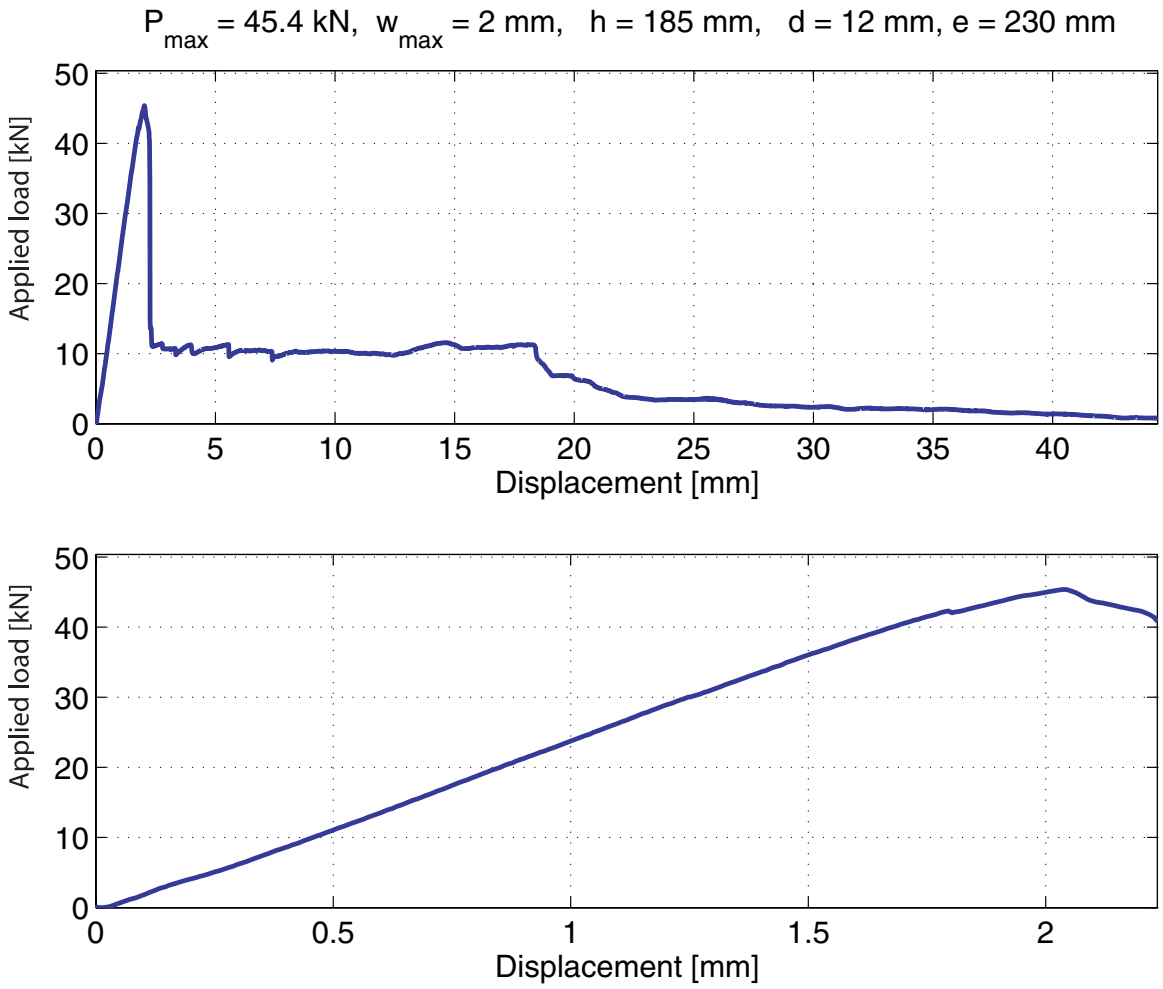

Figure A.132: *Load-deflection curve for the anchors pull-out*

A.4.4 Edge distance e = 100 mm, d = 16 mm

Figure A.133: *The failure mode observed*

Failure mode: Splitting failure in the brick

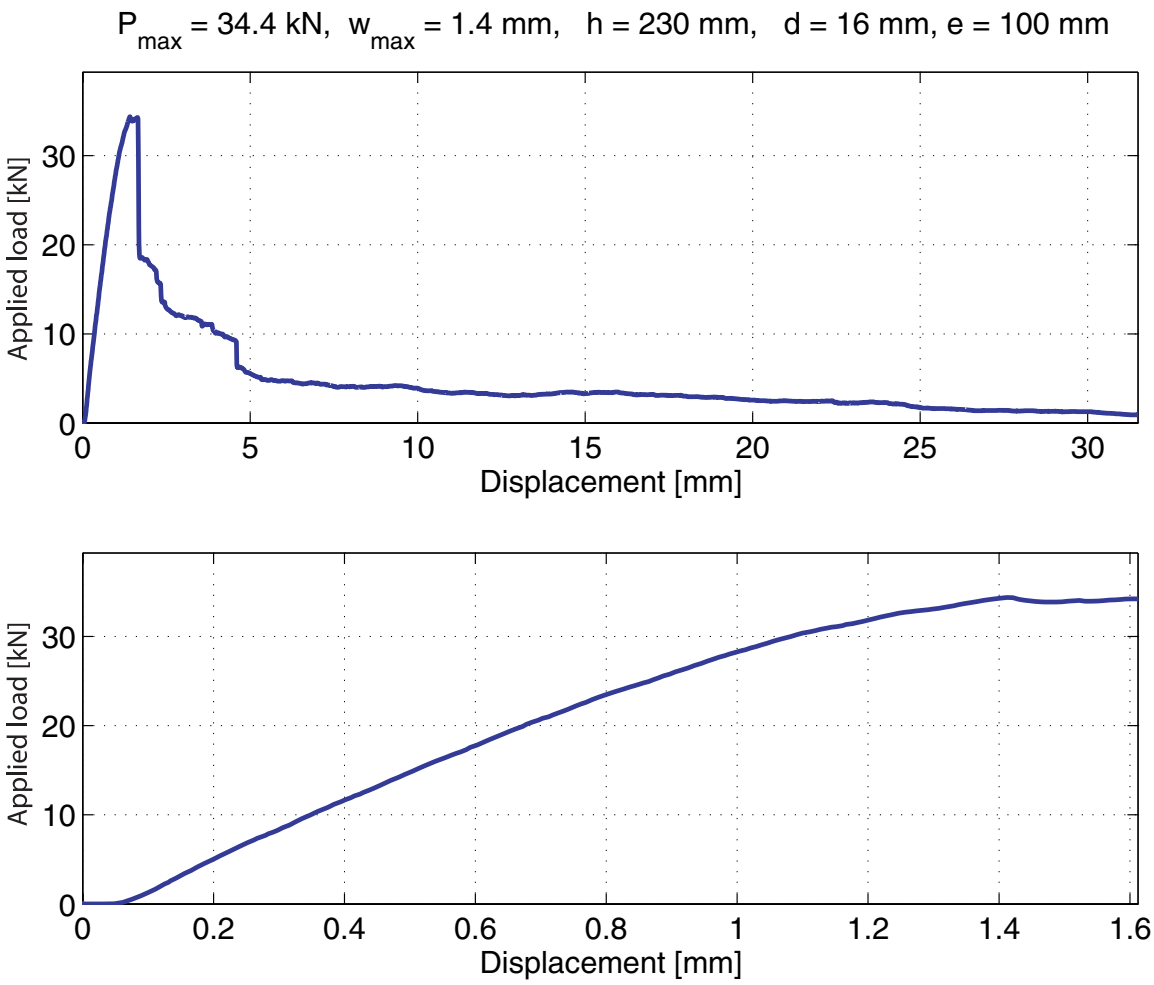

Figure A.134: *Load-deflection curve for the anchors pull-out*

A.4.5 Edge distance e = 160 mm, d = 16 mm

Figure A.135: *The failure mode observed*

Failure mode: Splitting failure in the wall

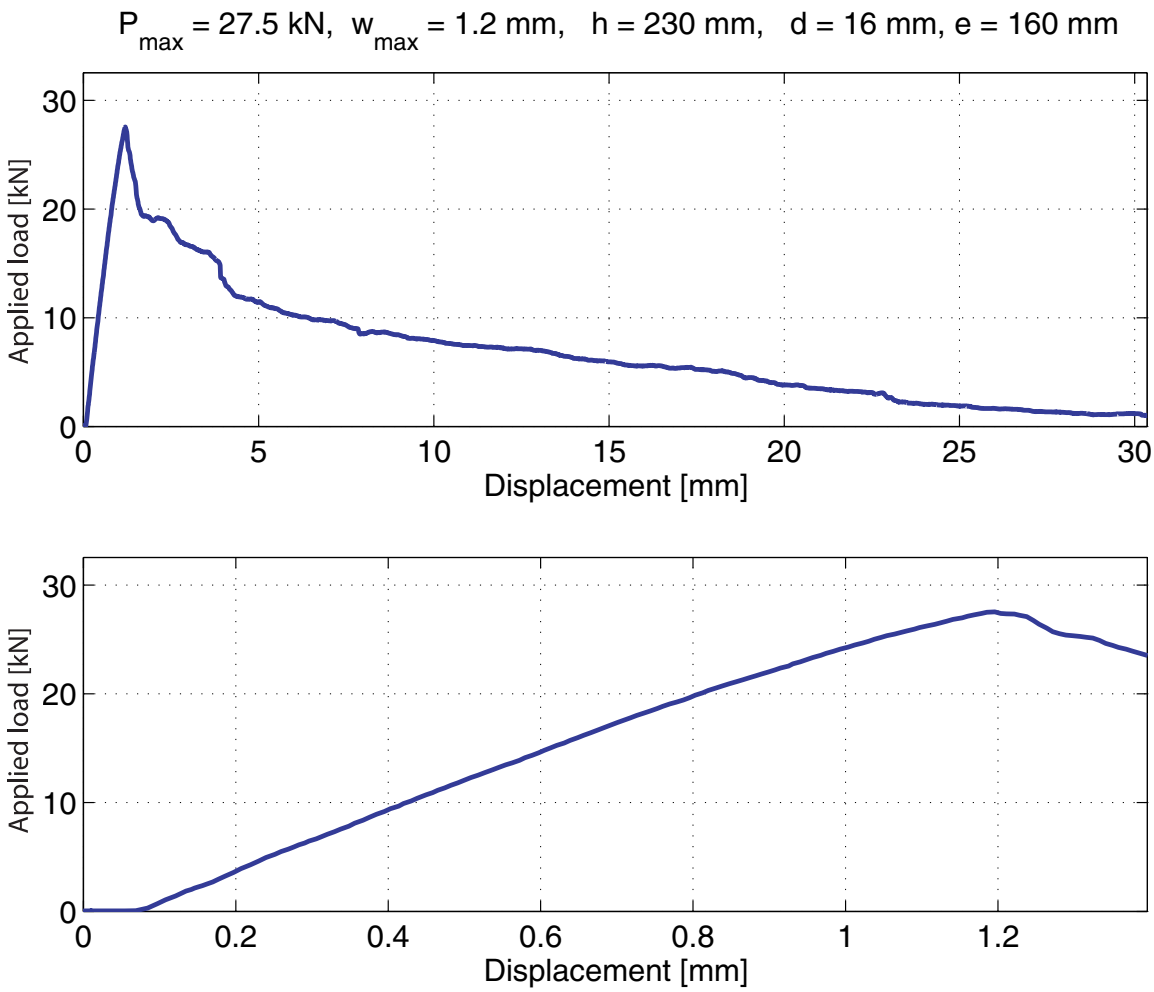

Figure A.136: *Load-deflection curve for the anchors pull-out*

A.4.6 Edge distance e = 230 mm, d = 16 mm

Figure A.137: *The failure mode observed*

Failure mode: Splitting failure in the brick

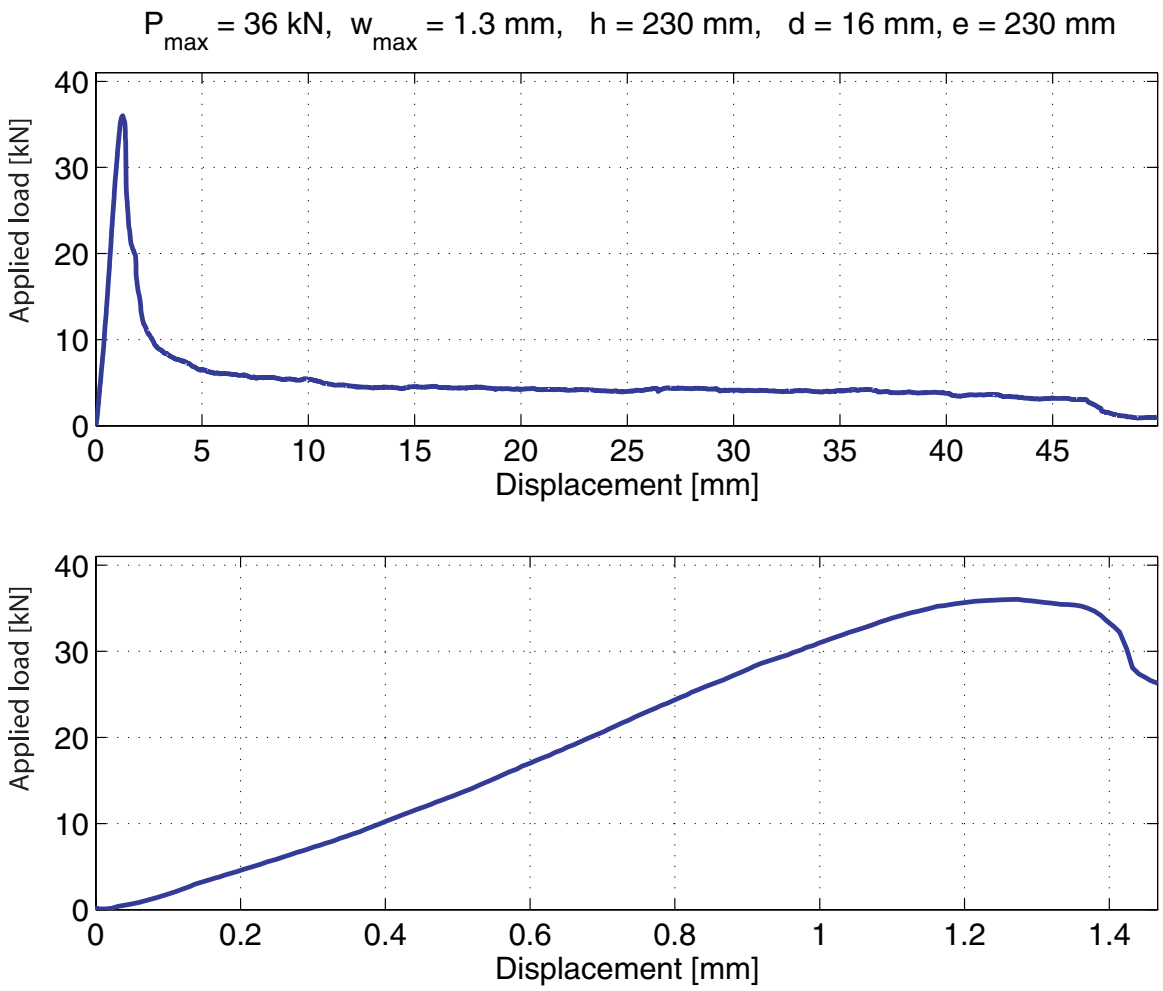

Figure A.138: *Load-deflection curve for the anchors pull-out*

A.5 Close to an edge - parallel to the bed joint

A.5.1 Edge distance e = 90 mm, d = 12 mm

Figure A.139: *The failure mode observed*

Failure mode: Cover bending failure

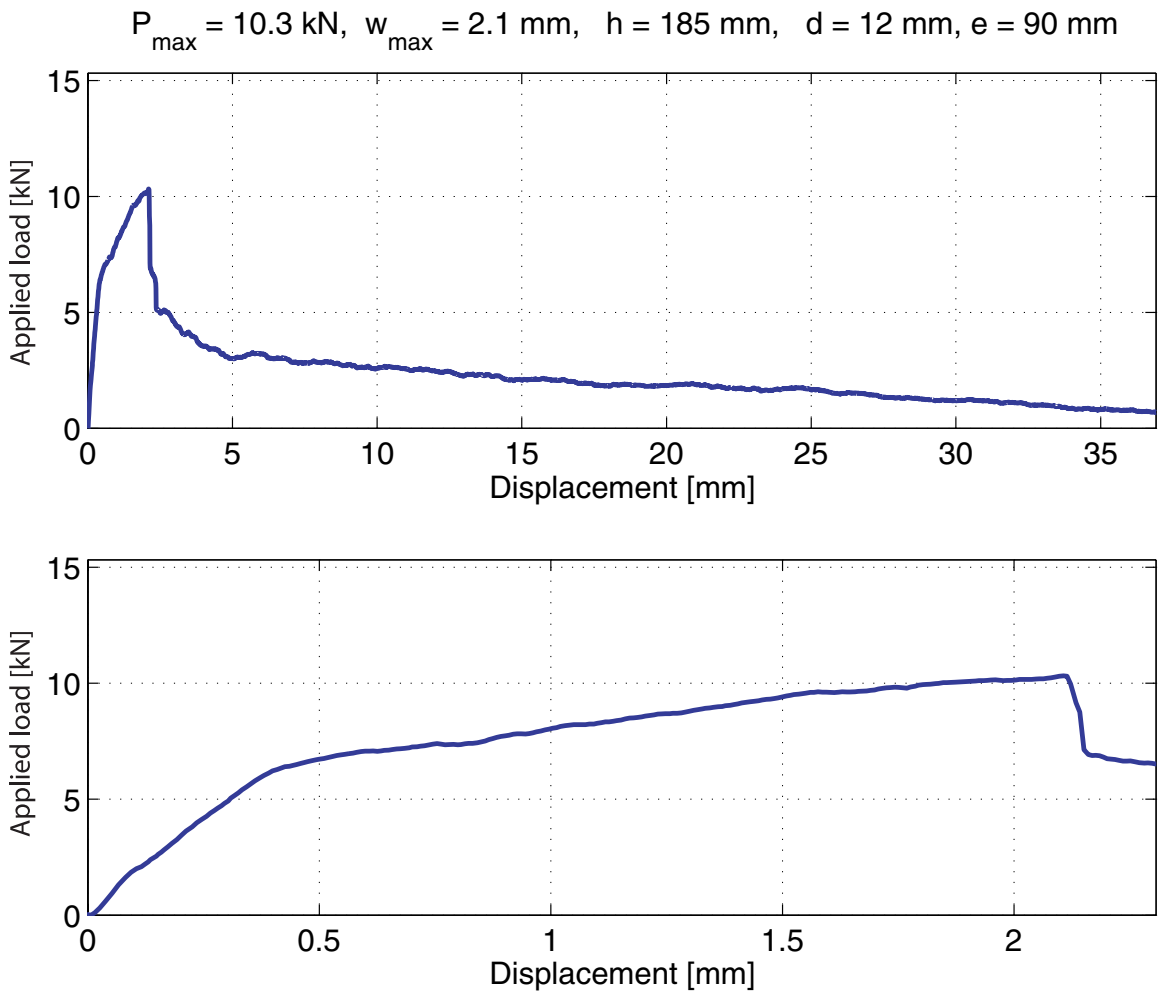

Figure A.140: *Load-deflection curve for the anchors pull-out*

A.5.2 Edge distance e = 160 mm, d = 12 mm

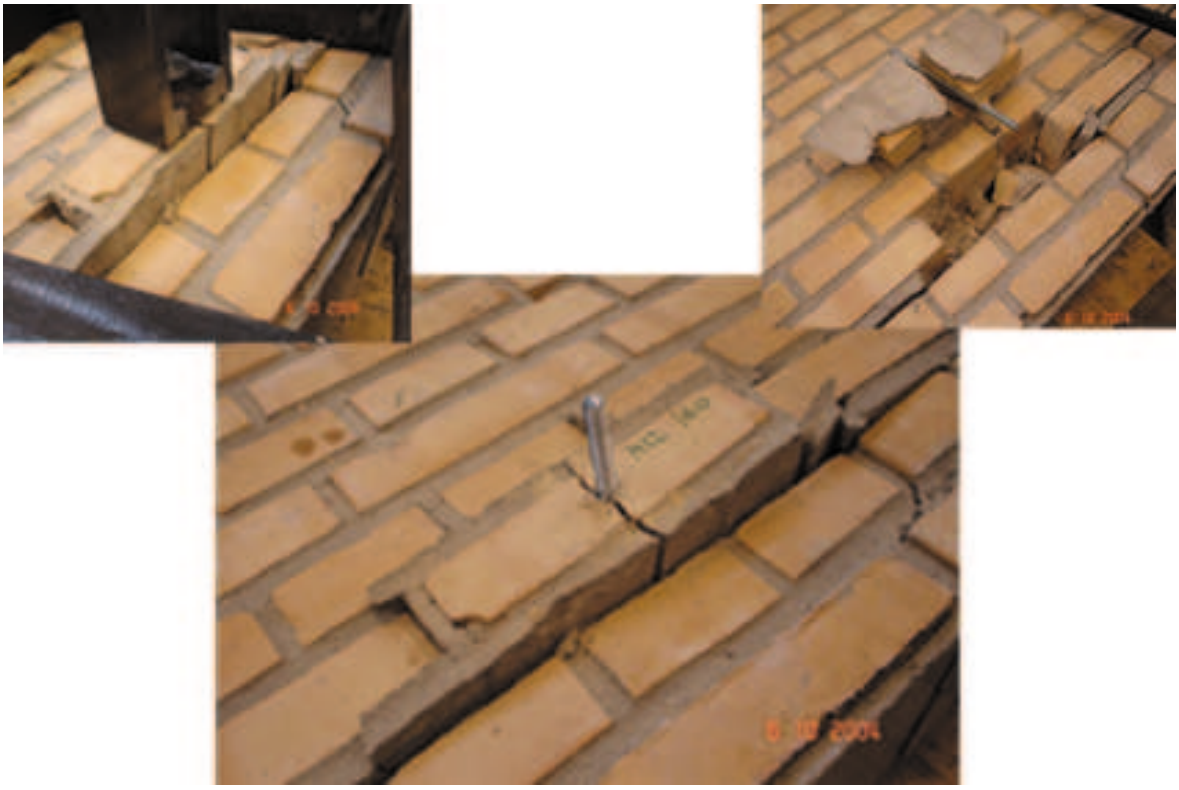

Figure A.141: *The failure mode observed*

Failure mode: Cover bending failure

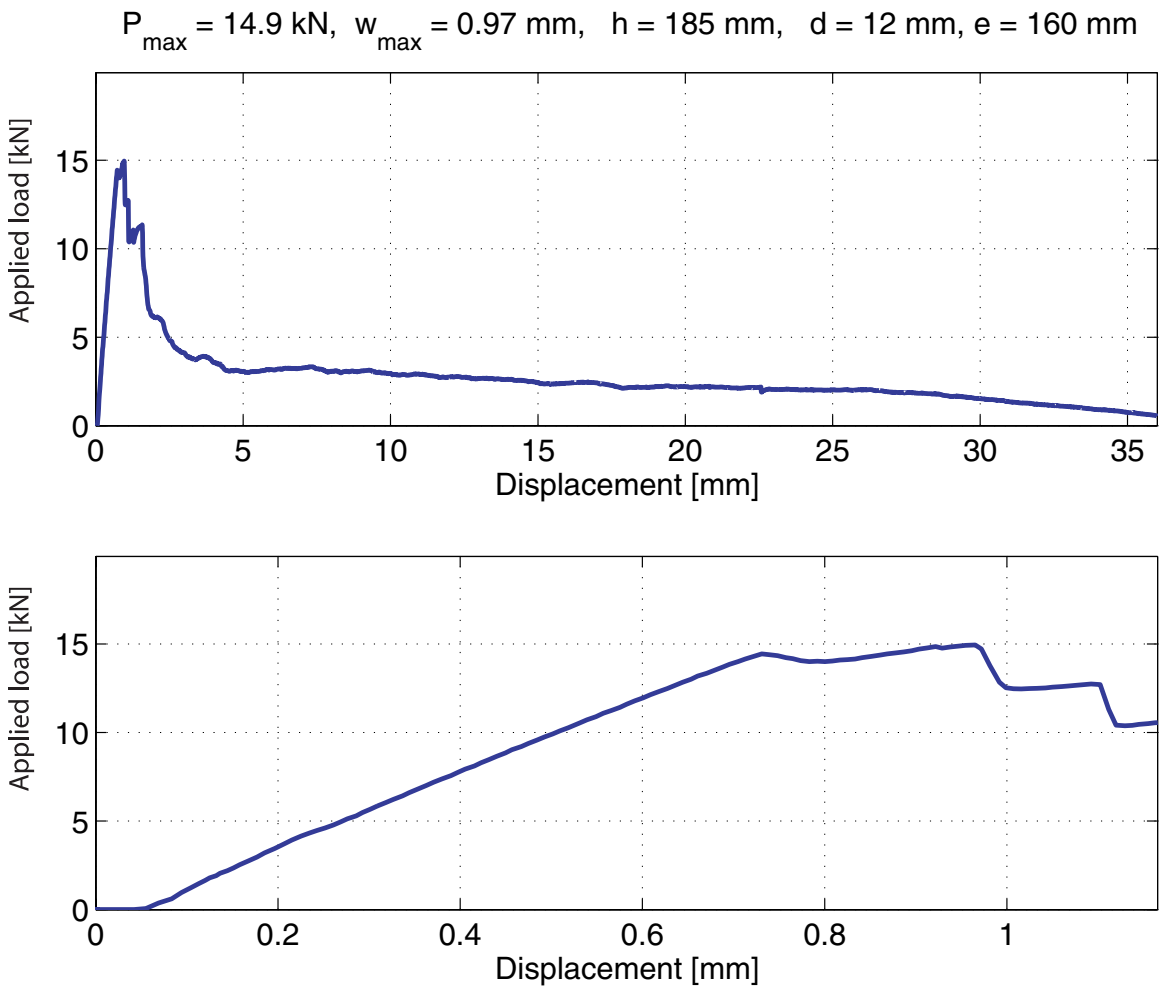

Figure A.142: *Load-deflection curve for the anchors pull-out*

A.5.3 Edge distance e = 230 mm, d = 12 mm

Figure A.143: *The failure mode observed*

Failure mode: Brick pull-out failure

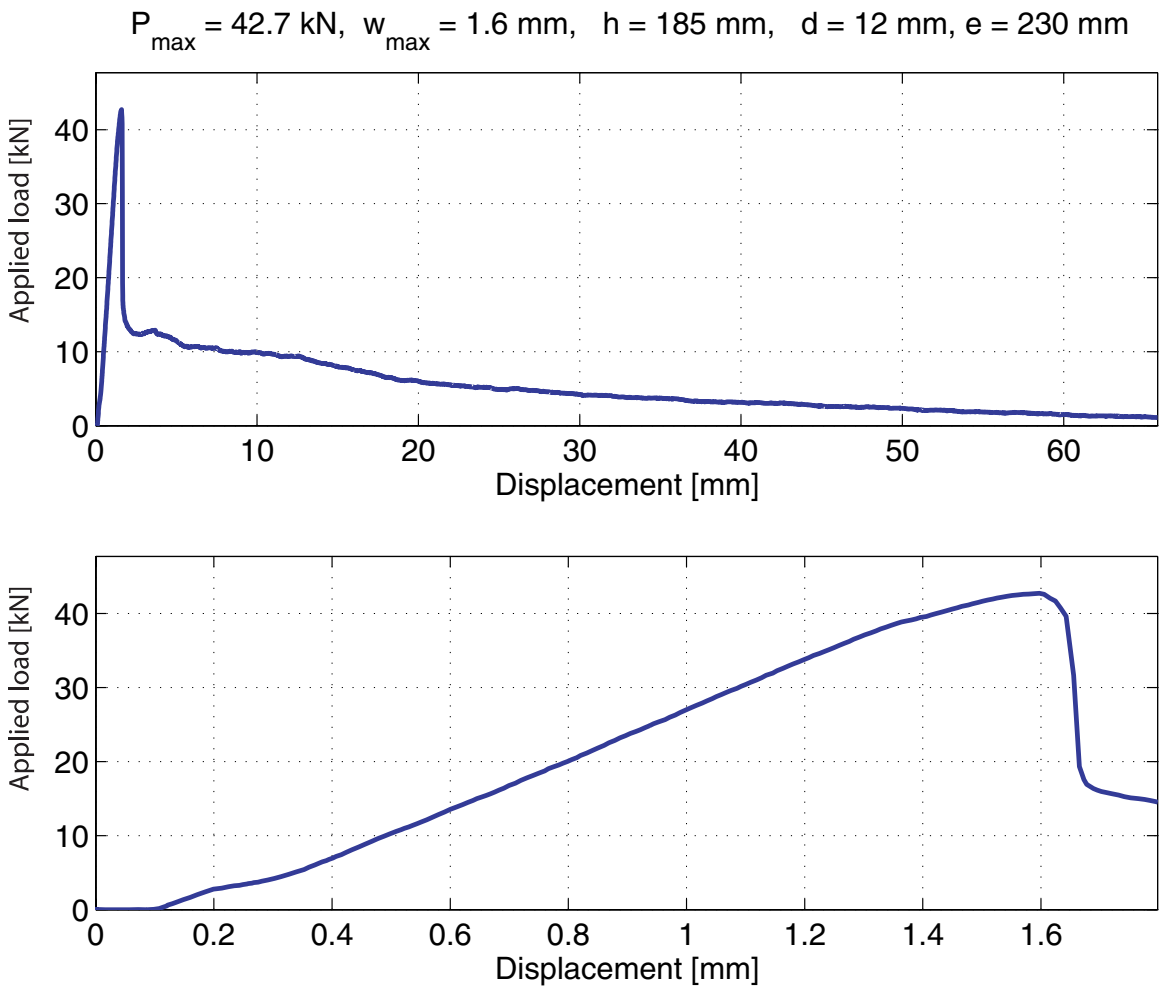

Figure A.144: *Load-deflection curve for the anchors pull-out*

A.5.4 Edge distance e = 100 mm, d = 16 mm

Figure A.145: *The failure mode observed*

Failure mode: Cover bending failure

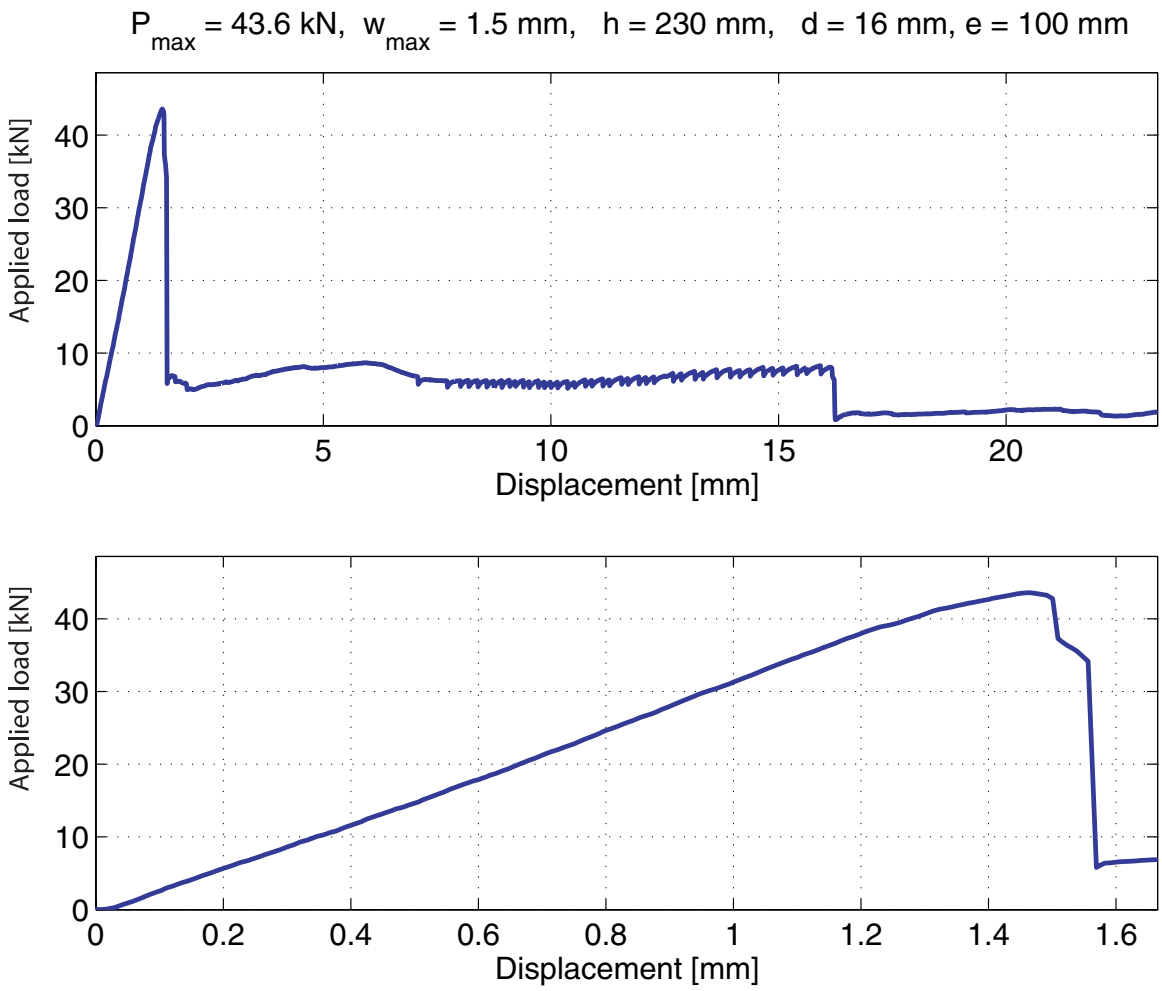

Figure A.146: *Load-deflection curve for the anchors pull-out*

A.5.5 Edge distance e = 160 mm, d = 16 mm

Figure A.147: *The failure mode observed*

Failure mode: Brick pull-out failure

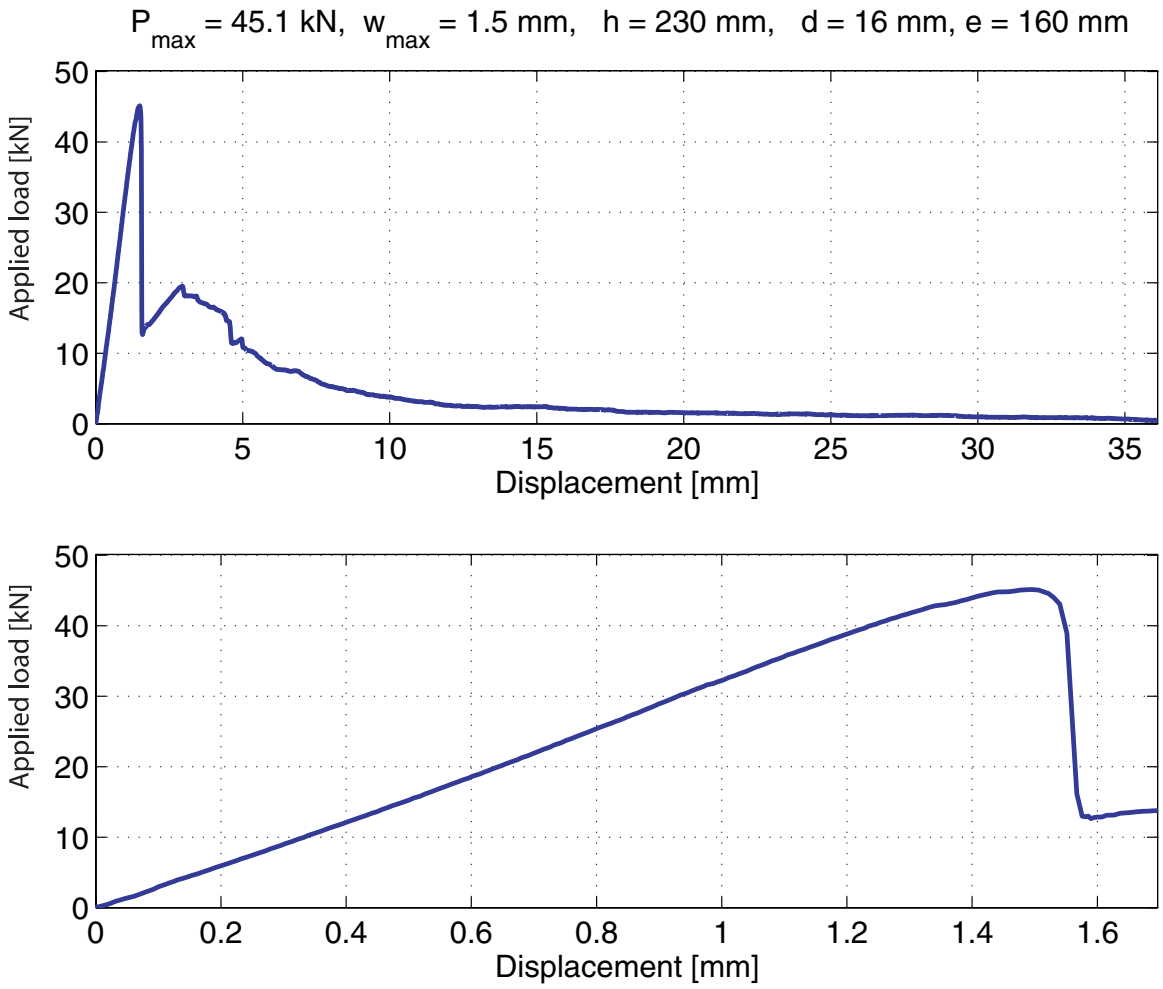

Figure A.148: *Load-deflection curve for the anchors pull-out*

A.5.6 Edge distance e = 230 mm, d = 16 mm

Figure A.149: *The failure mode observed*

Failure mode: Brick pull-out failure

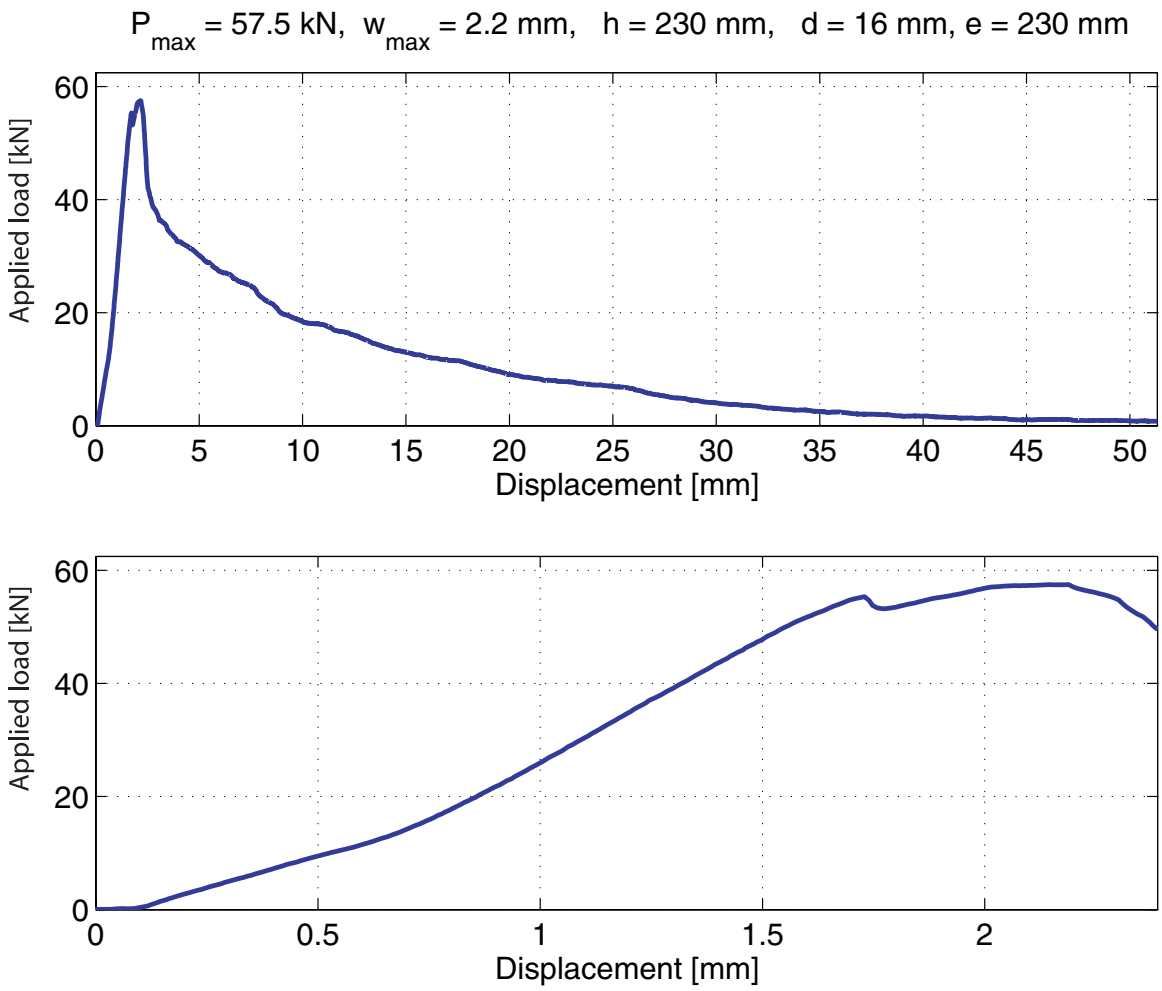

Figure A.150: *Load-deflection curve for the anchors pull-out*